National Library
of Canada

Bibliothèque nationale
du Canada

Canadian Theses Service

Services des thèses canadiennes

Ottawa, Canada
K1A 0N4

CANADIAN THESES

THÈSES CANADIENNES

NOTICE

The quality of this microfiche is heavily dependent upon the quality of the original thesis submitted for microfilming. Every effort has been made to ensure the highest quality of reproduction possible.

If pages are missing, contact the university which granted the degree.

Some pages may have indistinct print especially if the original pages were typed with a poor typewriter ribbon or if the university sent us an inferior photocopy.

Previously copyrighted materials (journal articles, published tests, etc.) are not filmed.

Reproduction in full or in part of this film is governed by the Canadian Copyright Act, R.S.C. 1970, c. C-30. Please read the authorization forms which accompany this thesis.

THIS DISSERTATION
HAS BEEN MICROFILMED
EXACTLY AS RECEIVED

AVIS

La qualité de cette microfiche dépend grandement de la qualité de la thèse soumise au microfilmage. Nous avons tout fait pour assurer une qualité supérieure de reproduction.

S'il manque des pages, veuillez communiquer avec l'université qui a conféré le grade.

La qualité d'impression de certaines pages peut laisser à désirer, surtout si les pages originales ont été dactylographiées à l'aide d'un ruban usé ou si l'université nous a fait parvenir une photocopie de qualité inférieure.

Les documents qui font déjà l'objet d'un droit d'auteur (articles de revue, examens publiés, etc.) ne sont pas microfilmés.

La reproduction, même partielle, de ce microfilm est soumise à la Loi canadienne sur le droit d'auteur, SRC 1970, c. C-30. Veuillez prendre connaissance des formules d'autorisation qui accompagnent cette thèse.

LA THÈSE A ÉTÉ
MICROFILMÉE TELLE QUE
NOUS L'AVONS REÇUE

NL 339 (r. 86/01)

Canada

44

0-315-26777-1

National Library
of Canada

Bibliothèque nationale
du Canada

Canadian Theses Division

Division des thèses canadiennes

Ottawa, Canada
K1A 0N4

PERMISSION TO MICROFILM — AUTORISATION DE MICROFILMER

- Please print or type — Écrire en lettres moulées ou dactylographier

Full Name of Author — Nom complet de l'auteur

STEPHEN JOHN KENNEDY

Date of Birth — Date de naissance 56.10.04	Country of Birth — Lieu de naissance CANADA.

Permanent Address — Résidence fixe

131 WOLF WILLOW CRES.
EDMONTON T5T 1T1

Title of Thesis — Titre de la thèse

END CONNECTION EFFECTS ON THE STRENGTH OF CONCRETE FILLED HSS BEAM COLUMNS.

University — Université

UNIVERSITY OF ALBERTA.

Degree for which thesis was presented — Grade pour lequel cette thèse fut présentée

M Sc.

Year this degree conferred — Année d'obtention de ce grade 1984	Name of Supervisor — Nom du directeur de thèse DR. J.G. MacGREGOR.

Permission is hereby granted to the NATIONAL LIBRARY OF CANADA to microfilm this thesis and to lend or sell copies of the film.

The author reserves other publication rights, and neither the thesis nor extensive extracts from it may be printed or otherwise reproduced without the author's written permission.

L'autorisation est, par la présente, accordée à la BIBLIOTHÈQUE NATIONALE DU CANADA de microfilmer cette thèse et de prêter ou de vendre des exemplaires du film.

L'auteur se réserve les autres droits de publication; ni la thèse ni de longs extraits de celle-ci ne doivent être imprimés ou autrement reproduits sans l'autorisation écrite de l'auteur.

Date 84.04.16	Signature

NL-91 (4/77)

THE UNIVERSITY OF ALBERTA

END CONNECTION EFFECTS ON THE STRENGTH OF CONCRETE FILLED HSS BEAM COLUMNS

by

ⓒ STEPHEN JOHN KENNEDY

A THESIS
SUBMITTED TO THE FACULTY OF GRADUATE STUDIES AND RESEARCH
IN PARTIAL FULFILMENT OF THE REQUIREMENTS FOR THE DEGREE
OF MASTER OF SCIENCE

DEPARTMENT OF CIVIL ENGINEERING

EDMONTON, ALBERTA
SPRING, 1984

THE UNIVERSITY OF ALBERTA

RELEASE FORM

NAME OF AUTHOR STEPHEN JOHN KENNEDY

TITLE OF THESIS END CONNECTION EFFECTS ON THE STRENGTH OF CONCRETE FILLED HSS BEAM COLUMNS

DEGREE FOR WHICH THESIS WAS PRESENTED MASTER OF SCIENCE

YEAR THIS DEGREE GRANTED SPRING, 1984

Permission is hereby granted to THE UNIVERSITY OF ALBERTA LIBRARY to reproduce single copies of this thesis and to lend or sell such copies for private, scholarly or scientific research purposes only.

The author reserves other publication rights, and neither the thesis nor extensive extracts from it may be printed or otherwise reproduced without the author's written permission.

(SIGNED) ....

PERMANENT ADDRESS:

131 WOLF WILLOW CRES
EDMONTON, ALBERTA
T5T 1T1

DATED MARCH 22nd 1984

THE UNIVERSITY OF ALBERTA

FACULTY OF GRADUATE STUDIES AND RESEARCH

The undersigned certify that they have read, and recommend to the Faculty of Graduate Studies and Research, for acceptance, a thesis entitled END CONNECTION EFFECTS ON THE STRENGTH OF CONCRETE FILLED HSS BEAM COLUMNS submitted by STEPHEN JOHN KENNEDY in partial fulfilment of the requirements for the degree of MASTER OF SCIENCE.

....

Supervisor

....

J.R. Colbourne

D.W. Murray

Janie Kennedy

Date MARCH 22nd 1984

ABSTRACT

Based on past experimentation, design recommendations from various codes and standards stipulate that a load path must be provided such that both the steel and the concrete of a concrete filled HSS beam column are loaded simultaneously. This, in effect, ensures strain compatibility of the two materials at this location. A preferred arrangement would be to forego this expensive and inconvenient connection detail and in its place use a standard HSS beam column connection in which the load is transferred through the connection into the steel shell without attempting to introduce the load directly into the concrete. In such a connection strain compatibility is not ensured.

The main objective of this study was to determine the change in behaviour and ultimate load capacity of concrete filled HSS beam columns when strain compatibility was not ensured. This was accomplished in four steps as summarized here.

1. A series of tests were conducted on bare steel, and concrete filled, strain compatible and non-strain compatible rectangular HSS beam columns, to obtain the necessary information for subsequent analyses.
2. A detailed analysis of the data from the non-strain compatible test series was done to determine the method and rate of load transfer from the steel shell to the concrete core. Four types of load transfer mechanisms

have been identified and are:

a. Adhesion

b. Micro-interlocking of surface irregularities of the steel tube with the cement paste

c. Macro-interlocking - Friction Type

d. Macro-interlocking - Binding Type

A mathematical model was developed for the micro-interlocking load transfer mechanism. The solution of the governing differential equation shows excellent agreement with corresponding test data.

3. A comparison was made of the ultimate loads obtained from the bare steel and concrete filled strain compatible HSS beam column tests and the values predicted for the corresponding columns by various codes or standards. With the exception of those beam columns approaching and including pure flexural behaviour, the ultimate load values were predicted with reasonable accuracy.

4. A further comparison of the non-strain compatible test series with the strain compatible test series suggests that there is no difference in flexural stiffness or general load deflection behaviour between the two types. Based on the limited data a simple empirical formula was developed to describe the reduction in ultimate load capacity from the strain compatible to the non-strain compatible case as a function of column slenderness and eccentricity of the applied load.

It is plausible that current code or standard formulations could be used to describe the strength of non-strain compatible HSS beam columns, if an ultimate load reduction capacity factor similar to the one described previously, was incorporated.

ACKNOWLEDGEMENTS

I am indebted to Professor J. G. MacGregor for his supervision and valued counsel throughout the course of this work.

In addition the author would like to express his appreciation to Dr. R.G. Redwood, Dr. D.J.L. Kennedy, Dr. D.W. Murray and Dr. T.Hrudey for their guidance and suggestions.

The assistance and cooperation of the technical staff of the I. F. Morrison Laboratory, Technical Services, Civil Engineering Machine Shop at the University of Alberta is acknowledged. In particular, I would like to thank L. Burden, R. Helfrich and H. Friedrich for their skill, craftmanship and assistance in fabricating and testing the test specimens.

The time, energy and personal interest that Tom Casey gave in his advice and assistance in programming source code and graphic packages, is truly unforgettable and for this I am very grateful.

I gratefully acknowledge the support, time and personal interest that Karen Baker put in for the preparation and completion of this thesis.

Table of Contents

Chapter Page

1. INTRODUCTION 1
    1.1 General 1
    1.2 Objectives 2
    1.3 Scope 3
    1.4 Outline 3
2. LITERATURE REVIEW 6
    2.1 General 6
    2.2 Experimentally Based Research 7
        2.2.1 Behaviour of Beam Columns 7
        2.2.2 Triaxial Effects 10
        2.2.3 Load Transfer Mechanisms 11
    2.3 Analytical Methods and Parametric Studies 13
    2.4 Development of Design Recommendations 16
    2.5 Summary 17
3. EXPERIMENTAL PROGRAM 32
    3.1 General 32
    3.2 Selection of Test Section 33
    3.3 Column Tests 34
        3.3.1 General 34
        3.3.2 Preparation of Test Specimens 36
        3.3.3 Test Set-Up 37
            3.3.3.1 Load and Reaction Devices 37
            3.3.3.2 Instrumentation and Measurement ...38
            3.3.3.3 Test Procedure 38
    3.4 Flexural Tests 40
        3.4.1 General 40

3.4.2 Preparation of Test Specimens 41

3.4.3 Test Set up 41

3.4.4 Test Procedure 42

3.5 Ancillary Tests 42

3.5.1 Stub Columns 43

3.5.2 Tension Coupons 43

3.5.3 Residual Stress Measurements 44

3.5.4 Concrete Strength 45

3.5.4.1 Cylinder Tests 45

3.5.4.2 Split Cylinder Tensile Tests 46

3.5.4.3 Modulus of Rupture 46

4. MATERIAL PROPERTIES AND BEHAVIOUR 57

4.1 Steel 57

4.1.1 Geometric Properties 57

4.1.1.1 Dimensions 57

4.1.1.2 Section Properties 58

4.1.2 Load Deformation Relationships 58

4.1.2.1 Modulus of Elasticity 59

4.1.2.2 Poisson's Ratio 63

4.1.2.3 Yield Strength 63

4.1.2.4 Stub Column Load Deformation Curves 65

4.1.2.5 Tension Coupon Stress Strain Curves 66

4.1.3 Residual Stresses 67

4.2 Concrete 68

4.2.1 Stress Strain Relationship 68

4.2.1.1 Uniaxial Compressive Strength 68

4.2.1.2 Modulus of Rupture 69

4.2.1.3 Modulus of Elasticity 69

4.2.1.4 Stress Strain Curve 70

4.3 Composite Stub Column Behaviour 71

4.3.1 Load Deformation Relationship 71

4.3.2 Concrete Contribution 72

5. TEST RESULTS AND GENERAL BEHAVIOUR 95

5.1 Knife Edge Fixtures 95

5.2 Column Test Results 96

5.2.1 Initial Out-of-straightness 96

5.2.2 General Behaviour 97

5.2.3 Deflected Shapes 99

5.2.4 Steel Strain Distributions 100

5.2.5 Concrete Strain Distributions 101

5.2.6 Slip Distributions 102

5.3 Flexural Tests 104

6. LOAD TRANSFER MECHANISMS 146

6.1 General 146

6.2 Load Transfer Mechanisms 147

6.2.1 Adhesion 147

6.2.2 Micro-Interlocking 148

6.2.2.1 Development of the Governing Differential Equation for Slip ...149

6.2.2.2 Solution of the Governing Differential Equation for Slip ...153

6.2.3 Macro-Interlocking - Friction 154

6.2.4 Macro-Interlocking - Binding 155

6.3 Non-Strain Compatible Column Tests 156

6.3.1 Loads in Steel 156

6.3.2 Loads in Concrete 158

6.3.2.1 Concentrically Loaded Columns (C205,C605,C1205) 160

6.3.2.2 Eccentrically Loaded Columns (C206,C606,C1206) 164

7. ULTIMATE LOADS 187

7.1 General 187

7.2 Strength of Hollow Structural Steel Sections ...188

7.3 Strength of Strain Compatible Concrete Filled Hollow Structural Sections 192

7.3.1 CAN3-S16.1-M84 192

7.3.2 CAN3-S16.1-M84 (Alternate Proposal, Not Adopted) 197

7.3.3 Structural Stability Research Council, SSRC - Task Group 20 200

7.3.4 ECCS Recommendations 203

7.3.5 Ultimate Moment Resistance of the Composite Section 208

7.4 Non-Strain Compatible Versus Strain Compatible Beam Columns 210

7.4.1 Comparison of General Behaviour 211

7.4.2 Comparison of Ultimate Loads 212

7.5 Summary 213

8. SUMMARY, CONCLUSIONS AND RECOMMENDATIONS 233

8.1 Summary 233

8.2 Conclusions and Recommendations 236

8.3 Future Work 241

REFERENCES 243

List of Tables

Table Page

2.1 Summary of Tests on Axially Loaded Concrete Filled Circular HSS Columns 19

2.2 Summary of Tests on Axially Loaded Concrete Filled Rectangular HSS Columns.............23

2.3 Summary of Tests on Eccentrically Loaded Concrete Filled Circular HSS Columns................24

2.4 Summary of Tests on Eccentrically Loaded Concrete Filled Rectangular HSS Columns.............28

2.5 List of Papers on the Development of Design Recommendations..............................30

3.1 Type of Measurement and Instrumentation.............47

4.1 Example Set of Calculations for the Modulus of Elasticity, Tension Coupon 6.............74

4.2 Single Variable Statistical Analysis of the Modulus of Elasticity..........................75

4.3 Single Variable Statistical Analysis of the Yield Stress....................................75

4.4 Coefficients Used to Describe the Stub Column Stress Strain Curve..........................76

4.5 Coefficients Used to Describe the Stub Column Load Strain Curve............................76

4.6 Characteristic Parameters Used in the Description of Stress Strain Curves for Flat, Corner, and Weld Sections....................77

4.7 Coefficients Used to Describe the Stress Strain Curve for the Flat Sections..................80

4.8 Coefficients Used to Describe the Stress Strain Curve For the Corner Sections.........81

4.9 Coefficients Used to Describe the Stress Strain Curve of the Weld Sections............82

4.10 Uniaxial-Compressive and Tensile Strength for Concrete.......................................83

Table Page

4.11 Coefficients Used in the Mathematical Expressions which Describe the Composite Stub Column Load Strain Curve........................84

5.1 Reduced Data Derived from the Out-of-Straightness Measurements for Column C604....................................105

5.2 Summary of Initial Curvatures Derived From Out-of-Straightness Measurements..............106

5.3 Column Test Results................................107

5.4 Flexural Test Results..............................108

6.1 Effective Load Transfer Mechanisms................166

7.1 Test to Predicted Ratios for Steel Beam Columns and Beams by CAN3-S16.1-M78...........215

7.2 Test to Predicted Ratios for Composite Beam Columns and Beams by CAN3-S16.1-M84...........216

7.3 Test to Predicted Ratios for Composite Beam Columns and Beams, CAN3-S16.1-M84 Alternate Method (Not Adopted).....................217

7.4 Test to Predicted Ratios for Composite Beam Columns and Beams by SSRC-Task Group 20.......218

7.5 Test to Predicted Ratios for Composite Beam Columns and Beams by ECCS.....................219

7.6 Test to Predicted Ratio Statistics.................220

List of Figures

Figure Page

3.1 Upper Connection of Strain Compatible and Non-Strain Compatible Concrete-Filled HSS Columns...50

3.2 Schematic Diagram of a Column Specimen..............51

3.3 Knife Edge Assembly..................................52

3.4 Schematic Diagram of Instrumentation on a Column Specimen...................................53

3.5 Schematic Diagram of a Beam Specimen................54

3.6 Schematic Diagram of Instrumentation on a Beam Specimen.....................................55

3.7 Identification and Location of the Tension Coupons and Residual Stress Sections........56

4.1 Decision Making Model for Determination of the Modulus of Elasticity for Steel Sections.....85

4.2 Modulus of Elasticity Distribution..................86

4.3 Static Yield Stress Distribution....................87

4.4 Stress Strain Curve for Steel Stub Column...........88

4.5 Stress Strain Curves from Tension Coupons...........89

4.6 Longitudinal Residual Stress Distribution...........90

4.7 Through the Thickness Distribution of Longitudinal Residual Stresses.....................91

4.8 Modulus of Elasticity of Concrete..................92

4.9 Idealized Uniaxial Stress Strain Curve for Concrete.......................................93

4.10 Composite Stub Column Analysis.....................94

5.1 End Rotation, Concentrically Loaded Columns........109

5.2 End Rotation, Concentrically Loaded Columns........110

5.3 Out-of-Straightness for Column C604................111

5.4 Load-Deflection Curves for Concentrically Loaded Steel Columns..............................112

Figure Page

5.5 Load-Deflection Curves for Eccentrically Loaded Steel Columns....................................113

5.6 Load-Deflection Curves for Concentrically Loaded Composite Columns..............................114

5.7 Load-Deflection Curves for Eccentrically Loaded Composite Columns..............................115

5.8 Typical Failure Modes for Beam Column Tests........116

5.9 Load Deflection Curves for Concentrically Loaded Column, C603..................................117

5.10 Load Deflection Curves for Eccentrically Loaded Column, C606..................................118

5.11 Load Deflection Curves for Concentrically Loaded Column, C203..................................119

5.12 Steel Strain Distributions for Concentrically Loaded Column C205, L/r=20..........120

5.13 Steel Strain Distributions for Concentrically Loaded Column C605, L/r=59.9........121

5.14 Steel Strain Distributions for Concentrically Loaded Column C1205, L/r=117.6......122

5.15 Steel Strain Distributions for Eccentrically Loaded Column C206, L/r=20...........123

5.16 Steel Strain Distributions for Eccentrically Loaded Column C606, L/r=59.9.........124

5.17 Steel Strain Distributions for Eccentrically Loaded Column C1206, L/r=117.6.......125

5.18 Concrete Strains on South Face of Column C205, as Measured with a Demec Gauge...............126

5.19 Concrete Strains on South Face of Column C605, as Measured with a Demec Gauge...............127

5.20 Concrete Strains on South Face of Column C1205, as Measured with a Demec Gauge..............128

5.21 Concrete Strains on South Face of Beam Column C206, as Measured with a Demec Gauge........129

Figure Page

5.22 Concrete Strains on South Face of Beam Column C606, as Measured with a Demec Gauge........130

5.23 Concrete Strains on North Face of Beam Column C606, as Measured with a Demec Gauge........131

5.24 Concrete Strains on South Face of Beam Column C1206, as Measured with a Demec Gauge.......132

5.25 Slip on South Face of Column C205, Method B........133

5.26 Slip on South Face of Column C205, Method A........134

5.27 Slip on South Face of Column C605, Method B........135

5.28 Slip on South Face of Column C1205, Method B...136

5.29 Slip on North Face of Column C1205, Method B...137

5.30 Slip on South Face of Beam Column C206, Method B...138

5.31 Slip on North Face of Beam Column C206, Method B...139

5.32 Slip on South Face of Beam Column C606, Method B...140

5.33 Slip on North Face of Beam Column C606, Method B...141

5.34 Slip on South Face of Beam Column C1206, Method B...142

5.35 Slip on North Face of Beam Column C1206, Method B...143

5.36 Moment Curvature Diagrams for the Flexural Tests....................................144

5.37 Typical Failure Modes for Flexural Tests..........145

6.1 Shear Transfer Function............................167

6.2 Free Body Diagrams Used for the Development of the Governing Differential Equation.168

Figure Page

6.3 Slip Distributions for C1205 Computed from the Governing Differential Equation...........169

6.4 Macro-Interlocking - Friction Load Transfer at Top of Column.........................170

6.5 Ratios of Predicted to Applied Loads of the Mean Loads for Steel Columns, Based on Stub Column Data...............................171

6.6 Ratio of Predicted to Applied Loads of the Mean Loads for Steel Columns, Based on Tension Coupons and Longitudinal Residual Stress Data...............................172

6.7 Concrete Load Distributions for Column C1205.......173

6.8 Concrete Load Distributions for Column C605........174

6.9 Concrete Load Distributions for Column C205........175

6.10 Concrete Load Distributions for Beam Column C1206.......................................176

6.11 Concrete Load Distributions for Beam Column C606..177

6.12 Concrete Load Distributions for Beam Column C206..178

6.13 Assumed and Predicted Concrete Load Distributions for Column C1205....................179

6.14 Assumed Concrete Load Distributions for Column C605..180

6.15 Assumed Concrete Load Distributions for Column C205..181

6.16 Assumed Concrete Load Distributions for Beam Column C1206................................182

6.17 Assumed Concrete Load Distributions for Beam Column C606.................................183

6.18 Assumed Concrete Load Distributions for Beam Column C206.................................184

Figure Page

6.19 Load Transfer Mechanisms in the Region just Below the Connection Plates for Concentrically Loaded Columns......................185

6.20 Load Transfer Mechanisms in the Region just Below the Connection Plates for Eccentrically Loaded Columns.......................186

7.1 Axial Load-Moment Interaction Diagram for Steel Columns, CAN3-S16.1-M78......................222

7.2 Column Curves for Steel Columns, CAN3-S16.1-M78....223

7.3 Axial Load-Moment Interaction Diagram for Composite Columns, CAN3-S16.1-M84..................224

7.4 Column Curves for Composite Columns, CAN3-S16.1-M84225

7.5 Axial Load-Moment Interaction Diagram for Composite Columns, CAN3-S16.1-M84 (Alternate Proposal, Not Adopted)..................226

7.6 Column Curves for Composite Columns, CAN3-S16.1-M84 (Alternate Proposal, Not Adopted)...227

7.7 Axial Load-Moment Interaction Diagram for Composite Columns, SSRC Method.....................228

7.8 Column Curves for Composite Columns, SSRC Method...229

7.9 Axial Load-Moment Interaction Diagram for Composite Columns, ECCS Recommendations............230

7.10 Column Curves for Composite Columns, ECCS Recommendations...................................231

7.11 Ultimate Load Capacity Ratio of Non-Strain Compatible to Strain Compatible Composite Beam Columns..................232

LIST OF SYMBOLS

A = Steel area; coefficient used to describe a load-deformation curve

A_c = Concrete area

A_s = Steel area

a = Constant defining the shape of the shear transfer function; concrete contribution factor

B = Coefficient used to describe a load-deformation curve

BFC_n = Modulus of elasticity that corresponds to the coefficient of determination closest to 1 for the n^{th} evaluation

B23 = Beam specimen identification number; B - beam test; first digit - beam length in meters; last digit - designates beam type, refer to Table 5.4

b = Outside dimension of a rectangular HSS; width of an unstiffened compression element; constant defining the shape of the shear transfer function

b_{eff} = Effective width of a compression element

b_f = Outside dimension of the tube parallel with the axis of bending

C = Coefficient used to describe a load-deformation curve

C_c = Slenderness ratio corresponding to an Euler stress $F_y/2.0$

C_e = Euler buckling strength of the steel column

C_{ec} = Euler buckling strength of a composite column

C_f = Compressive force in a member under axial load

C_r = Compressive resistance of a member

C_r' = Compressive resistance of the concrete member

C_{rc} = Compressive resistance of the composite member

C_{ro} = Squash load for a composite column

C605 = Column specimen identification number; C - column test; 60 - slenderness ratio; last digit - odd or even number indicates whether the column was loaded concentrically or eccentrically, respectively; last digit also designates column type, steel (1,2), composite strain compatible (3,4), composite non-strain compatible (5,6)

D = Diameter of a circular HSS; Coefficient used to describe a load-deformation curve

dx = Element length along the length of the column

E = Elastic modulus of steel; Coefficient used to describe a load-deformation curve

E_c = Elastic modulus of concrete

E_{ce} = Effective elastic modulus of concrete

E_{coupon} = Elastic modulus of a steel tension coupon

E_m = Modified modulus of elasticity for a composite column

E_s = Elastic modulus of steel

E_{stub} = Elastic modulus of a steel stub column

E_T = Tangent modulus

e = Eccentricity of the applied load

e_o = Initial out-of-straightness at midheight

F = Coefficient used to describe a load-deformation curve

F_{my} = Modified value of yield stress for a composite section

F_u = Ultimate tensile strength of the steel section

F_y = Yield stress of the steel section

f_c = Compressive strength of concrete expressed as a function of strain

f'_c = Uniaxial compressive strength of concrete

f_{cu} = Compressive strength of concrete

f_r = Modulus of rupture of concrete

f_{sy} = Yield strength of the steel section

G = Coefficient used to describe a load-deformation curve

h = Inside dimension of the tube perpendicular to the axis of bending

h/L = Non-dimensional column height

I = Moment of inertia of the steel section

I_c = Moment of inertia of the concrete section

I_s = Moment of inertia of the steel section

K = Effective length factor

Kl = Effective length

K_1 = Non-dimensional coefficient which describes the shape of column curve 'a' as a function of column slenderness

K_2 = Non-dimensional coefficient which defines the maximum axial load corresponding to an applied moment equal to the plastic moment capacity of the section as a function of column slenderness

$K_{2(l=0)}$ = Non-dimensional coefficient which defines the upper bound for K_2 as a function of the concrete contribution parameter

L = Length

LVDT = Linear variable differential transformer

l = Length

l_k = Effective column length

M_f = End moment of the beam column

M_r = Moment resistance of steel section

M_{rc} = Moment resistance of the composite section

M_u = Ultimate moment resistance of the composite section

M_{ult} = Ultimate moment capacity of a beam

N = Compressive force in the member

N_{cr} = Euler critical load of a composite member

N_u = Squash load for the composite section

N_{us} = Squash load for the steel section

n = Sample or population size; modular ratio,

P = Applied load

P_{csc} = Composite stub column load carrying capacity expressed as a function of strain

P_{cx} = Load carried by the concrete as a function of length along the column from the lower end

P_s = Squash load for the composite section

P_{stub} = Steel stub column load carrying capacity expressed as a function of strain

P_{sx} = Load carried by the steel as a function of length along the column from the lower end

P_{ult} = Ultimate load carrying capacity of a column

p = $0.48 \times 0.83 \times f_{cu}/f_{sy}$

R = Ratio of the ultimate load carrying capacity of non-strain compatible to strain compatible beam columns

r = Radius of gyration of the steel section; correlation coefficient

r_c = Radius of gyration of the concrete section

r_m = Modified radius of gyration for a composite section

r^2 = Coefficient of determination

S = Elastic section modulus of a steel section; short term load of the column

S_m = Modified section modulus for a composite section

s = Standard deviation

T = Long term load of the column

t = wall thickness

V = Coefficient of variation

v_x = Shear load transferred per mm at a distance x along the length of the column from the lower end

w_x = Relative Displacement between the two materials at a distance x along the length of the column from the lower end

$\bar{x}$ = Mean value

Z = Plastic section modulus of a steel section

β = The ratio of the smaller to the larger end moments

δ = Deflection of the column at midheight

ϵ = Strain

ϵ_{cx} = Longitudinal strain in the concrete due to a load, P_{cx}

ϵ_o = Strain at the maximum compressive strength, f'_c

ϵ_s = Longitudinal strain in the steel section due to the applied load

ϵ_{sx} = Longitudinal strain in the steel due to a load, P_{sx}

ϵ_u = Strain at the ultimate tensile strength of a steel section

ϵ_y = Yield strain

ζ = Ratio of the compressive resistance of steel to concrete

η = Coefficient reflecting the effects of long term loading

$\bar{\eta}$ = Coefficient relating material and geometric properties of the composite section

θ = End rotation of a pinned-ended column

λ = Non-dimensional slenderness ratio for a steel column

$\bar{\lambda}$ = Equivalent slenderness ratio for a composite column

λ_c = Non-dimensional slenderness ratio for a concrete column

λ_{comp} = Non-dimensional slenderness ratio for a composite column

ν = Poisson's ratio

π = 3.1416

ρ = Reinforcement ratio

σ = Stress; standard deviation

σ_{lr} = Longitudinal residual stress

σ_{p} = Stress at a proportional limit

σ_{stub} = Average stress on a steel stub column as a function of strain

σ_{sy} = Static yield stress

$\sigma_{sy_{coupon}}$ = Static yield stress for a tension coupon

$\sigma_{sy_{stub}}$ = Static yield stress for a steel stub column

σ_{ttr} = Through the thickness longitudinal residual stress

τ = Coefficient reflecting a decrease in strength in the steel section due to the development of a biaxial state of stress in the steel section

τ' = Coefficient reflecting an increase in strength in the concrete section due to the development of a triaxial state of stress in the concrete

ω = Coefficient used to determine equivalent uniform bending effect in beam-columns

1. INTRODUCTION

1.1 General

In all the tests conducted to establish the ultimate load carrying capacity and behaviour of concrete filled HSS beam columns in the last thirty years, as reported in the literature survey, the load was applied to the column in such a manner that both the steel and concrete were loaded simultaneously, thus ensuring strain compatibility at the ends of the column. Current codes or standards also ensure that this is the case by stipulating that some type of shear transfer mechanism be implemented such that both materials are loaded proportionately at the point where the load is introduced into the column by using, for example, a cover plate on the HSS section.

In multi-storey construction where the column lifts may be two or three storeys high, the most desirable approach from both an economical viewpoint and for ease of construction, would be to transfer loads from the beams of intermediate storey levels through connections into the steel shell without attempting to introduce the load directly into the concrete.

Generally the failure of columns or beam columns loaded in single curvature occurs at a critical section which is located about midheight where curvature is a maximum. It is conceivable that the concrete and steel may act compositely at that location even though strain compatibility is not ensured at the ends of the column. If this occurred the ultimate load and behaviour would be similar to that of the strain compatible case. In this circumstance, taking special measures to ensure strain compatibility would be uneconomic. The purpose of this thesis is to examine this premise in detail.

1.2 Objectives

The objectives of this experimental and analytical study are:

1. To determine the change in behaviour and ultimate load capacity of concrete filled HSS beam columns when strain compatibility is not ensured at the end of the beam column where the load is introduced.
2. To identify and give a physical interpretation of the various load transfer mechanisms between the steel shell and the concrete core for the non-strain compatible beam column series.
3. To compare the ultimate load values, as determined by current or proposed design methods, with the respective values obtained from the beam column tests.
4. To make recommendations for the design of non-strain compatible composite beam columns which reflect the change in behaviour and ultimate load capacity of this member type compared to strain compatible beam columns.
5. To outline areas of future work.

1.3 Scope

Bare steel and concrete filled strain compatible and non-strain compatible rectangular HSS beam columns were constructed and tested under laboratory conditions. These members were constructed from a cold formed steel HSS 152.4 x 152.4 x 4.78, and concrete purchased from a local batch plant. Columns with slenderness ratios which reflected short, intermediate and long column behaviour were tested as pinned ended members under concentric loads and constant eccentric loads of 65 mm. Flexural specimens were tested as simply supported beams with a two point load system with equal shear spans, producing a constant moment region. All loads were short term. Analyses of load transfer mechanism type and characteristics, and comparisons of ultimate loads with various codes and standards were made with the data acquired from these tests.

1.4 Outline

A review of existing literature on concrete filled HSS beam columns is presented chronologically in Chapter 2 under the following subheadings:

1. Experimentally based research
2. Analytical methods and parameter studies
3. Development of design recommendations

The objectives of the experimental program and the method by which they were achieved are outlined in Chapter 3. The purpose, number and type of tests, the instrumentation and experimental method are all described in detail.

Material properties and load deformation behaviour of the steel and concrete and the stub columns are defined in Chapter 4.

The test results presented in Chapter 5 include:

1. End fixture behaviour
2. Summary of the out-of-straightness measurements for the columns
3. General load deflection behaviour and failure modes for both the column and flexural tests
4. Steel and concrete strain distributions
5. Slip distributions

A detailed analysis of the load sharing characteristics of the steel section and the concrete core for non-strain compatible beam columns is presented in Chapter 6. Physical interpretations and limitations are presented for each load transfer mechanism. A mathematical model for the micro-interlocking mechanism is presented and compared to the appropriate test data.

In Chapter 7 a comparison is made of the ultimate loads obtained from tests of the bare steel beam columns and the concrete filled strain compatible HSS beam columns and the values predicted for the corresponding columns by various codes or standards. The change in behaviour and ultimate load carrying capacity for beam columns from the strain compatible test series to the non-strain compatible test series is discussed.

A summary, conclusions and recommendations are presented in Chapter 8.

2. LITERATURE REVIEW

2.1 General

This literature review delineates the development of the understanding of the behaviour of concrete filled HSS beam columns from the first significant work, an experimental study by Klöppel and Goder (1957), to the most recent work in standard development and design recommendations by Redwood (1983).

During this time span, a great number of tests have been conducted on concrete filled HSS beam columns, the majority on pinned-ended concentrically loaded columns with circular sections. In all cases the columns were loaded such that the load was applied to both the concrete and the steel ensuring strain compatibility at the ends of the columns. Experimentally based research is presented chronologically in Section 2.2 and is subdivided into three categories; behaviour of beam columns, the study of physical phenomenon associated with the behaviour of these members and the study of load transfer mechanisms.

In Section 2.3 analytical methods and parametric studies conducted to supplement the test data for beam columns subject to uniaxial and biaxial bending are reviewed. Discussion in Section 2.4 centres around those papers which review and consolidate all research done previously to derive a set of design recommendations. Salient points are summarized in Section 2.5.

2.2 Experimentally Based Research

Over the past thirty years a large number of experiments have been conducted to gain an understanding into the behaviour of concrete filled HSS members. These investigations can be categorized into three major areas of study.

1. Behaviour of beam columns.
2. Augmented strength due to triaxial effects.
3. Load transfer mechanisms.

2.2.1 Behaviour of Beam Columns

The largest area of study to date has been the behaviour of axially loaded columns and beam columns. This work has been summarized and presented chronologically in Tables 2.1, 2.2, 2.3 and 2.4 for axially and eccentrically loaded circular and rectangular section columns, respectively. The number of columns tested as a function of slenderness ratio based on the steel section alone, the ranges of size, ultimate load and eccentricity, and a summary of that work is given in the appropriate table.

Further examination of this work reveals that the various experiments had a common purpose, and were similar in instrumentation, end connections and method of load application. Since the objective of each experimental program was to observe the gross behaviour of beam columns, only a limited amount of data was sought and reported. In most cases this data included material and geometric properties (assumed or measured), load-midheight deflection, load-midheight strains (both longitudinal and transverse), ultimate load and failure mode. With the exception of the eight columns tested by Bertero et. al. (1970) and the stub column tests, all columns were tested as pinned-ended columns. The most significant feature of these tests was the type of end load condition imposed. The load was applied to both steel and concrete ensuring strain compatibility at both ends of the column; the only exception here being four stub columns tested by Gardner and Jacobson (1967) as part of a small series of tests investigating the effects of end loading conditions.

For the most part, the ultimate load for axially loaded columns was compared to the buckling load as determined by a tangent modulus approach. For eccentrically loaded columns the experimental load was compared to either a numerical solution based on determining the deflected shape, or to a tangent modulus solution, coupled with an interaction equation and an assumed ultimate moment capacity of the composite section. Furlong (1967) also compared his results to a reinforced concrete column by treating the concrete filled tube as an ordinary reinforced concrete section and determining the ultimate load by the ACI Code method (ACI, 1963).

Eight basic conclusions drawn from these works on the behaviour of concrete filled HSS beam columns are:

1. For axially loaded columns, the theoretical buckling

load determined by a tangent modulus approach predicts the experimental load closely.

2. The squash load of the composite section is adequately estimated as the sum of the squash load for the steel plus that of the concrete.
3. The strength of circular section stub columns is increased due to the development of a triaxial state of stress in the concrete core. This phenomenon is not experienced in rectangular columns and for circular columns it diminishes as the eccentricity of the applied load increases.
4. Concrete restrains the tube wall from local buckling.
5. Mechanical prestressing of the concrete core improves the mechanical behaviour of the composite column and appreciably increases the ultimate load carrying capacity.
6. The behaviour and load carrying capacity of a pinned-ended beam column can be accurately predicted using an iterative inelastic stability analysis based on load-moment-curvature relationships as derived from accurate stress-strain relationships for the materials and assuming perfect bond between the steel and concrete.
7. Estimates of the ultimate moment capacity for the composite section based on the plastic moment capacity of the steel section alone are usually low.
8. Prediction of the ultimate load of columns subject to

uniaxial bending by an interaction curve with an elliptical shape provides a reasonable lower bound solution. A straight line interaction curve, without an amplification factor, does not provide an accurate prediction of ultimate load.

It should be noted that the great majority of the columns tested have been circular in cross section and/or axially loaded. Relatively few tests have been conducted on columns or beam columns with Kl/r>90 and no tests have been done to establish the ultimate moment resistance of these composite sections.

2.2.2 Triaxial Effects

Experimental studies of physical phenomena associated with the behaviour of these members have been limited to examining the increased strength for concrete filled HSS columns due to the development of a triaxial state of stress in the concrete core.

Although an increase in the strength of composite columns due to triaxial effects was first recognized by Gardner and Jacobson (1967), the first major study of the phenomenon was done by Sen (1969) on circular hollow section columns. This information was confirmed by an extensive experimental study by Tomii, et al. (1977) on concrete filled steel tubular stub columns under concentric load. About 270 stub column tests were conducted on circular, octagonal and square sections. Tomii, et al. (1977) have shown that there is no increase in strength due to triaxial effects for square hollow section stub columns.

2.2.3 Load Transfer Mechanisms

The study of load transfer mechanisms has not been fully explored. Three different groups of researchers have investigated various facets of the method in which load is transferred from a beam through a connection, and into the steel shell and concrete core.

As part of a series of tests Gardner and Jacobson (1967) tested nine stub columns to investigate the effects of varied end loading conditions. These included columns filled with concrete and columns filled with coarse aggregate. Columns in which both the steel and the concrete were loaded, and other columns in which only the concrete core or a compacted aggregate core was loaded, failed at approximately the same load and had a pronounced barrel shape. The composite stub column in which only the steel was loaded had little gain in strength over a corresponding empty tube and the ultimate load was approximately 40 percent of that of the other columns. Both the empty tube and the composite tube in which only the steel was loaded failed by local buckling.

Only one paper has been presented on beam column assemblage and connection behaviour. Ansourian (1976) investigated the behaviour of various continuous frame connections between I-beams of normal and wide flange section and concrete filled rectangular HSS columns, as well as the behaviour of the beam columns subject to a range of constant axial load and increasing moment produced by a beam framing into the column about one axis. From the nine assemblages tested it was concluded that the concrete worked in conjunction with the steel tube to resist the axial load, bending moment, shear force and local action at the connection, enhancing their overall behaviour even though no attempt was made to load the concrete directly.

Virdi and Dowling (1980) conducted a series of pushout tests on concrete filled circular seamless mild steel tubes to examine the method of load transfer along the interface between the concrete core and the steel tube. It should be noted that in such a test, the effects of Poisson's Ratio will cause the concrete core to expand against the steel tube at the loaded end. Virdi and Dowling (1980) defined the ultimate bond strength on the basis of a critical bond strain which is related to the ultimate crushing strain of concrete. From this series of tests, the following conclusions were reported:

1. The bond strength is not affected by factors such as contact length, tube size to thickness ratio and concrete strength.
2. Surface roughness causes a micro-interlocking between the materials and is reflected as the initially stiff region of the load deformation curve, where the deformation is the relative movement of the concrete

core with respect to the steel shell.

3. Macro-interlocking of the concrete with the undulating surface of the steel contributes to the frictional resistance and is related to the flat part of the load deflection curve.
4. Bond is broken when the concrete interface attains a local strain greater than that associated with the compressive crushing of the concrete, a value of 0.0035.
5. A characteristic ultimate bond strength is approximately 1 MPa.

Aside from series of tests conducted by Ansourian (1976) no attempt has been made to determine the method and rate of load transfer for typical beam to column connections.

2.3 Analytical Methods and Parametric Studies

It is evident from the information given in Tables 2.1 to 2.4 that an insufficient number of tests have been conducted to describe adequately the behaviour and ultimate load carrying capacity for all possible types of concrete filled HSS beam columns subjected to uniaxial and biaxial bending. It is necessary then, to supplement that information through parametric studies via calibrated analytical methods. In all cases, the behaviour and load carrying capacity of the beam column, has been predicted by an iterative inelastic stability analysis based on numerical integration of load-moment-curvature relationships derived from assumed or known stress-strain relationships of the materials and on the assumption of full composite action. These studies have led to the development of semi-empirical design recommendations.

An analytical method based on inelastic column theory was developed by Basu (1967) for eccentrically loaded rectangular composite section columns subjected to uniaxial bending. Using assumed stress-strain relationships, excluding the effects of residual stresses in the steel section, incorporating initial out-of-straightness and assuming that the deflected shape was part of a cosine curve, Basu found good agreement between the failure loads predicted by this method and forty corresponding test values. Comparisons were also made with exact solutions for the two limiting sections, steel I-sections and unreinforced rectangular concrete sections. The error in either case was small. Good agreement was also found by Neogi, Sen and Chapman (1969) when they compared all known test results to a similar numerical analysis for circular section columns.

Further development of this method by Basu and Hill (1968) led to a more "exact" solution in which the failure load for columns subjected to equal and unequal end eccentricities could be determined and was based on a derived deflected shape rather than an assumed profile. The accuracy of this solution was established by comparison with "exact" solutions for steel I-sections with end eccentricity ratios of 1 and 0 presented by Galambos and Ketter (1957).

The effects of initial out-of-straightness and applicability of a straight-line interaction equation for uniaxial bending were examined.

Subsequently Basu and Sommerville (1969) used this modified method to develop semi-empirical design recommendations. A large number of parameters and their effect on the load carrying capacity of columns subject to uniaxial bending were investigated.

Virdi and Dowling (1973) developed an analytical method for computing the failure load for biaxially loaded, pinned-ended columns in symmetrical single curvature bending, by determining the load-deflection response of such columns from biaxial moment-thrust-curvature relationships and selecting the failure load as the peak of that curve. The solution, although applicable to concrete filled HSS columns, has only been tested against concrete encased H-section columns. The agreement between test and predicted values was found to be satisfactory. The effects of residual stress and initial out-of-straightness were examined. Bresler's empirical formula was shown to be conservative in obtaining biaxial failure loads from uniaxial loads. Bridge (1976) compared the behaviour and the ultimate load carrying capacity of eight tests on concrete filled rectangular HSS columns with a similar analysis and found good agreement.

A general method for the calculation of the ultimate load of biaxially restrained columns has been developed by Virdi and Dowling (1976). The solution is based on the

Newton-Raphson iterative procedure for solving a system of non-linear equations. Comparisons of calculated ultimate loads were made with corresponding experimentally obtained values from tests on concrete encased H-section columns and the correlation was found to be good.

2.4 Development of Design Recommendations

The development of design recommendations generally involves a process by which all previous experimental and analytical work on a particular structural element is synthesized into a simple, logical sequence of concepts and/or equations which reflect the behaviour of these elements. The design recommendations are then calibrated against known test results as a measure of their applicability, reliability and accuracy. Fourteen papers or reports related to the development of design recommendations for concrete filled HSS beam columns are listed chronologically in Table 2.5.

From these, four sets of design recommendations have evolved and are currently used or under consideration for use in various codes or standards. They are as follows:

1. CAN3-S16.1-M84, Redwood (1983)
2. CAN3-S16.1-M84, Redwood (1983) (Alternate Proposal, not adopted)
3. Structural Stability Research Council (SSRC) - Task Group 20 (1979)
4. European Convention for Constructional Steelwork (ECCS),

Recommendations on Composite Structures, Technical General Secretariat of the ECCS (1981)

For each of these, the pertinent sections relating to concrete filled rectangular HSS beam columns are presented in detail in Chapter 7. In all cases provisions were made for strength and stability calculations, as well as application and fabrication requirements. It is important to note that as a direct result of the loading conditions imposed on all beam columns tested, provisions exist in each Standard or Code which require that the load be applied appropriately to both steel and concrete at the point in which it is introduced into that member.

2.5 Summary

In total, 526 tests have been conducted on concrete filled HSS beam columns, 309 tests on stub columns of various sections, 207 and 43 tests of circular and rectangular concrete filled HSS columns, respectively. In the majority of cases, the beam columns were tested as pinned ended members with the load being applied to the specimen such that both the steel and concrete were loaded, ensuring strain compatibility at the ends. The phenomenon of augmented strength due to the development of triaxial stresses in the concrete core has been adequately examined by Sen (1969) and Tomii, et al. (1977). A limited number of tests have been conducted by Ansourian (1976) on beam column assemblage and connection behaviour, and by Virdi and

Dowling (1980) on the bond strength between the two materials for this type of section. No tests have been done to establish the ultimate moment capacity of these sections.

The consensus amongst researchers is that the tangent modulus approach closely predicts the buckling load for axially loaded columns. The behaviour and load carrying capacity for columns subject to uniaxial and biaxial loads has been successfully predicted by Basu (1967), Basu and Hill (1968), Virdi and Dowling (1973, 1976), and Bridge (1967), using an iterative inelastic stability analysis based on load-moment-curvature relationships, stress-strain characteristics of both materials, and the assumption of full composite action.

Thirty years of experimental and analytical work on concrete filled HSS beam columns has been synthesized into three unique sets of design recommendations, one for Canada (CSA CAN3-S16.1-M84), one for the United States of America (AISC, LFRD) and one for Europe (ECCS Recommendations on Composite Structures).

Table 2.1 Summary of Tests on Axially Loaded Concrete Filled Circular HSS Columns[1]

NO. OF TESTS				SIZE RANGE D, mm	ULTIMATE LOAD RANGE, kN	SUMMARY
STUB[3] COLUMNS	PINNED-ENDED COLUMNS[2] Kl/r <30	30-90	>90			
KLÖPPEL AND GODER, DER STAHLBAU, 1957						
-	31	30	-	95 - 216	403 - 2746	Development of a rational formula to predict the load carrying capacity of a composite column as a function of an equivalent slenderness ratio and a ratio of steel to concrete area.
SALINI AND SIMS, ACI JOURNAL, 1964						
-	-	7	10	25.4 - 76.2	14.4 - 320	Theoretical buckling loads as calculated by a tangent modulus formulation correspond to the observed buckling load.
GARDNER AND JACOBSON, ACI JOURNAL, 1967						
20	5	5	-	76.4 - 152.4	245 - 1201	Theoretical buckling loads determined by a tangent modulus approach. The strength of concrete for circular stub columns is increased due to the development of triaxial stresses.

Table 2.1 con't

NO. OF TESTS				SIZE RANGE D, mm	ULTIMATE LOAD RANGE, kN	SUMMARY
STUB^1 COLUMNS	PINNED-ENDED COLUMNS^2 Kl/r					
	<30	30-90	>90			
GARDNER AND JACOBSON, ACI JOURNAL, 1967 (con't)						
						Local buckling of the tube is restrained. Various end loading conditions were tested on eight composite stub columns.
FURLONG, ASCE JOURNAL, 1967						
-	8	-	-	114.3 - 152.4	623 - 756	The capacity of axially loaded short segments were adequately estimated as the squash load of the steel plus that of the concrete. Calculations of strength and external measurements of strain suggested that the steel and concrete sustain load somewhat independently of one another. Concrete restrains local buckling of the steel wall.

Table 2.1 con't

NO. OF TESTS				SIZE RANGE D, mm	ULTIMATE LOAD RANGE, kN	SUMMARY
STUB[3] COLUMNS	PINNED-ENDED COLUMNS[2] Kl/r					
	<30	30-90	>90			
GARDNER, ACI JOURNAL, 1968						
11	-	8	-	168.8	357 - 1984	Concrete filled spiral welded steel tubes were tested to compare their behaviour with corresponding concrete filled seamless steel tubes. Ultimate loads were compared with conventional design methods.
KNOWLES AND PARK, ASCE JOURNAL, 1968						
1	5	6	-	82.6 - 88.9	225 - 992	Buckling loads for long columns can be accurately predicted by summing the tangent modulus loads for the steel tube and the concrete core acting as independent columns. Due to the development of a triaxial stress state in the concrete, short circular section columns show an increase in load carrying capacity.

Table 2.1 con't

NO. OF TESTS				SIZE RANGE D, mm	ULTIMATE LOAD RANGE, kN	SUMMARY
STUB[3] COLUMNS	PINNED-ENDED COLUMNS[2] Kl/r <30	30-90	>90			
GUIAUX AND JANSS, CRIF PUBLICATION, 1969						
-	14	13	3	95 - 356	154.9 - 8385	The maximum strength of the composite section was determined assuming compatibility of longitudinal strains in the two materials.
BERTERO AND MOUSTAFA[3], ASCE JOURNAL, 1970						
-	8	-	-	101.6	1290 - 2260	A study of improving the mechanical behaviour of composite columns under load by prestressing the concrete core with expansive concrete and/or additional mechanical prestressing.

NOTES: 1. For all columns with the exception of four columns tested by Gardner and Jacobson (1967), the loads were applied to both the steel and concrete such that strain compatibility was ensured at both ends of the column.
2. Slenderness ratio is based on the steel section alone.
3. All stub columns and the columns tested by Bertero et al. (1970) were tested between flat plates.

Table 2.2 Summary of Tests on Axially Loaded Concrete Filled Rectangular HSS Columns

NO. OF TESTS				SIZE RANGE D, mm	ULTIMATE LOAD RANGE, kN	SUMMARY
STUB[3] COLUMNS	PINNED-ENDED COLUMNS[2] Kl/r					
	<30	30-90	>90			
				FURLONG, ASCE JOURNAL, 1967		
-	5	-	-	101.6 - 127	448 - 1601	Same comments as Furlong (1967), Table 2.1.
				KNOWLES AND PARK, ASCE JOURNAL, 1969		
1	2	3	-	76.2 -	356 - 539	Same comments as Knowles and Park (1969), Table 2.1. The phenomenon of increase load carrying capacity due to the development of a triaxial stress state in the concrete does not occur for rectangular section columns.
				GUIAUX AND JANSS, CRIF PUBLICATION, 1970		
-	4	-	-	329 - 333	7992 - 8140	Same comments as Guiaux and Janss (1970), Table 2.1.

NOTES:
1. For all columns tested, the loads were applied to both the steel and concrete such that strain compatibility was ensured at both ends of the column.
2. Slenderness ratio is based on the steel section.
3. Stub columns were tested between flat plates.

Table 2.3 Summary of Tests on Eccentrically Loaded Concrete Filled Circular HSS Columns

NO. OF TESTS PINNED-ENDED COLUMNS[a] Kl/r			SIZE RANGE D, mm	e/D RANGE	ULTIMATE LOAD RANGE, kN	SUMMARY
<30	30-90	>90				
						KATO AND KANATANI, TOKYO UNIVERSITY LAB REPORT, 1966
3	5	-	318	0.220 - 0.628	1069 - 2785	Test results reported by Neogi, Sen and Chapman (1969).
						FURLONG[a], ASCE JOURNAL, 1967
22	-	-	114.3 152.4	0.115 - 2.65	43.6 - 56.8	Columns were loaded to failure with the application of a constant concentric axial force and increasing end moments (single curvature, uniaxial bending). Estimates of pure bending strength based on the plastic moment capacity of the steel alone were usually low. Uniaxial bending interaction equation in the form of an ellipse was conservative for most data and formed a reasonable lower bound solution. Accurate estimates of beam-column strength were made by treating the concrete filled tubes as ordinary reinforced concrete sections.

Table 2.3 con't

NO. OF TESTS PINNED-ENDED COLUMNS[3] Kl/r			SIZE RANGE D, mm	e/D RANGE	ULTIMATE LOAD RANGE, kN	SUMMARY
<30	30-90	>90				
NEOGI, SEN AND CHAPMAN, THE STRUCTURAL ENGINEER, 1969						
-	18	-	127 - 169.4	0.050 - 0.283	153.5 - 467	Non-linear behaviour of pin-ended concrete filled tubular steel columns loaded either eccentrically or concentrically about one axis were studied numerically by determining the exact deflected shape. Increase strength due to the development of a triaxial stress state of stress in the concrete core diminishes as the eccentricity of the applied load increases. Increased moment capcity as calculated at mid-height of the columns tested was probably due to triaxial augmentation of the concrete strength.

Table 2.3 con't

NO. OF TESTS			SIZE RANGE D, mm	e/D RANGE	ULTIMATE LOAD RANGE, kN	SUMMARY
PINNED-ENDED COLUMNS[a] Kl/r						
<30	30-90	>90				
KNOWLES AND PARK, ASCE JOURNAL, 1969						
4	2	-	826 - 88.9	0.217 - 0.371	400 - 919	Ultimate moment capacity of the section is based on the plastic moment capacity of the steel section alone. Straightline interaction formula (without amplification factor) does not accurately predict the ultimate load and moment of acomposite column given the ultimate compressive resistance as determined from the tangent modulus approach and the moment resistance of the composite section as the elastic moment capacity of the steel section alone.

Table 2.3 con't

NOTES:
1. For all columns tested the loads were applied to both the steel and concrete such that the strain compatibility was ensured at both ends of the column.
2. Slenderness ratio is based on the steel section alone.
3. The eccentricity for the e/D ratios for Furlong 1967 were calculated as the ultimate moment divided by the ultimate load.

Table 2.4 Summary of Tests on Eccentrically Loaded Concrete Filled Rectangular HSS Columns

NO. OF TESTS PINNED-ENDED COLUMNS[2] Kl/r <30	30-90	>90	SIZE RANGE b, mm	e/b RANGE	ULTIMATE LOAD RANGE, kN	SUMMARY
			FURLONG[3], ASCE JOURNAL, 1967			
17	-	-	101.6	0.132 - 0.000	0 - 1112	Same comments as Furlong (1967), Table 2.3.
			KNOWLES AND PARK, ASCE JOURNAL, 1969			
2	2	-	76.2	0.1617- 0.485	156 - 346	Same comments as Knowles and Park (1969), Table 2.3.
			BRIDGE, CIVIL ENGINEERING TRANSACTIONS, 1976			
3	5[4]	-	150- 200	0.190 - 0.427	513 - 2869	Eight test were performed on concrete filled HSS to examine the effect of the eccentricity of loading, slenderness and inclination of loading axis (uniaxial and biaxial bending). Concrete stabilizes the walls of tube, preventing local buckling.

Table 2.4 con't

NO. OF TESTS PINNED-ENDED COLUMNS[2] Kl/r <30	 30-90	 >90	SIZE RANGE b, mm	e/b RANGE	ULTIMATE LOAD RANGE, kN	SUMMARY
BRIDGE, CIVIL ENGINEERING TRANSACTIONS, 1976 con't						
						The behaviour and load carrying of a pin-ended member can be accurately predicted using an iterative inelastic stability analysis based on load-moment curvature relationships derived from accurate stress-strain relationships for the materials assuming perfect bond between the steel and concrete.

NOTES:
1. For all columns tested, the loads were applied to both the steel and concrete such that the strain compatibility was ensured at the both ends of the column.
2. Slenderness ratio is based on the steel section alone.
3. The eccentricity and e/b ratios for Furlong were calculated as the ultimate moment divided by the ultimate load.
4. One column was loaded axially to provide a control specimen.

Table 2.5 List of Papers on the Development of Design Recommendations

DATE	AUTHOR	PUBLICATION	TITLE
1968	Furlong	ASCE Journal	Design of Steel-Encased Concrete Beam Columns
1969	Basu and Sommerville	ICE Proceedings	Derivation of Formulae for the Design of Rectangular Composite Columns
1970	Knowles and Park	ASCE Journal	Axial Load Design for Concrete Filled Steel Tubes
1976	Virdi and Dowling	IABSE Memoires	A Unified Design Method for Composite Columns
1976	Furlong	AISC Engineering Journal	AISC Column Design Makes Sense for Composite Columns, Too
1976	Dowling, Janss and Virdi	Introductory Second International Colloquim on Stability, ECCS	The Design of Composite Steel-Concrete Columns
1977	Wakabayashi	Proceedings International Colloquim on Stability of Structures Under Static and Dynamic Loads	A New Design Method of Long Composite Beam-Columns
1977	Roik, Bode and Bergman	Preliminary Report Second Colloquim on Stability of Structures	Composite Column Design
1979	SSRC Task Group 20	AISC Engineering Journal	A Specification for the Design of Steel-Concrete Composite Columns

Table 2.5 con't

DATE	AUTHOR	PUBLICATION	TITLE
1981	Bode and Bergman	Merkblatt 167	Concrete Filled Structural Hollow Sections
1981	Redwood	S16 Task Group on Composite Construction Report	The Treatment of Composite Columns in S16.1
1982	Redwood	S16 Task Group on Composite Construction Report	CSA S16 Subcommittee on Composite Construction Report to S16 Committee
1983	Redwood	S16 Task Group on Composite Construction Report	Design of Concrete Filled HSS
1983	Burdijanto	Project Report 483.6 McGill University	Design Methods for Composite Columns

3. EXPERIMENTAL PROGRAM

3.1 General

The experimental program was designed to examine:

1. The change in behaviour and ultimate load carrying capacity of concrete filled HSS beam columns when strain compatibility is not ensured at the point on the beam column where the load is introduced.
2. The method and rate of load transfer between the steel shell and the concrete core for non-strain compatible cases.

Nineteen pinned-ended columns with slenderness ratios of 20, 60, and 118, based on the radius of gyration of the steel alone, were tested to establish the ultimate load capacity, the load-deflection behaviour, and the load sharing characteristics of the steel and concrete along the length of the column. Bare steel tubes and concrete filled tubes with and without strain compatibility at the upper end were loaded concentrically and at an eccentricity of 65 mm (0.43b). In addition, six simply supported beams with a two point load system with equal shear spans producing a constant moment region, were tested to establish the general behaviour and ultimate moment capacity of empty HSS members and concrete filled members with and without strain compatibility.

Ancillary tests included four stub column tests, two on bare steel tubes and two on concrete filled strain compatible tubes, residual stress measurements, tension coupons and concrete cylinder tests.

3.2 Selection of Test Section

A geometric programming technique was used to determine the optimum test section size from the following objective and constraint functions.

1. Objective - Class 2 behaviour

$$\frac{b_{eff}}{t} \leqslant \frac{525}{\sqrt{F_y}} \tag{3.1}$$

where, $b_{eff} = b - 4t$

2. Objective - long column or Euler column behaviour

$$90 \leqslant \frac{Kl}{r} \leqslant 120 \tag{3.2}$$

3. Constraint - maximum test specimen height in which the MTS testing machine can accommodate

$$L \leqslant 7400 \text{ mm} \tag{3.3}$$

4. Constraint - squash load of the composite section must be less than the working load capacity of the knife edge assemblages

$$A_sF_y + A_cf'_c \leqslant 2000 \text{ kN} \tag{3.4}$$

5. Constraint - the inner dimension of the HSS member must be large enough so that the concrete for a long specimen can be placed. This led to:

$$b - 2t \geqslant 100 \text{ mm} \tag{3.5}$$

Based on size as determined by this technique, the steel section was selected as a grade 350W 152.4 x 152.4 x 4.78 HSS and the concrete specified as a type 10 with a 28 day strength of 30 MPa, a maximum aggregate size of 12 mm and a slump of 100 mm.

3.3 Column Tests

3.3.1 General

Three types of rectangular HSS beam columns with slenderness ratios of 20, 60 and 118 as determined from the steel section alone, and which reflect short, intermediate and long column behaviour respectively, were tested under a concentric load and a constant eccentric load of 65 mm.

The bare steel column test series was used as a control series and as a means of calibrating end fixture performance and steel load prediction models as discussed in Section 5.1 and 6.3.1 respectively.

The strain compatible and non-strain compatible test series were conducted to get a direct comparison of load-deflection behaviour, ultimate load capacity and failure modes for corresponding columns when strain compatibility at the point on the column where the load is introduced was not ensured. The upper end connections used to achieve strain compatibility and non-strain compatibility are shown in Figure 3.1. The test set up and knife edge assemblies are shown in Figure 3.2 and 3.3. The connection plates shown in Figure 3.1 were intended to represent the beam to column connection through which the loads are transferred. For both types the load was applied to the column through a knife edge plate which bore against the load bearing surface as shown in Figure 3.1. Grout was used in the strain compatible case to ensure that the knife edge plate made constant contact with and loaded both materials simultaneously. In the non-strain compatible specimens the connection plates extended 6.4 mm above the end of the tube so that the loads would be applied only to these plates, simulating the case where no attempt is made to load the concrete core.

The column specimen identification numbers refer to the slenderness ratio, loading and type of column. Odd and even numbered specimens were tested concentrically and eccentrically, respectively. The last digit of the specimen identification number designates the type of column, steel (1,2), composite strain compatible (3,4), and composite non-strain compatible (5,6). Specimen C205 is a concentrically loaded non-strain compatible composite column with a slenderness ratio of 20.

3.3.2 Preparation of Test Specimens

Special attention was given at this stage of the experimental program in the preparation of the column ends of all specimens. To ensure proper loading of the column ends and to reduce alignment difficulties of the columns at set-up, the end surfaces of the column were milled at right angles to the length of the column, before and after the base plate and connection plates were welded to the tube. These milled surfaces bore against the associated milled surfaces of the knife edge plates providing uniform bearing and transfer of load.

Concrete strains and slip between the concrete core and the steel shell were measured at six sections along the length of the member, using a removeable mechanical extensometer (Demec gauge). The gauge points were mounted on both ends of 6 mm diameter steel rods 150 - 175 mm long, which were embedded in the concrete core and passed directly through 12 mm diameter holes made on opposite sides of the steel section. At each of the six sections, four gauge points were located such that the Demec gauge readings from two pairs of points would give an adequate description of the strain distribution in the concrete core about the axis of bending, and that the holes made in the steel shell to accommodate the steel rod would mean the removal of a minimum amount of stressed material. During construction rubber hose inserts were used to:

1. Center and secure the steel rods in the respective holes

2. Prevent concrete from plugging the space between the rods and the steel shell, allowing for unrestricted movement of the rod when slip occurred.

One batch of ready mix concrete was used for all test specimens. The concrete was placed through one end of the vertical standing tubes via a hopper and vibrated with pencil vibrators. An external vibrator was used in addition to the pencil vibrators for the 4 - 7 m long columns. The exposed concrete at one end of each tube was wrapped in polyethylene while the concrete cured. The polyethylene was removed just prior to testing. The concrete was 27 to 69 days old when the specimens were tested.

3.3.3 Test Set-Up

The test set-up consisted of the MTS testing machine, two knife edge end fixtures, the electronic instrumentation which includes strain gauges and LVDT'S, an automatic data acquisition system, and the test specimen. Figure 3.2 is a schematic diagram of a column in the test apparatus. For clarity the instrumentation has not been included in this figure.

3.3.3.1 Load and Reaction Devices

The load was applied to column test specimens, by the MTS testing machine, through a pair of reaction devices called knife edge assemblages. One of these devices was bolted to the compression head of the MTS testing machine and the other to the lower platten as shown in Figure 3.2.

The original design, May (1978), was modified to provide rotational freedom about one axis only, and to provide the capability of adjusting the column-knife edge assemblage location so that, both concentric and constant eccentric loads could be applied to columns without major modifications to the test set-up. Each knife edge assemblage consists of a diamond shaped steel knife and two steel plates as shown in Figure 3.3. The knives were case hardened and the plates left soft to allow each groove to deform plastically and take up the shape of the knife where necessary.

As indicated in Figure 3.2, the column length is defined as the distance between the knife edges or points of rotation.

3.3.3.2 Instrumentation and Measurement

Loads, steel and concrete strains, end fixture rotations, column displacements and relative movement slip between the steel shell and the concrete core were measured throughout the duration of each test. The locations of the measurements made on the column are shown schematically in Figure 3.4. Table 3.1 provides the type of measurement, instrumentation used, location, purpose and the frequency of which the measurements were made.

3.3.3.3 Test Procedure

Prior to this series of tests, the knife edge devices were set in the MTS system, aligned with one another, and fixed in place.

The ends of each column were placed into the center of the steel housing provided, aligned, and secured in place by the adjustment of eight machine bolts as shown in Figures 3.1 and 3.3.

Out-of-straightness measurements were made using an instrument consisting of a series of mechanical dial gauges firmly attached to an aluminum angle. One such instrument was constructed for each length of column to be tested. Each instrument had a dial gauge at each end for reference measurements, and a sufficient number of intermediate gauges to describe the initial curvature. The instrument was fastened to the steel housings with clamps and two sets of readings were taken on each face of the column. These readings subsequently were compared to a set of calibrated readings to obtain the out-of-straightness of the column. These readings were analyzed, as described in Section 5.2, to give the out-of-straightness of the column about both major axes.

The alignment of the column was further refined on the basis of strain gauge readings taken on four faces of the tube at each end of the specimen while under a predetermined load, Estuar and Tall (1967). The alignment was considered satisfactory when the deviation of any four strain gauge readings was less than 5 per cent of the average value at the alignment load. This criterion was applied to both gauged sections.

For each test, an initial load of about 1/10th of the calculated ultimate load was applied to the column. Further load was applied to the column in appropriate increments as determined by the load deflection curve. All loads were applied to the column test specimen under stroke control. Tests were concluded at a point well beyond that defined as failure of the column. Measurements were made and recorded as described in the previous section. A photographic and written record was kept.

3.4 Flexural Tests

3.4.1 General

The purpose of this test series was to determine the ultimate moment capacity and load deformation response of empty HSS and concrete filled HSS. Tests were conducted on:

1. Two - 2000 mm long bare steel tubes.
2. One - 2000 mm long concrete filled HSS where strain compatibility was ensured at both ends of the beam.
3. Two - 2000 mm long non-strain compatible concrete filled HSS. The effect of adhesion, as a load transfer mechanism, on the ultimate strength of the beam test specimen was examined by coating the interior of one tube with form oil prior to the placing of the concrete.
4. One - 4000 mm long non-strain compatible concrete filled HSS was tested to observe the effect of a longer shear span on the method and rate of load transfer.

A total of six simply supported beams were tested under a two point load system which produced a constant moment region of 1 metre in length. The specimen identification numbers are given in Table 5.4.

3.4.2 Preparation of Test Specimens

At the load and reaction points on the beam specimens, 12 x 50 x 150 mm plates were welded to the loaded surface of the tube to prevent local buckling and to aid in the distribution of the stresses at these points. Additional plates were tack welded to the ends of the tubes to retain the concrete. These plates were removed from the non-strain compatible specimens prior to testing. The concrete in the beam test specimens was from the same batch as that in the column test specimens, and was placed and cured in the same way. The concrete was 64 to 69 days old when the beam test specimens were tested.

3.4.3 Test Set up

The test set up consisted of the MTS testing machine, rollers which provided translational and rotational degrees of freedom, distributing beams, electronic instrumentation, an automatic data acquisition system, and the test specimen. Figure 3.5 is a schematic diagram of a beam in the test apparatus.

As in the column tests, measurements were made to provide the information necessary to determine the load sharing characteristics and the method and rate of load transfer. Figure 3.6 gives schematic diagrams showing the locations of these measurements. Steel strain, concrete strain, and slip measurements were taken in the middle of the constant moment region, in the middle of the shear spans, and at the ends of the beam. End rotations, translations, and deflections at center line and under the point loads were measured with LVDT'S.

3.4.4 Test Procedure

Each beam was aligned and centered under the compression head of the MTS testing machine. For each test, an initial load of about 1/10th of the calculated ultimate load was applied to the beam. Further load was applied to the beam in appropriate increments as determined by the moment curvature curve. All loads were applied to the beam test specimen under stroke control. Measurements were made and recorded as previously described. A photographic and written record was kept.

3.5 Ancillary Tests

Due to the complexity of determining the load sharing characteristics between the steel shell and the concrete core, and the method and rate of load transfer a rigorous examination of material properties was required. This involved stub column tests, tension coupons, residual stress mesurements, and concrete strength tests.

3.5.1 Stub Columns

Two bare steel and two strain compatible concrete filled stub columns were each tested in compression to obtain an average load-strain relationship for their complete cross-sections.

The length of the steel stub columns was determined according to guidelines of SSRC (1976) to be 585 mm. The composite stub columns were made the same length. At midheight, eight strain gauges were placed equidistant from one another around the tube, four on the flats and four on the corners. Centred about midheight, Demec points were mounted in the centre of the four flats, to obtain a mechanical measurement of the average strain. These values were used to calibrate the electronic strain gauge system.

The test specimens were prepared, aligned, and tested as specified by SSRC (1976). Grout was used on both ends of the composite stub columns to provide a smooth surface for uniform bearing of the steel tube and concrete core against the loading and reaction plates, enforcing strain compatibility at both ends.

3.5.2 Tension Coupons

Tension coupons were used to determine the stress-strain characteristics of the steel from three distinct regions around the tube. Sixteen specimens were sawn from one section of tube. In total, 2 sets of 16 coupons were tested, 8 from the corners, 2 including welds, and 22 cut from the flat sides. The coupon numbers and locations are given in Figure 3.7. The flat and weld type coupons were made according to ASTM A370-77, Part 1. The corner coupons were cut and milled such that the specimen had a constant cross-sectional area along its length. A lead packing around the ends of the corner coupons prevented the tension grips of the testing machine from gouging the specimen, and causing a premature failure of the specimen.

A pair of strain gauges was mounted on opposite faces of each coupon and were wired in conjunction with two dummy gauges and a Budd Strain Indicator to form a full bridge system. This arrangement allowed the average strain to be measured, with double the sensitivity, up to values of two percent strain. Calipers and a scale were used to measure large strains and percent elongation. Rectangular rosette gauges were mounted on three flat coupons, numbers 7, 11 and 15 to determine Poisson's Ratio experimentally.

Prior to testing, the cross-sectional areas were determined from measurements of the necked down area for flat and weld coupons and by a volumetric method for corner coupons. The coupons were tested in the Baldwin testing machine, according to ASTM 370-77, Part (1). Load and corresponding strain measurements were taken.

3.5.3 Residual Stress Measurements

Residual strain measurements were made on forty-four sections cut from one section of the tube, Figure 3.7, to determine the distribution and magnitude of the longitudinal and through thickness residual stresses around the tube. These values, in conjunction with the stress-strain data, were used to predict the load carried by the steel section, given the strain distribution across the section.

Longitudinal residual stresses were determined by the method of sectioning as described by Tebedge, Alpsten, and Tall (1971). The through thickness variation of longitudinal residual stresses was determined from the curvature of the deformed shape of the longitudinal sections.

3.5.4 Concrete Strength

One batch of concrete was used for all the test specimens. Compressive and tensile strength tests were conducted to determine the parameters necessary to define the stress-strain curve as a function of time. The concrete was 27 to 69 days old when the columns and beams were tested.

3.5.4.1 Cylinder Tests

Twenty-three cylinders were tested in accordance with CSA A23.2, to determine the modulus of elasticity, and the maximum compressive strength. The cylinders were cast in steel molds and covered with polyethylene and cured in the lab along with the columns and beams. The curing process and steel molds were used to simulate the conditions of the concrete within the tubes. Tests were carried out at ages from 7 to 63 days.

3.5.4.2 Split Cylinder Tensile Tests

Two cylinders were tested in accordance with CSA A23.2-13C, to determine the splitting tensile strength. The concrete was 56 and 63 days old when tested.

3.5.4.3 Modulus of Rupture

Three 150 x 150 x 915 mm prisms were tested, in accordance with CSA A23.2-8C to determine the modulus of rupture. The prisms were moist cured. The concrete was 35, 42, and 49 days old when tested.

Table 3.1 Type of Measurement and Instrumentation

INSTRUMENTATION	LOCATION	PURPOSE	FREQUENCY OF MEASUREMENTS
	Steel Strains		
Electronic Resistance Gauges	Two gauges at fifteen locations along the length of the column (eleven located as a function of non-dimensional column height and four just below the connection plate). One gauge was mounted in the centre of the sides of the tube parallel to the axis of bending. Additional sets of gauges were mounted on the connection plates.	Provides a steel strain distribution across the section from which the load carried by the steel at that location may be determined. For the bare steel column tests, loads calculated from the measurements were compared with the applied load to determine the accuracy of the steel load prediction, Section 6.3.1.	Continuous
	Concrete Strains		
Mechanical Extensometer (Demec Gauge)	A pair of measurements on both sides of the column about the axis of bending, at six locations along the length of the column as shown in Figure 3.4. Gauge lengths as shown.	Provides a concrete strain distribution across the section from which the load carried by the concrete at that location may be determined.	Discrete 12-16 sets of readings per test.

Table 3.1 con't

INSTRUMENTATION	LOCATION	PURPOSE	FREQUENCY OF MEASUREMENTS
Slip			
Mechanical Extensometer (Demec Gauge)	Same relative locations as the concrete strain measurements, as shown in Figure 3.4. Gauge lengths as shown.	Provides values of relative movement of the steel shell with respect to the concrete core.	Discrete 12-16 sets of readings per test.
Rotation of Knife Edge Devices			
LVDT[2]	Two LVDT'S at both the upper and lower ends of the column as shown in Figure 3.4.	Used to determine the end fixity of the knife edge devices (hinges). Measurements define the slope of the column ends.	Continuous

Table 3.1 con't

INSTRUMENTATION	LOCATION	PURPOSE	FREQUENCY OF MEASUREMENTS
	Column Displacements (Deflected Shape)		
LVDT[2]	Eleven LVDT'S located as a function of non-dimensional column height as shown in Figure 3.4.	Used to monitor the load-deflection response of the test specimen under load. Deflection measurements could be used in determining thrust-moment-curvature relationships for each section type.	Continuous

Notes: 1. Load was applied under stroke control and measured internally by the MTS testing machine. Readings were taken continuously.

2. LVDT - linear variable differential transformer

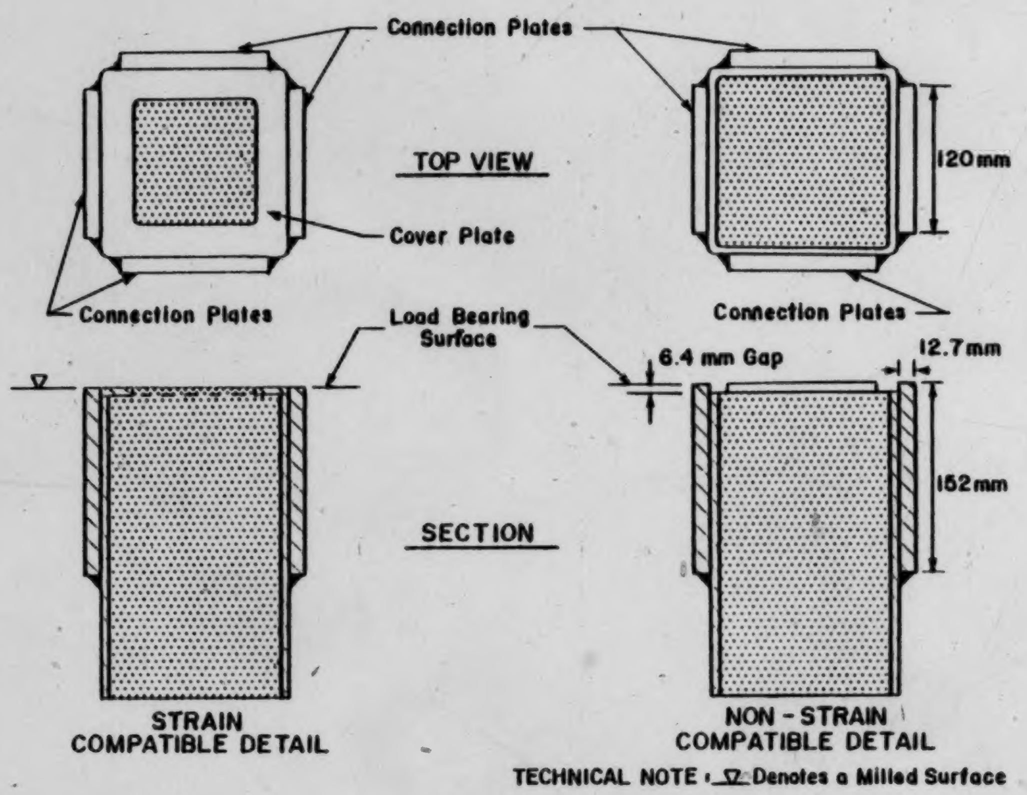
Connection Plates
TOP VIEW
Cover Plate
Connection Plates
Connection Plates
120mm
Load Bearing Surface
6.4 mm Gap
12.7mm
152mm
SECTION
STRAIN COMPATIBLE DETAIL
NON - STRAIN COMPATIBLE DETAIL
TECHNICAL NOTE : ∇ Denotes a Milled Surface

Figure 3.1 Upper Connection of Strain Compatible and Non-Strain Compatible Concrete-Filled HSS Columns

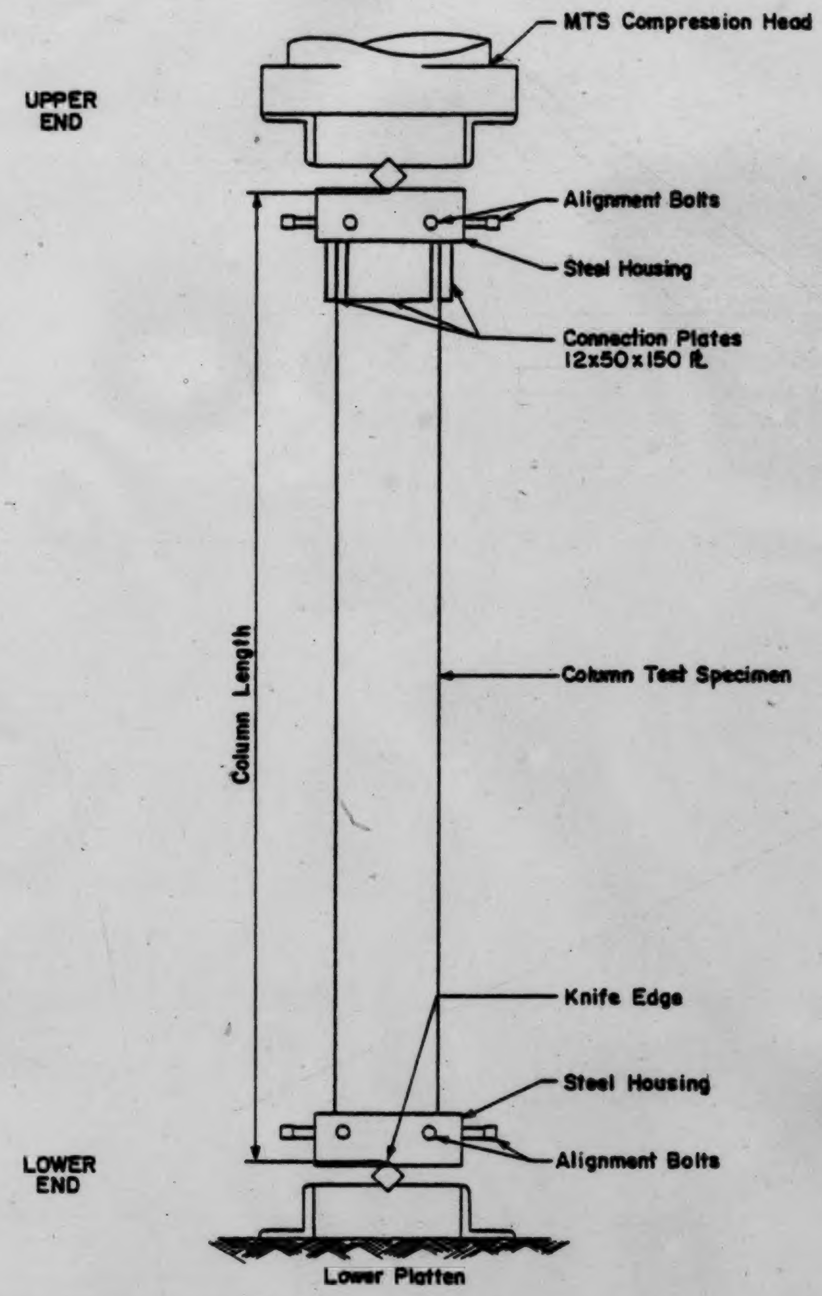
MTS Compression Head
UPPER END
Alignment Bolts
Steel Housing
Connection Plates 12x50x150 P.
Column Length
Column Test Specimen
Knife Edge
Steel Housing
Alignment Bolts
LOWER END
Lower Platten

Figure 3.2 Schematic Diagram of a Column Specimen

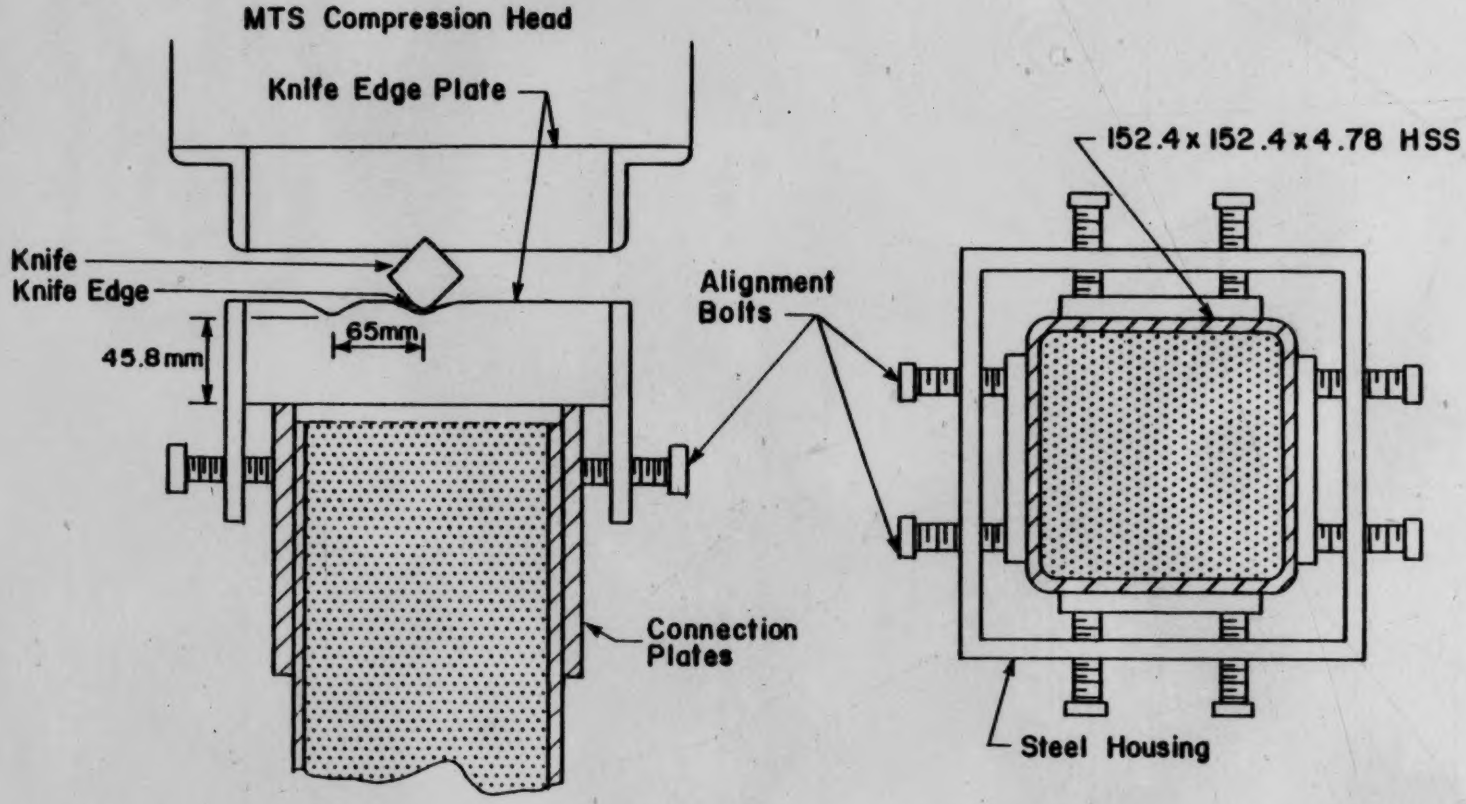
MTS Compression Head
Knife Edge Plate
Knife
Knife Edge
45.8mm
65mm
Alignment Bolts
Connection Plates
152.4 x 152.4 x 4.78 HSS
Steel Housing

CROSS - SECTION OF COLUMN
AND KNIFE EDGE ASSEMBLY

CROSS-SECTION OF COLUMN
IN STEEL HOUSING

Figure 3.3 Knife Edge Assembly

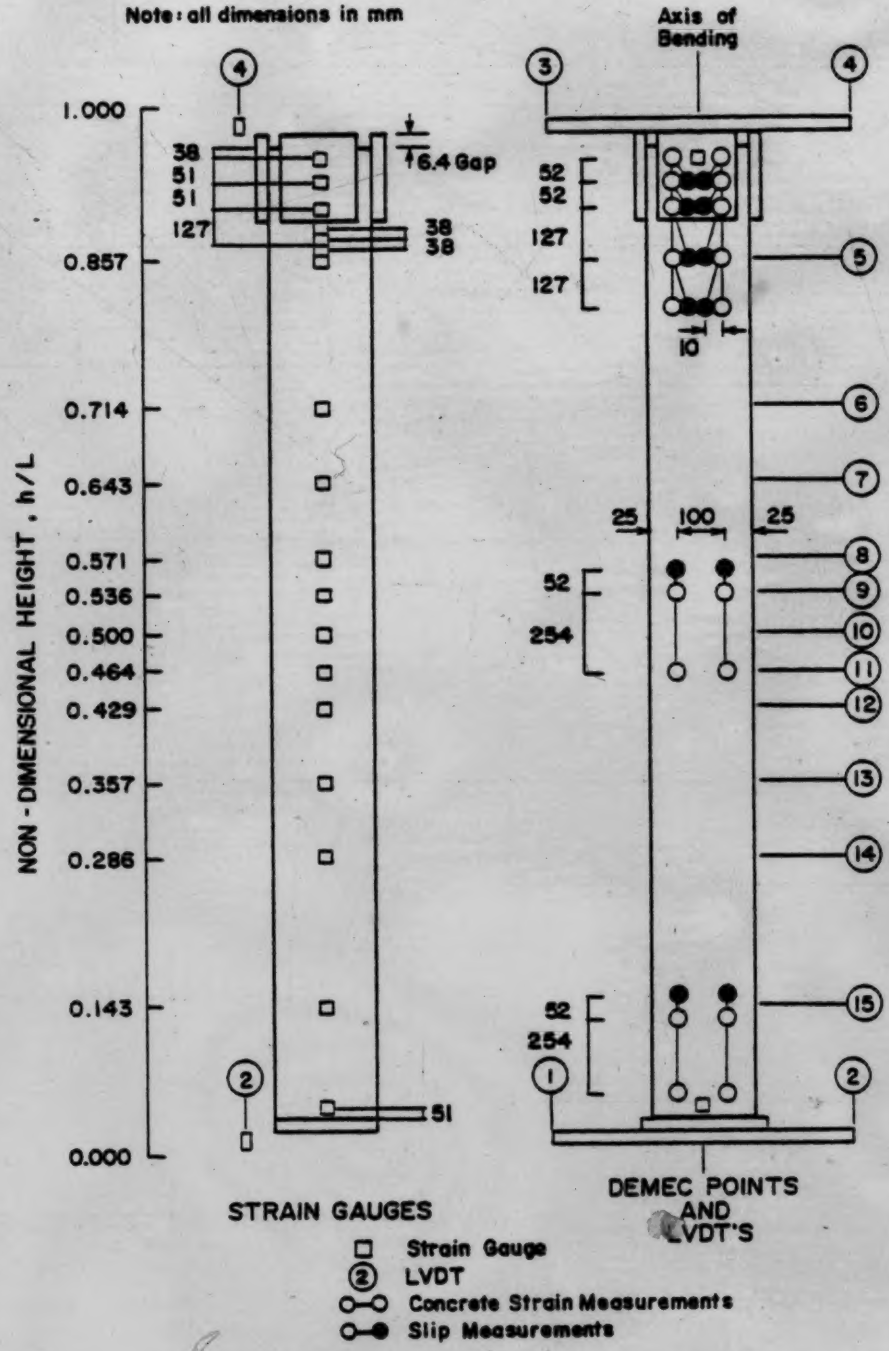
Note: all dimensions in mm
Axis of Bending
NON-DIMENSIONAL HEIGHT, h/L
1.000
0.857
0.714
0.643
0.571
0.536
0.500
0.464
0.429
0.357
0.286
0.143
0.000
38
51
51
127
6.4 Gap
38
38
51
52
52
127
127
10
25
100
25
52
254
52
254
①
②
③
④
⑤
⑥
⑦
⑧
⑨
⑩
⑪
⑫
⑬
⑭
⑮
STRAIN GAUGES
DEMEC POINTS AND LVDT'S
□ Strain Gauge
② LVDT
○–○ Concrete Strain Measurements
○–● Slip Measurements

Figure 3.4 Schematic Diagram of Instrumentation on a Column Specimen

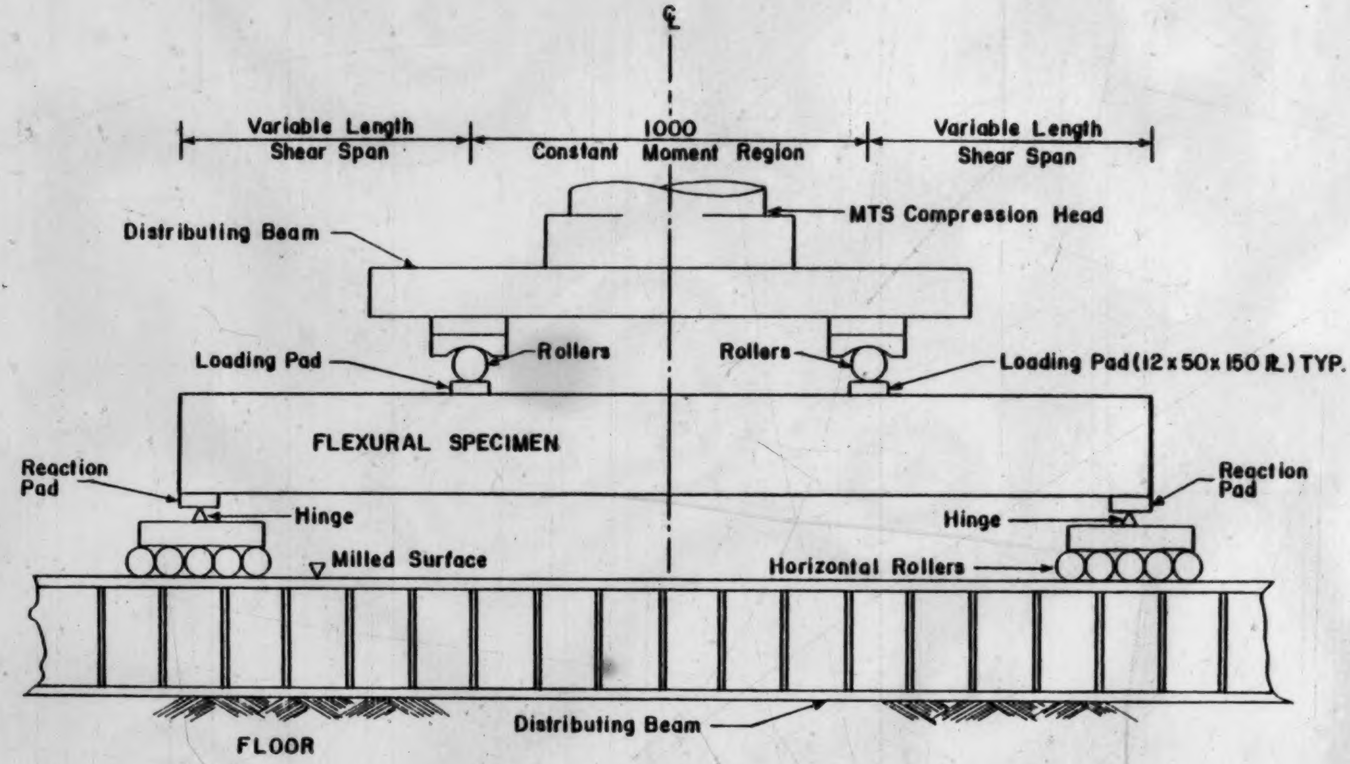
℄
Variable Length
Shear Span
1000
Constant Moment Region
Variable Length
Shear Span
MTS Compression Head
Distributing Beam
Loading Pad
Rollers
Rollers
Loading Pad (12 x 50 x 150 PL) TYP.
FLEXURAL SPECIMEN
Reaction Pad
Reaction Pad
Hinge
Hinge
Milled Surface
Horizontal Rollers
FLOOR
Distributing Beam

Figure 3.5 Schematic Diagram of a Beam Specimen

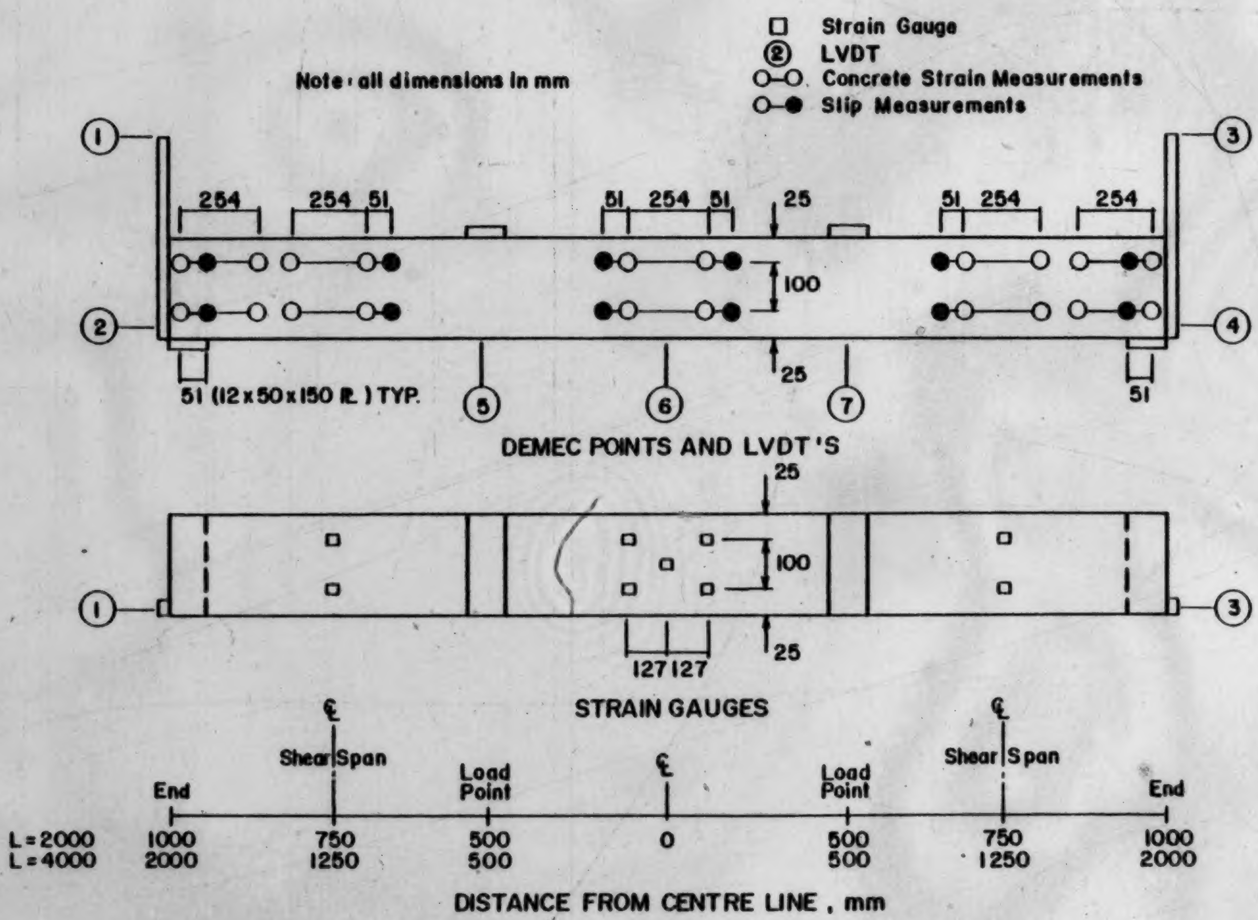
Note: all dimensions in mm
Strain Gauge
② LVDT
Concrete Strain Measurements
Slip Measurements
①
②
③
④
⑤
⑥
⑦
254
254
51
51
254
51
25
100
25
51
254
254
51 (12 x 50 x 150 R.) TYP.
51
DEMEC POINTS AND LVDT'S
25
100
25
127 127
①
③
STRAIN GAUGES
℄
Shear Span
End
Load Point
℄
Load Point
℄
Shear Span
End
L=2000
L=4000
1000
2000
750
1250
500
500
0
500
500
750
1250
1000
2000
DISTANCE FROM CENTRE LINE, mm

Figure 3.6 Schematic Diagram of Instrumentation on a Beam Specimen

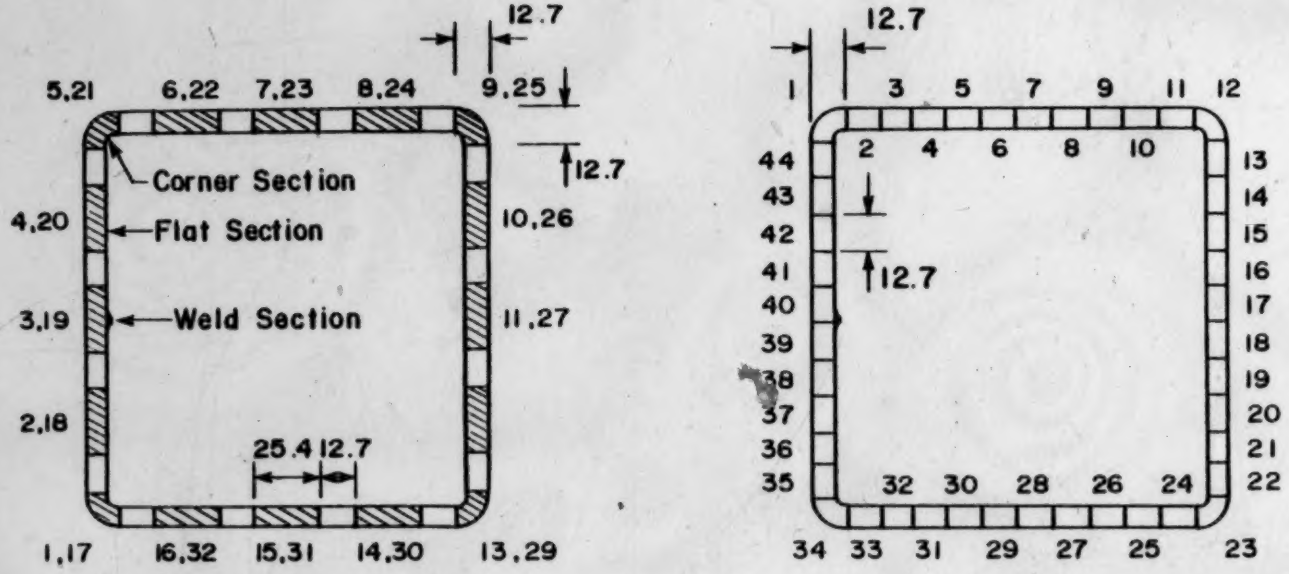
12.7
5,21
6,22
7,23
8,24
9,25
12.7
Corner Section
4,20
Flat Section
10,26
3,19
Weld Section
11,27
2,18
25.4
12.7
1,17
16,32
15,31
14,30
13,29
12.7
1
2
3
4
5
6
7
8
9
10
11
12
13
14
15
16
17
18
19
20
21
22
23
24
25
26
27
28
29
30
31
32
33
34
35
36
37
38
39
40
41
42
43
44
12.7

TENSION COUPONS

RESIDUAL STRESS SECTIONS

Note: typical dimensions are shown in mm

Figure 3.7 Identification and Location of the Tension Coupons and Residual Stress Sections

4. MATERIAL PROPERTIES AND BEHAVIOUR

4.1 Steel

The section selected for this study, a grade 350 W 152.4 x 152.4 x 4.78 HSS was manufactured by Standard Tube Canada Limited. All test specimens were cut from eight 40 foot pieces which were all from one heat, number 32714. The chemical composition of this heat was: 0.18% C, 0.82% Mn, 0.009% P, and 0.016% S. These values lie within the limits for grade 350 W HSS as specified by CAN3 - G40.21 - M81.

4.1.1 Geometric Properties

The dimensions for this section were found to lie within the allowable fabrication tolerances as described in the CISC Handbook of Steel Construction, 1980. Measured values of wall thickness, section depth and width were used to calculate section properties.

4.1.1.1 Dimensions

The wall thickness was determined from 344 measurements to have a mean value of 4.43 mm with a coefficient of variation of 0.0099. The actual wall thickness was equal to 0.927 times the specified wall thickness of 4.78 mm. Measurements of the outside dimensions b and d show that these dimensions lie within the ± 1.5 mm specified tolerance. The value of 152.4 mm will be used for b and d in subsequent analysis. Based on the measured dimensions, the section was a Class 3 section although the nominal properties would classify it as a Class 2 section, as defined in Clauses 11.2 and 11.3.2(b) from S16.1-77M.

4.1.1.2 Section Properties

Based on measured values of mass and length, and given that rolled steel has a density of 7850 kg/mm^3, the cross-sectional area was calculated by the volumetric method to be 2570 mm^2. Given the dimensions as determined, and a simple geometric relationship, the cross-sectional area was calculated to be 2571 mm^2. Agreement of these two values gives confidence to the dimensions as measured and the value of 2570 mm^2 was selected for the cross-sectional area. The moment of inertia, elastic section modulus and plastic section modulus were determined geometrically to be 9.29 x 10^6 mm^4, 121.6 x 10^3 mm^3 and 142.2 x 10^3 mm^3, respectively.

4.1.2 Load Deformation Relationships

The establishment of load deformation relationships was essential for the transformation of strain gauge data to values of stress and load. These values of predicted steel load have been used in subsequent analyses for statical checks, load prediction verification, determination of concrete load distributions, and for the identification of load transfer mechanisms. An accurate assessment of the characteristic properties of the material was required.

4.1.2.1 Modulus of Elasticity

Section 2.1 of ASTM E111-61 'Standard Test Method for Young's Modulus at Room Temperature', states the definition of Young's Modulus as, "the ratio of normal stress to corresponding strain for tensile or compressive stresses below the proportional limit of the material". The description from 7.3 of the section entitled, 'Interpretation of Data', suggests that errors that may be introduced in fitting graphically a straight line can be reduced by determining Young's Modulus as the slope of the straight line fitted to the appropriate data by the method of least squares.

For a set of data that exhibits linear and non-linear behaviour and is coupled with random variations, the problem is not the application of the method of least squares to the data set to determine the best fit straight line, but, the determination of the appropriate data to apply it to.

When using the method of least squares to determine the best fit curve, the correlation coefficient r is used as the criterion to determine closeness of fit, with a value of r equal to one indicating a perfect correlation between the data set and the best fit curve. By conducting a continuous least squares analysis to a set of stress strain data, the slope of the best fit straight line curve with a correlation coefficient closest to one may be deemed as the best selection for the modulus of elasticity, E, where, a continuous least squares analysis is the application of the method of least squares to determine the best fit curve to the first two points of the data set and then to the first 3, 4, 5, ...etc.. Each subsequent calculation includes the influence of an additional point on the best fit straight line curve, the slope and the correlation coefficient. As the set of data being evaluated becomes larger the influence of each additional point becomes less and by the correlation coefficient criterion alone the point in which the data set begins to exhibit nonlinear behaviour becomes unclear. However, this point is easily detectable by examining the trend of the data by evaluating the tangent modulus from point to point with a moving average technique. The upper limit of the appropriate data set can now be defined.

The possibility of small offsets of zero load and random variations in establishing the load path during the first small increments of load, suggest that a lower limit exists to the appropriate data set and that a number of points in this region should not be used in the calculation of the modulus of elasticity. The standard recognizes this and specifies that the best fit curve should not be constrained to pass through the zero point. It was found that the inclusion of the points in this region, with the exception of the zero point, did not affect the value of E selected as long as a sufficient number of points were used in the analysis.

The evaluation of the modulus of elasticity for tension coupon 6 has been included to illustrate the problems and procedures as outlined. An example set of data and calculations is given in Table 4.1. Figure 4.1 is a graphical representation of the decision making model for the determination of the modulus of elasticity. Three sets of moduli are plotted in this figure, with moduli on the vertical axis and applied stress on the horizontal axis. The square and triangular symbols represent the elastic moduli values as determined from a continuous least squares analysis for the entire data set, and the entire set of data excluding the first three points, respectively. BFC_1 and BFC_2 are the respective elastic modulus values as selected by the correlation coefficient criterion. It can be clearly seen here and from the trend of tangent moduli values in Table 4.1, that the material was exhibiting non-linear behaviour prior to the points as determined by the correlation criterion. The proportional limit or upper limit for the appropriate data set was selected as 187.0 MPa and the corresponding modulus of elasticity, E_s was 209.6 x 10^3 MPa. In summary, the modulus of elasticity for all steel test specimens were calculated by the following procedure:

1. Evaluate the tangent modulus between sets of data points.
2. Apply the moving average technique over 4 to 6 points to establish the trend of the data and select the proportional limit.
3. Apply the method of least squares to the bounded set of data. The slope of the best fit straight line curve is

the modulus of elasticity for that test specimen.

The distribution of modulus of elasticity values for two sample sets of tension coupons taken around the tube are shown graphically in Figure 4.2 as solid and dashed lines which represent a ratio of coupon to stub column E values. The tube shape outline indicates a ratio of E values equal to one. Solid or dashed lines outside this tube outline have a ratio of E values greater than one and the converse is true for lines inside the tube outline. A single solid line indicates that both samples at that point on the tube have the same value of the modulus of elasticity value. The actual values for the tension coupons are given in Table 4.6.

The mean modulus of elasticity values, standard deviations and coefficients of variation for corner, weld and flat coupons and for the steel stub columns have been established by a single variable statistical analysis and are given in Table 4.2. Bessel's correction has been applied to populations less than 30 and in all cases Chauvenet's Criterion was used for the rejection of outliers. The mean values obtained here were used in conjunction with other pertinent stress strain parameters to develop mathematical expressions which describe load deformation behaviour for each section type.

Examination of tension coupon results indicate that there are two distinct groups of modulus of elasticity values, a value of 225.9 x 10^3 MPa for the corners and a value close to 210.1 x 10^3 MPa for the flats and welds. The differences in behaviour and in particular the modulus of elasticity values is a result of the plastic deformation that takes place in the corners of the tube during the shaping process when the tubes are made. This deformation is a result of the metal crystals deforming by slip on a glide system. Cottrel (1967) states that an important effect of the slip process is lattice rotation of which one effect is the development of preferred orientation. The higher values of the modulus of elasticity are due to this reorientation of the crystals. The metal crystals in the corner regions of the tubes are no longer randomly orientated and therefore are considered anisotropic.

4.1.2.2 Poisson's Ratio

Poisson's ratio was determined experimentally and is given as the mean of three values, a value of 0.28, with a coefficient of variation of 0.0043. The test procedure and evaluation of the data was done in accordance with ASTM E132-61, 'Standard Test Method for Poisson's Ratio at Room Temperature'.

4.1.2.3 Yield Strength

As defined bt ASTM Standard A370-77, the yield strength is the "stress, corresponding to the load which produces in a material, under specific conditions of the test, a specified limiting plastic strain". A strain offset of 0.002 is suggested as the yield criterion when gradual yielding (no definite yield plateau), a phenomena characteristic of heavily cold worked materials, occurs.

Based on this criterion the static yield stress values for the stub columns and the tension coupons were determined. The distributions of static yield stress values of the tension coupons are shown graphically in Figure 4.3 as the ratio of coupon to stub column static yield stress values. The interpretation of this figure is similar to that for the modulus of elasticity in Figure 4.2. The static yield stress values for the tension coupons are given in Table 4.6.

The mean static yield strength values, standard deviations and coefficients of variation for corner, weld and flat coupons and for the steel stub columns have been established by a single variable statistical analysis and are given in Table 4.3. Bessel's correction and Chauvenet's Criterion were applied as before. The mean values obtained here were used in the development of mathematical expressions which describe the load deformation behaviour for each section type.

The results indicate that there are three distinct groups of static yield values. The variation between the flats and the corners is attributed to cold working of the corner material during the tube forming process. The distinct static yield stress for the weld section is attributed to the inclusion in this section of weld metal which has different mechanical properties.

4.1.2.4 Stub Column Load Deformation Curves

The average stress strain curve for a steel stub column given in Figure 4.4 can be described by a series of mathematical expressions of the form:

$$\sigma_{stub} = A\,\varepsilon + B\,\varepsilon^{1/2} + C\,\varepsilon^{1/3} + D\,\varepsilon^{1/4} + E\,\varepsilon^{1/5} \qquad (4.1)$$

The strain ranges and corresponding coefficients are given in Table 4.4. The strain values are the average of the eight gauges shown on the stub column in Figure 4.4. Stress strain curve information, including Young's modulus of elasticity, proportional limit stress, yield strength, yield stress level, elastic range, and elastic-plastic range are clearly marked on Figure 4.4. Because the steel stub column behaved as a Class 3 section the plastic range, onset of strain hardening, strain hardening range, and the strain hardening modulus could not be defined.

The average load strain curve for a steel stub column given in Figure 4.10, was modeled from the experimentally obtained curve and can be described by a series of mathematical expressions of the form:

$$P_{stub} = A\,\varepsilon + B\,\varepsilon^{1/2} + C\,\varepsilon^{1/3} + D\,\varepsilon^{1/4} + E\,\varepsilon^{1/5} \qquad (4.2)$$

The strain ranges and corresponding coefficients are given in Table 4.5. This load deformation curve, as described by this series of mathematical expressions, is used in conjunction with steel strain measurements in subsequent analyses to predict the load carried by the steel at specified locations. The accuracy of these predictions is discussed in Section 6.3.1.

4.1.2.5 Tension Coupon Stress Strain Curves

Based on the characteristic parameters of the stress strain curves as determined from the tension coupon tests and given in Table 4.6, a series of mathematical expressions have been developed to describe their shapes. These expressions take the form:

$$\sigma = A + B\varepsilon + C\varepsilon^{1/2} + D\varepsilon^{1/3} + E\varepsilon^{1/4} + F\varepsilon^{1/5} + G\varepsilon^{1/6} \qquad (4.3)$$

The strain ranges and corresponding coefficients for flat, corner, and weld sections are given in Tables 4.7, 4.8 and 4.9 respectively. The stress strain curve for each of these sections as described by these expressions is found in Figure 4.5.

Given the strain distribution across depth of the HSS relative to the axis of bending, and given that plane sections remain plane after bending, the strain at any location around the tube can be determined. The corresponding stresses can be determined with the use of the previously described stress strain curves. Combining these stresses with the associated residual stresses, and multiplying these values by the appropriate area, the load for any discrete section can be determined. The load carried by the HSS on the plane is determined by integrating the loads for all the sections over the entire cross-section. The accuracy of using these curves to predict the load carried by the steel is discussed in Section 6.3.1.

4.1.3 Residual Stresses

By the method of sectioning, forty-four longitudinal and forty-four through the thickness residual strain measurements were made. The residual strain values were converted to residual stress values using the appropriate stress strain curve. Statics was checked and corrections were made to ensure that the sum of the axial forces on the section and the sum of the moments about both principal axes were zero. It should be noted that, the residual strain measurements include the effect of temperature change on the specimens between the initial and final readings. An apparent net residual tensile strain of 29.4×10^{-6} was determined from statics.

The longitudinal residual stress distribution is shown graphically in Figure 4.6 as a ratio of longitudinal residual stress on the section to the stub column static yield stress. Negative values indicate a residual compressive stress and are plotted on the outside of the tube outline. From this single determination of residual stresses, it appears that effects of plastically deforming the corners of the tube are localized. The sections containing and affected by the weld have a net residual tensile stress. The through the thickness distribution of longitudinal residual stresses is shown graphically in Figure 4.7 as a ratio of the through the thickness variation to the stub column static yield stress. The residual stress on the inside and outside face of each section has been plotted on the outside of the tube outline. Negative values are residual compressive stresses. These residual compressive stresses always occurred on the inside face of the tube and are shown in the figure as a dashed line. A single solid line indicates that both the residual stress on the inside and outside faces are of the same magnitude but opposite sign. The cold formed HSS residual stress patterns, although slightly different in shape and relative magnitude, concur with those reported by Davison and Birkemoe (1983).

4.2 Concrete

4.2.1 Stress Strain Relationship

4.2.1.1 Uniaxial Compressive Strength

A least squares best fit third degree polynomial was derived to express the uniaxial compressive strength of the concrete as a function of time in days for the sixteen cylinders cast in steel molds. The polynomial is of the form:

$$f'_c = 5.69 + 2.03t - 0.034t^2 + 0.0002t^3 \qquad (4.4)$$

The strengths predicted by this expression are only valid for the age of concrete during the test period, 21 to 69 days. Experimental and empirically determined values are given in Table 4.10.

4.2.1.2 Modulus of Rupture

Because the number of split cylinder tests and modulus of rupture tests was small and owing to the scatter of results obtained by other researchers, the maximum tensile strength for the uniaxial stress strain curve was set equal to the modulus of rupture as defined by Clause 7.6.2.2.2 of CAN3 - A23.3 - M77. Although conclusive statements cannot be made, experimental values were comparable with this definition of strength, as shown in Table 4.10.

4.2.1.3 Modulus of Elasticity

Twenty-nine tests were conducted on fifteen cylinders, in accordance with CSA A23.2-9C, to determine the modulus of elasticity. These tests were conducted regularly throughout the test period in order to obtain a relationship for the modulus of elasticity as a function of time.

Each set of test data was evaluated according to the CSA standard. The modulus of elasticity was calculated by dividing the difference between the stress at 40% of the ultimate load and the stress at 0.005% strain by the corresponding difference in strain values. These values were compared with the corresponding values obtained from the method of least squares. This data has been fitted with an expression of the form:

$$E_c = 4200\sqrt{f'_c} \tag{4.5}$$

where the compressive strength was determined by Equation 4.4. The empirical and experimentally determined values are shown in Figure 4.8. It should be noted that Equation 4.5 gives values of E_c that are 84 per cent of those given by CSA standard CAN3-A23.3-M77.

4.2.1.4 Stress Strain Curve

This curve has been developed to predict the unconfined resistance of the concrete given the strains measured during the column and beam tests. The experimentally based stress strain curve shown in Figure 4.9 consists of three parts.

1. An elastic-brittle stress strain relationship was assumed for concrete in tension. The modulus of elasticity in tension was set equal to the modulus of elasticity in compression, the value determined by Equation 4.5. The maximum tensile stress was taken as the modulus of rupture.
2. An elastic stress strain relationship was assumed for concrete in compression up to a value of stress equal to 0.4 times the compressive strength. The modulus of elasticity was determined from Equation 4.5.
3. The inelastic compressive stress portion is described by the Todeschini et al. (1964) stress strain curve. The value ϵ_0 is the strain at the maximum compressive

strength, f'_c . By constraining the Todeschini curve to pass through the point corresponding to a stress equal to $0.4f'_c$ and a strain of $0.4f'_c/E_c$, the value of ϵ_o was evaluated and is equal to 4.79 times the strain at $0.4f'_c$.

Given a time in days and the polynomial expression for f'_c a complete stress strain curve can easily be developed. Figure 4.9 shows this idealized uniaxial stress strain curve for a 28 day old concrete with the properties of the concrete used in this test series. The value for ϵ_o is 2420 microstrains.

4.3 Composite Stub Column Behaviour

4.3.1 Load Deformation Relationship

The average load strain curve in Figure 4.10, modelled after the experimentally obtained curve, can be described by a mathematical expression of the following form:

$$P_{csc} = A + B\varepsilon + C\varepsilon^{1/2} + D\varepsilon^{1/3} + E\varepsilon^{1/4} + F\varepsilon^{1/5} + G\varepsilon^{1/6} \qquad (4.6)$$

The strain ranges and corresponding coefficients are given in Table 4.11. The triangular symbols in this figure denote the point at which initiation of local buckling was observed on the surface of the steel tube. The ultimate load of 1794 kN, which is equal to 1.021 times the squash load, was calculated using Equation 4.7 and the experimentally determined material properties.

$$P_s = A_s\sigma_{sy_{stub}} + A_c f'_c \qquad (4.7)$$

where, $A_c = 20550\ mm^2$

$A_s = 2570\ mm^2$

$f'_c = 36.9$ MPa

$\sigma_{sy_{stub}} = 389$ MPa

The axial load versus longitudinal strain relationship is classified according to Tomii, et al. (1977) as being a degrading type in which there is a decrease in the axial load in the load deformation curve after the ultimate load was reached. The stub column failed by a crushing of the concrete and outward local buckling of the steel tube.

4.3.2 Concrete Contribution

The composite and steel stub column load deformation curves as described by previously defined mathematical expressions are shown in Figure 4.10. The concrete load deformation curve shown in this figure is the difference between these two curves.

Based on sixty tests on square composite stub columns, Tomii, et al. (1977) suggest that there is no confinement action on the concrete by the steel tube for columns displaying a degrading type load deformation curve. Based on this premise, the concrete load deformation curve should be equivalent to the uniaxial unconfined concrete load deformation curve as predicted by the proposed stress-strain model. As shown in Figure 4.10, the predicted curve over-estimates the concrete load by a maximum value of 12.1 percent at a strain of 1100 microstrains and under estimates the concrete load by a maximum value of 6.3 percent at a strain of 3000 microstrains. A single variable statistical analysis on the ratio of fifty predicted to observed concrete load values gives a mean value of 1.010 and a coefficient of variation of 5.7 percent. Although this result concurs with those reported by Tomii, et al. (1977), it may not be true for all HSS beam columns.

The difference between the observed and the predicted curves shown in Figure 4.10 is a measure of error. Included in this measure are errors in measurement for the stub column tests, errors in approximating these curves with mathematical expressions and any error in assuming the proposed stress strain curve model for concrete.

Due to the restraining action of the concrete core on the wall of the steel tube, the steel was able to sustain load for increasing deformations. This curve, shown as a dashed line in Figure 4.10, was approximated as the difference between the composite stub column and the predicted concrete load deformation curves.

Table 4.1 Example Set of Calculations for the Modulus of Elasticity, Tension Coupon 6

STRESS MPa	STRAIN x10^{-6} mm/mm	TANGENT MODULUS x10^{3}MPa	MOVING AVERAGE MODULUS x10^{3}MPa	AS DETERMINED BY THE METHOD OF LEAST SQUARES	
				MODULUS OF ELASTICITY x10^{3}MPa	r^2
11.7	63	-	-	-	-
23.4	128	179.8	-	179.8	0.999960
35.1	184	208.7	-	192.8	0.999624
46.8	236	224.7	-	202.7	0.999113
58.4	288	224.7	-	208.9	0.998900
70.1	347	198.1	207.2	209.3	0.999196
81.8	403	208.7	213.0	209.3	0.999393
93.5	467	182.6	207.8	206.8	0.999583
105.2	512	259.7	214.8	208.4	0.999576
116.9	568	208.7	211.6	209.3	0.999613
128.5	626	201.5	212.2	209.4	0.999676
140.2	684	201.5	210.8	209.2	0.999737
151.9	738	216.4	217.6	209.2	0.999773
163.6	790	224.7	210.6	209.7	0.999785
175.3	848	201.5	209.1	209.8	0.999810
187.0	907	198.1	208.4	209.6[2]	0.999839
192.8	939	182.6	204.6	209.1	0.999864
198.7	966	216.4	204.7	208.9	0.999882
204.5	997	188.5	197.4	208.6	0.999898
210.4	1032	166.9	190.5	207.9[1]	0.999964
216.2	1061	201.5	191.2	207.4	0.999910
222.0	1094	177.1	190.1	206.8	0.999911
227.9	1130	162.3	179.3	206.0	0.999899
233.7	1165	166.9	174.9	205.2	0.999831
239.6	1205	146.1	170.8	204.0	0.999831

NOTES: 1. BFC$_1$, Modulus of Elasticity that corresponds to the coefficient of determination, r^2 closest to 1.
2. The value of E_s selected based on the trends indicated by the moving average technique.
3. Correlation coefficient, r.
4. Calculations based on the entire data set.

Table 4.2 Single Variable Statistical Analysis of the Modulus of Elasticity

TYPE	n	$\bar{x}$ x10^3 MPa	σ x10^3 MPa	V %
STEEL STUB COLUMNS	2	210.7	0.14	0.07
CORNER COUPONS[1]	7	225.9	1.75	1.50
WELD COUPONS	2	210.0	2.90	1.38
FLAT COUPONS[2]	21	210.1	1.72	0.82

NOTES: 1. One sample was rejected as an outlier, based on Chauvenet's Criterion.
2. One sample was rejected due to an accidental preload to the specimen.

Table 4.3 Single Variable Statistical Analysis of the Yield Stress

TYPE	n	$\bar{x}$ MPa	σ MPa	V %
STEEL STUB COLUMN[1]	1	389.0	-	-
CORNER COUPONS	8	472.6	8.69	1.83
WELD COUPONS	2	474.1	6.5	1.37
FLAT COUPONS[2]	21	364.5	8.25	2.26

NOTES: 1. One sample was rejected due to an uneven loading of the end specimen.
2. One sample was rejected due to an accidental preload to the specimen.

Table 4.4 Coefficients Used to Describe the Stub Column Stress Strain Curve

COEFFCIENTS	STRAIN RANGE x10^{-6} mm/mm	
	0-844	844-4936
A	210,700	-596,424
B	-	738,419
C	-	-1,334,012
D	-	1,281,168
E	-	-465,681

NOTE: 1. $\sigma_{stub} = A\,\varepsilon + B\,\varepsilon^{1/2} + C\,\varepsilon^{1/3} + D\,\varepsilon^{1/4} + E\,\varepsilon^{1/5}$

Table 4.5 Coefficients Used to Describe the Stub Column Load Strain Curve

COEFFCIENTS	STRAIN RANGE x10^{-6} mm/mm	
	0-844	844-4936
A	541,028	-77,819
B	-	-195,865
C	-	294,888
D	-	-186,661
E	-	41,838

NOTE: 1. $P_{stub} = A\,\varepsilon + B\,\varepsilon^{1/2} + C\,\varepsilon^{1/3} + D\,\varepsilon^{1/4} + E\,\varepsilon^{1/5}$

Table 4.6 Characteristic Parameters Used in the Description of Stress Strain Curves for Flat, Corner, and Weld Sections

COUPON NO.	E $\times 10^3$ MPa	σ_p MPa	ϵ_y $\times 10^{-6}$ mm/mm	F_y MPa	ϵ_u $\times 10^{-6}$ mm/mm	F_u MPa	$\Delta L/L$[3] %
				FLATS			
2	209.0	139.4	3670	350.1	145,700	439.7	26.3
4	210.1	116.4	3830	365.7	160,000	459.7	27.5
6	209.6	187.0	3390	381.2	160,000	466.3	28.0
7	208.6	221.4	3820	363.5	160,400	454.5	26.3
8'	-	-	-	-	-	-	-
10	210.8	185.8	3850	367.5	130,000	448.2	24.5
11	210.1	237.4	3860	370.2	159,800	448.1	28.3
12	211.1	140.9	3820	367.3	149,600	444.4	25.9
14	208.5	182.0	3860	365.4	137,200	442.1	25.4
15	208.3	176.5	3810	359.1	160,000	448.3	26.8
16	210.9	175.9	3810	362.7	160,800	442.8	26.4
18	211.0	127.8	3750	353.6	160,000	438.6	25.8
20	208.6	160.6	3820	361.5	169,600	458.3	28.2
22	212.9	189.3	3880	379.6	162,900	463.9	25.6
23	211.9	166.8	3780	355.9	145,700	454.2	20.6
24	213.7	129.5	3820	370.7	193,000	450.4	27.3
26	207.0	175.1	3850	367.5	164,200	449.4	28.1
27	211.1	222.3	3820	363.3	150,000	444.6	27.5
28	207.5	142.5	3840	361.7	188,500	446.9	28.3
30	210.7	176.0	3830	366.8	158,600	442.9	25.6

TABLE 4.6 (continued)

COUPON NO.	E $\times 10^3$ MPa	σ_p MPa	ϵ_y $\times 10^{-6}$ mm/mm	F_y MPa	ϵ_u $\times 10^{-6}$ mm/mm	F_u MPa	$\Delta L/L$[3] %
				FLATS			
31	209.1	175.7	3790	355.7	160,000	442.9	27.6
32	211.3	181.2	3860	366.7	140,000	442.6	25.0
x	(210.1)	(171.9)	(3820)	(364.5)	(157,900)	(449.0)	(26.4)
				CORNERS			
1	226.2	315.7	4180	465.8	18,000	544.1	–[3]
5	225.6	300.8	4260	479.0	19,200	557.7	–[3]
9	226.3	141.3	4210	466.2	25,000	546.2	–[3]
13	214.3	181.8	4340	472.8	29,900	545.4	7.9
17	222.8	124.7	4200	460.6	22,400	544.9	–[3]
21	232.6	143.9	4180	484.8	18,750	556.7	–[3]
25	225.2	145.3	4240	482.2	17,500	550.6	–[3]
29	222.7	146.7	4210	469.2	22,500	546.3	7.3
x	(225.9)	(187.5)	(4230)	(472.6)	(21,700)	(549.0)	(7.6)

TABLE 4.6 (continued)

COUPON NO.	E x10^3 MPa	σ_p MPa	ϵ_y x10^{-6} mm/mm	F_y MPa	ϵ_u x10^{-6} mm/mm	F_u MPa	$\Delta L/L$[3] %
				WELDS			
3	207.9	232.9	4510	478.7	57,900	550.2	10.8
19	212.0	166.4	4320	469.5	43,700	549.3	10.1
x	(210.0)	(199.7)	(4420)	(474.1)	(50,800)	(549.8)	(10.45)

NOTES: 1. Data not evaluated due to an accidental preloading of the specimen.
2. Failure outside gauge length.
3. ΔL/L, elongation of the gauge length in per cent.

Table 4.7 Coefficients Used to Describe the Stress Strain Curve for the Flat Sections

COEFF-CIENTS	STRAIN RANGE $x10^{-6}$ mm/mm						
	0-815	815-3820	3820-30000	30000-94500	94500-157900	157900-220000	220000-264000
A	-	-	-	435.8	449.0	471.9	-
B	210,100	32,025,629	181,783	139.5	-	-144.9	-50,973,495
C	-	-110,462,169	-1,902,846	-	-	-	782,887,402
D	-	389,369,471	9,581,852	-	-	-	-3,103,559,452
E	-	-725,232,557	-21,279,617	-	-	-	4,340,036,863
F	-	644,399,388	20,993,148	-	-	-	-1,969,298,895
G	-	216,220,243	-7,548,679	-	-	-	-

NOTE: 1. $\sigma = A + B\,\varepsilon + C\,\varepsilon^{1/2} + D\,\varepsilon^{1/3} + E\,\varepsilon^{1/4} + F\,\varepsilon^{1/5} + G\,\varepsilon^{1/6}$

Table 4.8 Coefficients Used to Describe the Stress-Strain Curve For the Corner Sections

COEFF-CIENTS	STRAIN RANGE x10^{-6} mm/mm				
	0-830	830-4230	4230-18220	18220-21700	21700-76000
A	-	-	-	549.0	-
B	225,900	42,486,981	26,689	-	-110,923
C	-	-146,212,228	-1,560,006	-	509,079
D	-	514,407,892	9,452,648	-	-1,358,179
E	-	-956,970,311	-22,641,060	-	1,554,358
F	-	849,619,406	23,280,824	-	-623,420
G	-	-284,915,222	-8,593,548	-	0

NOTE: 1. $\sigma = A + B\,\varepsilon + C\,\varepsilon^{1/2} + D\,\varepsilon^{1/3} + E\,\varepsilon^{1/4} + F\,\varepsilon^{1/5} + G\,\varepsilon^{1/6}$

Table 4.9 Coefficients Used to Describe the Stress-Strain Curve of the Weld Sections

COEFF-CIENTS	STRAIN RANGE $x10^{-6}$ mm/mm				
	0-951	951-4420	4420-28700	28700-50800	50800-104500
A	-	-	-	536.7	-
B	210,000	-28,444,247	-987,409	262.4	-1,198,938
C	-	94,467,798	8,755,744	-	9,259,263
D	-	-329,955,827	-42,271,664	-	-29,204,869
E	-	612,003,112	92,124,549	-	36,427,565
F	-	-542,450,426	-89,940,250	-	-15,431,656
G	-	181,714,074	32,134,453	-	-

NOTE: 1. $\sigma = A + B\varepsilon + C\varepsilon^{1/2} + D\varepsilon^{1/3} + E\varepsilon^{1/4} + F\varepsilon^{1/5} + G\varepsilon^{1/6}$

Table 4.10 Uniaxial-Compressive and Tensile Strength for Concrete

TIME (t) days	COMPRESSIVE STRENGTH MPa		TENSILE STRENGTH MPa		
	EXPERIMENTAL	EMPIRICAL[1]	MODULUS OF RUPTURE	SPLIT 'T' CYLINDER	EMPIRICAL[3]
21	24.6	23.9	-	-	2.93
28	29.1 26.9	29.0	-	-	3.23
35	33.9 33.6 31.7	32.4	3.45	-	3.42
42	34.4 33.8 33.7	34.5	3.78	-	3.52
49	38.0 37.4 34.6	35.7	4.14	-	3.58
56	35.2 34.9	36.4	-	3.02 (4.53)	3.62
63	38.0 37.1	37.1	-	2.76 (4.14)	3.65

NOTES: 1. $f'_c = 5.69 + 2.03t - 0.034t^2 + 0.0002t^3$

2. The flexure strength of 1/3 point loaded 6 in. x 6 in. beams = 1.35 to 1.65 (average 1.50) times the split cylinder strength. The average adjusted value is found in the brackets.

3. $f_r = 0.6\sqrt{f'_c}$, where f'_c is based on the empirical Equation 4.4.

Table 4.11 Coefficients Used in the Mathematical Expressions which Describe the Composite Stub Column Load-Strain Curve

COEFF-CIENTS	STRAIN RANGE $x10^{-6}$ mm/mm			
	0-637	637-4955	4955-5506	5506-6171
A	-	-	1665.0	1635.0
B	1,035,219	57,473,448	-54,446	-45,865
C	-	-196,666,987	-	-
D	-	684,439,482	-	-
E	-	-1,264,776,681	-	-
F	-	1,118,022,065	-	-
G	-	-373,791,061	-	-

COEFF-CIENTS	STRAIN RANGE $x10^{-6}$ mm/mm			
	6171-6652	6652-6936	6936-7500	7500-7981
A	1604.5	1543.8	1483.3	1424.0
B	-126,195	-213,732	-105,142	-19,751
C	-	-	-	-
D	-	-	-	-
E	-	-	-	-
F	-	-	-	-
G	-	-	-	-

NOTE: 1. $P_{csc} = A + B\varepsilon + C\varepsilon^{1/2} + D\varepsilon^{1/3} + E\varepsilon^{1/4} + F\varepsilon^{1/5} + G\varepsilon^{1/6}$

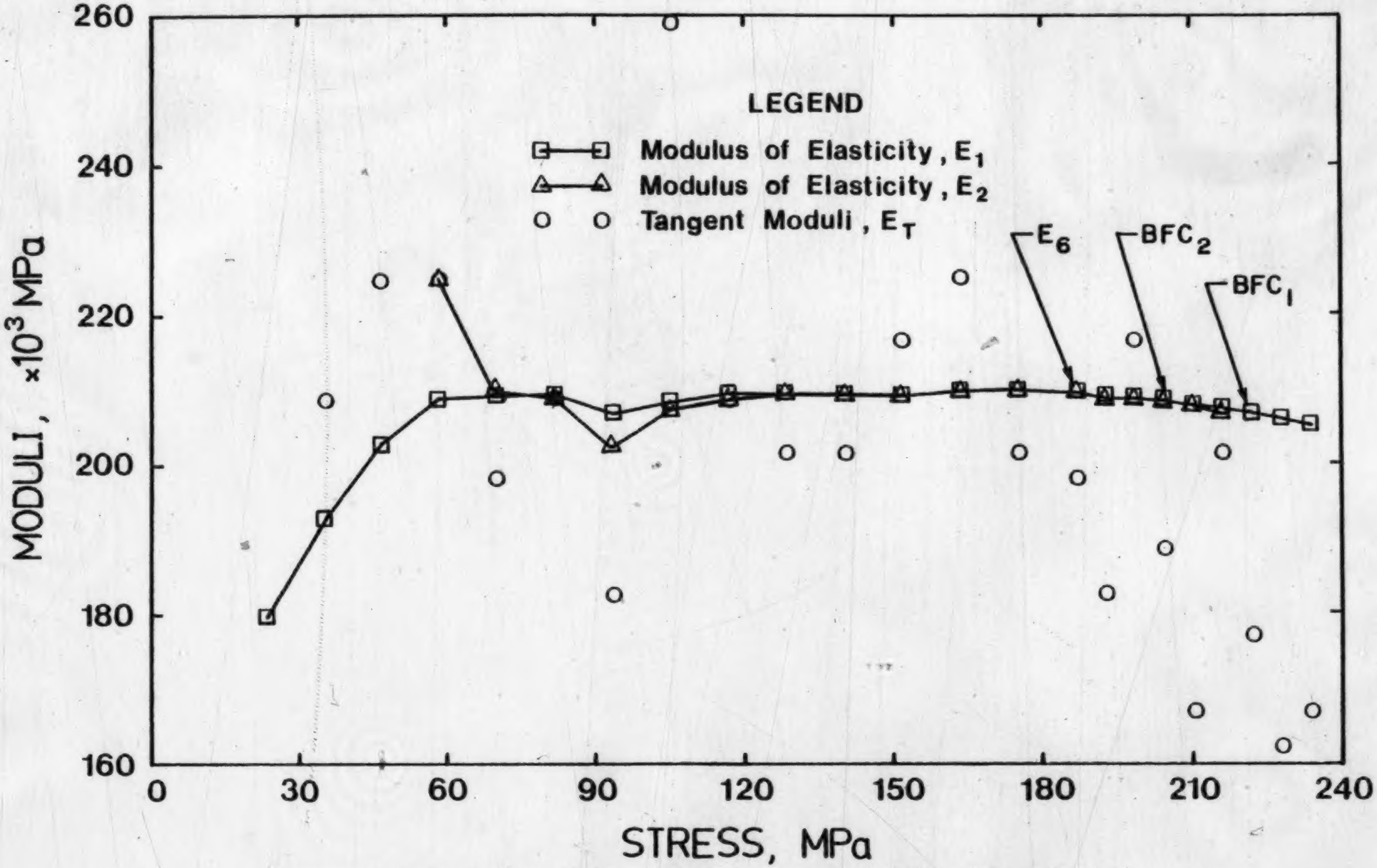

Figure 4.1 Decision Making Model for Determination of the Modulus of Elasticity for Steel Sections

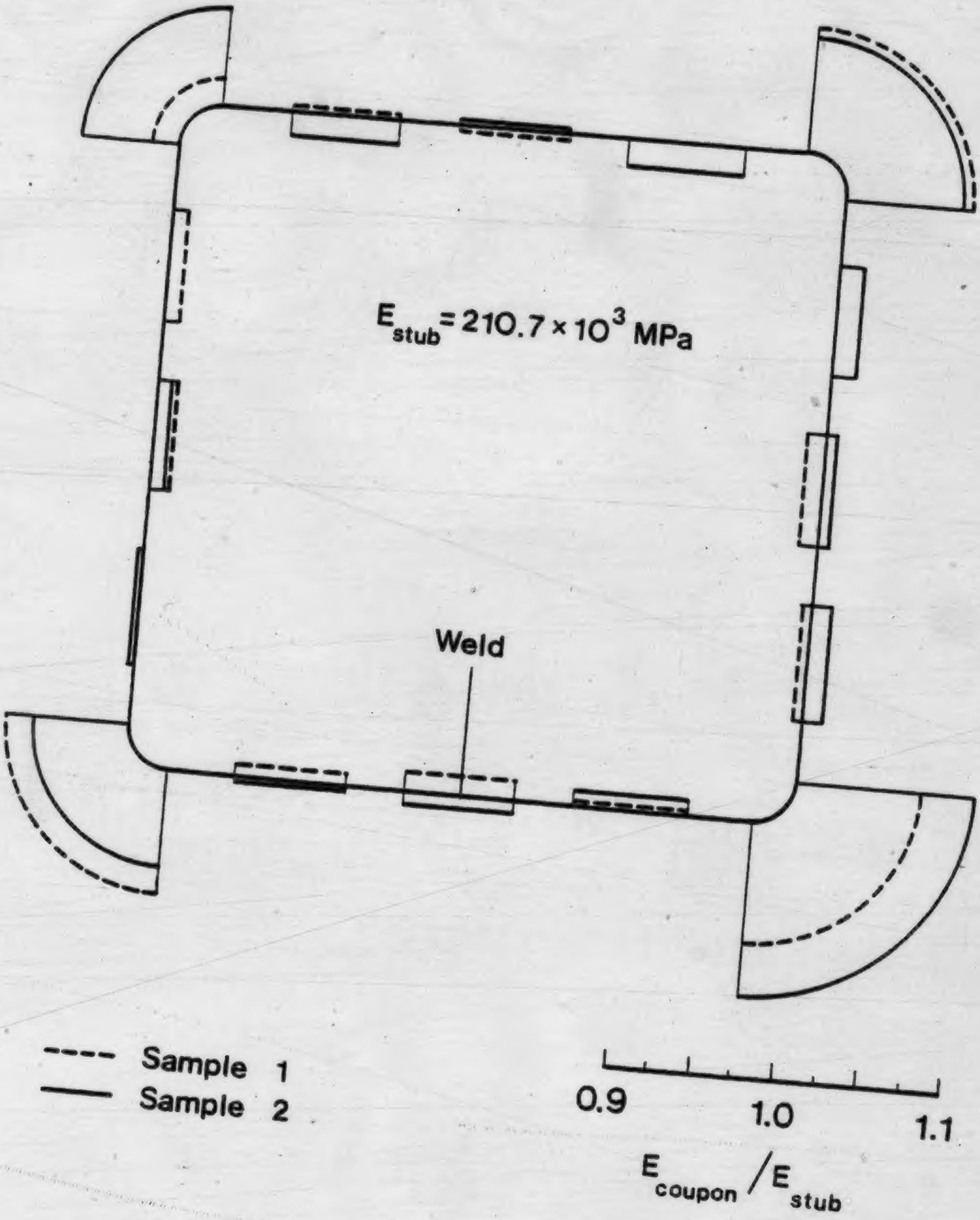

Figure 4.2 Modulus of Elasticity Distribution

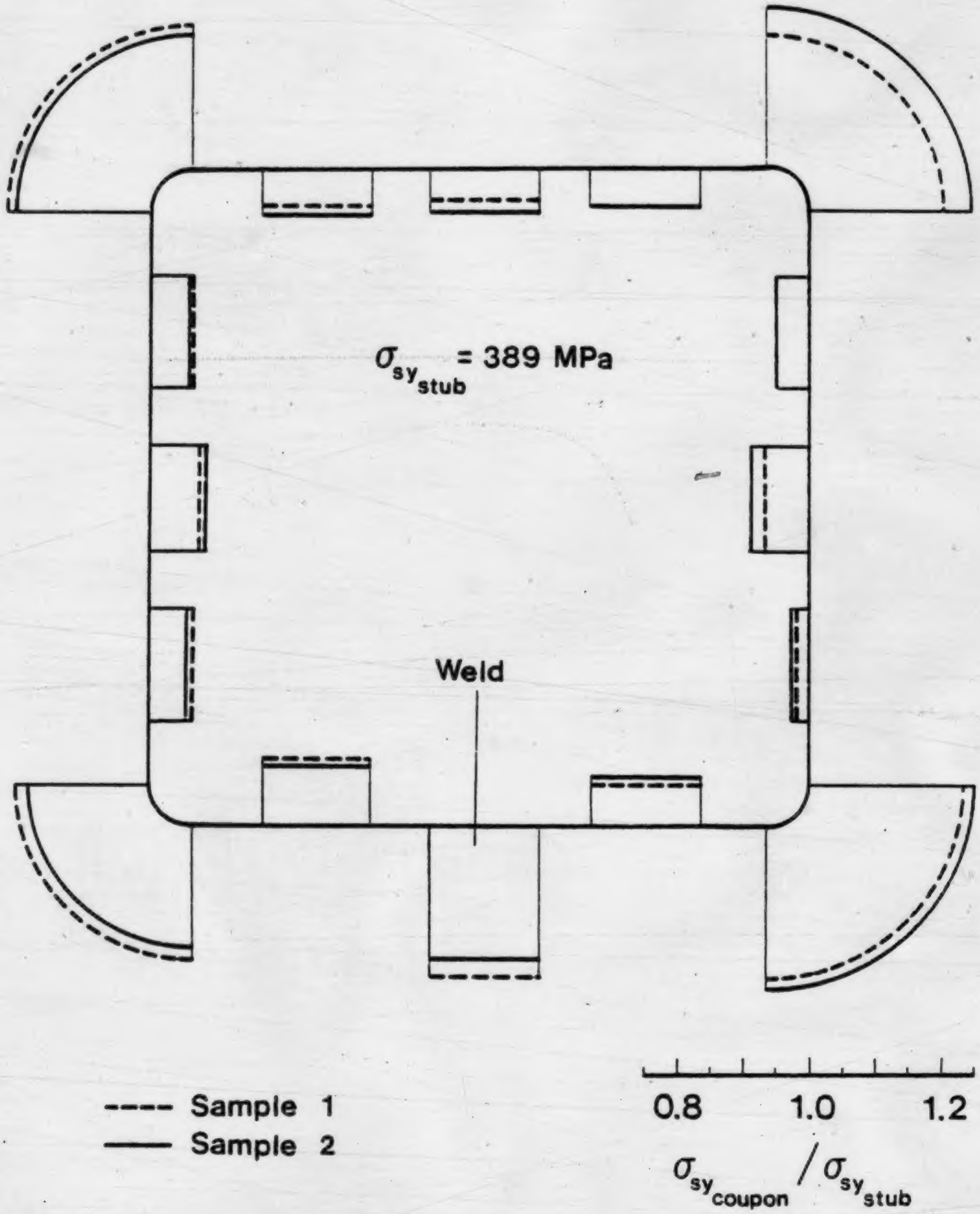

Figure 4.3 Static Yield Stress Distribution

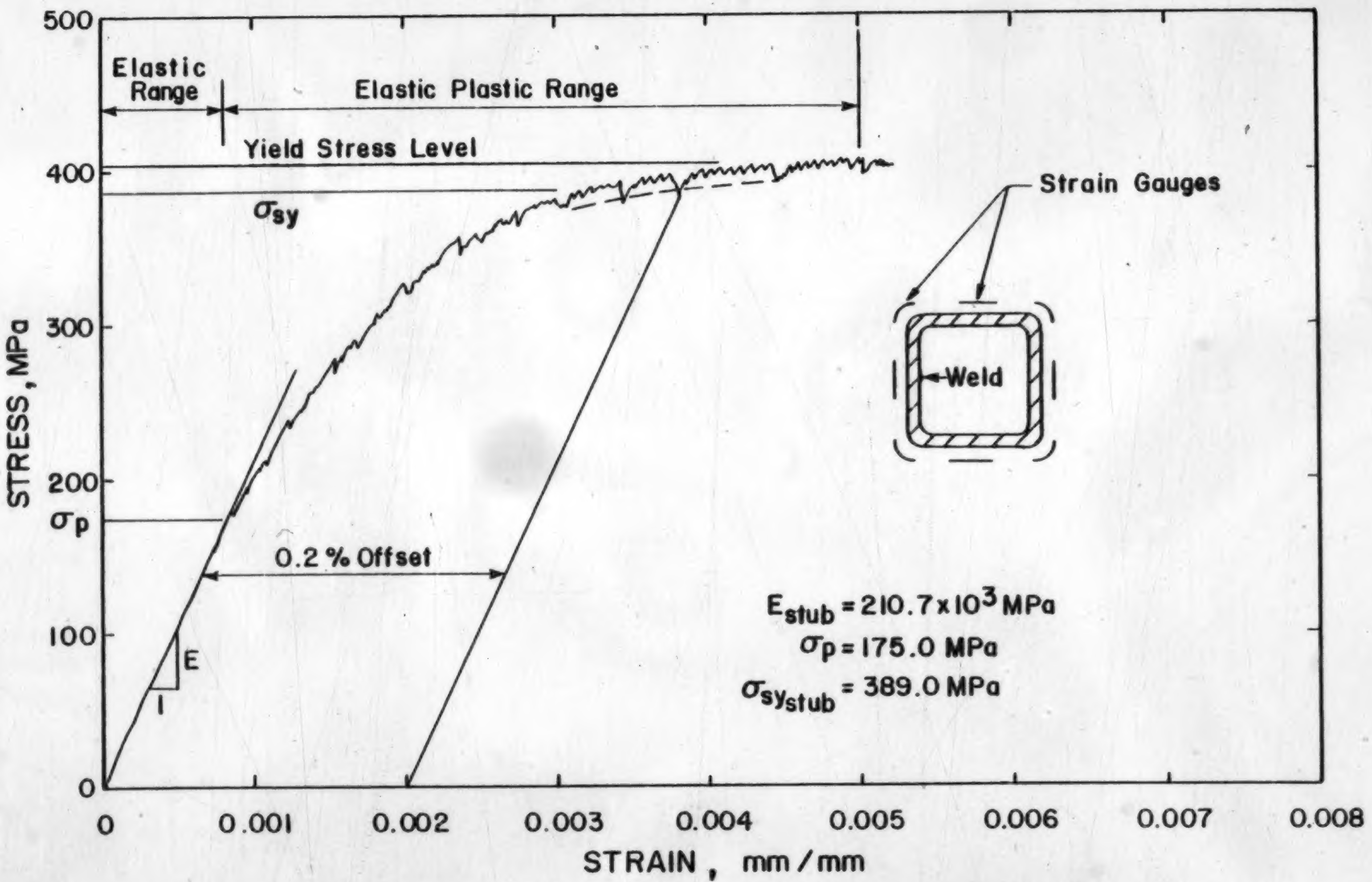

Figure 4.4 Stress Strain Curve for Steel Stub Column

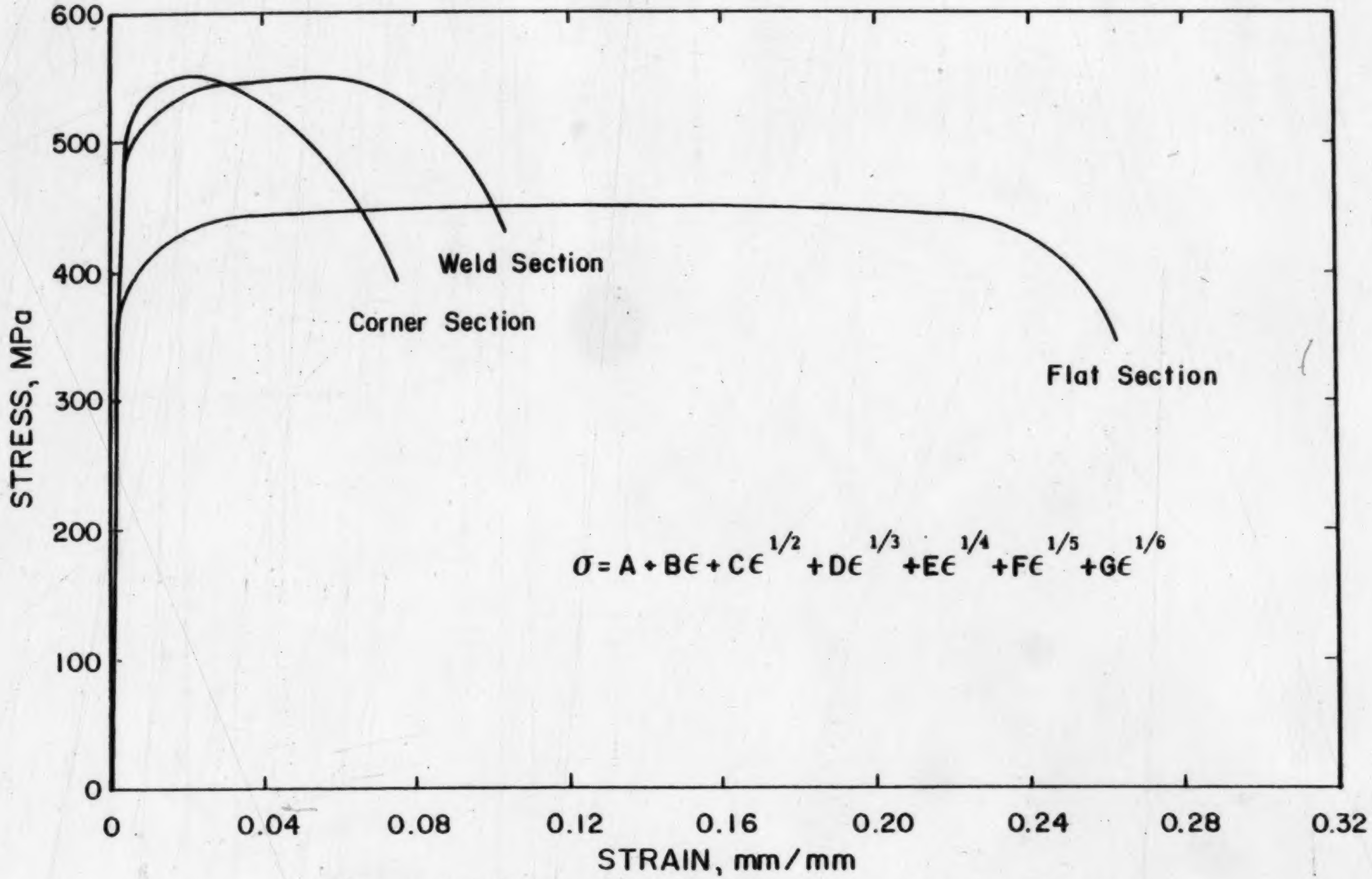

Figure 4.5 Stress Strain Curves from Tension Coupons

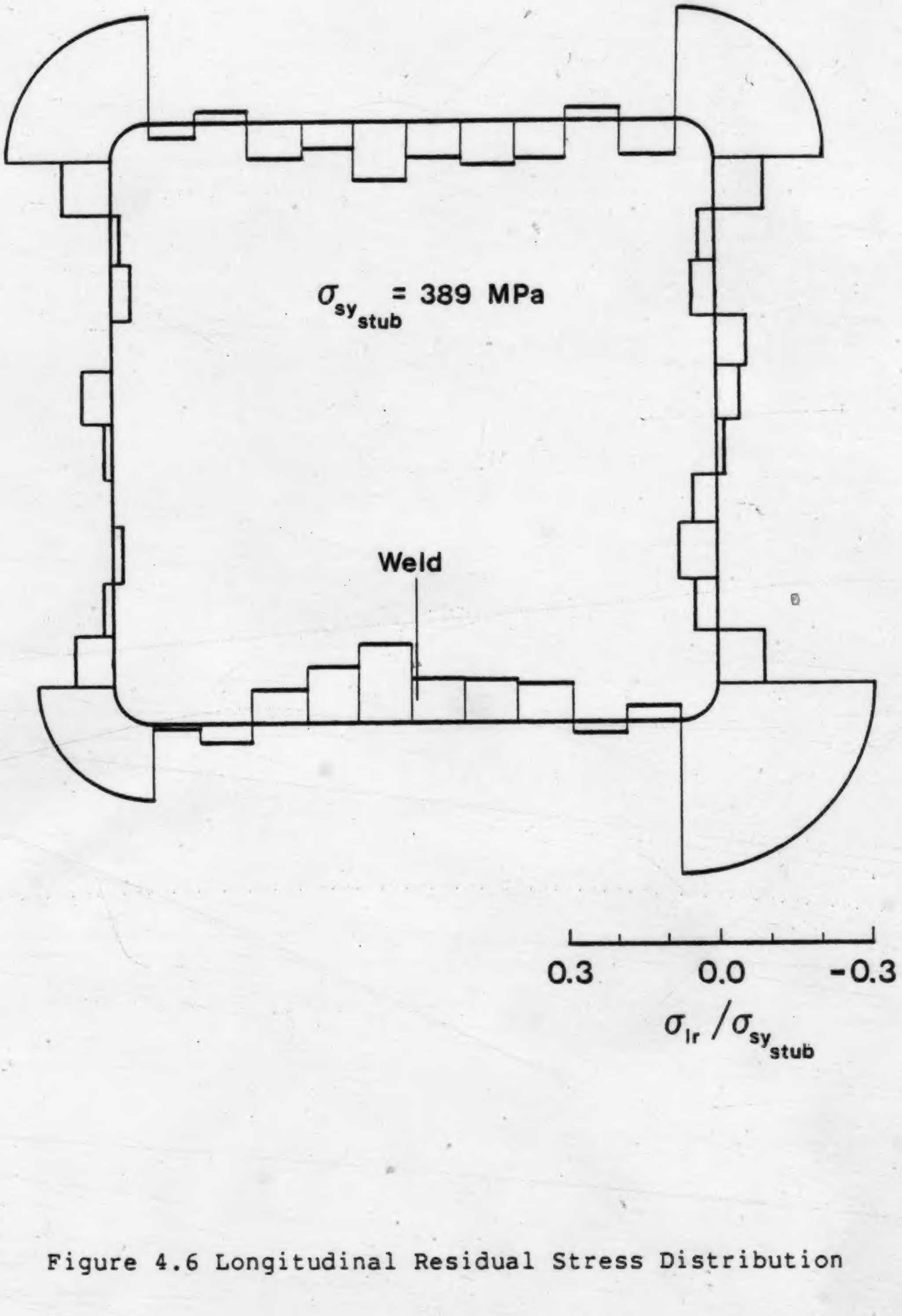

Figure 4.6 Longitudinal Residual Stress Distribution

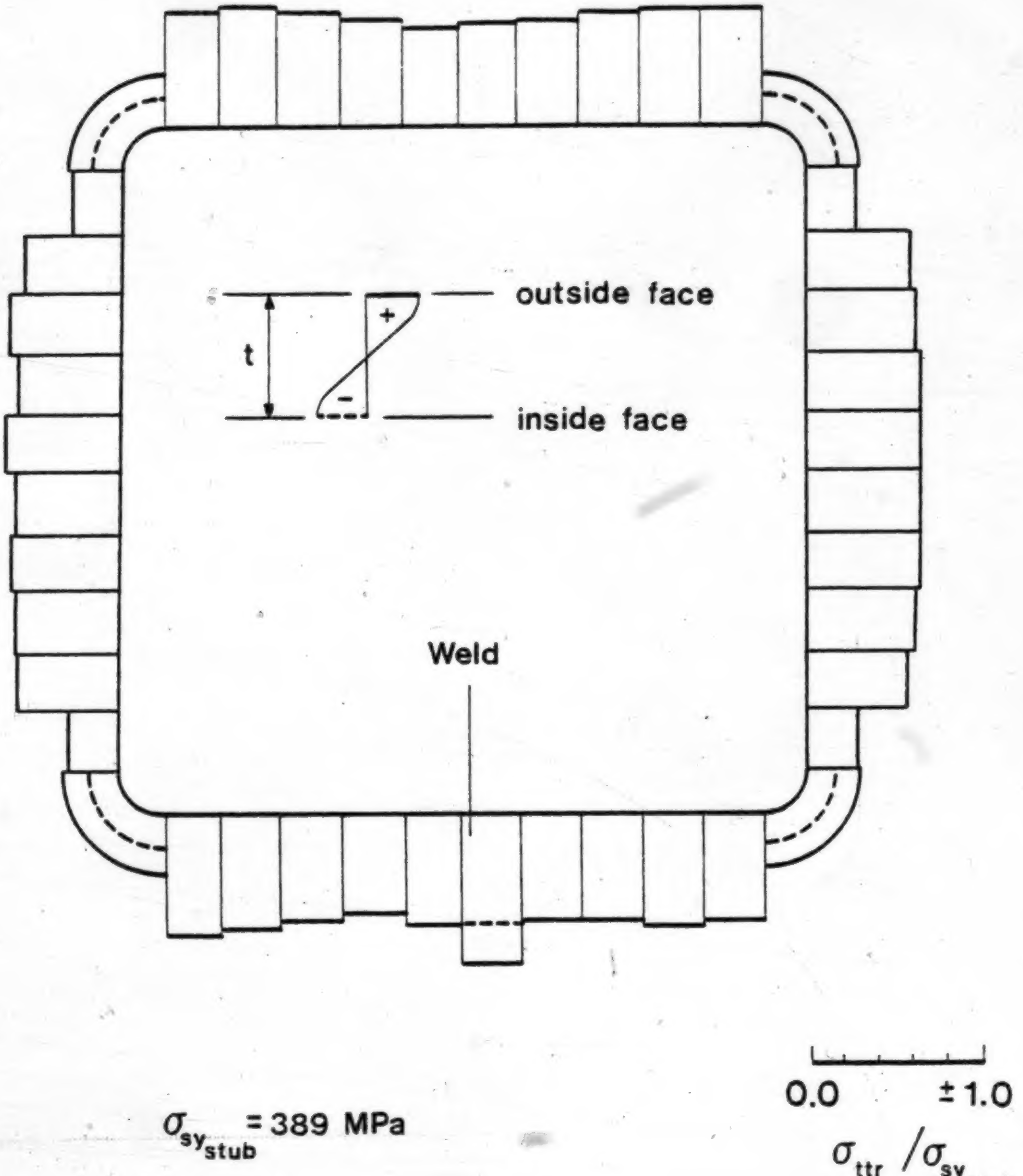
outside face
inside face
t
+
-
Weld
$\sigma_{sy_{stub}}$ = 389 MPa
0.0
±1.0
$\sigma_{ttr} / \sigma_{sy_{stub}}$

Figure 4.7 Through the Thickness Distribution of Longitudinal Residual Stresses

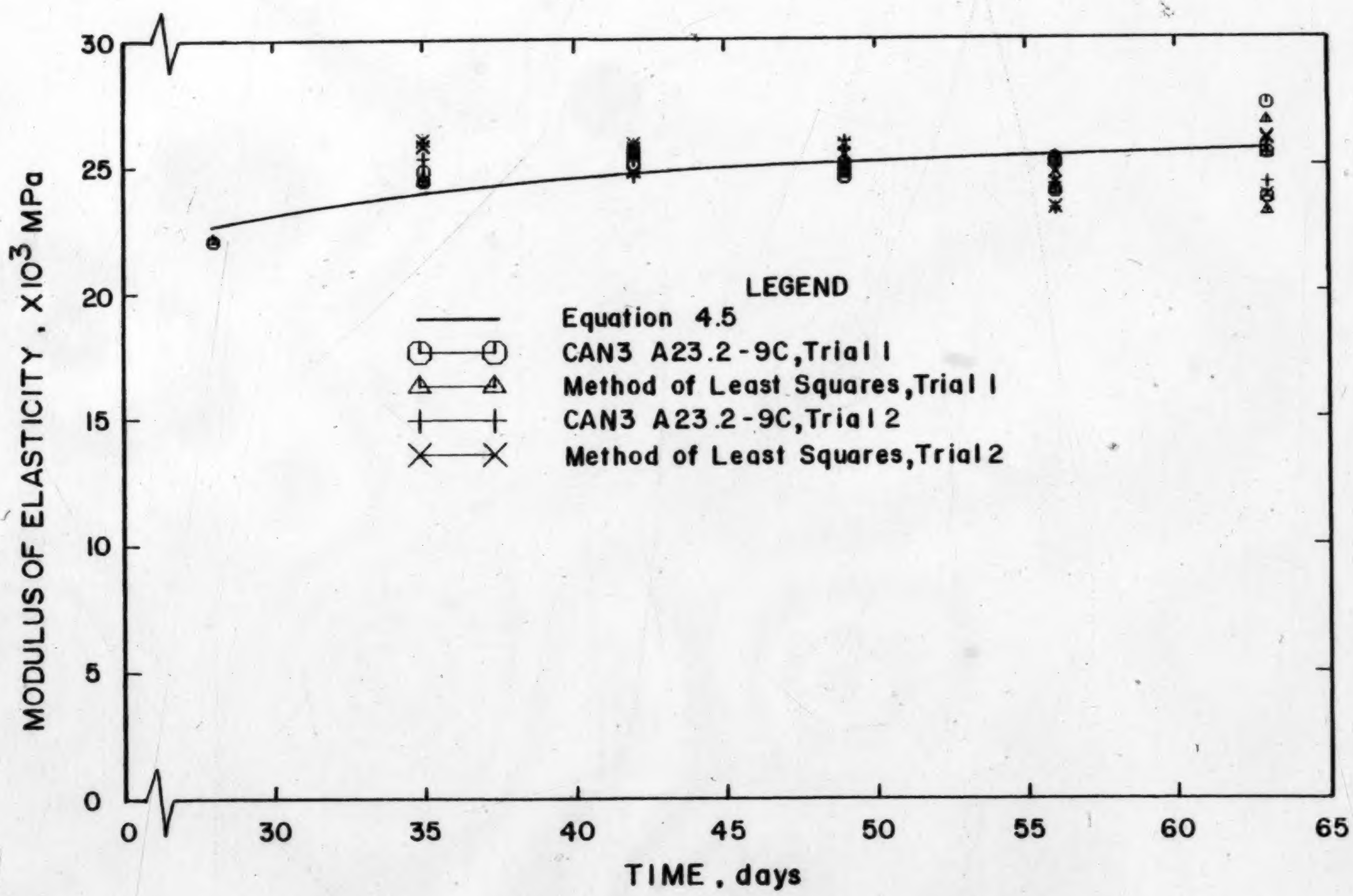

Figure 4.8 Modulus of Elasticity of Concrete

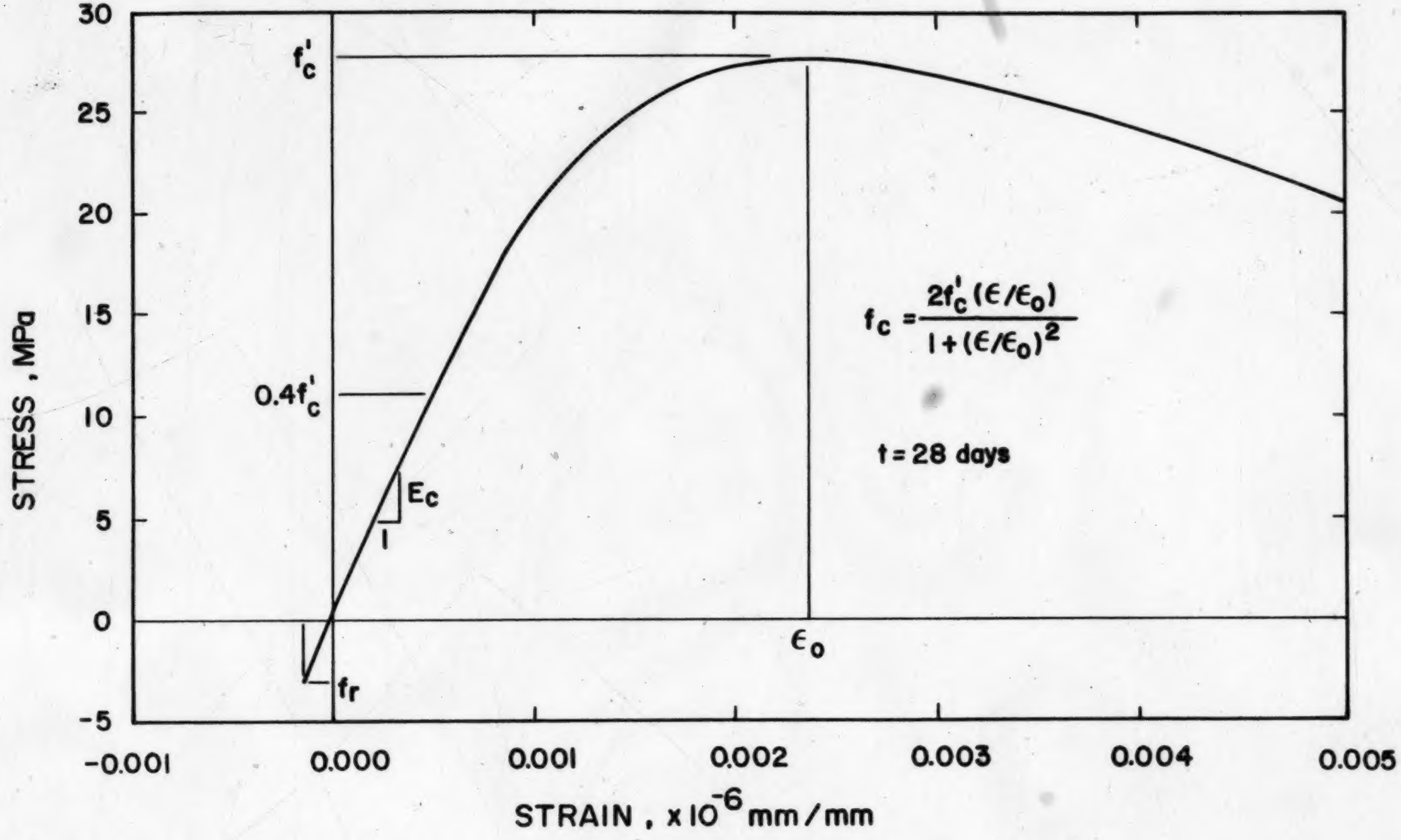

Figure 4.9 Idealized Uniaxial Stress Strain Curve for Concrete

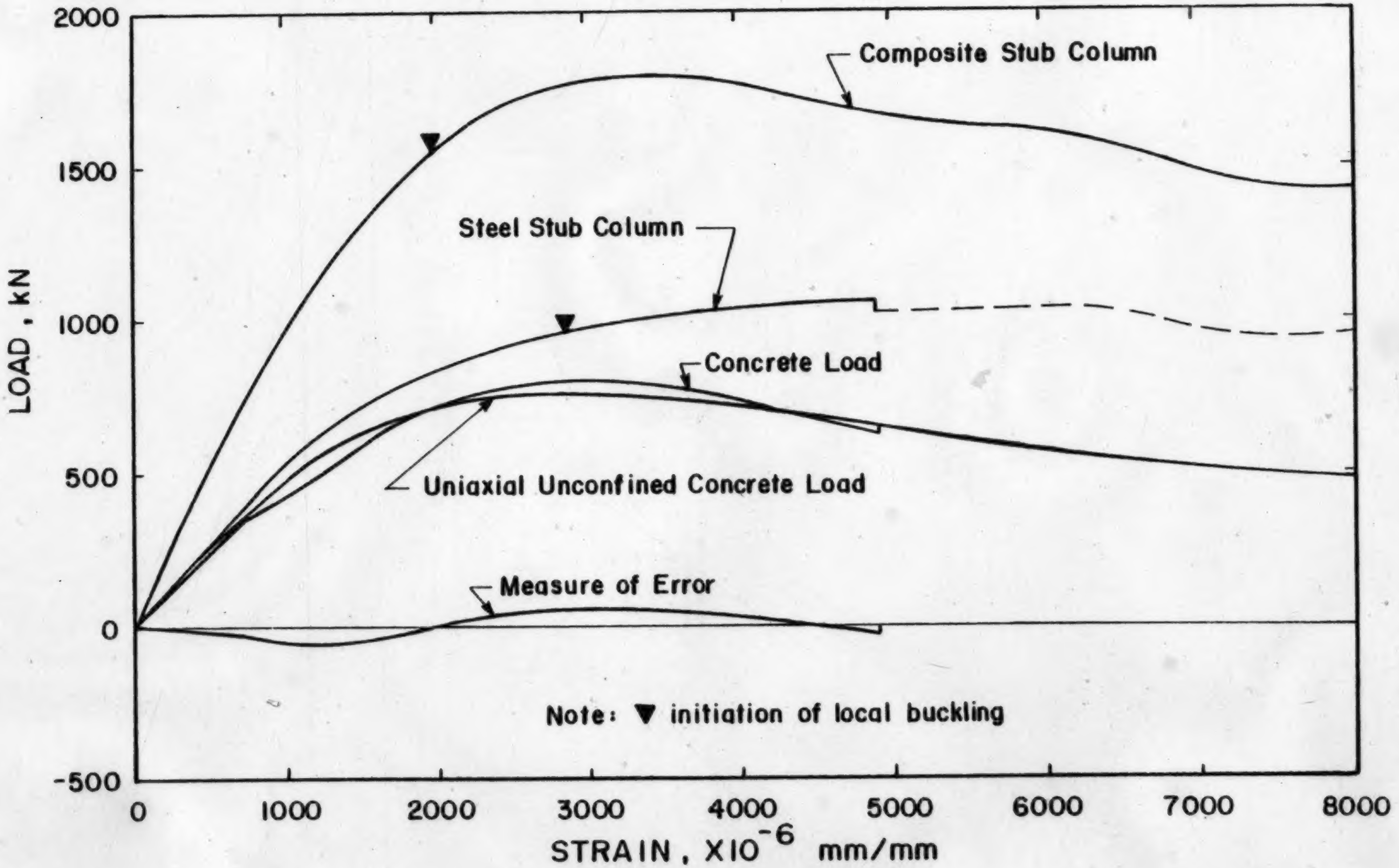

Figure 4.10 Composite Stub Column Analysis

5. TEST RESULTS AND GENERAL BEHAVIOUR

5.1 Knife Edge Fixtures

All columns were tested as pinned-end specimens. During the test end-rotations were monitored to ascertain whether the knife edge assemblages allowed pinned-end rotations to occur. It is commonly recognized that it is practically impossible to obtain absolutely perfect pinned ends, since some friction and other resistance will always be present. The end rotations were calculated from Equation 5.1 on the assumption that the deflected shape of a perfectly pinned-ended specimen is a half sine wave.

$$\theta = \frac{PeL}{2EI} + \frac{P\left(e_o + \delta\right)L}{\pi EI} \tag{5.1}$$

where, θ = end rotation of a pinned end column, radians
P = applied load, kN
L = distance between the points of rotation, mm
E = modulus of elasticity for the section, MPa
I = moment of inertia for the section, mm^4
e = eccentricity of applied load, mm
e_o = initial out-of-straightness at midheight, mm
δ = center-line deflection at midheight of the column under the applied load, mm

Experimental and predicted values of end rotations for the steel column tests have been plotted as a function of applied load for concentrically and eccentrically loaded test specimens in Figure 5.1 and 5.2, respectively. The measured values are accurate to ± 350 microradians and the predicted values are only valid within the elastic range. Comparison of the measured and predicted end rotations shows that the knife edge assemblages modelled pinned-ended connections closely.

5.2 Column Test Results

5.2.1 Initial Out-of-straightness

The initial out-of-straightness for each column was established in the north-south and east-west directions from a series of measurements taken from dial gauges mounted on a stiff aluminum angle. These values were adjusted to determine the relative out-of-straightness with respect to the reference measurements. As shown in Figure 5.3, the average of the difference between the sum of the two measurements made on one face from the sum of the measurements made on the opposite face, is the initial out-of-straightness of the column at that level. The out-of-straightness values for a typical column, C604, are given in Table 5.1. The maximum out-of-straightness, expressed as a ratio of column length and given by Equation 5.2 for all columns are given in Table 5.2.

$$\frac{e_o}{L} = \frac{1}{Z} \qquad (5.2)$$

where, Z = out-of-straightness

The maximum out-of-straightness was 1/1590 for test specimen C605. In the plane of bending, the north-south direction, the mean value for initial out-of-straightness of 1/12600 is significantly less than the specified maximum for hollow structural sections of 1/500.

5.2.2 General Behaviour

Table 5.3 gives the pertinent details for the nineteen columns tested and Figures 5.4 through 5.7 illustrate the load deflection curves for these tests. The load-deflection curves for both strain compatible and non-strain compatible composite columns with concentrically and eccentrically applied load are shown in Figures 5.6 and 5.7, respectively, to permit a direct evaluation of end connection effect. The load-deformation curves are based on load measurements made as the load was being applied, with the maximum strength being represented by the peak of each curve. The maximum static column strength was obtained at the same point by recording the maximum load at a zero strain rate, which is characterized by the stabilization of the column i.e. - no further deflection at midheight.

The load-deflection curves for the steel column series, Figures 5.4 and 5.5, exhibit normal characteristics. For concentrically loaded columns C201 and C601 the effect of any initial out-of-straightness is virtually negligible. Extensive yielding had occurred in both columns C201 and C202 by the time they had failed by local buckling of the tube wall. Figure 5.8(a) shows this typical failure mode. All other columns of this series failed through overall buckling of the specimen. Note that columns C601 and C602 eventually failed by local buckling of the tube at midheight of the column. Column C1201 with a slenderness ratio of 117.6 failed through overall elastic buckling. This specimen was unloaded and regained its original shape as verified by out-of-straightness measurements. It was retested with an applied load at a constant eccentricity of 65 mm, column C1201E, and exhibited identical behaviour to its counterpart column C1202.

The load-deflection curves for the composite column series, Figures 5.6 and 5.7 are similar to the steel columns all exhibiting normal characteristics with the exception of column C205. Column C205, a non-strain compatible column, with a length of 1200 mm and an initial out-of-straightness of 1/19700, was tested under a concentrically applied load. Essentially the steel shell slid down the concrete core and buckled outwardly on four faces at three levels. Yield lines were evident on all four connection plates. This failure mode is shown in Figure 5.8(b). Strains along the length of the column were two to three times the static yield strain for the section. Column C203, the counterpart to C205, failed by outward buckling of the steel wall on three sides and simultaneous crushing of the concrete. This failure mode is typified by a sketch, as shown in section in Figure 5.8(c).

The eccentrically loaded 1200 mm long columns, C204 and C206, failed through overall buckling and eventually developed the failure mode previously described. Composite columns of the 600 and 1200 series all failed through overall buckling.

Apart from the ultimate loads obtained, the general load deflection behaviour of the non-strain compatible beam columns is comparable to the corresponding strain compatible beam columns. There is no difference in the flexural stiffness between the two types. When strain compatibility is not ensured, the reduction in load carrying capacity varies from 0 per cent to 18 per cent for concentrically loaded columns of slenderness ratios of 118 and 20, respectively and less for eccentrically loaded columns. In general, the effect of the concrete is to increase the flexural stiffness and to stabilize the tube wall against local buckling.

5.2.3 Deflected Shapes

Figures 5.9 and 5.10 are typical examples of the load deformation history of concentrically and eccentrically loaded columns which failed through overall buckling. The half sine wave shapes shown here are consistent with the assumption made in Section 5.1 and they illustrate quite clearly that the knife edge assemblages functioned as pinned-ended connections. The small and erratic behaviour of column C203, as shown in Figure 5.11, is indicative of columns with small slenderness ratios which realize high strains along the length of the column before failing by local buckling. As shown in Figures 5.9 through 5.11, relatively small deflections for most of the load history are attributed to small values of initial out-of-straightness and to the precise alignment of the column in the loading apparatus.

5.2.4 Steel Strain Distributions

The resulting steel strain distributions for the non-strain compatible column series are presented in Figures 5.12 through 5.17 as a function of non-dimensional height for a series of loads depicting the load history.

Figures 5.12, 5.13 and 5.14 gives the steel strain distributions for concentrically loaded columns with slenderness ratios of 20, 59.9 and 117.6, respectively. The predominant features of these distributions are noted here.

1. At small loads, the strains along both sides of the column are virtually equal and constant, indicating that the load was applied concentrically at the section.
2. The erratic distribution of strain values at the upper end of the column just below the connection plates, as in C605 and C1205, and those for C205 of ultimate load are attributed to out-of-plane displacements of the tube wall (localized bending effects).
3. The general shape of the average steel strain distribution for tests C605 and C1205 is one which decreases in magnitude, from a maximum value at the upper end, asympotically to a constant value at the lower end of the column.

4. Differences of strain values from one side of the column to the other are due to overall bending of that column.

Figures 5.15 through 5.17 show the steel strain distributions for eccentrically loaded columns with the same series of slenderness ratios. Similar observations can be made about the strain differences and erratic distributions for the eccentrically loaded columns.

Although the magnitude of the strain values for the steel and strain compatible column series may differ from the non-strain compatible column series, the shape, and relative increase in strain value to increase in load is similar to that presented in Figures 5.12 through 5.17 for corresponding column lengths and load applications.

5.2.5 Concrete Strain Distributions

The resulting compressive concrete strain distributions for the south face of the non-strain compatible column series are presented in Figure 5.18 through 5.22 and 5.24 as a function of non-dimensional column height for a series of loads depicting the load history. Figure 5.23 is a similar presentation of concrete strain data for the north face of test specimen C606.

In these figures two reference lines have been drawn, a zero strain line and a parallel line, which mark the maximum tensile strain before rupture, as described for the uniaxial stress-strain model for concrete in Section 4.2.1.4.

Strains that are not considered reliable, due to a loosening of the embedded bars during installation are marked as spurious points. When these bars reached their maximum travel, i.e. the bars made contact with the steel shell, the readings at these locations were discontinued and therefore not reported.

5.2.6 Slip Distributions

Slip distributions are descriptions of the relative movement of the concrete core with respect to the steel shell at any point along the length of the column. These were determined for the non-strain compatible test series by two methods.

1. Method A - slip distributions were calculated by integrating the difference in measured steel and concrete strains from the lower end of the column where no slip occurred to the upper end.
2. Method B - slip distributions were measured directly as the difference in movement between a demec point on the steel shell and one mounted on a horizontal bar embedded in the concrete and modified to account for the change in length of the steel tube under the applied load, over the gauge length of the slip measurement.

The slip distributions as determined by Method B are considered more reliable than those by Method A. With the exception of one for comparison, the distributions as determined by Method B are the only ones presented. Due to the limited travel of the embedded bar with respect to the shell, the maximum measureable slip was approximately 3.2 mm. This limit is shown on all slip distribution figures.

The slip distributions for concentrically loaded non-strain compatible columns are shown in Figures 5.25 through 5.29. Figures 5.25 and 5.26 are comparable slip distributions for the south face of column C205, as determined by Method B and Method A, respectively. The pertinent features of these distributions are:

1. The maximum slip value, which occurs at the upper end of the column, decreases as the column becomes more slender.
2. Virtually no slip occurred at midheight on either face of column C1205.
3. The slip distributions for C205 and C605 are linear.

Slip distributions for both the north and south faces of the eccentrically loaded non-strain compatible columns are shown in Figures 5.30 through 5.35. The most significant feature is the decrease in the maximum slip value as the column becomes more slender and as the eccentricity of the applied load increases. For example, the maximum slip for the eccentrically loaded column C1206 is approximately 0.2 mm, one-fifth of the value of its concentrically loaded counterpart C1205. Spurious measurements are marked.

5.3 Flexural Tests

Table 5.4 gives pertinent details for the six beams tested and Figure 5.36 illustrates the moment-curvature curves for these tests. The moments have been calculated from dynamic load measurements and the curvature, based on the strain distribution at center span, was calculated from the values of strain as measured by gauges mounted on the steel, top and bottom of the beam. These curves exhibit normal characteristics.

Both steel beams failed by local buckling of the tube wall, typified by an inward buckle on the compression flat and outward buckles of the web flats, as shown in Figure 5.37(a). All composite sections failed with a tensile failure of the bottom chord flat, crushing of the concrete core and outward local buckling of the compression flat, as shown in section, in Figure 5.37(b). Failure was initiated in the region of the steel rods which were embedded in the concrete and used as mounts for Demec points, as discussed in Section 3.3.2. In the non-strain compatible cases the relative displacement of the concrete core with the steel shell at both ends of the beam, was negligible. Apart from the ultimate moment capacities the results of these tests are not discussed further.

Table 5.1 Reduced Data Derived from the Out-of-Straightness Measurements for Column C604

LOCATION h/L	EAST		WEST		
	5	6	1	2	NET
0.9397[3]	0.0	0.0	0.0	0.0	0.0
0.8675	0.869	3.099	0.523	0.109	0.833
0.7450	2.436	3.223	1.615	0.767	0.820
0.6225	1.638	2.375	0.495	-0.605	1.031
0.5000	1.554	2.327	0.257	-0.767	1.097
0.3775	1.085	1.819	0.025	-0.856	0.935
0.2550	1.951	2.626	1.194	0.696	0.673
0.1325	0.295	0.587	-0.290	-0.549	0.429
0.0281[3]	0.0	0.0	0.0	0.0	0.0

LOCATION h/L	NORTH		SOUTH		
	3	4	7	8	NET
0.9397[3]	0.0	0.0	0.0	0.0	0.0
0.8675	-0.475	-1.514	1.956	0.0528	-1.118
0.7450	0.008	-2.090	2.515	2.202	-1.699
0.6225	-1.255	-3.683	2.002	1.560	-2.126
0.5000	-1.341	-3.536	2.116	1.735	-2.182
0.3775	-1.295	-3.005	1.796	1.516	-1.902
0.2550	0.414	-0.478	2.814	2.751	-1.417
0.1325	-0.577	-0.963	0.676	0.0742	-0.726
0.0281[3]	0.0	0.0	0.0	0.0	0.0

NOTE: 1. The net value is equal to the average of the sum of readings on one face less the sum of the readings on the opposite face.
2. All measurements are in millimeters.
3. The measurements at these levels were used as reference measurements.

Table 5.2 Summary of Initial Curvatures Derived From Out-of-Straightness Measurements

TEST	EAST-WEST DIRECTION Z	NORTH-SOUTH DIRECTION Z
C201	39370	11520
C202	20540	5030
C203	3030	18900
C204	8750	78740
C205	13500	19690
C206	5560	7870
C601	3143	17284
C602	4030	4040
C603	2760	6880
C604	3280	1650
C605	2560	1590
C606	3440	2310
C1201	13850	7790
C1201E	7480	7571
C1202	4250	1600
C1203	12250	12700
C1204	8480	15570
C1205	5900	8180
C1206	6630	9990

Table 5.3 Column Test Results

SPECIMEN	P_{ult} kN	FAILURE MODE AND REMARKS
		C200 COLUMN SERIES, 1200 mm long, Kl/r=20
C201	1007	local buckling at a distance d from the bottom end, see figure 5.8(a);
C202	485	local buckling at a distance d/2 from the bottom end, see figure 5.8(a);
C203	1517	local buckling / crushing of concrete, see figure 5.8(c);
C204	721	overall buckling;
C205	1179	outward local buckling of steel wall, see figure 5.8(b);
C206	635	overall buckling;
		C600 COLUMN SERIES, 3600 mm long, Kl/r=59.9
C601	868	overall buckling (load applied by load control);
C602	347	overall buckling;
C603	1271	overall buckling;
C604	479	overall buckling;
C605	1214	overall buckling;
C606	465	overall buckling;
		C1200 COLUMN SERIES, 7070 mm long, Kl/r=117.6
C1201	357	overall elastic buckling;
C1201E	197	overall buckling;
C1202	197	overall buckling;
C1203	476	overall buckling;
C1204	243	overall buckling;
C1205	481	overall buckling;
C1206	242	overall buckling;

Notes: 1. P_{ult} is the static maximum load (zero strain rate).

2. All test were tested under stroke control except C601 which was tested under load control.
3. K=1.0 for pinned end specimens and the radius of gyration is based on the steel section properties alone.
4. Odd and even numbered specimens were tested concentrically and eccentrically respectively.
5. The last digit of the specimen identification number designates the type of column: steel (1,2), composite strain compatible (3,4), and composite non-strain compatible (5,6).

Table 5.4 Flexural Test Results

SPECIMEN and TYPE	LENGTH mm	M_{ult} kNm	FAILURE MODE AND REMARKS
B21 Steel	2000	67.9	Inward local buckling of the upper flange in the shear span, 110 mm from the loading pad;
B25 Steel	2000	62.2	Inward local buckling of the upper flange in the constant moment region, 155 mm from the loading pad, Figure 5.37(a);
B22 Composite	2000	83.2	Tensile failure of the lower flange, outward buckling of the upper flange with crushed concrete, at a demac point location 125 mm from center span, Figure 5.37(b);
B23[2] Composite non-strain compatible	2000	76.9	Similar to B22, Figure 5.37(b);
B24 Composite non-strain compatible	2000	80.2	Similar to B22, Figure 5.37(b);
B41 Composite	4000	75.0	Similar to B22, Figure 5.37(b);

Notes:
1. The displacement of the concrete core with respect to steel shell at either end was negligible for all composite non-strain compatible flexural tests.
2. The inside of the tube was coated with form oil.

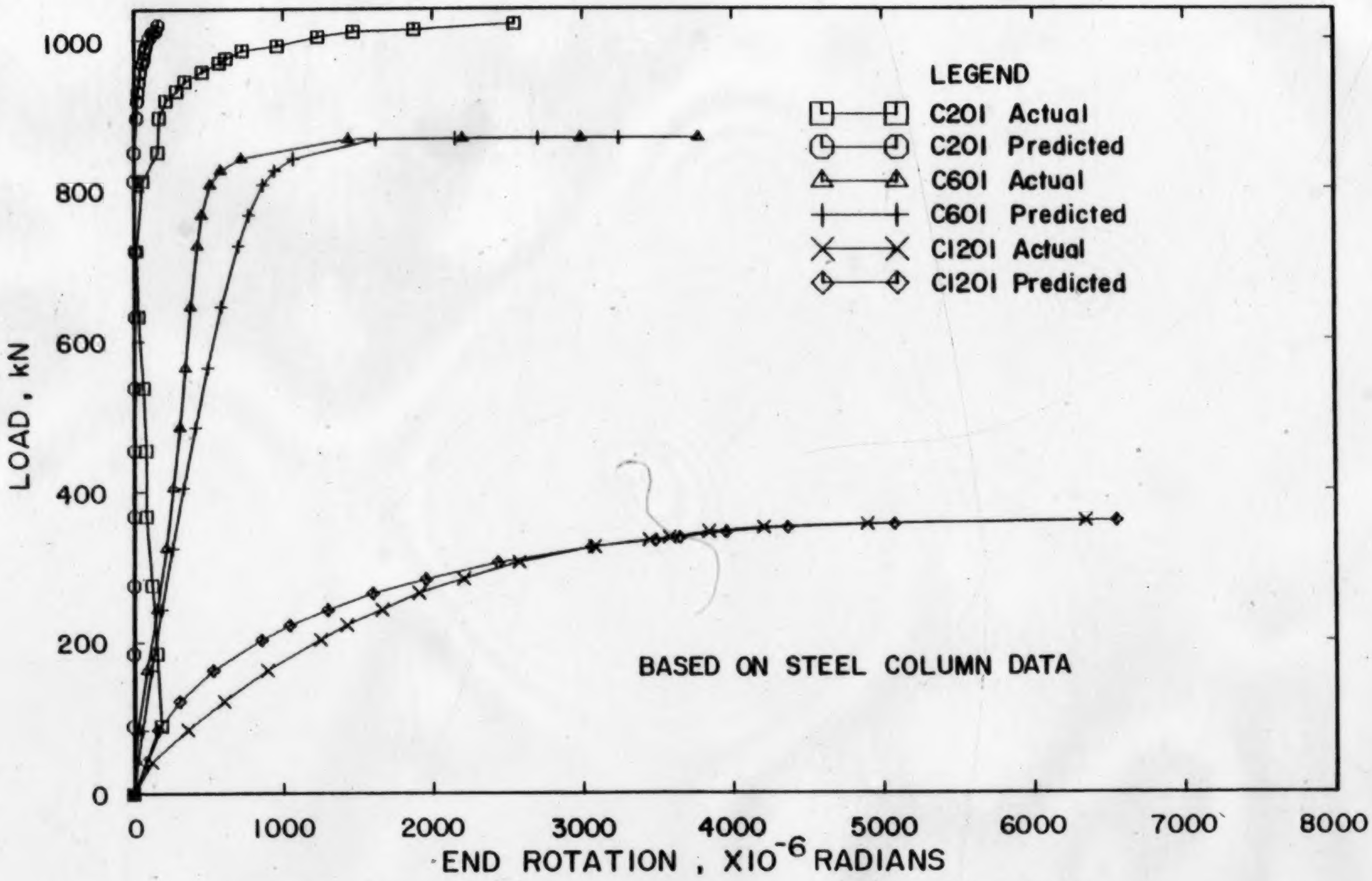

Figure 5.1 End Rotation, Concentrically Loaded Columns

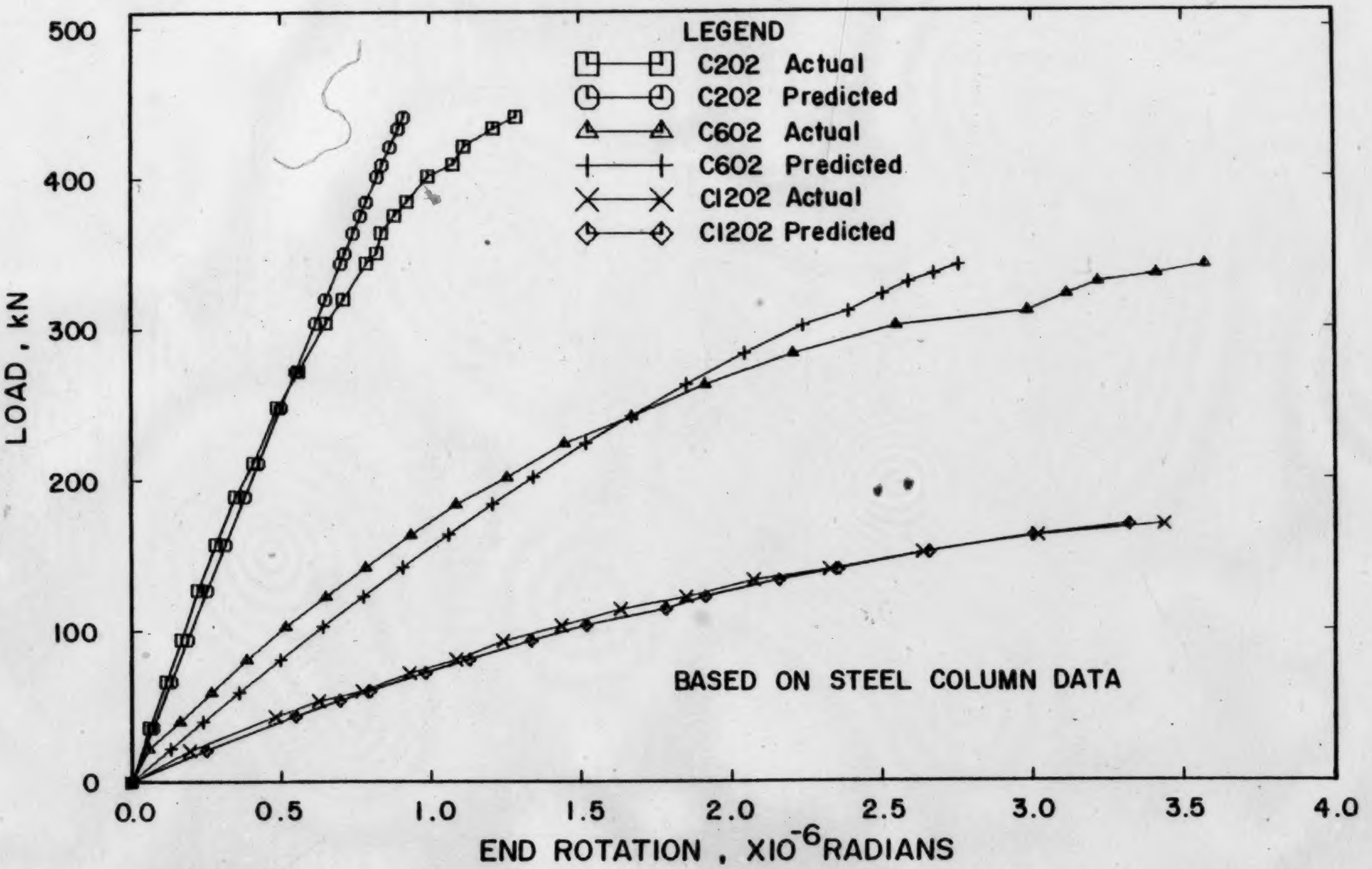

Figure 5.2 End Rotation, Concentrically Loaded Columns

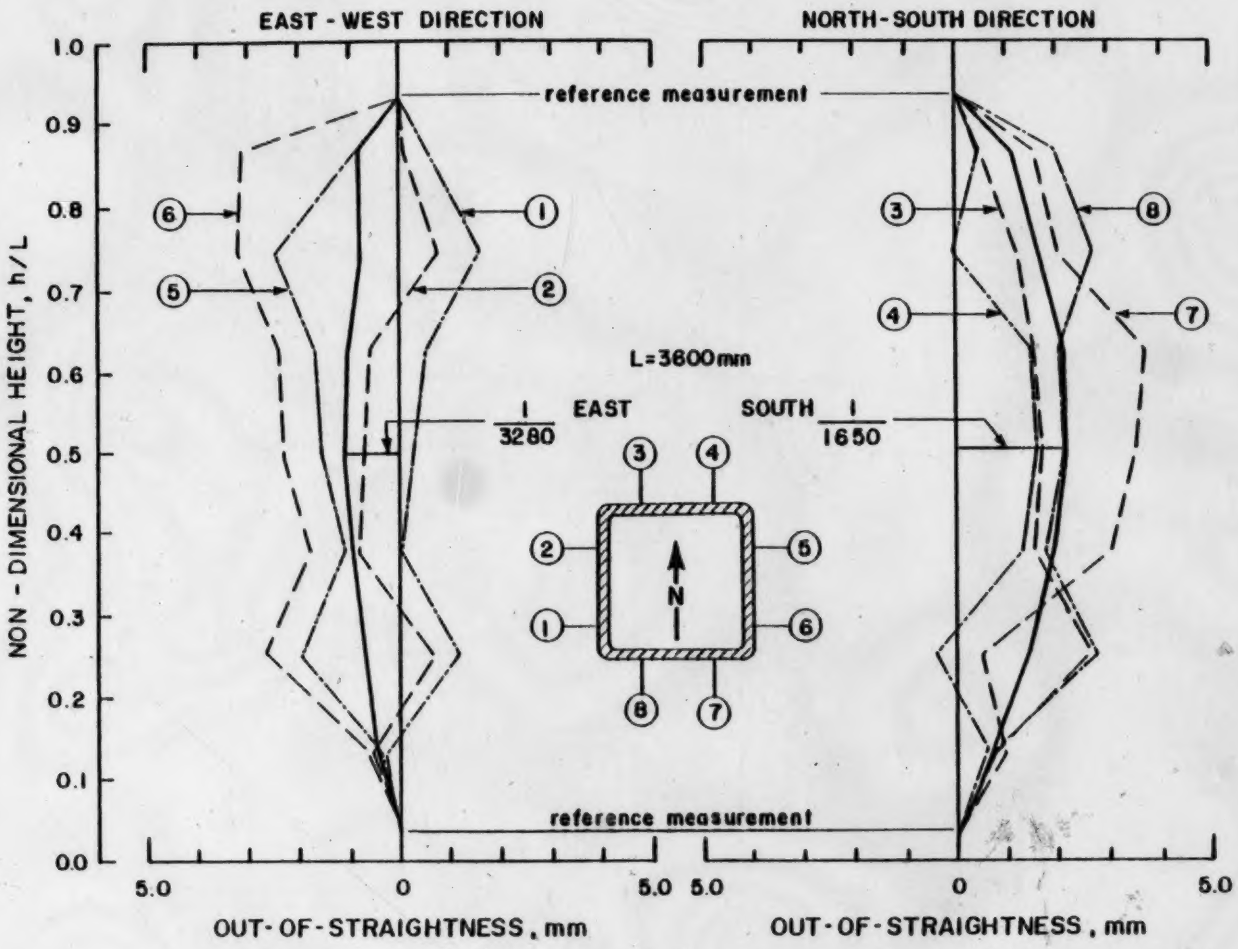

Figure 5.3 Out-of-Straightness for Column C604

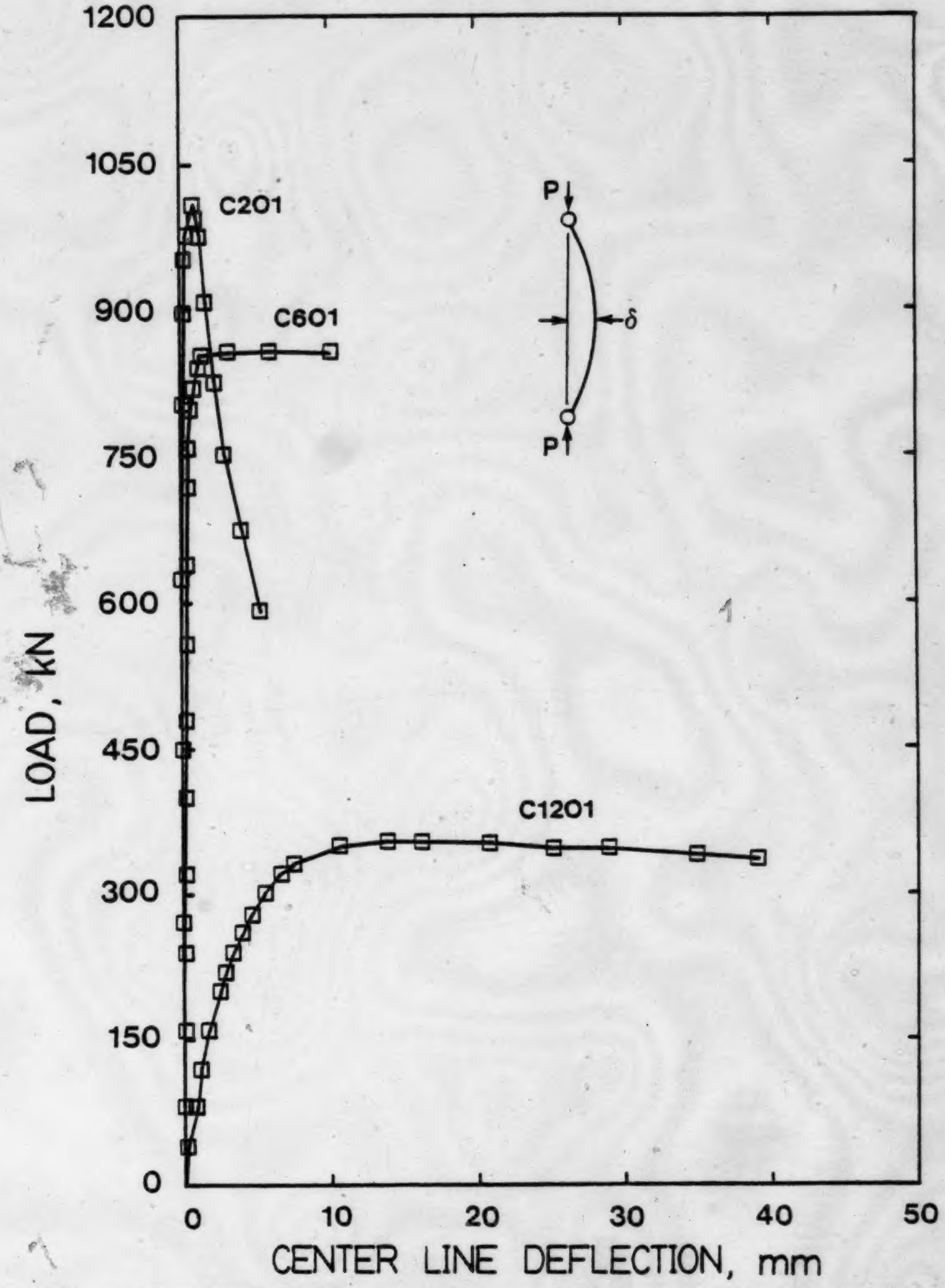

Figure 5.4 Load-Deflection Curves for Concentrically Loaded Steel Columns

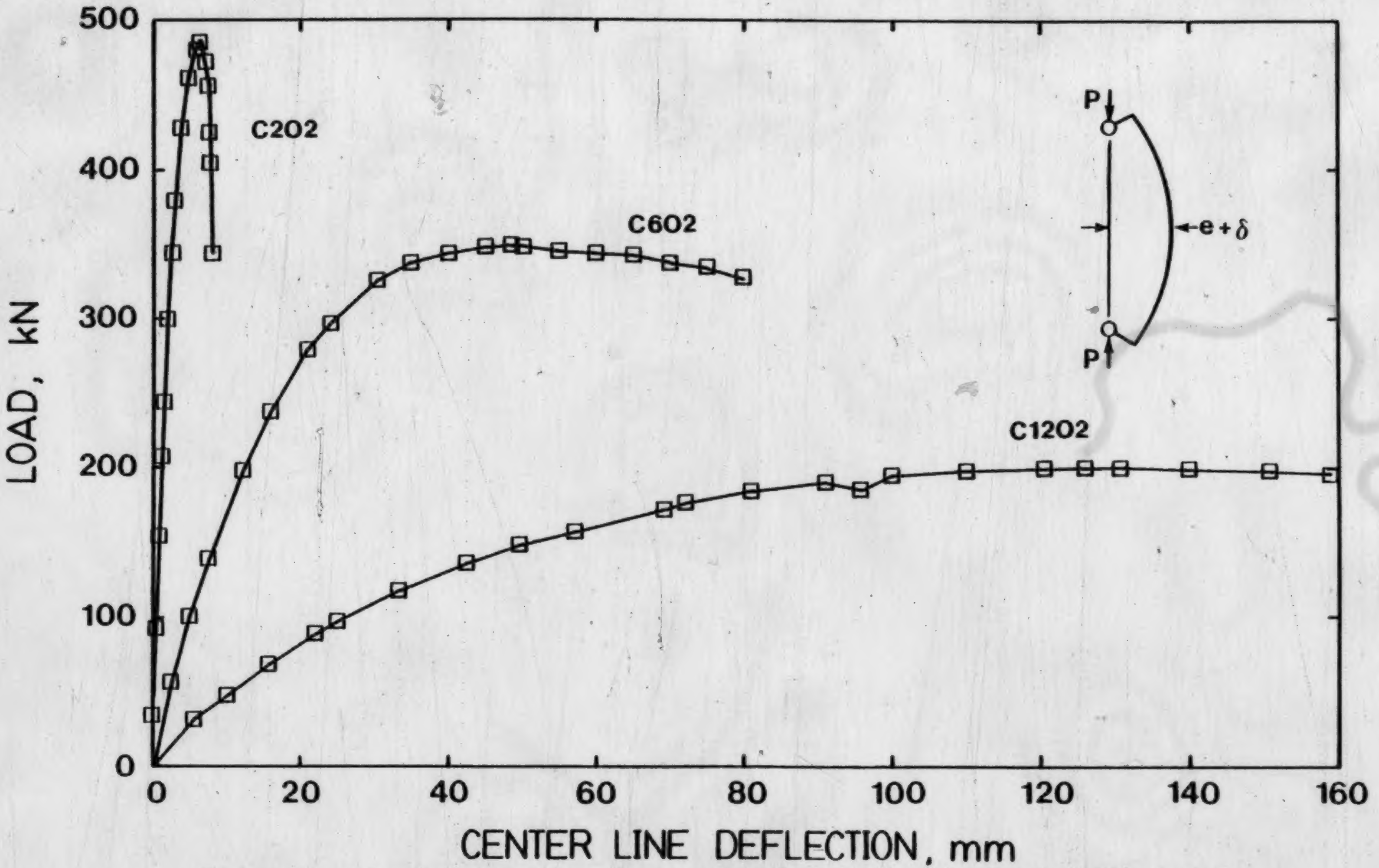

Figure 5.5 Load-Deflection Curves for Eccentrically Loaded Steel Columns

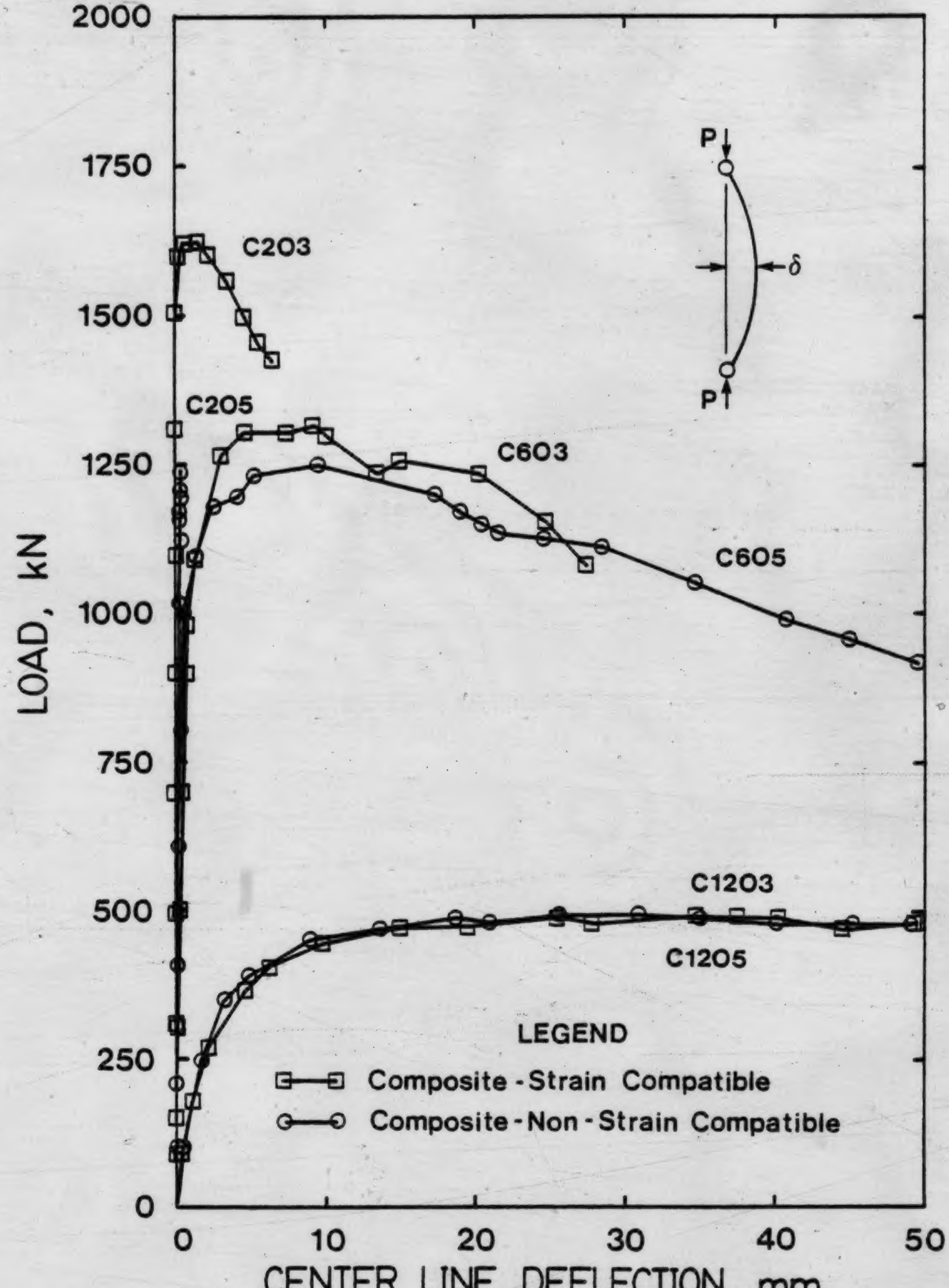

Figure 5.6 Load-Deflection Curves for Concentrically Loaded Composite Columns

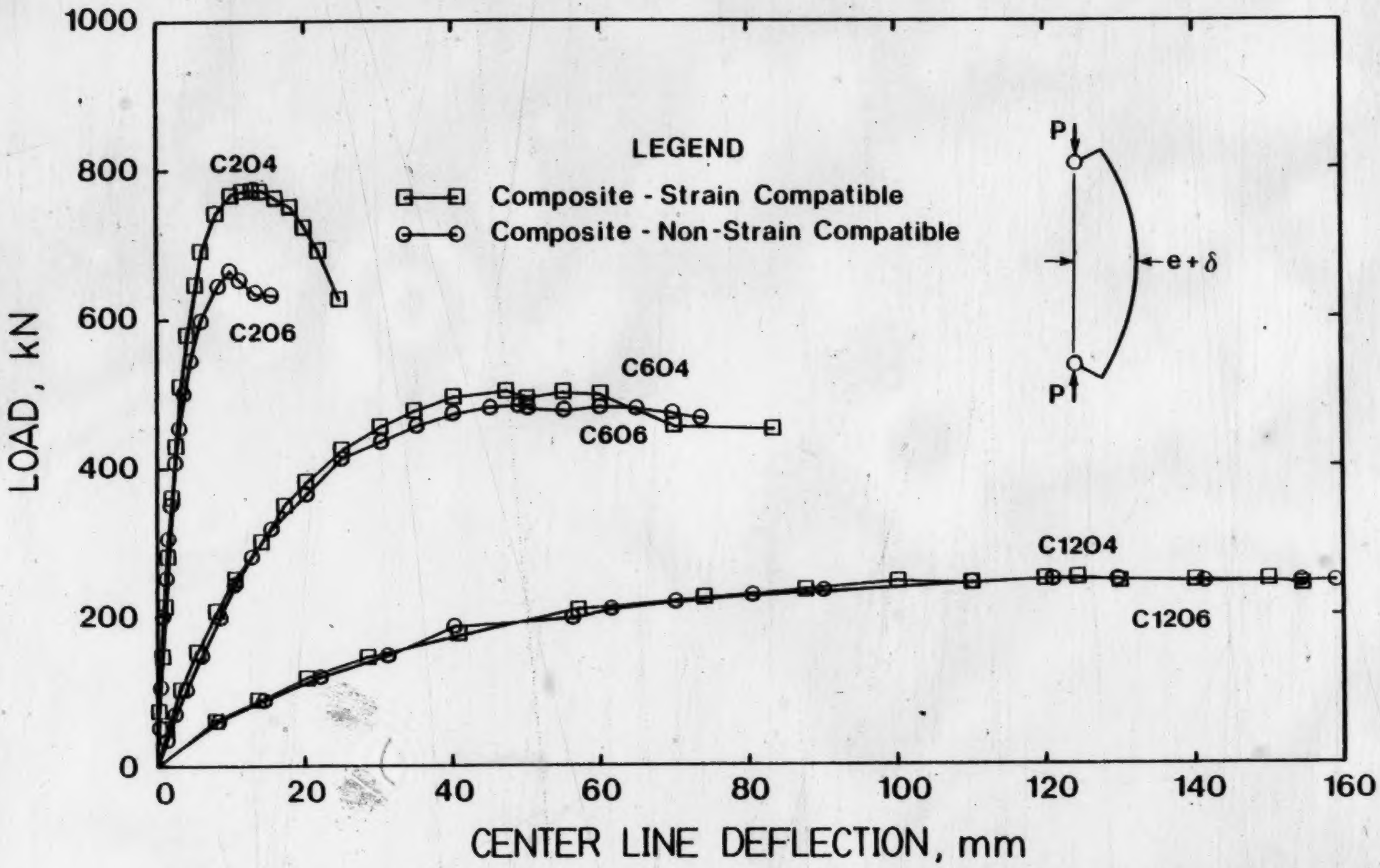

Figure 5.7 Load-Deflection Curves for Eccentrically Loaded Composite Columns

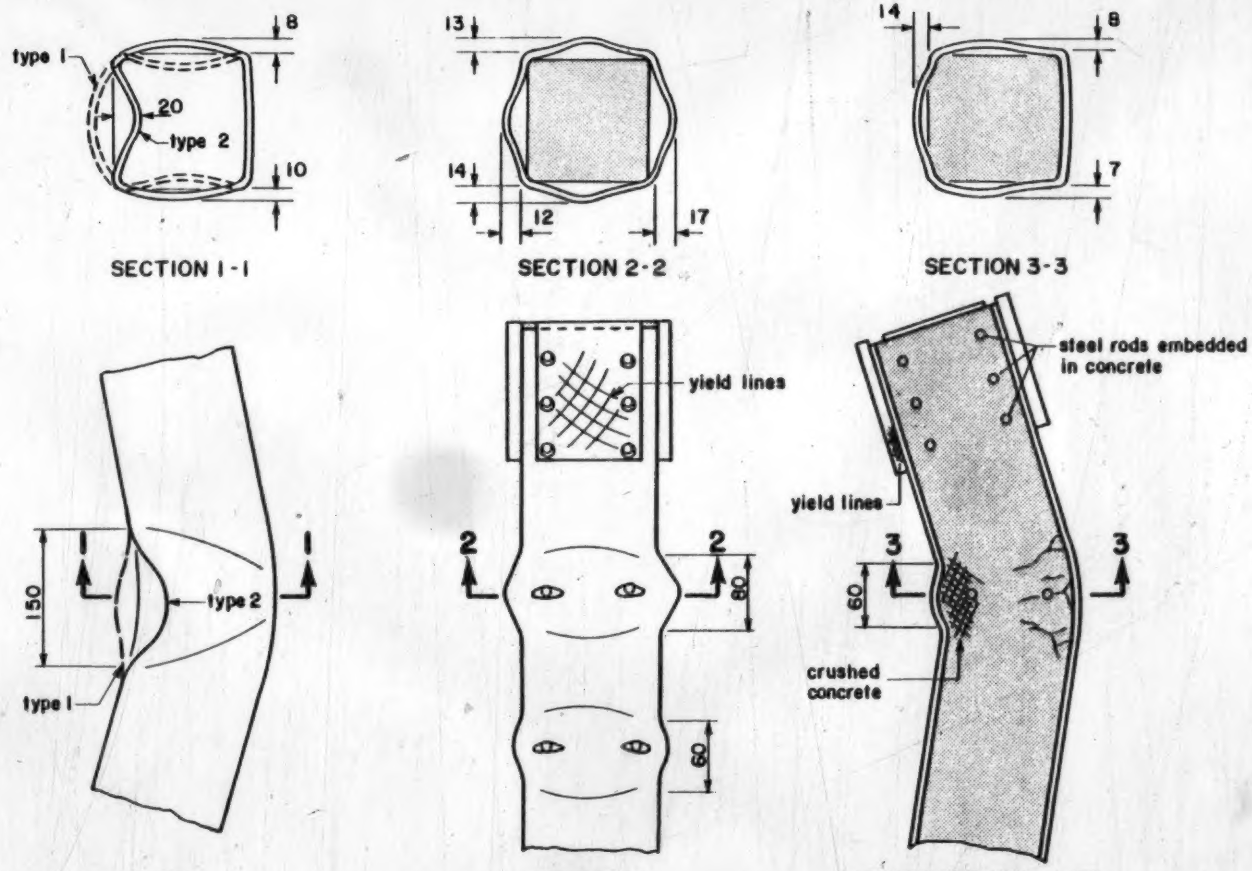
type I
20
type 2
8
10
SECTION I-I
13
14
12
17
SECTION 2-2
14
8
7
SECTION 3-3
I
I
150
type 2
type I
2
2
80
60
yield lines
steel rods embedded in concrete
yield lines
3
3
60
crushed concrete

STEEL
(a)

TEST C205
(b)

COMPOSITE, Kl/r = 20
(c)

Figure 5.8 Typical Failure Modes for Beam Column Tests

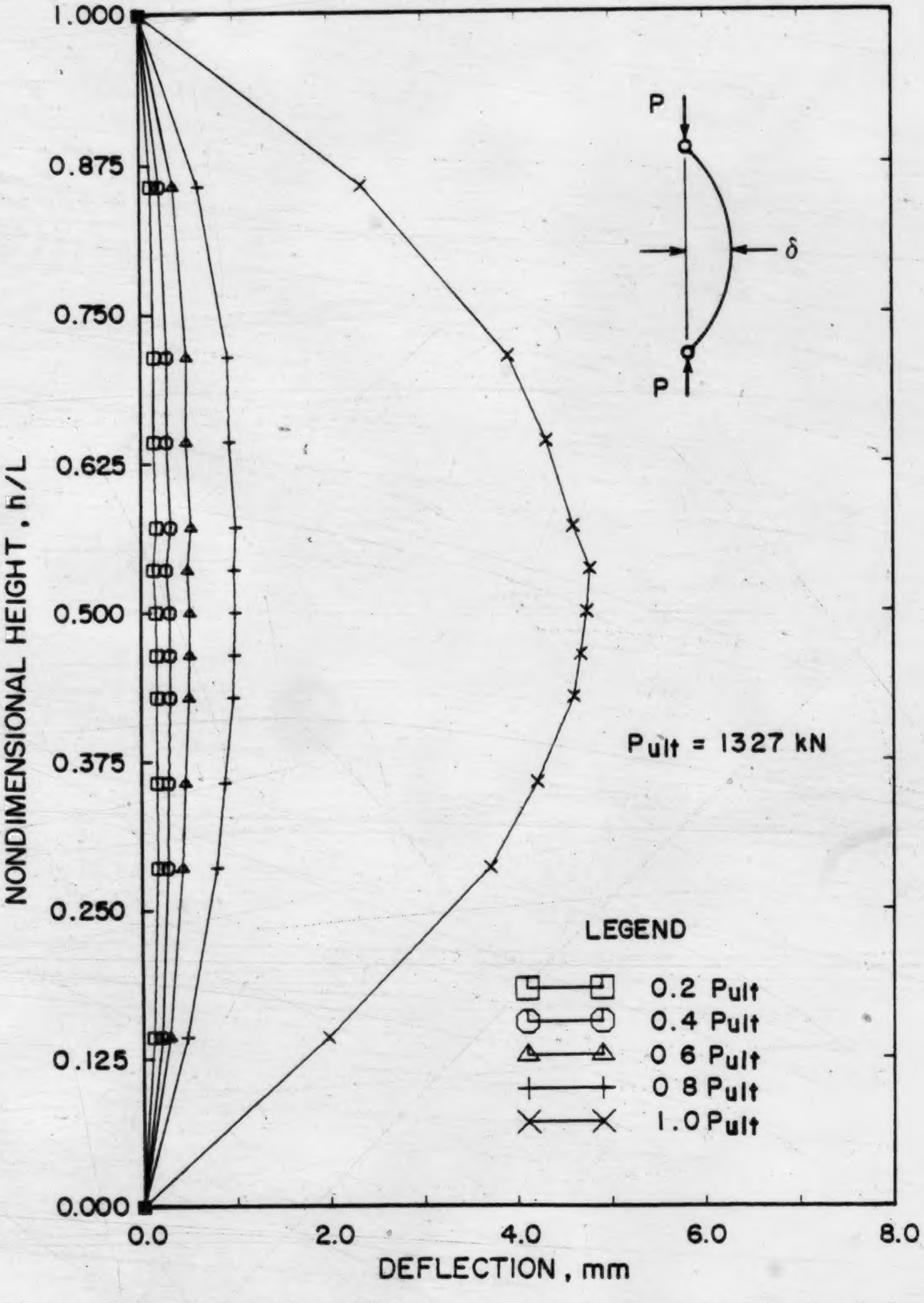

Figure 5.9 Load Deflection Curves for Concentrically Loaded Column C603

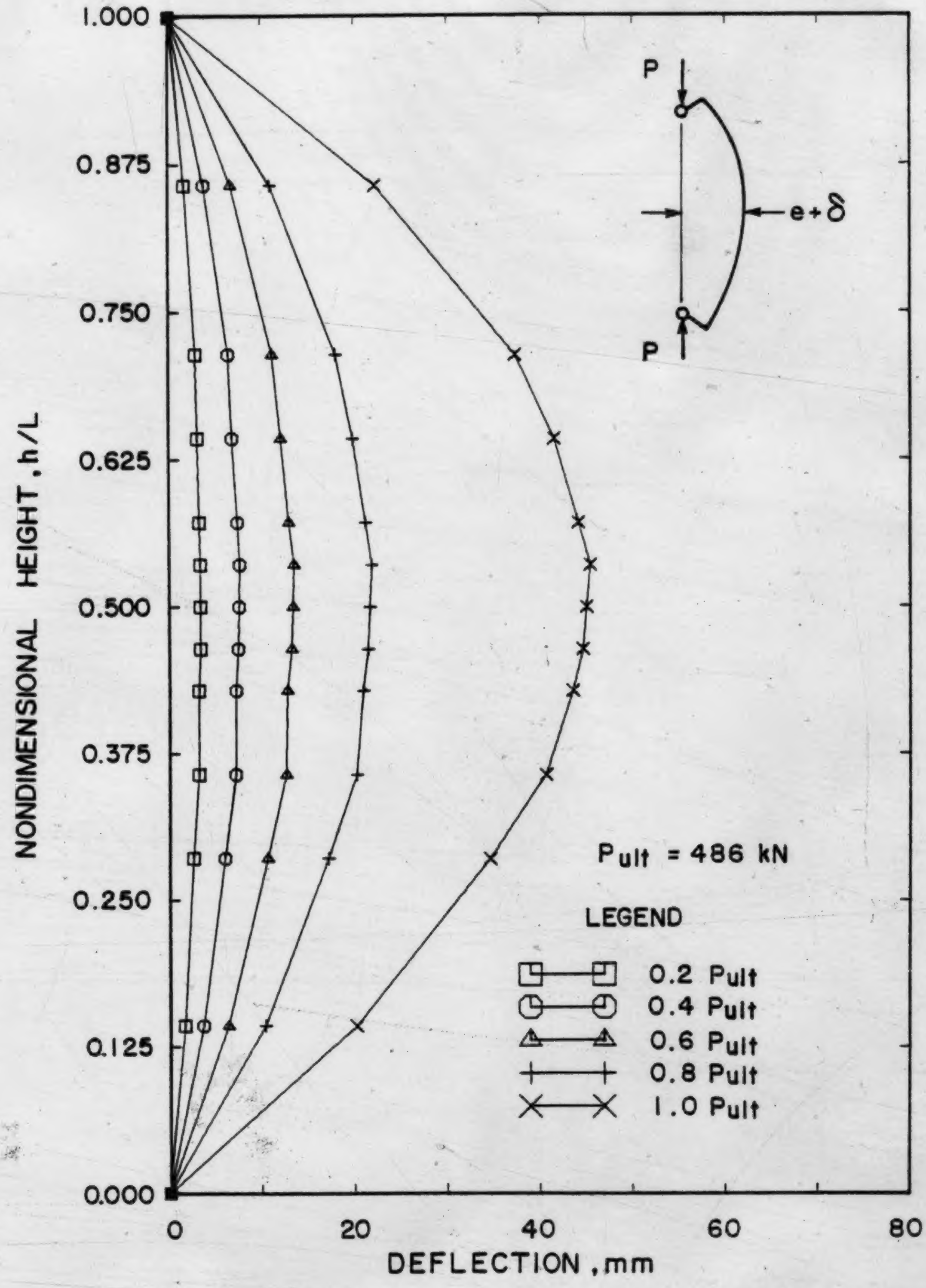

Figure 5.10 Load Deflection Curves for Eccentrically Loaded Column C606

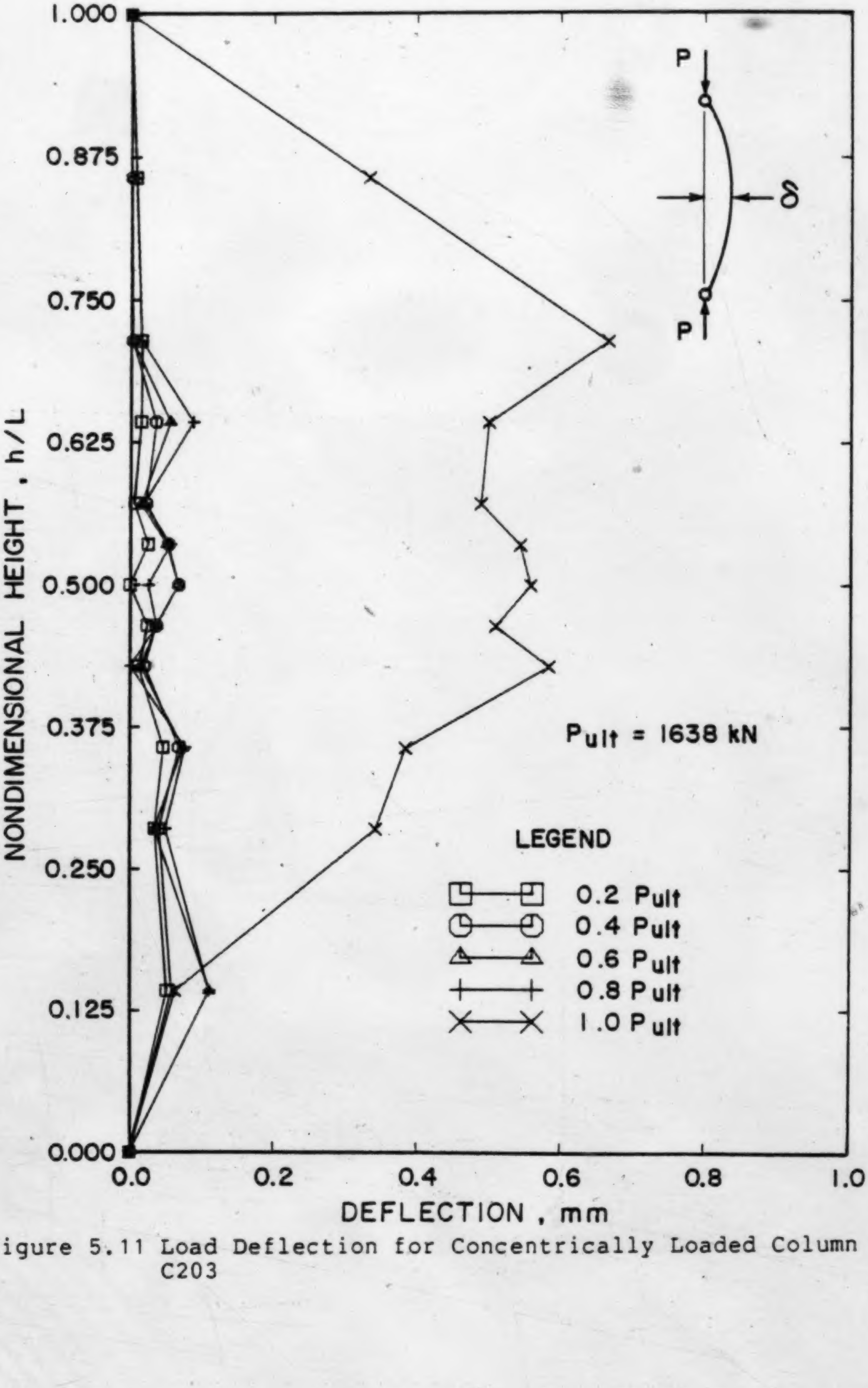

Figure 5.11 Load Deflection for Concentrically Loaded Column C203

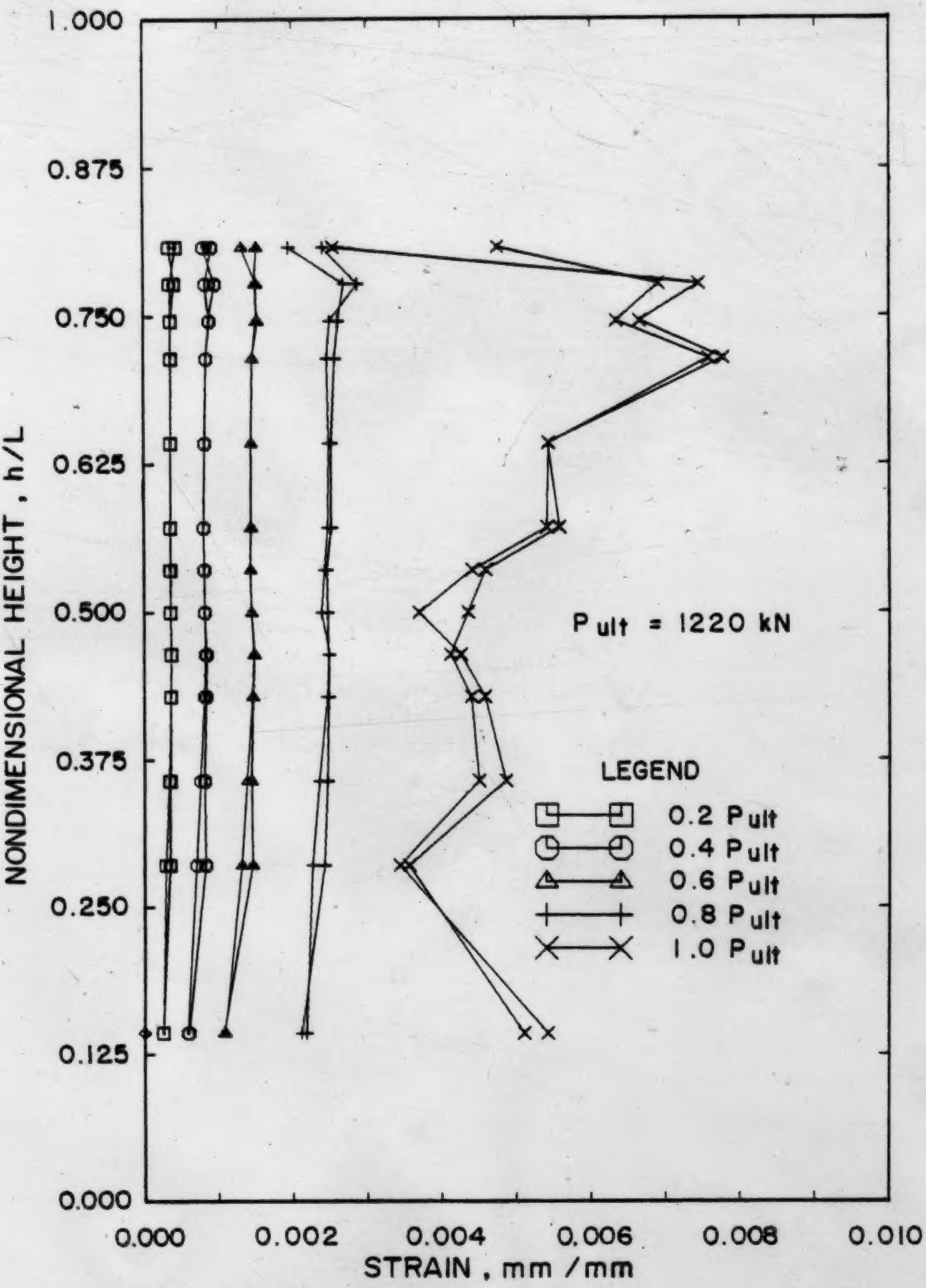

Figure 5.12 Steel Strain Distributions for Concentrically Loaded Column C205, L/r=20

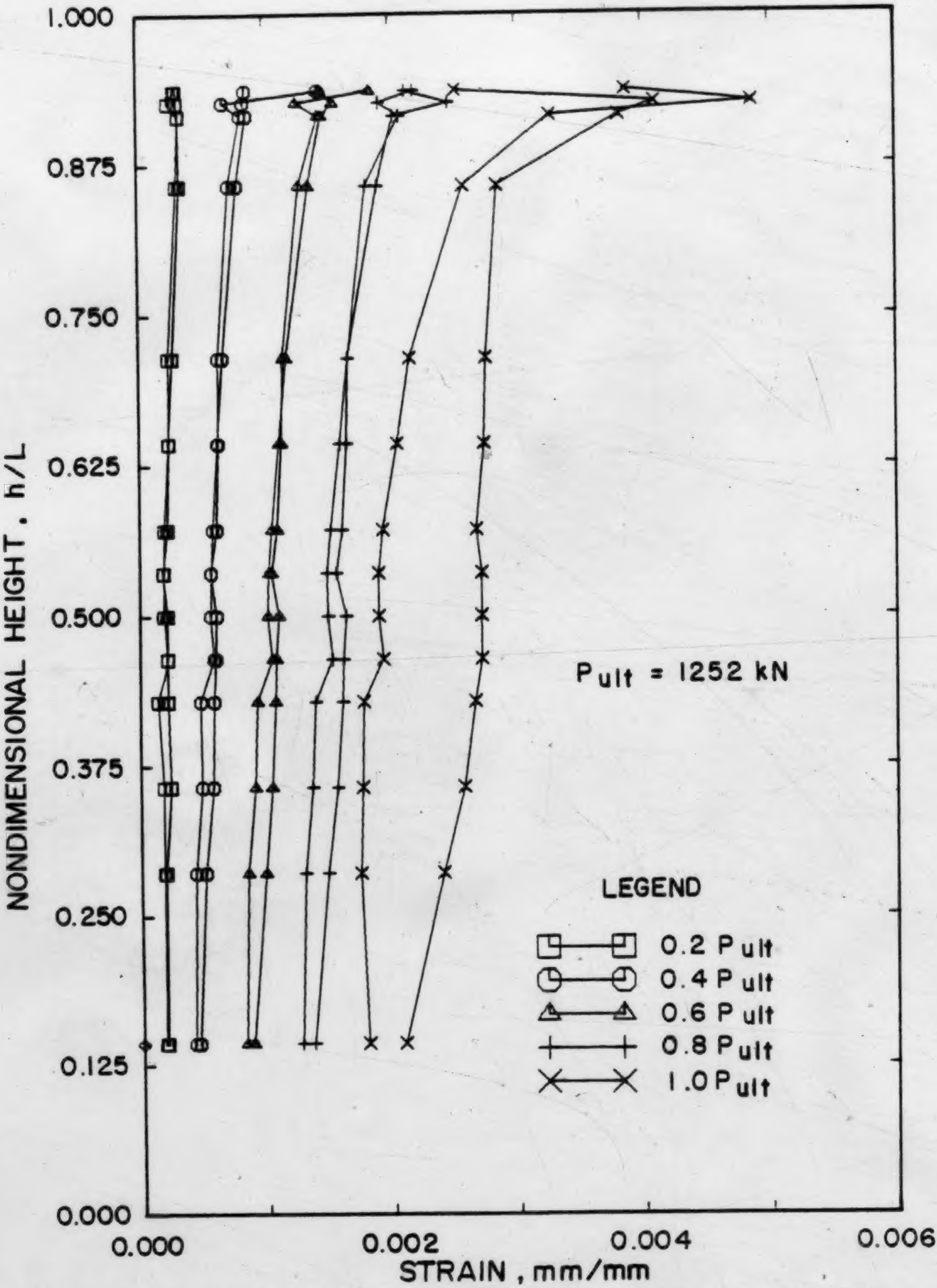

Figure 5.13 Steel Strain Distributions for Concentrically Loaded Column C605, L/r=59.9

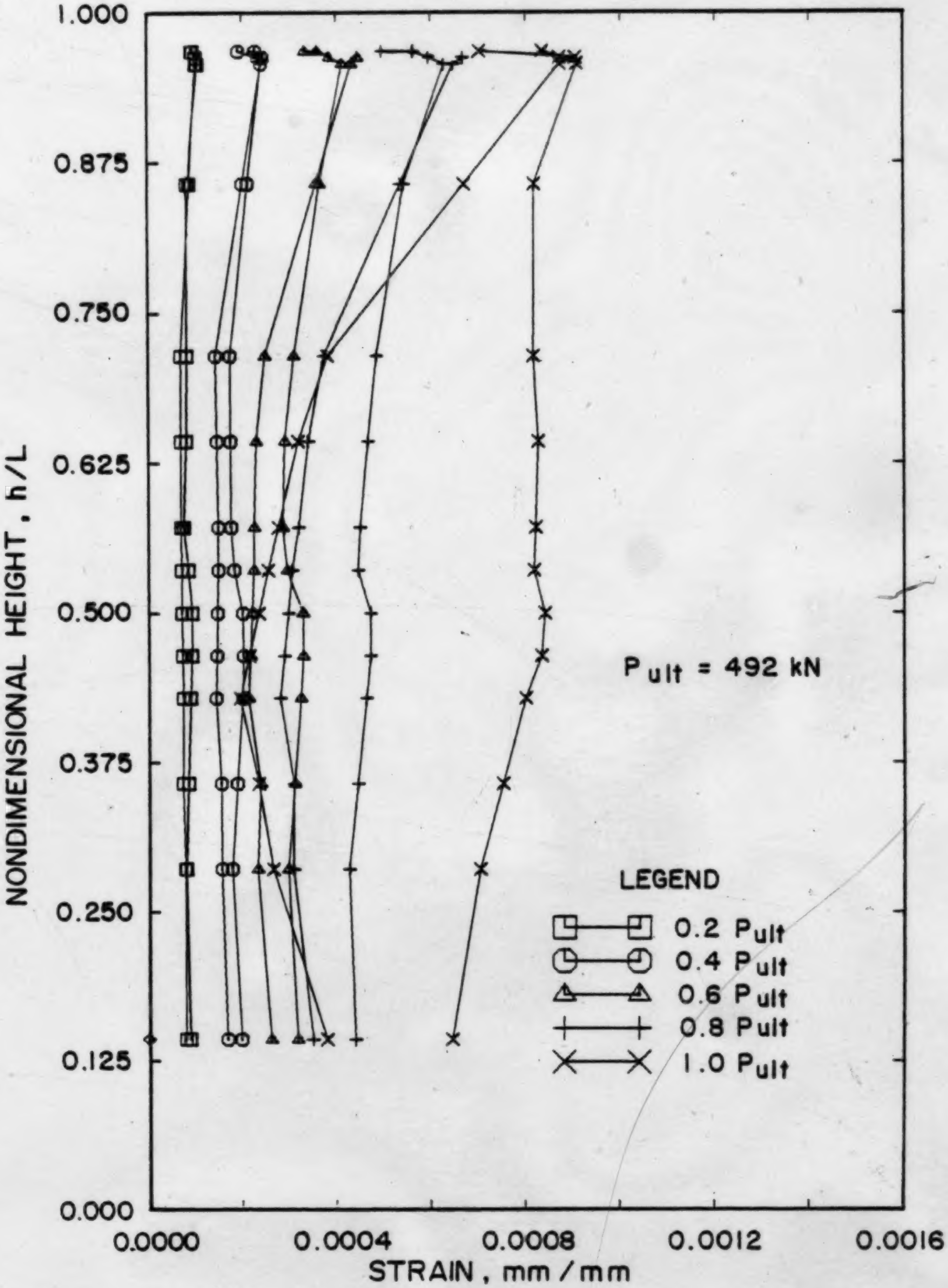

Figure 5.14 Steel Strain Distributions for Concentrically Loaded Column C1205, L/r=117.6

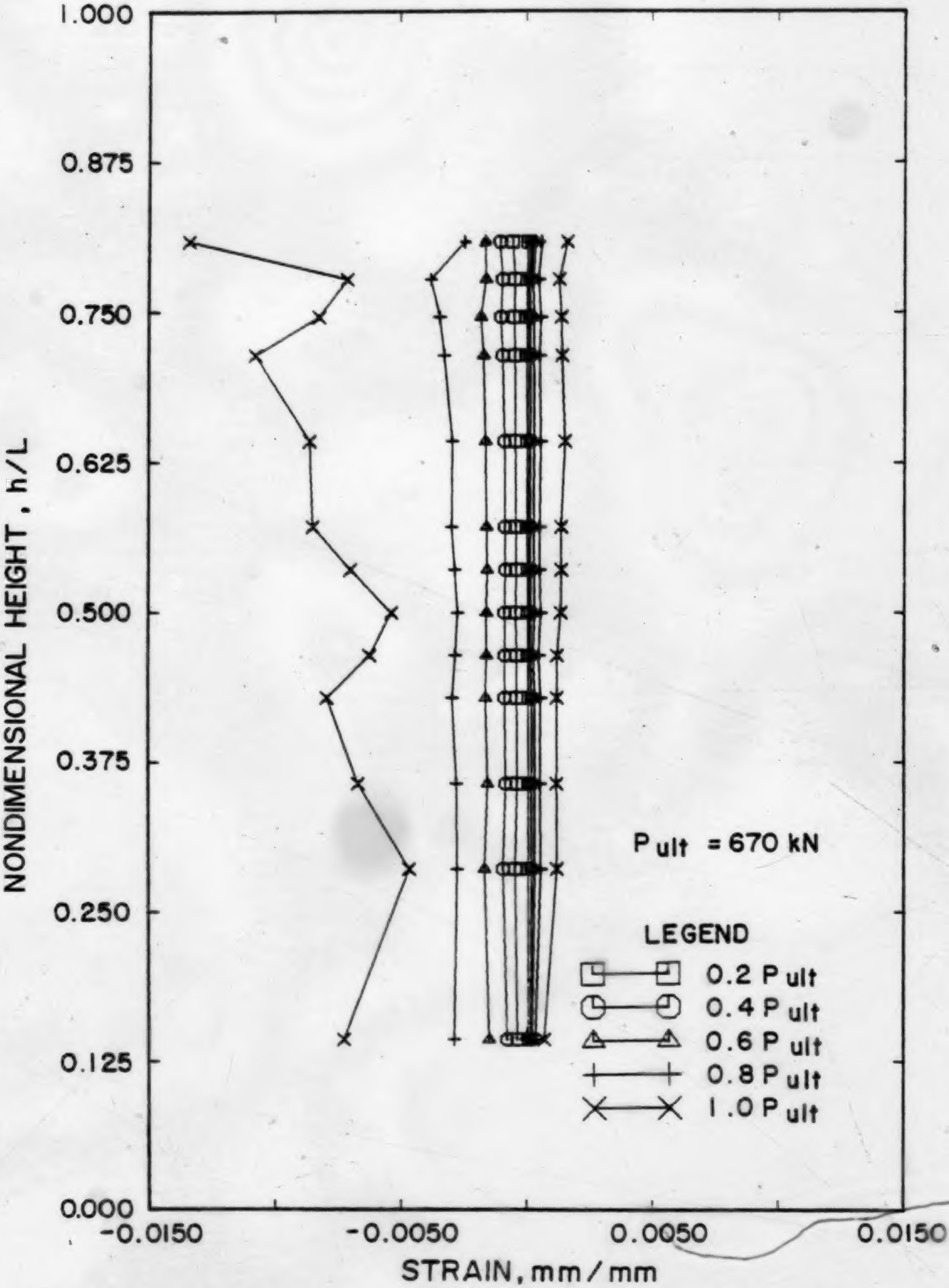

Figure 5.15 Steel Strain Distributions for Eccentrically Loaded Column C206, L/r=20

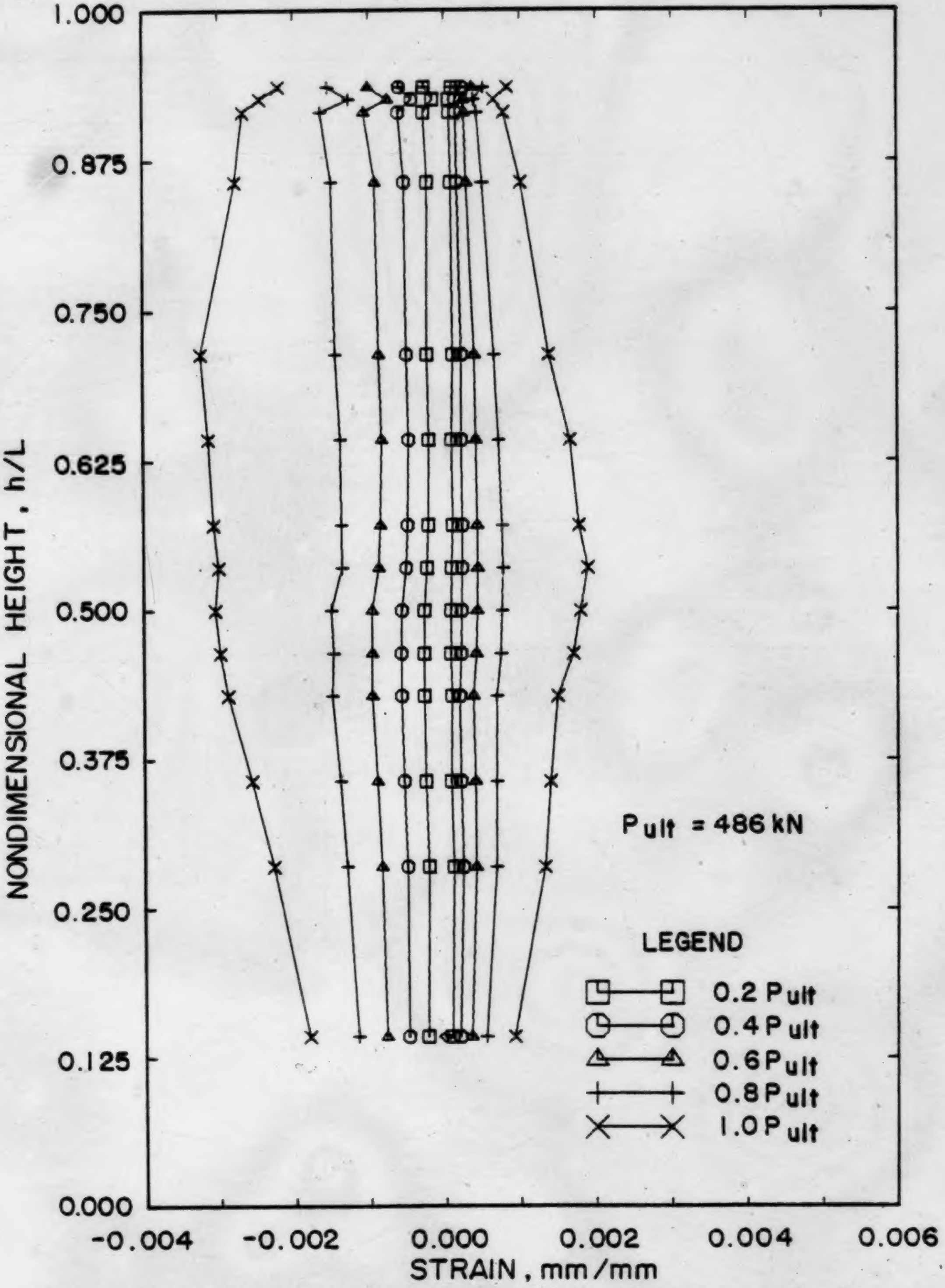

Figure 5.16 Steel Strain Distributions for Eccentrically Loaded Column C606, L/r=59.9

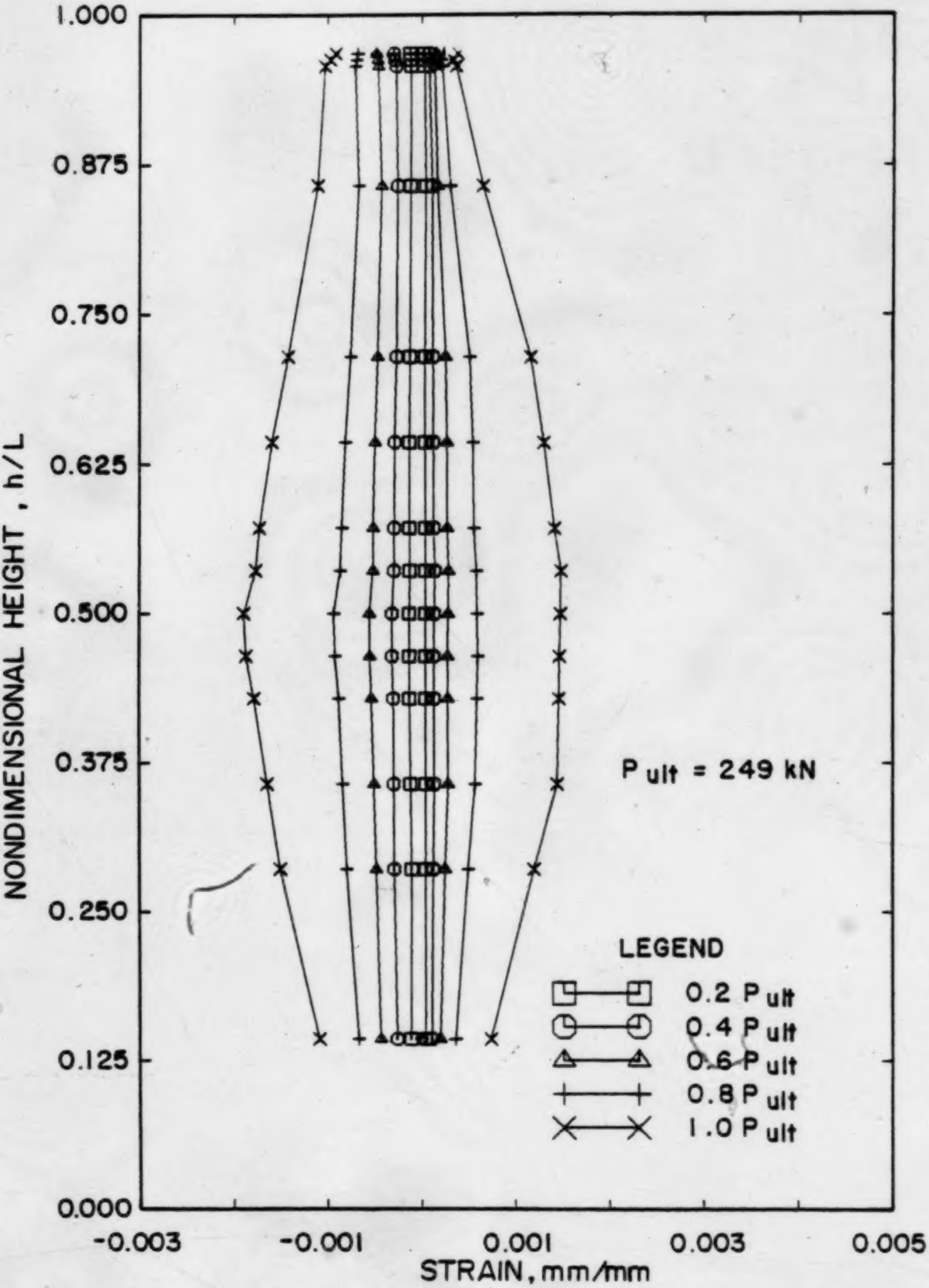

Figure 5.17 Steel Strain Distributions for Eccentrically Loaded Column C1206, L/r=117.6

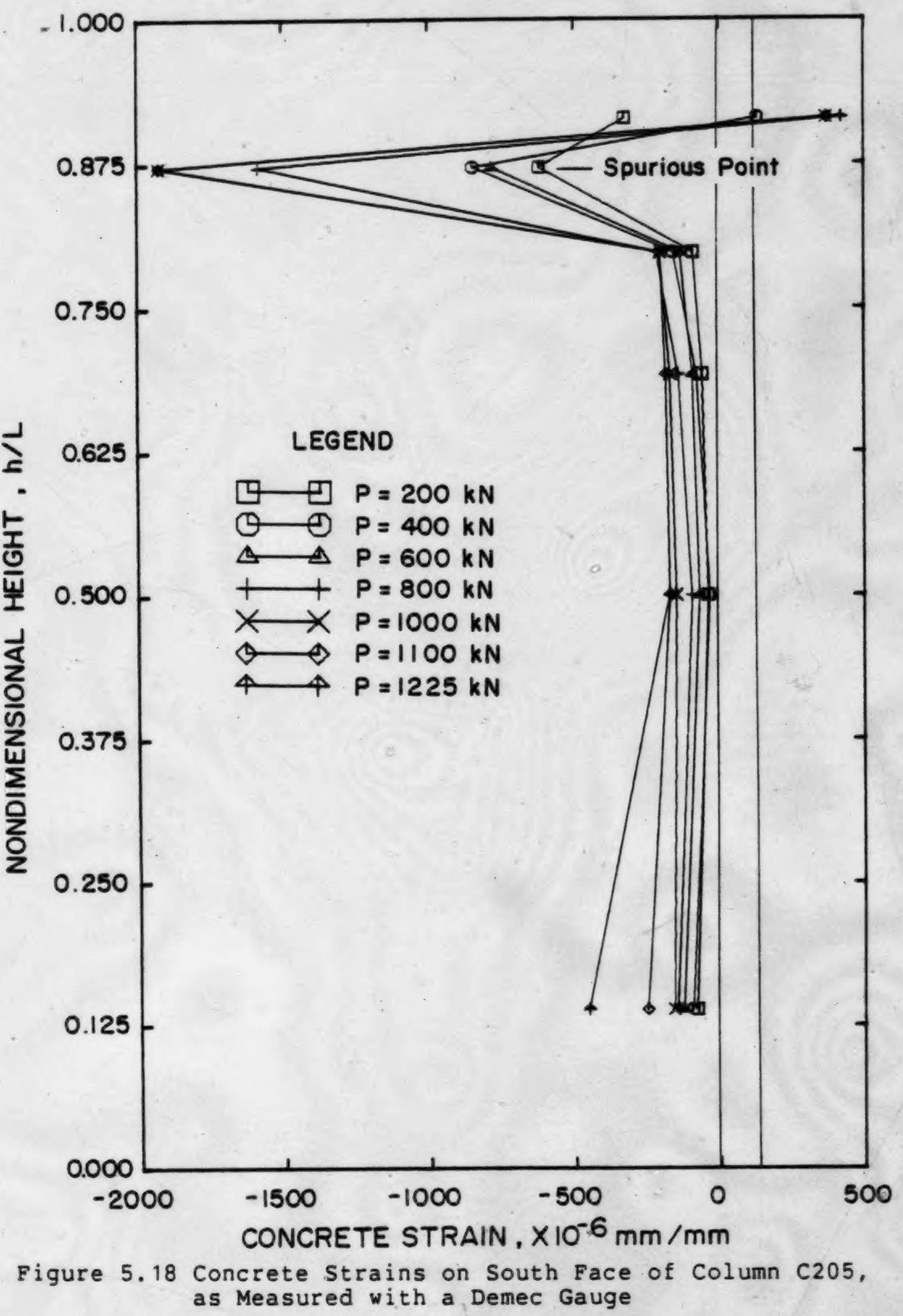

Figure 5.18 Concrete Strains on South Face of Column C205, as Measured with a Demec Gauge

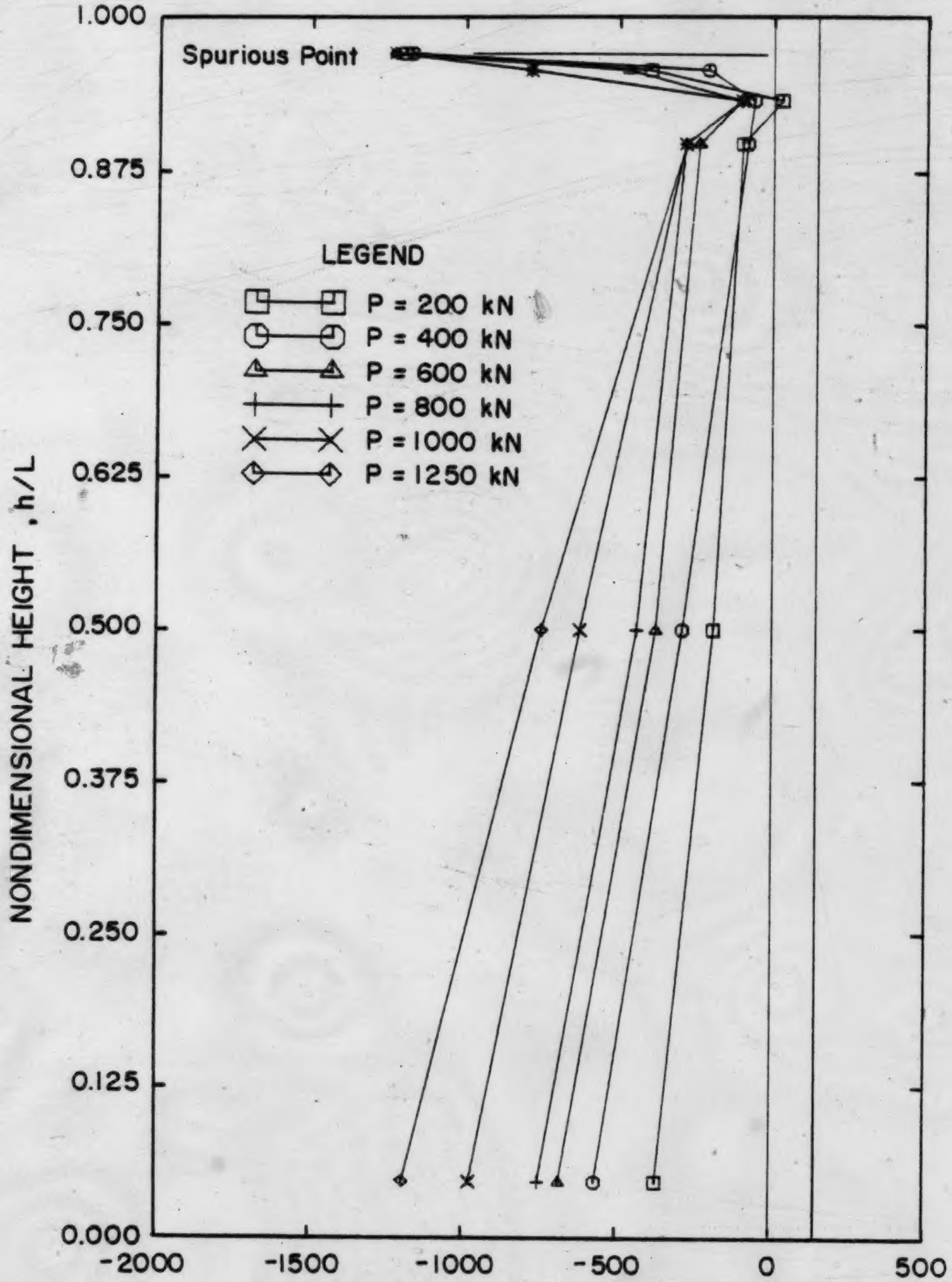

Figure 5.19 Concrete Strains on South Face of Column C605, as Measured with a Demec Gauge

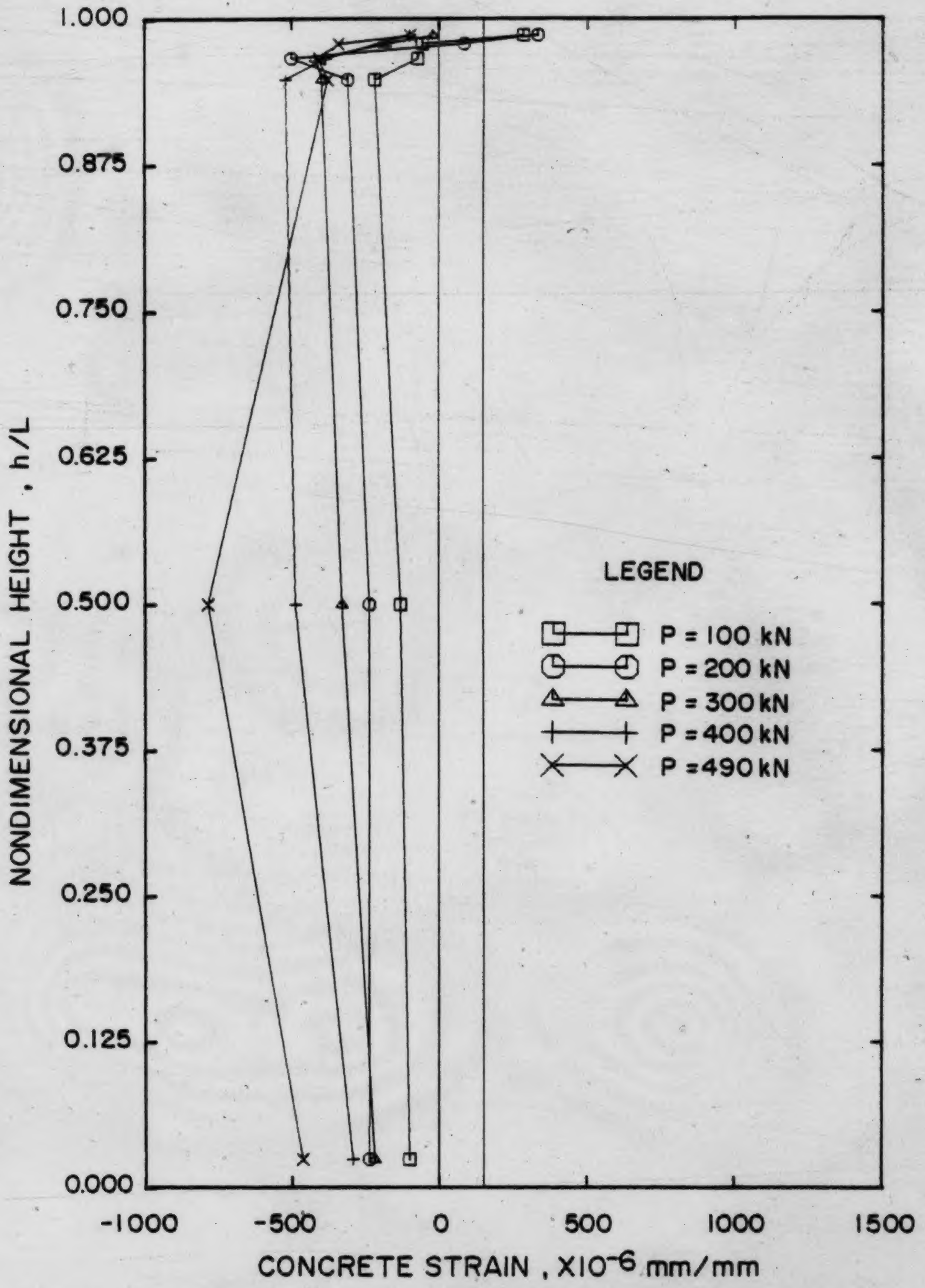

Figure 5.20 Concrete Strains on South Face of Column C1205, as Measured with a Demec Gauge

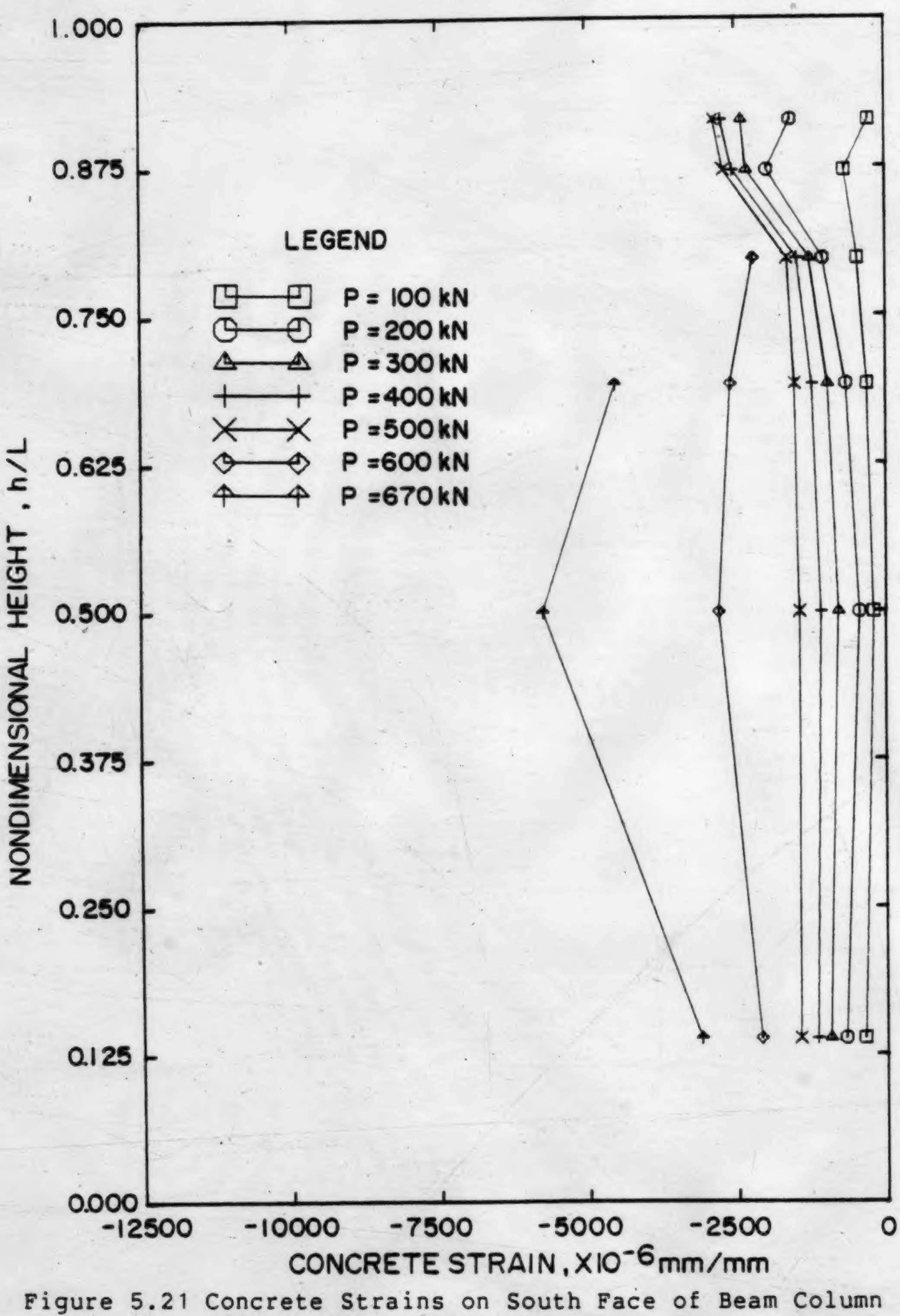

Figure 5.21 Concrete Strains on South Face of Beam Column C206, as Measured with a Demec Gauge

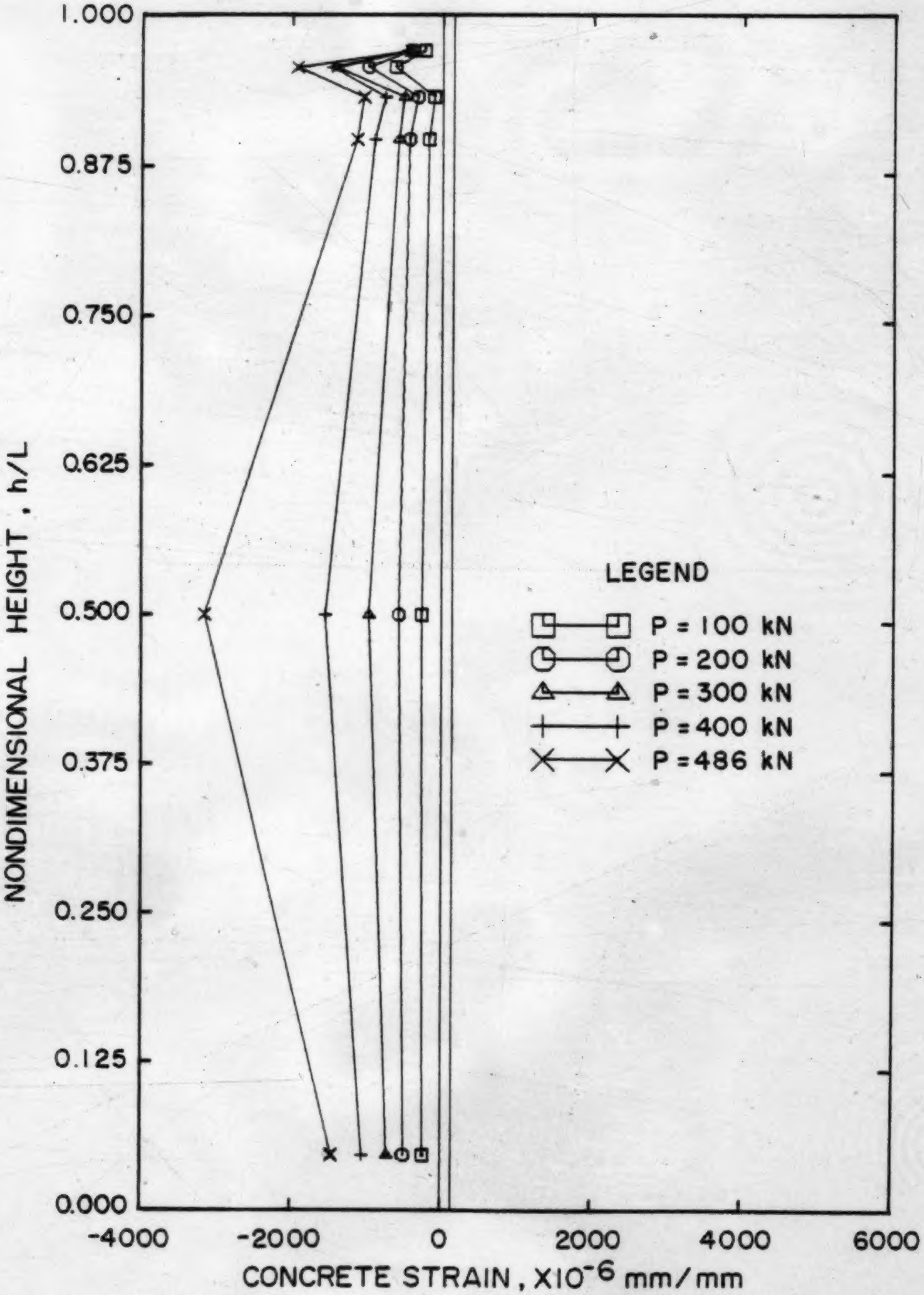

Figure 5.22 Concrete Strains on South Face of Beam Column C606, as Measured with a Demec Gauge

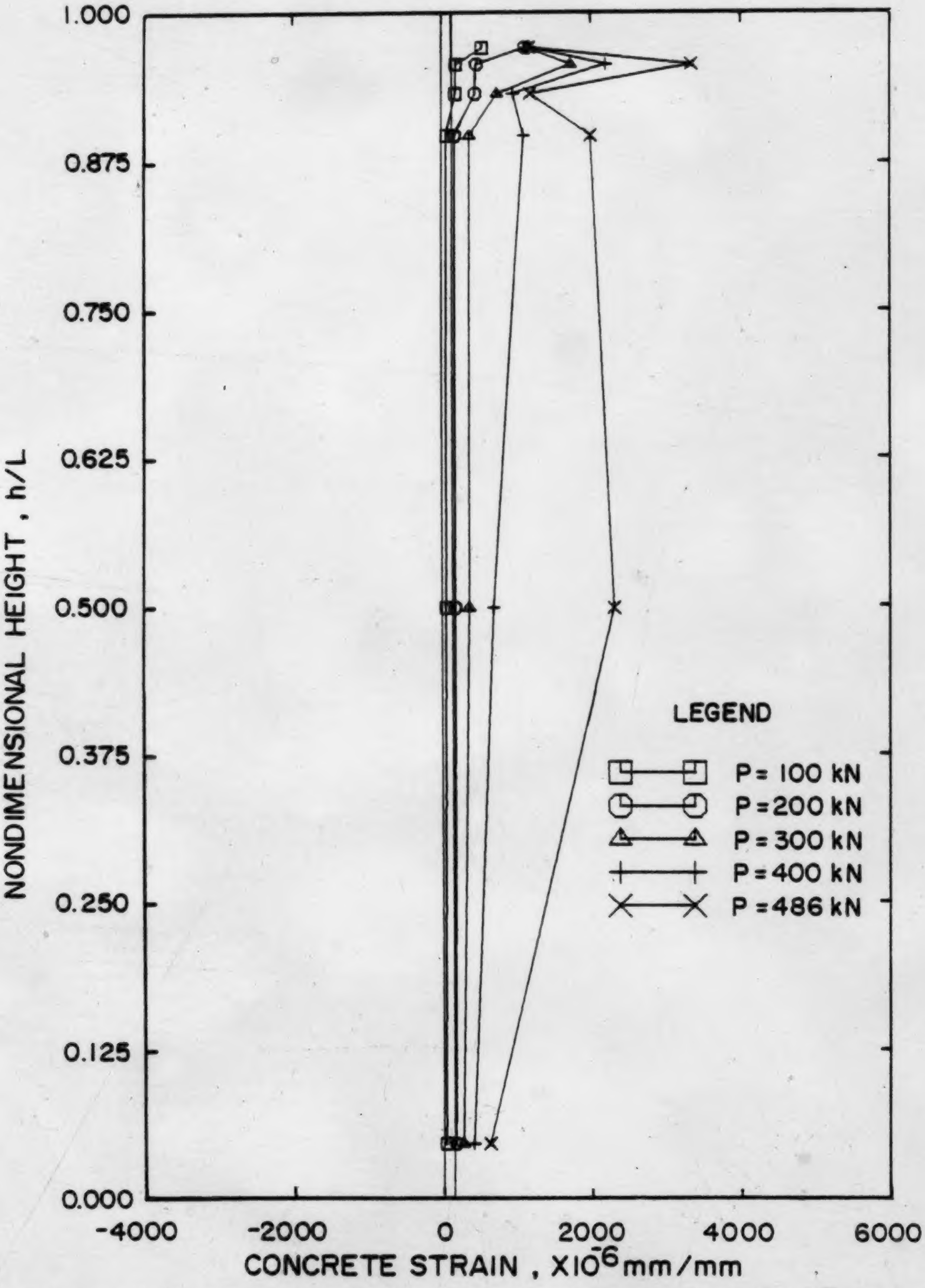

Figure 5.23 Concrete Strains on North Face of Beam Column C606, as Measured with a Demec Gauge

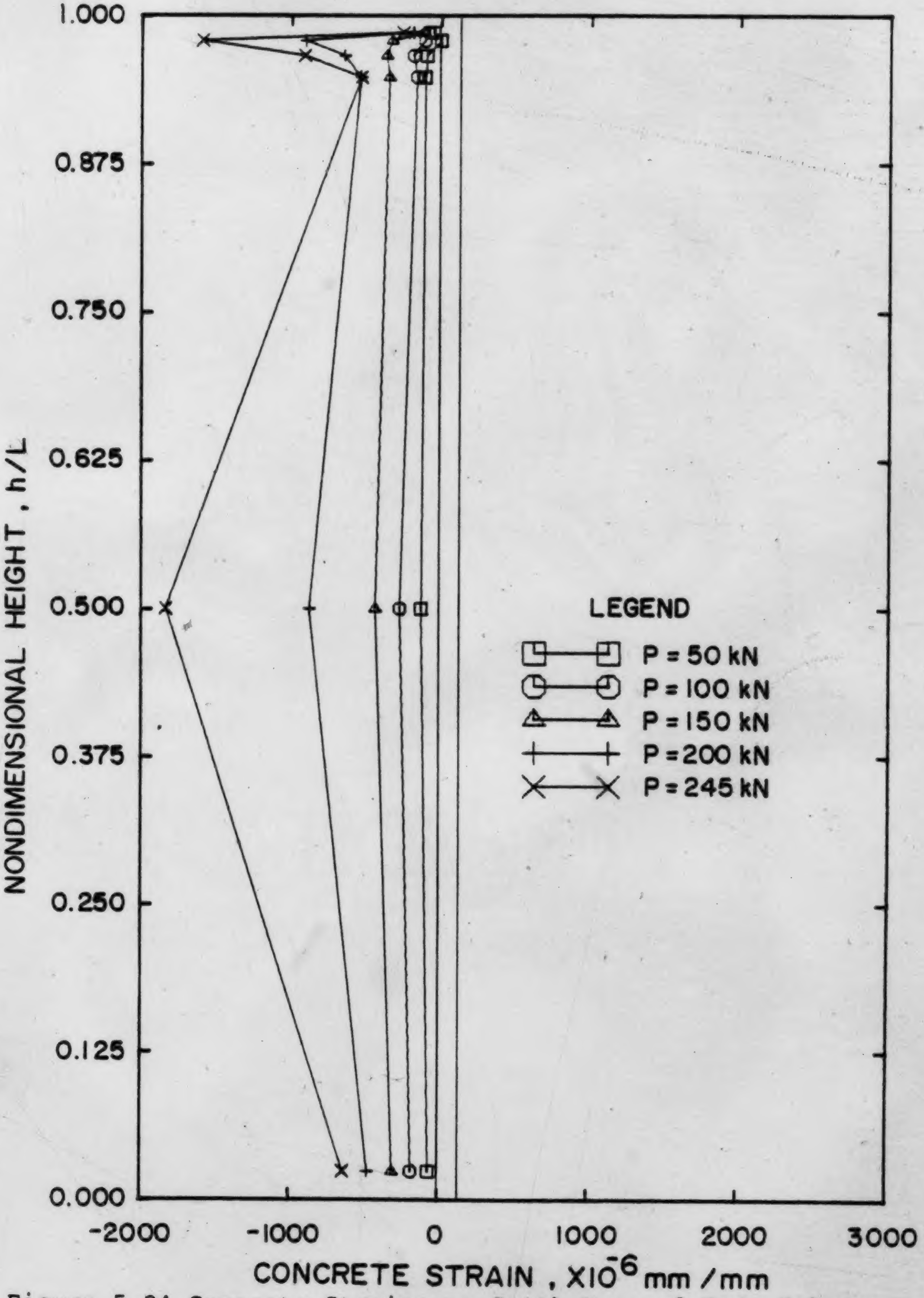

Figure 5.24 Concrete Strains on South Face of Beam Column C1206, as Measured with a Demec Gauge

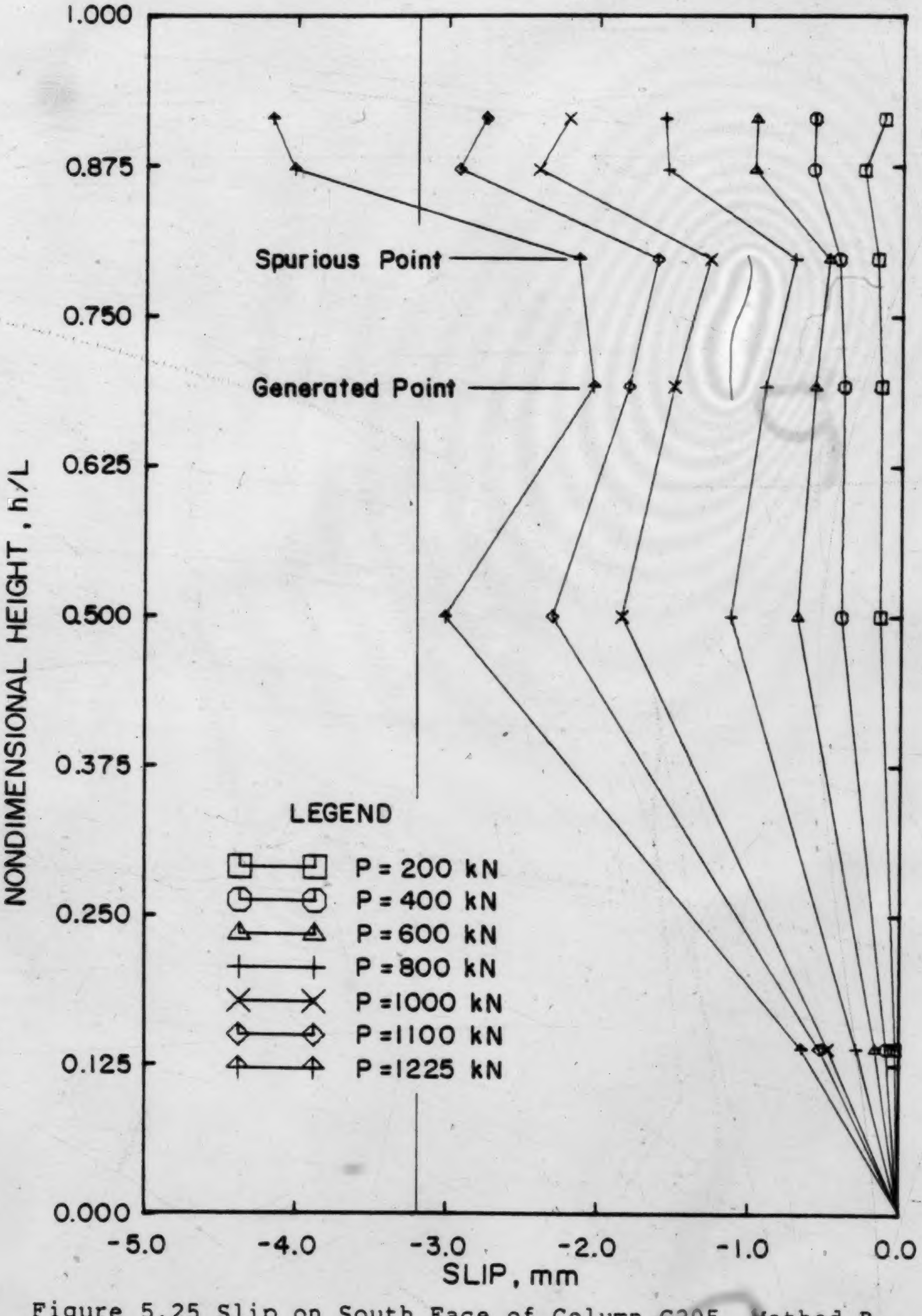

Figure 5.25 Slip on South Face of Column C205, Method B

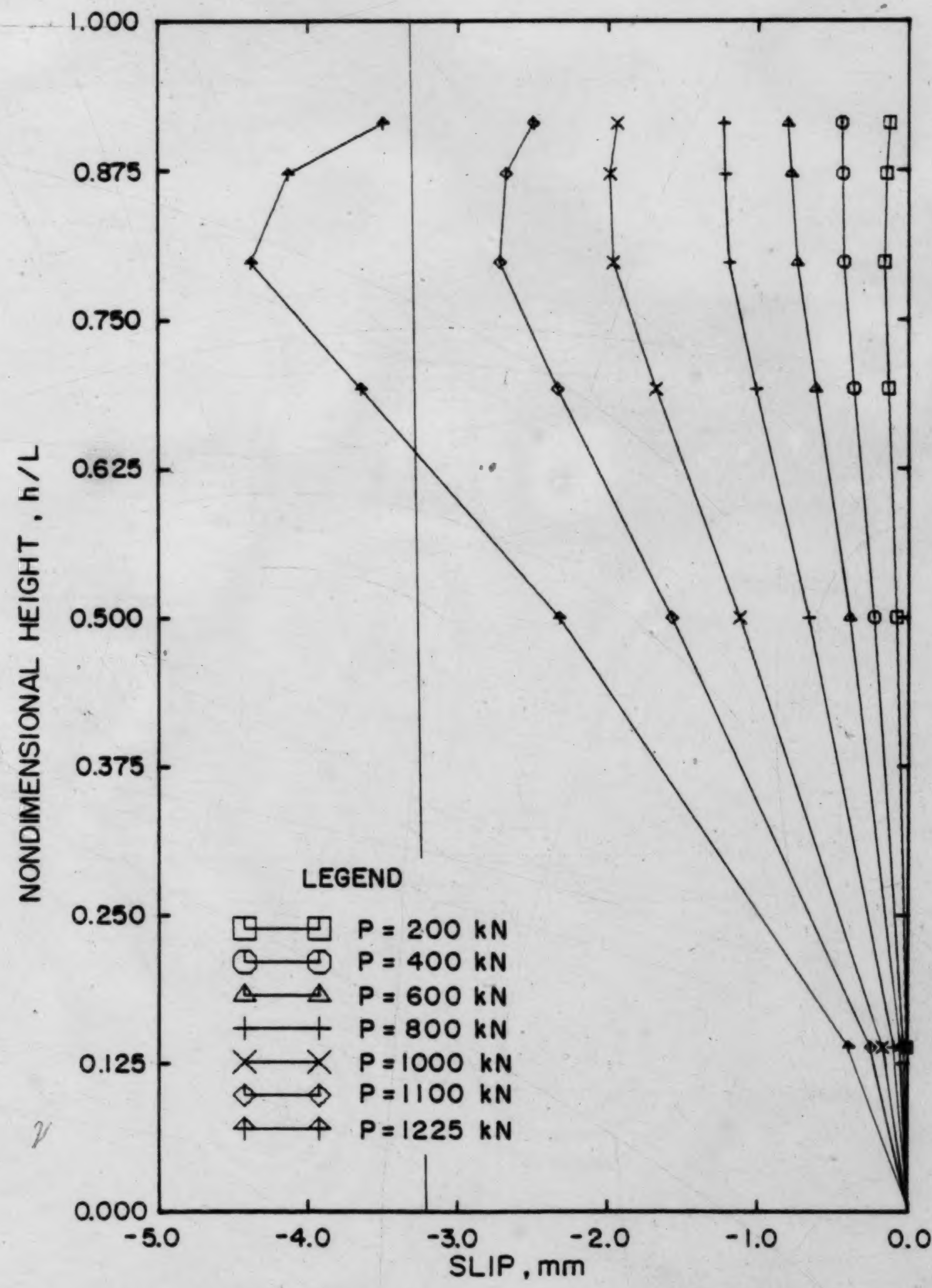

Figure 5.26 Slip on South Face of Column C205, Method A

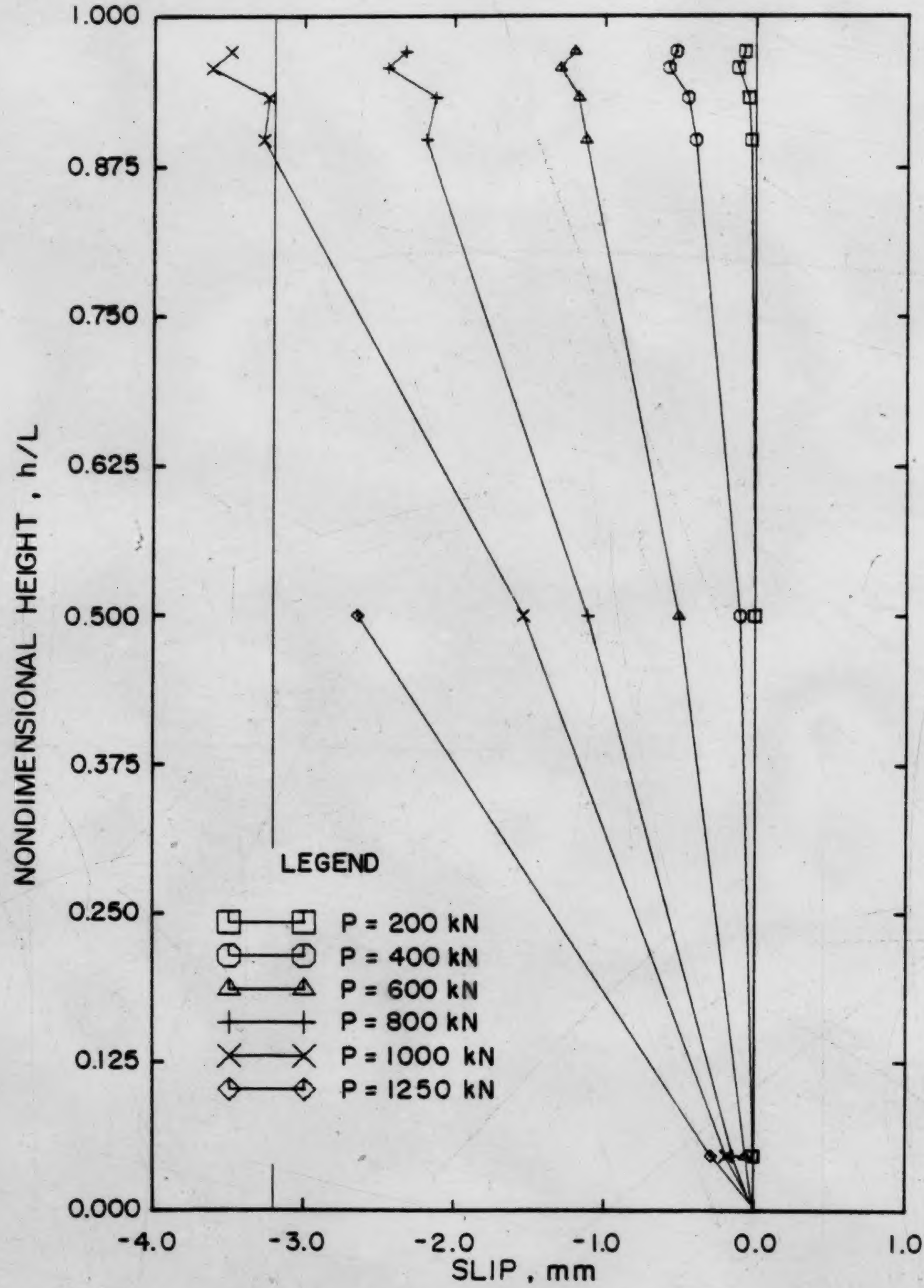

Figure 5.27 Slip on South Face of Column C605, Method B

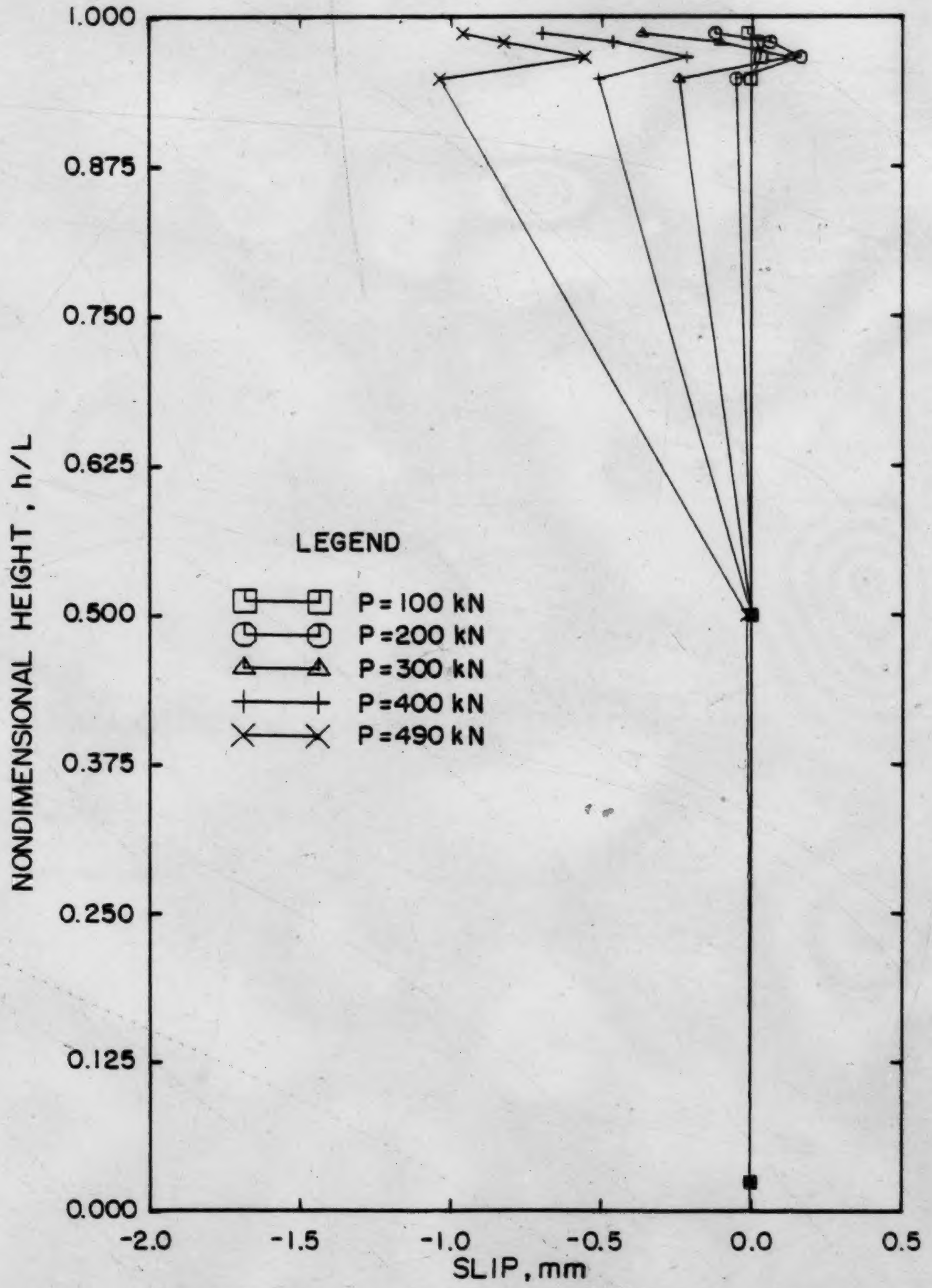

Figure 5.28 Slip on South Face of Column C1205, Method B

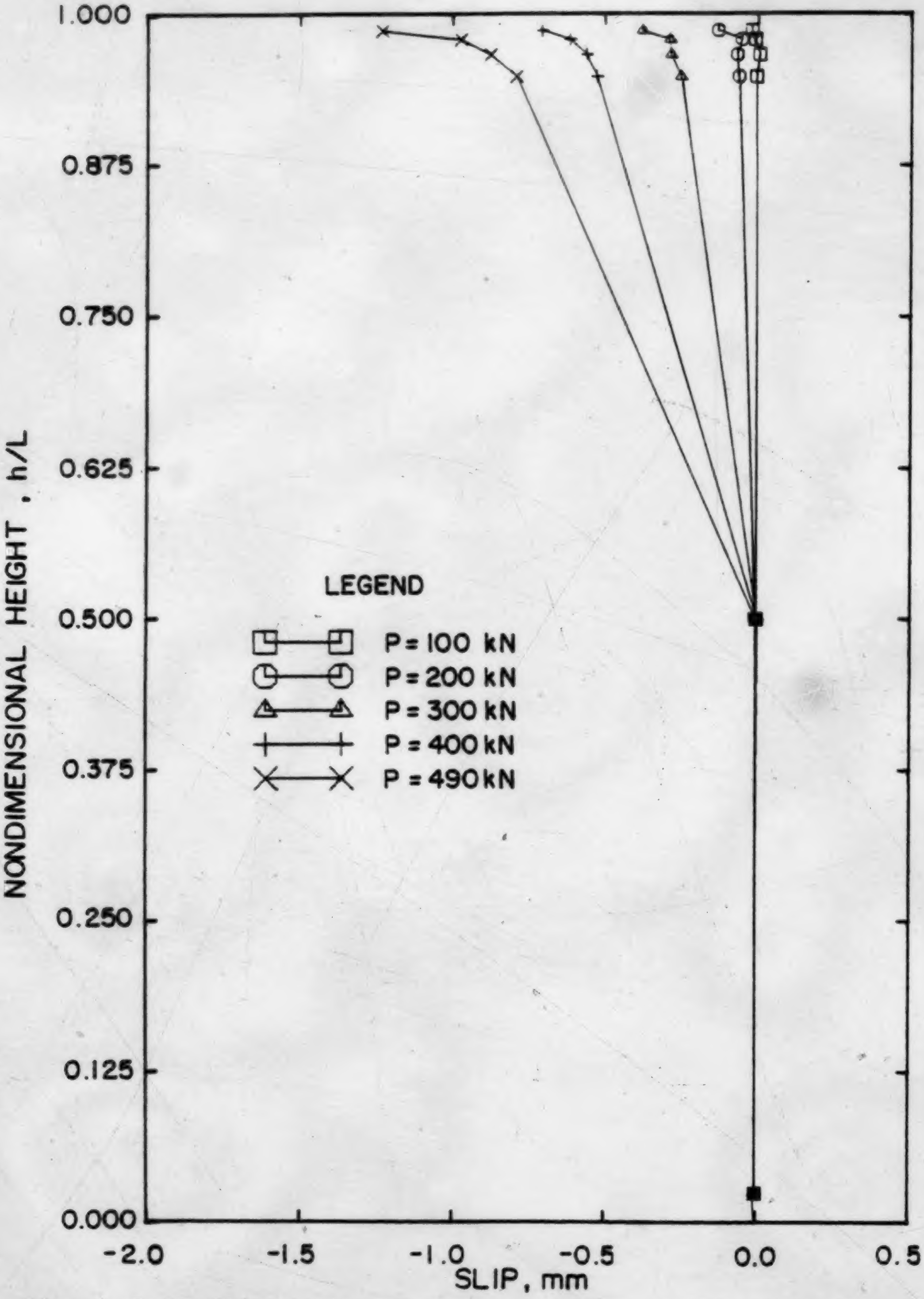

Figure 5.29 Slip on North Face of Column C1205, Method B

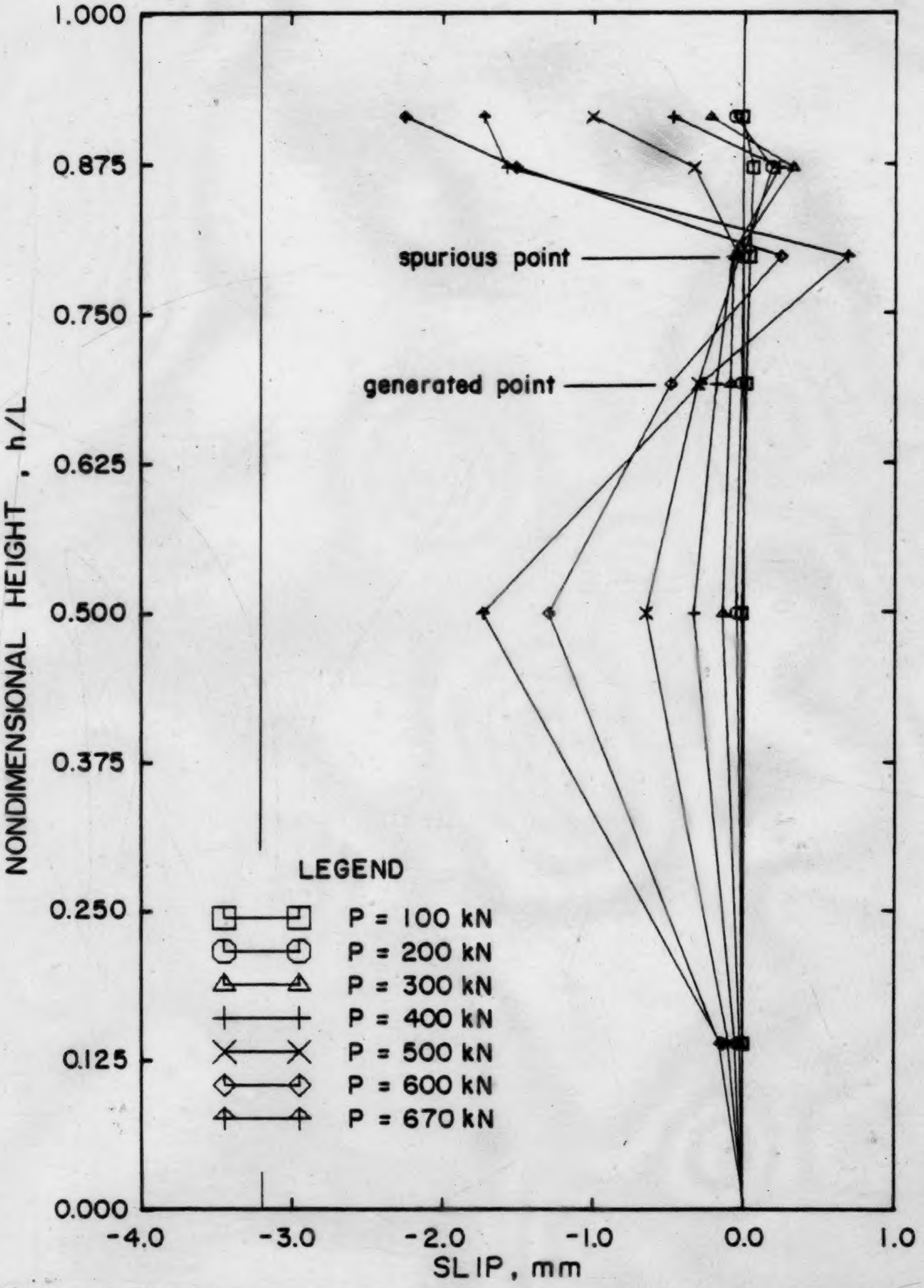

Figure 5.30 Slip on South Face of Beam Column C206, Method B

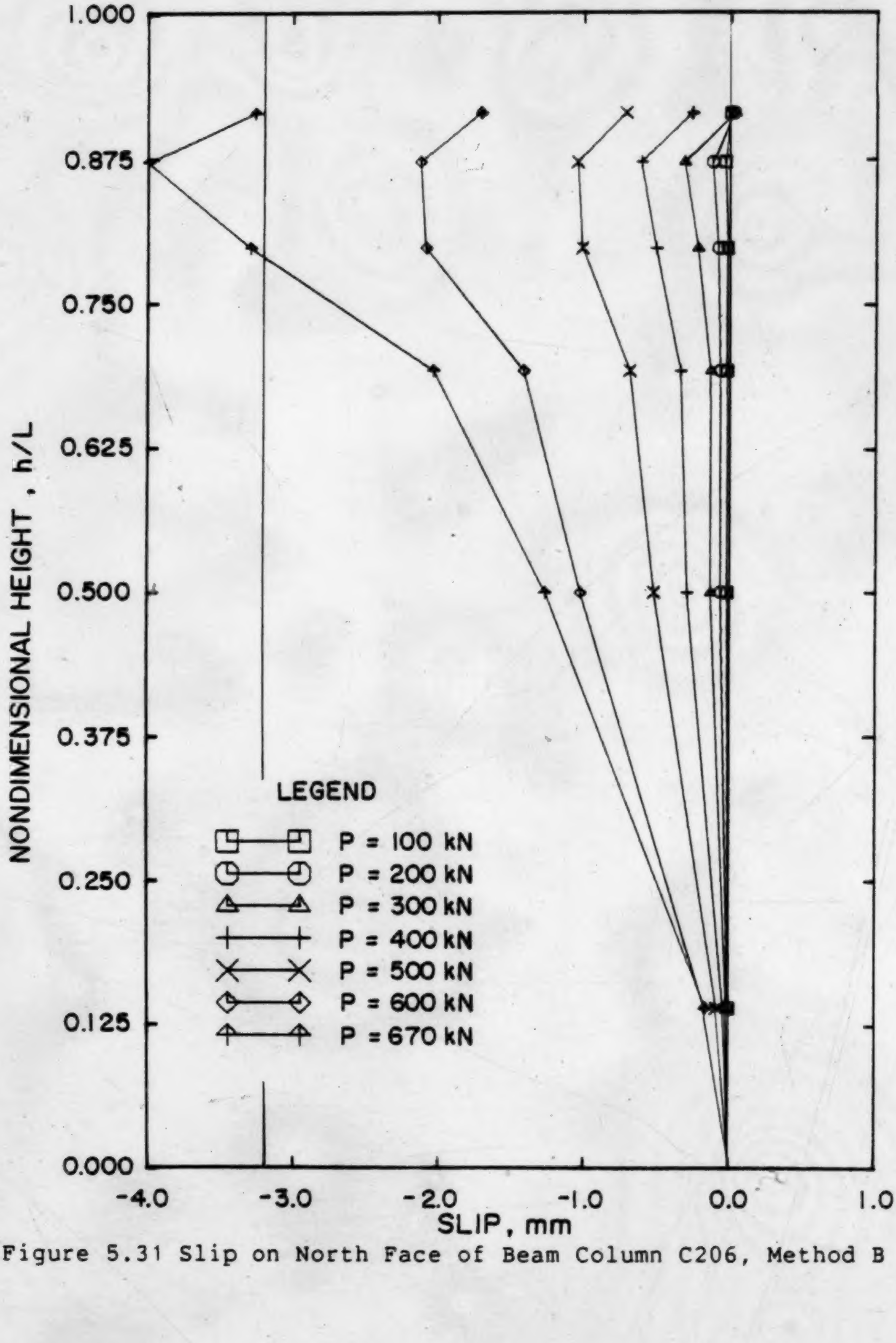

Figure 5.31 Slip on North Face of Beam Column C206, Method B

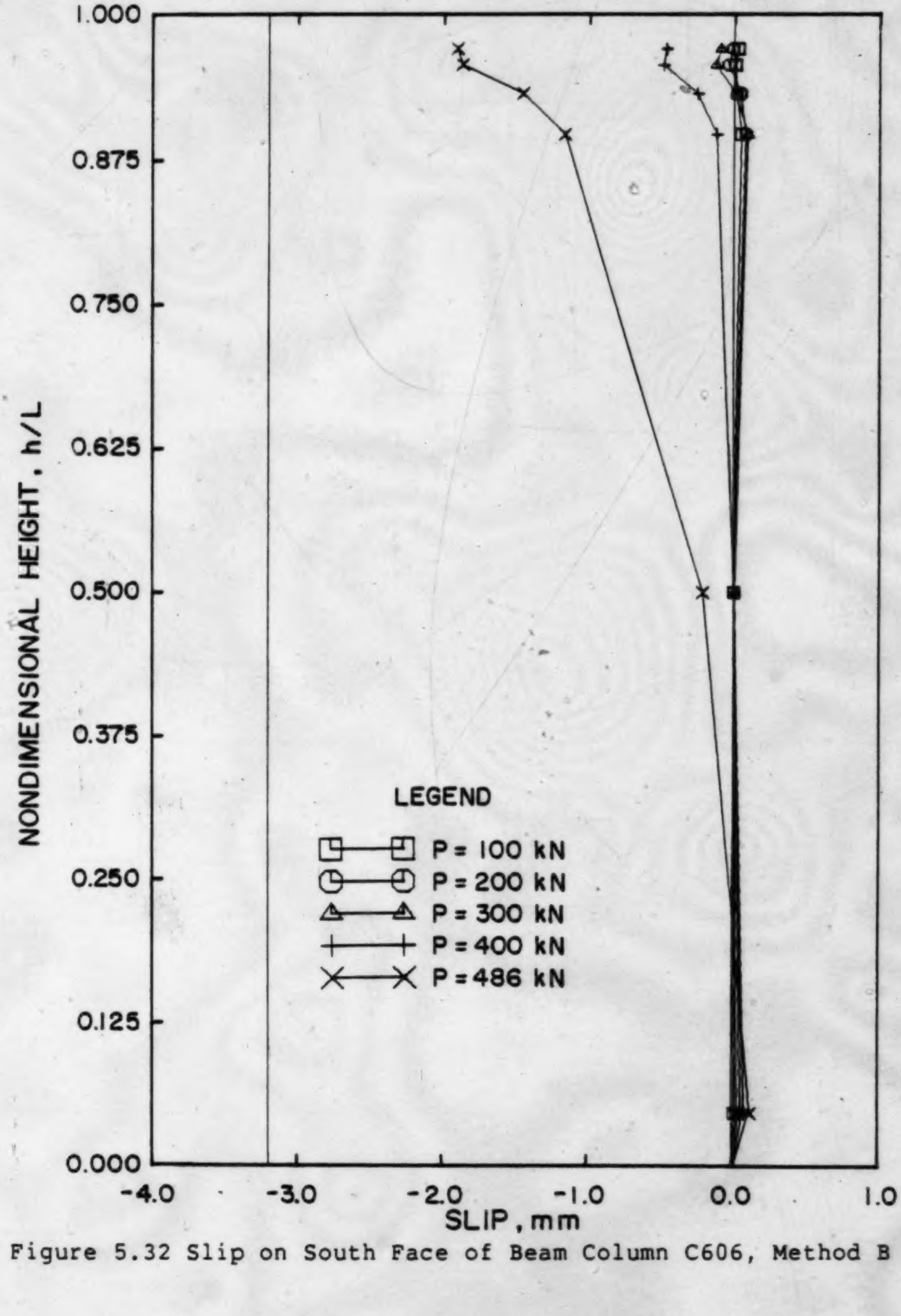

Figure 5.32 Slip on South Face of Beam Column C606, Method B

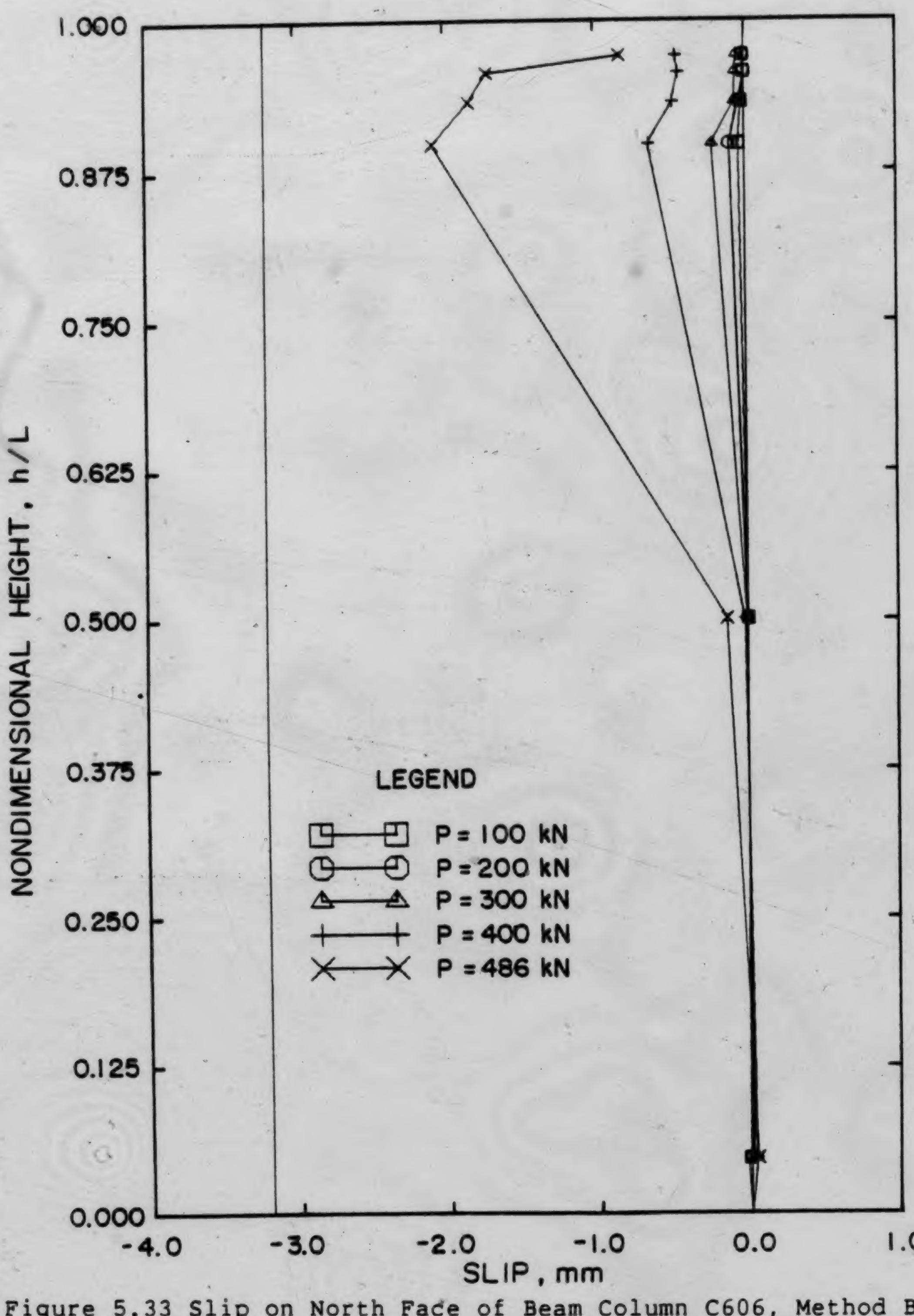

Figure 5.33 Slip on North Face of Beam Column C606, Method B

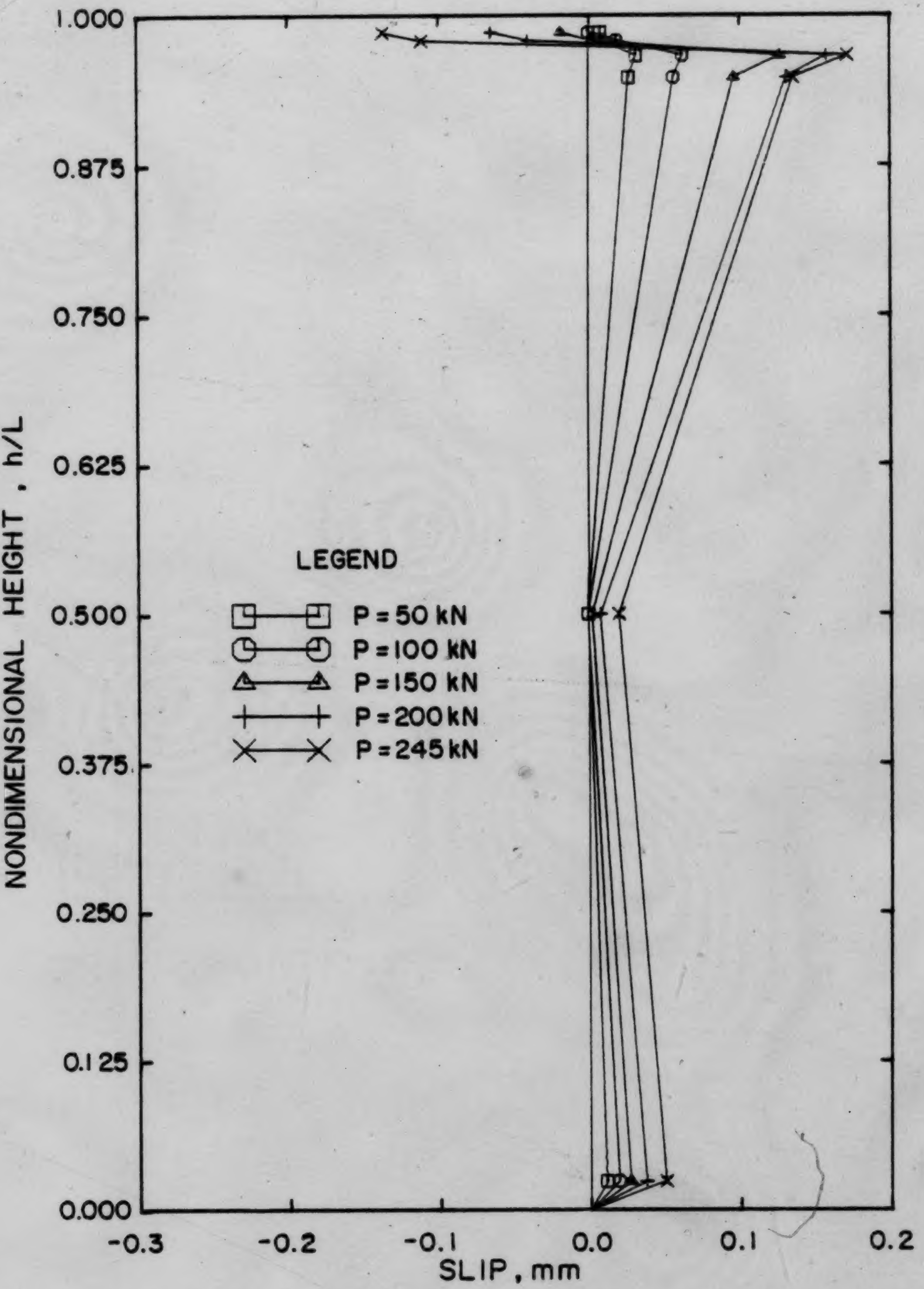

Figure 5.34 Slip on South Face of Beam Column C1206, Method B

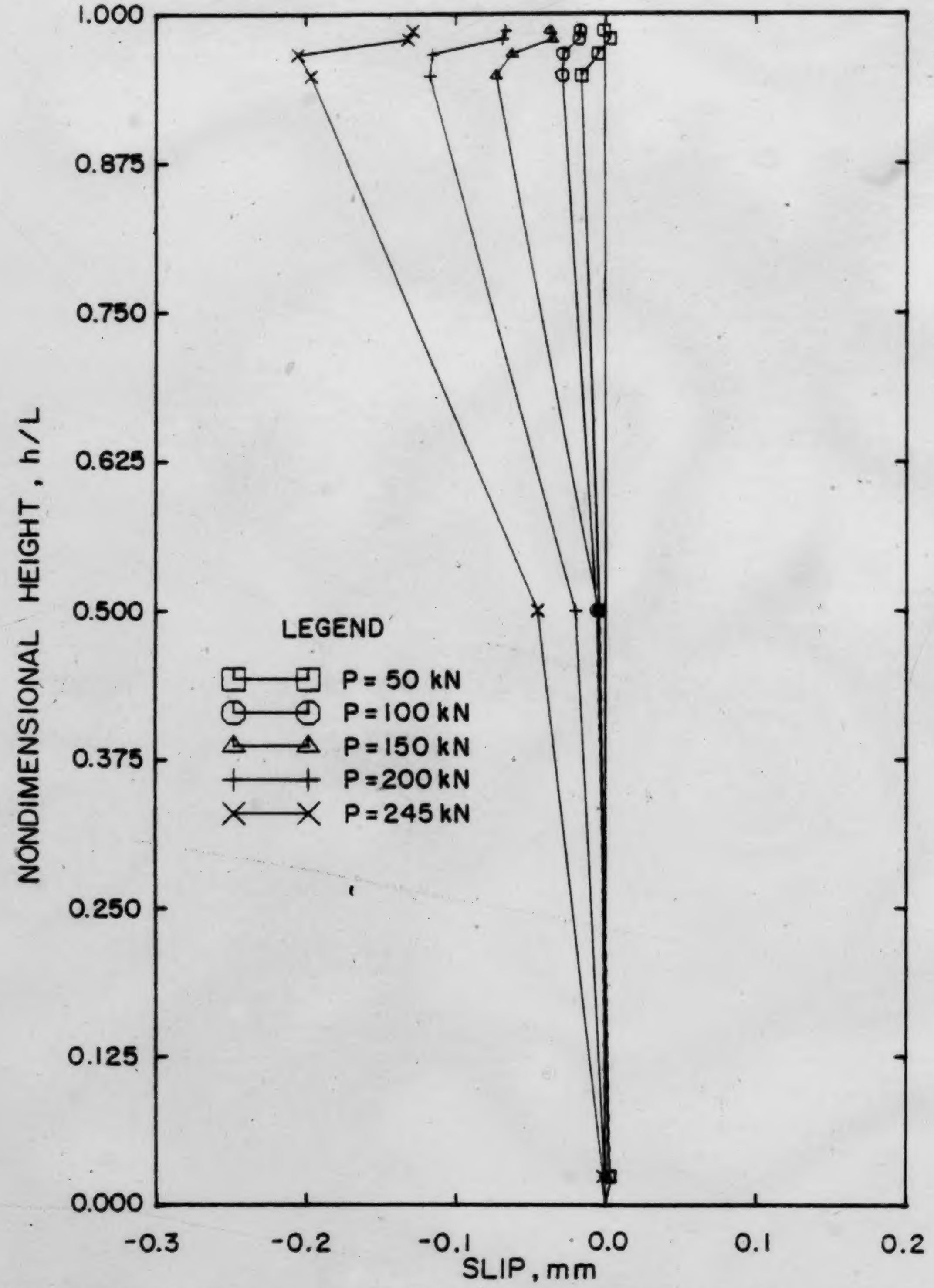

Figure 5.35 Slip on North Face of Beam Column C1206, Method B

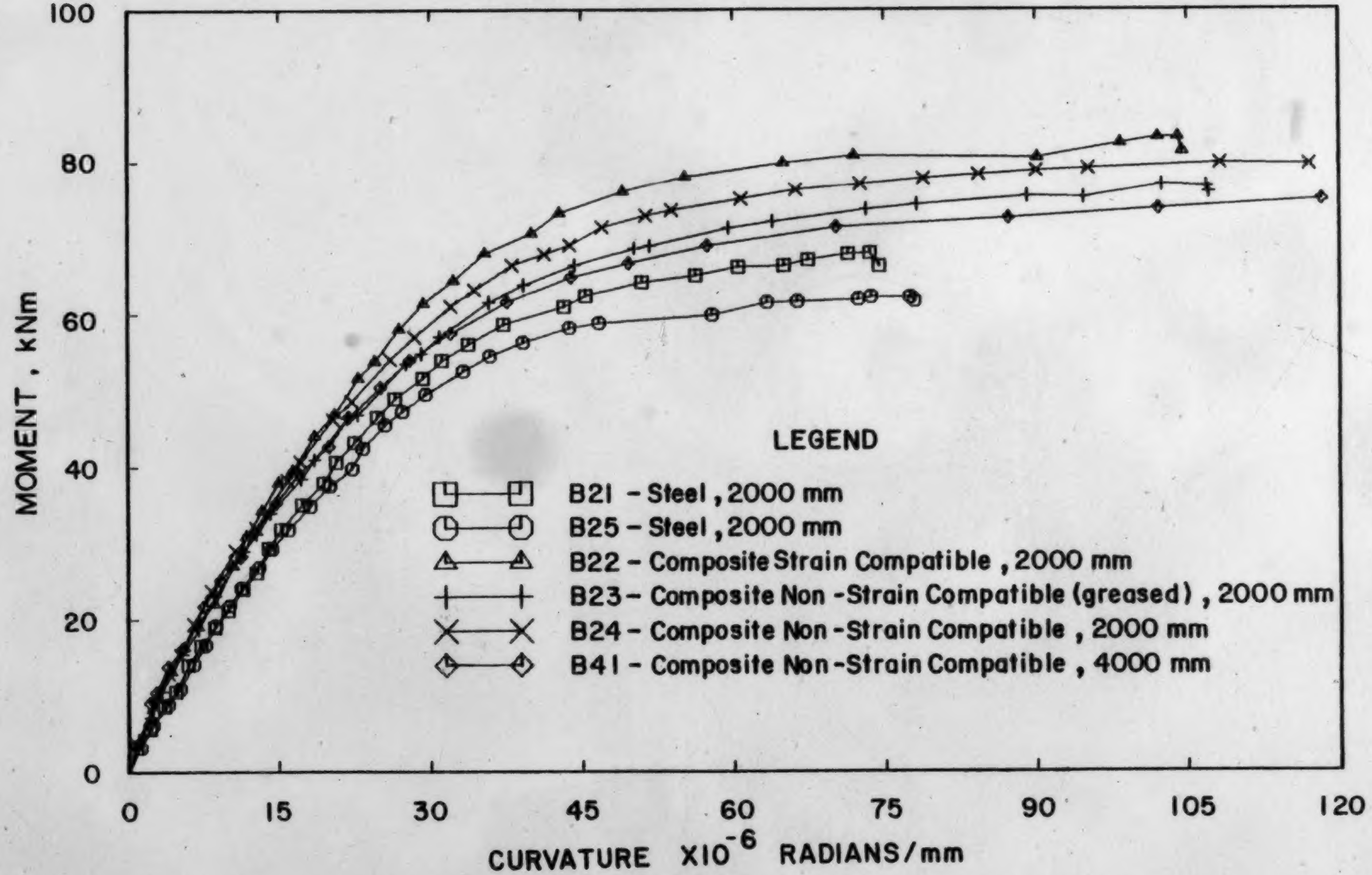

Figure 5.36 Moment Curvature Diagrams for Flexural Tests

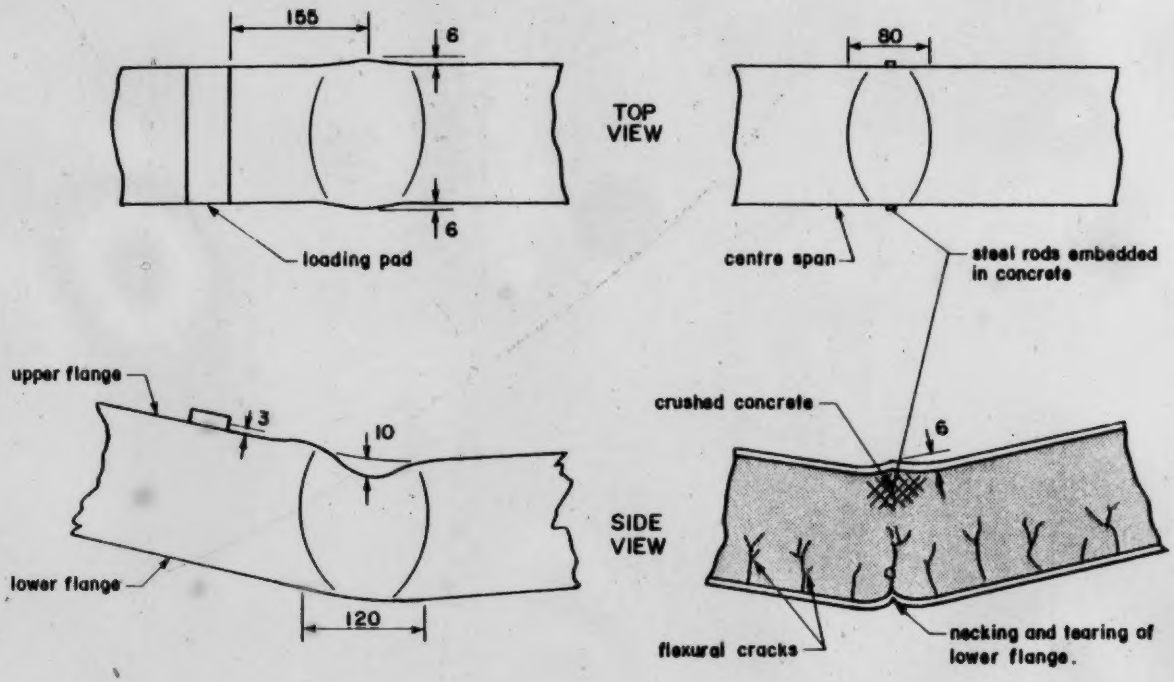
155
6
6
loading pad
TOP
VIEW
80
centre span
steel rods embedded
in concrete
upper flange
3
10
lower flange
120
SIDE
VIEW
crushed concrete
6
flexural cracks
necking and tearing of
lower flange.

STEEL
(a)

COMPOSITE
(b)

Figure 5.37 Typical Failure Modes for Flexural Tests

6. LOAD TRANSFER MECHANISMS

6.1 General

For non-strain compatible composite columns to obtain ultimate load capacities greater than that of their counterpart steel columns, some type of interaction and hence load transfer is required between the two materials. The manner in which the load is transferred from the steel shell to the concrete core will be referred to as a load transfer mechanism. For this test series four different mechanisms have been identified as follows:

1. Adhesion due to chemical reactions and/or suction forces resulting from capillary action during the hydration process.
2. Micro-interlocking of surface irregularities of the steel shell with the cement paste to which it is mated.
3. Friction due to pinching of the concrete core by the steel shell resulting from the eccentricity of the applied loads on the connection and/or buckling restraint provided by the concrete.
4. Binding or curvature effect which results from imposing compatible deformations on two materials of different flexural stiffnesses.

These can be classified into two groups according to scale: adhesion and micro-interlocking as micro effects and friction and binding as macro effects.

A mathematical solution has been developed to describe the micro-interlocking mechanism case and is presented in Section 6.2.2.1. Plausible scenarios are presented for the other load transfer mechanisms. The load transferred by these mechanisms is compared to the concrete load distributions derived from experimental data in Section 6.3.3.

6.2 Load Transfer Mechanisms

6.2.1 Adhesion

Adhesion of the two materials may be the result of chemical reactions and/or suction forces along the interface. Theories, as put forth by Wüzner, Nacken and von Rodt, and Pogany on the development and action of adhesive forces between steel and concrete are summarized by Rehm (1961). Rehm concludes that regardless of which concept corresponds more closely to actual conditions, adhesion exists between the two materials and that it should not be discounted as a viable load transfer mechanism during the early stages of loading when relative displacements are small. For concrete filled tubes, shrinkage of the concrete, would have an adverse effect on the development of adhesive forces.

The adhesive forces bind adjacent steel and concrete elements together forcing the concrete to undergo deformations that are equal to that of the steel. Adhesion is an elastic brittle load transfer mechanism. In the case of non-strain compatible composite HSS beam columns its contribution to transfer load is neglected since the adhesion forces are overcome at slip values less than 0.01 mm, Rehm (1961).

6.2.2 Micro-Interlocking

The concept of load being transferred by shear from steel to concrete through a series of cement paste keys interlocked and mated with the surface irregularities of the steel was first presented by Rehm (1961). Rehm surmised, after extensive work on load slip relationships of steel bars of varying surface roughnesses, that the load transferred and the rate of load transfer is dependent on the load deformation response of the shear keys, which is a function of the size, shape, spacing and material properties of the keys.

A shear transfer function of the form given in Equation 6.1 has been selected to model the shear deformation response of the system of cement paste shear keys.

$$v_x = a w_x e^{-b w_x} \tag{6.1}$$

where, v_x = shear load transferred per mm at a distance x along the length of the column from the lower end, N/mm

w_x = relative displacement between the two materials , that is as slip, mm

a,b = are constants defining the shape of the function

This function shown in Figure 6.1 is consistent with the load deformation response found by Rehm. The tail of this curve represents the frictional resistance provided by the cement paste rubble which lies between the steel shell and the concrete core. Both Rehm (1961), and Somayaji and Shah (1981) developed a governing differential equation for slip along the length of a reinforcing bar, as a function of a bond stress versus slip relationship and the applied load. A similar treatment of the problem is used here to determine the slip distribution along the length of a perfectly straight, concentrically loaded, concrete filled HSS column where strain compatibility is not ensured at the upper end. Given the slip distribution and the shear transfer function the distribution of load transfer from the steel to the concrete can be determined.

6.2.2.1 Development of the Governing Differential Equation for Slip

For the purpose of this discussion, the composite column is represented in Figure 6.2(a) as two rectangles, where the shaded area represents concrete and the plain area steel. At any distance x from the lower end, the load P, applied to the upper end of the column is shared by the concrete and the steel as shown in Figure 6.2(b). From equilibrium of the vertical forces in the x-direction for the section shown in Figure 6.2(b),

$$P = P_{cx} + P_{sx} \tag{6.2}$$

Assuming that both materials behave elastically, Equation 6.2 can be written as,

$$P = A_c E_c\left(\varepsilon_{cx} + \varepsilon_{sx} n \rho\right) \tag{6.3}$$

where, A_c = cross-sectional area of the concrete
E_c = modulus of elasticity of the concrete
ϵ_{cx} = longitudinal strain in the concrete at a distance x from the lower end
ϵ_{sx} = longitudinal strain in the steel at a distance x from the lower end
n = modular ratio, E_s/E_c
ρ = reinforcement ratio, A_s/A_c
= cross-sectional area of the steel
= modulus of elasticity of steel

At a distance x=l from the lower end of the column, the applied load is carried by the steel section alone, which causes a longitudinal strain in the steel ε_s.

$$\varepsilon_s = \frac{P}{A_s E_s} \tag{6.4}$$

Rearranging Equation 6.4 in terms of the load P, and substituting it into Equation 6.3, the longitudinal strain in the concrete at a distance x can be expressed as

$$\varepsilon_{cx} = \rho\, n\left(\varepsilon_s - \varepsilon_{sx}\right) \tag{6.5}$$

The local slip, w_x, is defined as the total difference in the elongation of the two materials from the lower end of the column where x=0, to the section at a distance x from that end.

$$w_x = \int_o^x \left(\varepsilon_{sx} - \varepsilon_{cx}\right) dx \tag{6.6}$$

Differentiating equation 6.6 with respect to x gives,

$$\frac{dw_x}{d_x} = \varepsilon_{sx} - \varepsilon_{cx} \tag{6.7}$$

Substituting the expression for concrete strain, Equation 6.5, into Equation 6.7 and rearranging the terms, dw_x/dx can be expressed as,

$$\frac{dw_x}{dx} = (1 + \rho n)\,\varepsilon_{sx} - \rho n \varepsilon_s \tag{6.8}$$

Differentiating Equation 6.8 with respect to x,

$$\frac{d^2 w_x}{dx^2} = \left(1 + \rho\ n\right) \frac{d\varepsilon_{sx}}{dx} \tag{6.9}$$

From equilibrium of the forces in the x-direction for a steel element of length dx and located a distance x from the lower end, as shown in Figure 6.2(c), the shear force at that point can be expressed as,

$$v_x = - \frac{dP_{sx}}{dx} \tag{6.10}$$

At a distance x, the steel load is given as,

$$P_{sx} = \varepsilon_{sx} A_s E_s \tag{6.11}$$

Similarily a small change in steel load with respect to x, at x, can be expressed as,

$$\frac{dP_{sx}}{dx} = \frac{d\varepsilon_{sx}}{dx} A_s E_s \tag{6.12}$$

Substituting Equation 6.12 into Equation 6.10 and rearranging the expression to give the rate of change of steel strain with respect to x, gives

$$\frac{d\varepsilon_{sx}}{dx} = - \frac{v_x}{A_s E_s} \tag{6.13}$$

Substituting Equation 6.13 into Equation 6.9 gives the governing differential equation for slip as a function of the shear transfer function,

$$\frac{d^2 w_x}{d_x^2} + (1 + \rho n) \frac{v_x}{A_s E_s} = 0 \tag{6.14}$$

The boundary conditions as shown in Figure 6.2(a), are as follows:

1. A steel plate across the lower end of the column forces the slip, w_x, to be zero at x=0.
2. At the upper end of the column, x=1, the concrete strain is zero and the steel strain is equal to ϵ_s. From Equation 6.7, at x=1, $dw_x/dx=\epsilon_s$.

6.2.2.2 Solution of the Governing Differential Equation for Slip

In order to solve this governing equation for slip, an iterative step-by-step numerical integration method had to be applied. The solution process takes on the form:

1. Treat the problem as an initial value problem - i.e. the initial values of the dependent variable w_x and its derivative dw_x/dx are known at x=0, however, because dw_x/dx is unknown in this case, a trial value is used instead.
2. Transform the second order differential equation into a set of two first order differential equations, apply two sets of Runge Kutta formulas and integrate over the length of the column from x=0 to x=l.
3. Compare the value dw_x/dx at x=l as calculated by this step-by-step integration, with dw_x/dx at x=l given as a boundary condition. If the difference in the two values is outside acceptable limits of accuracy, then a new trial value of dw_x/dx at x=0 must be used, and the solution process repeated. If the difference between the two values is acceptable, then the solution has been found.

Based on the solution process and given the shear transfer function defined in Figure 6.1, the slip distributions for three different loads have been determined for test specimen C1205 and are shown in Figure 6.3. Square, octagonal and triangular symbols represent the average slip values, as determined by Method B, for the north and south faces of column C1205 for applied loads of 100 kN, 300 kN, and 490 kN, respectively. For the given set of loads, the calculated slip distributions correspond closely to those measured in both magnitude and shape as can be seen by comparing the curves in Figure 6.3 with the corresponding test values as shown.

6.2.3 Macro-Interlocking - Friction

At the top of the non-strain compatible composite columns, load was applied to plates welded to the outside of the tube as shown in Figure 3.1. These were eccentric to the resultant of the load in the tube and concrete below the connection, as shown in a free body diagram of the upper end connection in Figure 6.4. To equilibriate this couple, tensions are developed in the wall of the tube at the top of the connection and compressions in the concrete at the bottom of the connection, as shown in Figure 6.4. Friction develops between the steel and concrete due to the normal force exerted by the concrete on the steel. Later in the loading sequence a similar action occurs where local buckling of the tube develops. The magnitude of the friction force developed is a function of the b/t ratio of the tube (local stability due to inplane forces), the flexural rigidity of the tube wall, the eccentricity of the connection, the moment rotation characteristics of the connection, and the loads applied to the column.

Characteristically, for the non-strain compatible tests, the load transfer to the concrete by this mechanism occurred in a very short length just below the connection plates at the upper end of the column. It was observed that this pinching action was not significant until the compressive strains for the steel wall exceeded the yield strain, after which the loads transferred by this action increased in proportion to the applied load. At the present time the information necessary to determine the normal force between the steel and the concrete is not available. No attempt has been made to develop a model for the friction macro-interlocking load transfer mechanism.

6.2.4 Macro-Interlocking - Binding

The load transferred by this mechanism was done through forced deformation. The two materials are bound together by imposing compatible global deformations on two materials of different flexural stiffnesses. This effect is further enhanced due to a volumetric increase or swelling of the concrete as a result of micro-cracking, which the concrete experiences when subjected to large compressive strains.

The mechanical binding of these two materials forces the concrete to undergo some deformation along the length of the column which is proportional to that of the steel in the same region. The rate and quantity of load transferred due to forced deformation depends upon the quality of the binding effect, which is a function of the applied load, curvature and length of the column, and the relative movement of the concrete with respect to the steel. For beam columns, the effect of this mechanism diminishes as the column length becomes shorter and increases as the eccentricity of the applied load increases.

This mechanism is the dominant load transfer mechanism for those beam column members subject to or approaching a state of pure flexure. For beam column test specimens C1206 and C606, the mechanism is characterized by a steady transfer of load up to a maximum value which occurred at a distance of less than half the column length from the free surface of the concrete, for the entire range of applied loads.

6.3 Non-Strain Compatible Column Tests

6.3.1 Loads in Steel

Loads carried by the steel shell at any location along the length of the tube were determined from a pair of electrical resistant strain measurements which described the linear strain distribution across the section about the axis of bending. For calculated steel loads based on the steel stub column tests, the stress was found for the corresponding strains of each of twenty-two points across the width of the section from the stub column curve as described in Section 4.1.2.4, and integrated over the area to give the total force in the steel. As discussed in

Section 4.1.2.5 a similar procedure was used to determine load from the tension coupon test data except that the effects of residual stresses, automatically accounted for in the stub column tests, had to be incorporated.

The accuracy of these procedures was assessed by examining the ratio of the predicted load to the applied load for the steel column tests, as shown in Figures 6.5 and 6.6. Each point on these figures represents the mean of fifteen predicted to applied load values made along the length of the column. In all cases the fifteen measuring stations considered were below the loading plate area. Outliers from each of these subsets have been rejected using Chauvenet's criterion.

In general, as the applied load was increased, the ratio of predicted to test mean values approached a value of one, indicating that this procedure for evaluating the load carried by the steel was satisfactory. At low loads, where the magnitude of the steel strains are in the order of 10 microstrains, these strains are comparable to the sensitivity of the measurement - i.e. one per cent of full scale. The results obtained from strains that are not much in excess of the sensitivity of the gauges are suspect and may not be considered reliable.

Using Chauvenet's criterion, seven outliers were rejected for the population of means shown in Figure 6.5. Based on stub column data the mean value of the predicted to test value is determined to be 0.974 with a coefficient of variation of 0.035. From Figure 6.6, based on the tension coupons and longitudinal residual stress distribution data, six outliers were rejected from the population and the mean value is determined to be 0.953 with a coefficient of variation of 0.036. For subsequent analyses loads in the steel have been taken to be those predicted on the basis of stub column test data.

6.3.2 Loads in Concrete

For any given test, load level, and location along the length of the column, the load in the concrete was determined simply as the difference between the applied load and the load calculated in the steel based on the corresponding steel strains.

$$P_{cx} = P - P_{sx} \tag{6.15}$$

Figures 6.7 to 6.12 give the distributions of load in the concrete as a function of the distance from the upper surface of the concrete over the history of the tests. In each of these figures an insert has been included which identifies the column as being loaded concentrically or at a constant eccentricity of 65 mm. Irregularities in the concrete load distributions are the direct result of the variations in the steel strains used to determine the concrete loads in these distributions.

For columns with slenderness ratios of 60 and 118, the variations are reflected in the concrete load distributions as small fluctuations about a best fit curve for the data. Large variations in adjacent concrete load values occur at the upper end of the column just below the connection plates for all columns and along the entire length of columns with a slenderness ratio of 20, for a range of applied loads approaching the ultimate load. These variations are attributed to localized straining of the tube as a result of out-of-plane movement of the tube wall. As an example, an increase in steel strain over the expected value, where the expected value is that value which would be obtained without variations of any nature, translates as a decrease in corresponding concrete load.

Due to the manner in which the load was applied to the column, load was transferred to the concrete from the steel, and not vice versa. It is reasonable then, to suggest that the load carried by the concrete at any location along the length of the column from the free surface of the concrete at the upper end is equal to or greater than the load carried by the concrete at a location nearer to the free surface. Based on this premise, an understanding of the irregularities in the concrete load distributions, and a knowledge of the general behaviour of each column, smooth curves have been constructed to fit the calculated concrete loads.

The concrete load distributions given in Figures 6.13 and 6.14 for the two longer concentrically loaded columns, are reasonable approximations of the measured curves plotted in Figures 6.7 and 6.8, except for points close to the upper end of the column. This is less true for column C205, plotted in Figures 6.15 and 6.9 for smooth curves and measured values, respectively. In fitting the curves in Figure 6.15, the data points at 1000 mm were disregarded due to the spurious nature of the points in the region which is influenced by end effects.

The concrete load distributions given in Figure 6.16 and 6.17 for the two longer eccentrically loaded columns closely resemble the corresponding measured curves in Figures 6.10 and 6.11, while Figure 6.18 is an ideal estimate of the data in Figure 6.12. As will be seen in the next section the characteristic shapes of these curves are indicative of the load transfer mechanisms that were effective.

6.3.2.1 Concentrically Loaded Columns (C205,C605,C1205)

Test C1205 exhibited the general behavioural characteristics of a column in which the predominant load transfer mechanism is micro-interlocking. Applying the proposed shear transfer function, the governing differential equation for slip, and the appropriate boundary conditions, the slip distributions for the specified range of loads were determined. As shown in Section 6.2.2.2, there is excellent correlation in magnitude and shape between those slip distributions and those determined experimentally, as shown in Figures 6.3, 5.28 and 5.29, respectively.

As given by Equation 6.16, the concrete load distributions can be determined by integrating the shear values corresponding to the slip values from the shear transfer function and given by the slip distributions, along the length of the column from the free surface of the concrete at the upper end of the column.

$$P_{cx} = \int_{l}^{o} v_x dx \qquad (6.16)$$

The concrete load distributions, for the applied loads of 100, 300, and 490 kN, are shown as dashed lines for the predicted values and solid lines for the experimentally determined values in Figure 6.14. The two sets of curves are similar in shape and magnitude. The differences are accountable as follows:

1. For applied loads of 100 and 300 kN during the early stages of loading where the strains measured in the steel were small, the loads predicted to be carried by the steel tended to be less than the expected value, as previously discussed in Section 6.3.1. This leads to an over-estimation of the concrete load component for these applied loads as shown in Figure 6.14. This over-estimation, expressed as the percentage of the total load carried by the concrete, decreases with an increase in the applied load. This coincides with the better steel load prediction as shown in Figure 6.5.
2. The mathematical model for micro-interlocking is

restricted to determining the load transferred for a perfectly straight, concentrically loaded column which undergoes no deflections for the range of specified loads. For an applied load of 490 kN the two curves are essentially identical except for the maximum transferred load attained. At this load the column had deflected laterally 30 mm. The difference in the curve can be attributed in part to the inability of the model to account for the deflected shape of the column under load.

Regardless of the inability of the model to predict precisely the quantity and the rate of load transferred, it indicates that micro-interlocking of the two materials exists and that given the appropriate conditions a substantial amount of load can be effectively transferred from one material to the other by this mechanism.

The remaining tests in this series C205 and C605 have, for the range of applied loads, a combination of effective mechanisms transferring load from the steel to the concrete. This is illustrated, by examining the average concrete load as a function of applied load, in a region 76 mm long just below the connection plates. As shown in Figure 6.19, all three columns of this series exhibit the same behavioural characteristics in this region for applied loads less than 500 kN. The difference in the maximum concrete load attained between test C205, and tests C605 and C1205 is believed to be the result of shrinkage. Column C205 was the only specimen in which shrinkage cracks were noticed at the top end prior to testing.

Figure 6.19 suggests that load was transferred by one mechanism for loads less than 500 kN and by a combination of mechanisms above this load. In this region of the column and for loads less than 500 kN, the dominant load transfer mechanism is micro-interlocking. The descending branch of this part of the curve coincides with increasing slip in the region, which is consistent with the behaviour described by the shape of the shear transfer function. As shown by the dashed lines in this figure, the load transferred by the micro-interlocking mechanism is negligible in that region after an applied load of about 600 kN and a measured slip between 0.8 mm and 1.3 mm. For larger loads, for both tests C205 and C605, load is transferred to the concrete by the friction resulting from macro-interlocking of the two materials. This is shown in Figure 6.19 as exponential increase in concrete load, and in Figures 6.14 and 6.15 as a sharp increase in concrete load in the region just below the connection plates. For both tests C205 and C605 further load is introduced into the concrete along the length of the column via the micro-interlocking mechanism. In Figures 6.14 and 6.15 for tests C605 and C205, the constant increase in concrete load, beyond the region in which macro-interlocking takes place and for load greater than 500 kN, infers that there is a minimum load transferred by micro-interlocking regardless of the slip and has a value between 15 N and 25 N per millimeter of length along the column.

6.3.2.2 Eccentrically Loaded Columns (C206,C606,C1206)

Up to an applied load of 150 kN the predominant load transfer mechanism for the columns of the test series is micro-interlocking. The characteristic shapes of the concrete load distribution curves for applied loads in this range, as shown in Figures 6.16 through 6.18, are the same as those for the concentrically loaded column series. Columns C206 and C205 were tested when the concrete was fifty and fifty-five days old, respectively. The apparent shift of the concrete load distribution curve, such that load is being introduced into the concrete at some distance from the free surface and continuing translation of these curves away from that surface as the applied load increases, is believed to be the result of the concrete shrinking away from the walls of the tube as was the case for test C205. For test C206, this reduces the load transferred by this mechanism in the region affected by shrinkage of the concrete to a value of zero.

The average concrete load in a 76 mm long region directly below the connection plate is plotted as a function of applied load for the eccentrically loaded columns. It should be noted that the applied load scale in Figure 6.20 is twice that in Figure 6.19. Load transfer because of forced deformation through macro-interlocking-binding of the two materials becomes evident for applied loads greater than 150 kN which corresponds to a curvature of approximately 10 microradians per millimeter. These values are based on a comparison of the rate of load transfer, the maximum concrete load obtained as a ratio of applied load, and the location along the length of the column in which that load was achieved, for concentrically loaded and eccentrically loaded columns. The load transfer by this mechanism is characterized by the concrete load curves for the region below the connection plates. As shown in Figure 6.20, there is no decrease in load carried by the concrete in this region, as was the case for the concentric series. Measured slips for these columns were less than their counterparts for the concentric series, with the greatest difference being an order of magnitude for column C1206. These values of slip reinforce the concept of forced deformation through binding.

Again the exponential increase in concrete load for the region below the connection plate for columns C206 and C606 indicates a pinching action of the tube on the concrete and an introduction of load into the concrete through friction. Although this action is less pronounced for test C606, it is well developed for test C206 and is defined as a sharp increase in concrete load in the region just below the connection plates as shown in Figure 6.17 and 6.18 respectively. A summary of the effective load transfer mechanisms and associated load ranges is given for both test series in Table 6.1.

Table 6.1 Effective Load Transfer Mechanisms

Concentrically Applied Load, e = 0.0 mm		
Specimen	Load Ranges, kN	
	0 - 500	500 - failure
C205	2	2, 3
C605	2	2, 3
C1205	2	-

Eccentrically Applied Load, e = 65.0 mm				
Specimen	Load Ranges, kN			
	0-150	150-350	350-500	500-failure
C206	2	2, 4	2, 4	3, 4
C606	2	2, 4	2, 3, 4	-
C1206	2	2, 4	-	-

Notes: 1. The adhesion mechanism as a load transfer mechanism is of no practical significance since the adhesive forces are overcome at low values of relative displacement (w < 0.01 mm), Rehm (1961).

2. Load Transfer Mechanism Identification Numbers
   1 - Adhesion
   2 - Micro-Interlock, surface irregularities
   3 - Friction, pinching or restrained buckling action
   4 - Binding, curvature effect

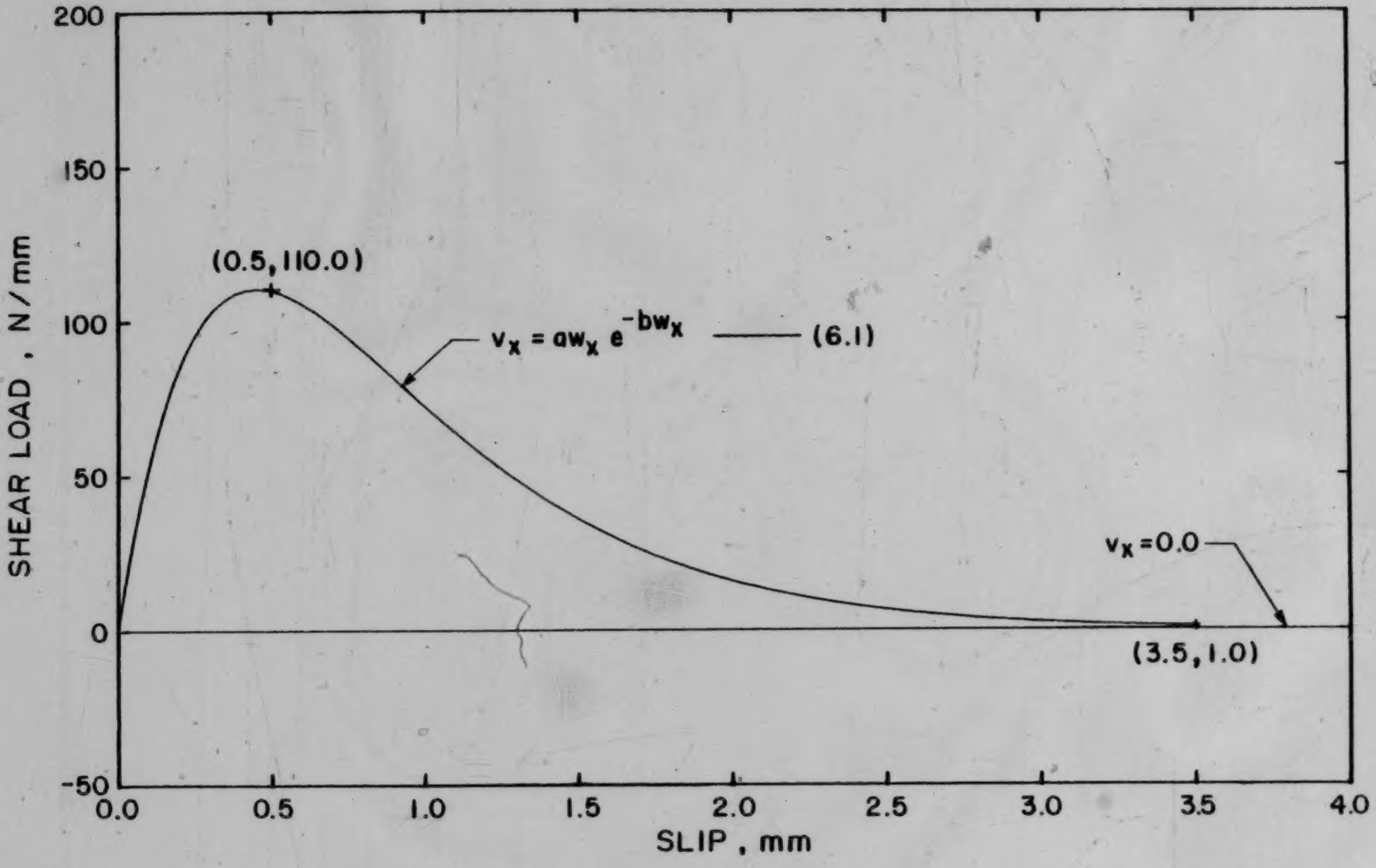

Figure 6.1 Shear Transfer Function

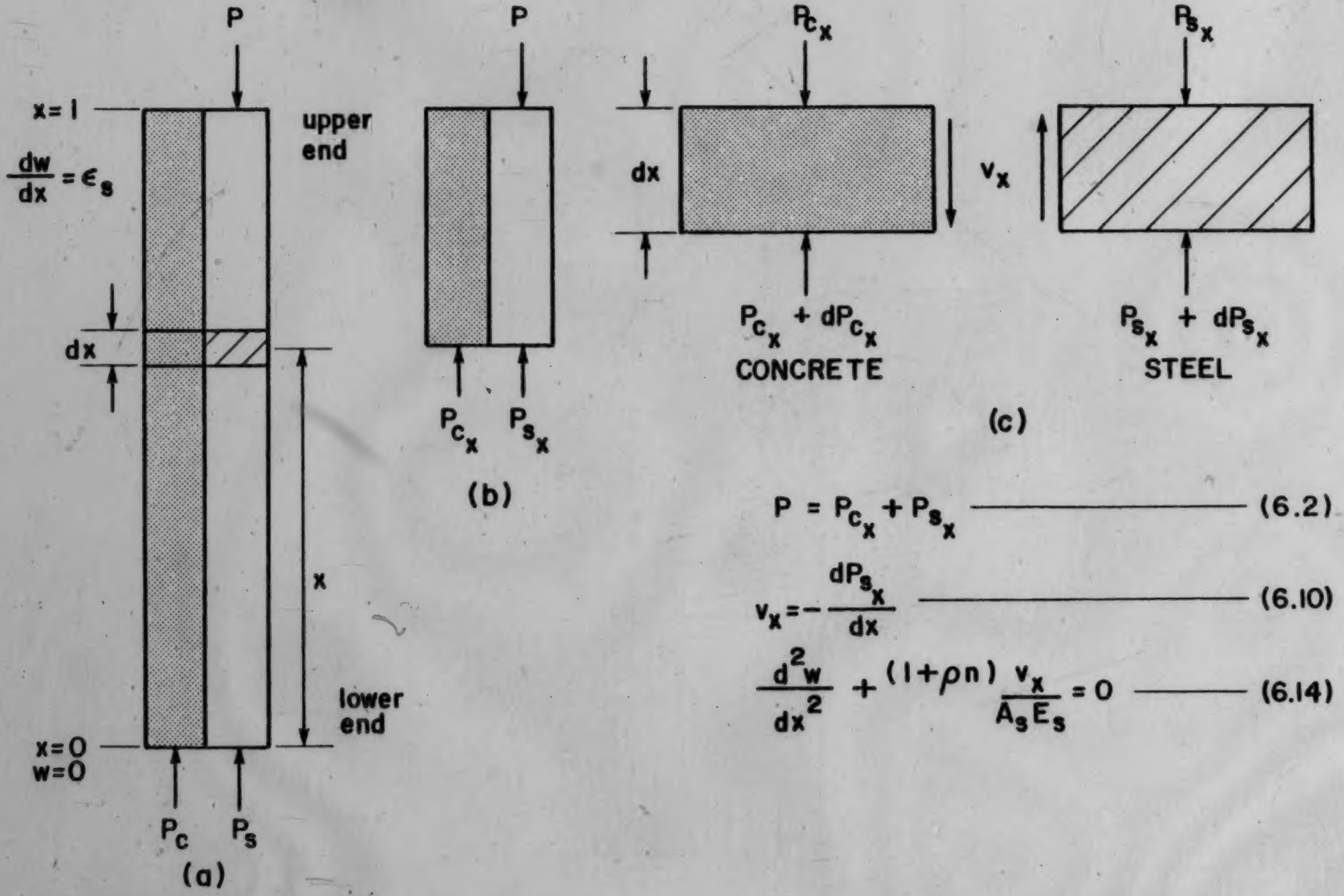
P
P
P_{c_x}
P_{s_x}
x = l
$\frac{dw}{dx} = \epsilon_s$
upper end
dx
dx
v_x
x
lower end
x=0
w=0
P_c
P_s
(a)
P_{c_x}
P_{s_x}
(b)
$P_{c_x} + dP_{c_x}$
CONCRETE
$P_{s_x} + dP_{s_x}$
STEEL
(c)

$$P = P_{c_x} + P_{s_x} \text{ ———— } (6.2)$$

$$v_x = -\frac{dP_{s_x}}{dx} \text{ ———— } (6.10)$$

$$\frac{d^2w}{dx^2} + (1+\rho n)\frac{v_x}{A_s E_s} = 0 \text{ ———— } (6.14)$$

Figure 6.2 Free Body Diagrams Used for the Development of the Governing Differential Equation

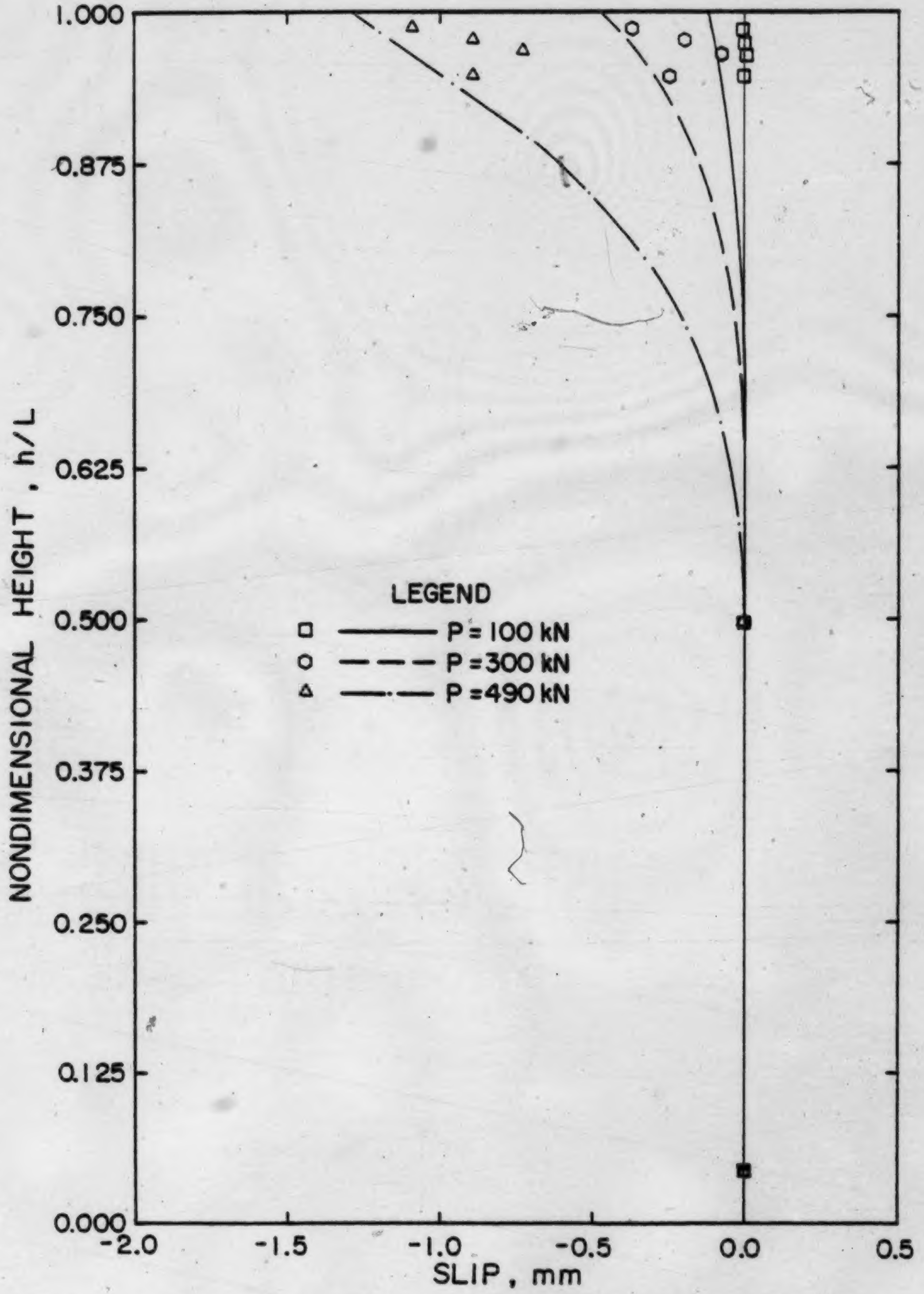

Figure 6.3 Slip Distributions for C1205 Computed from the Governing Differential Equation

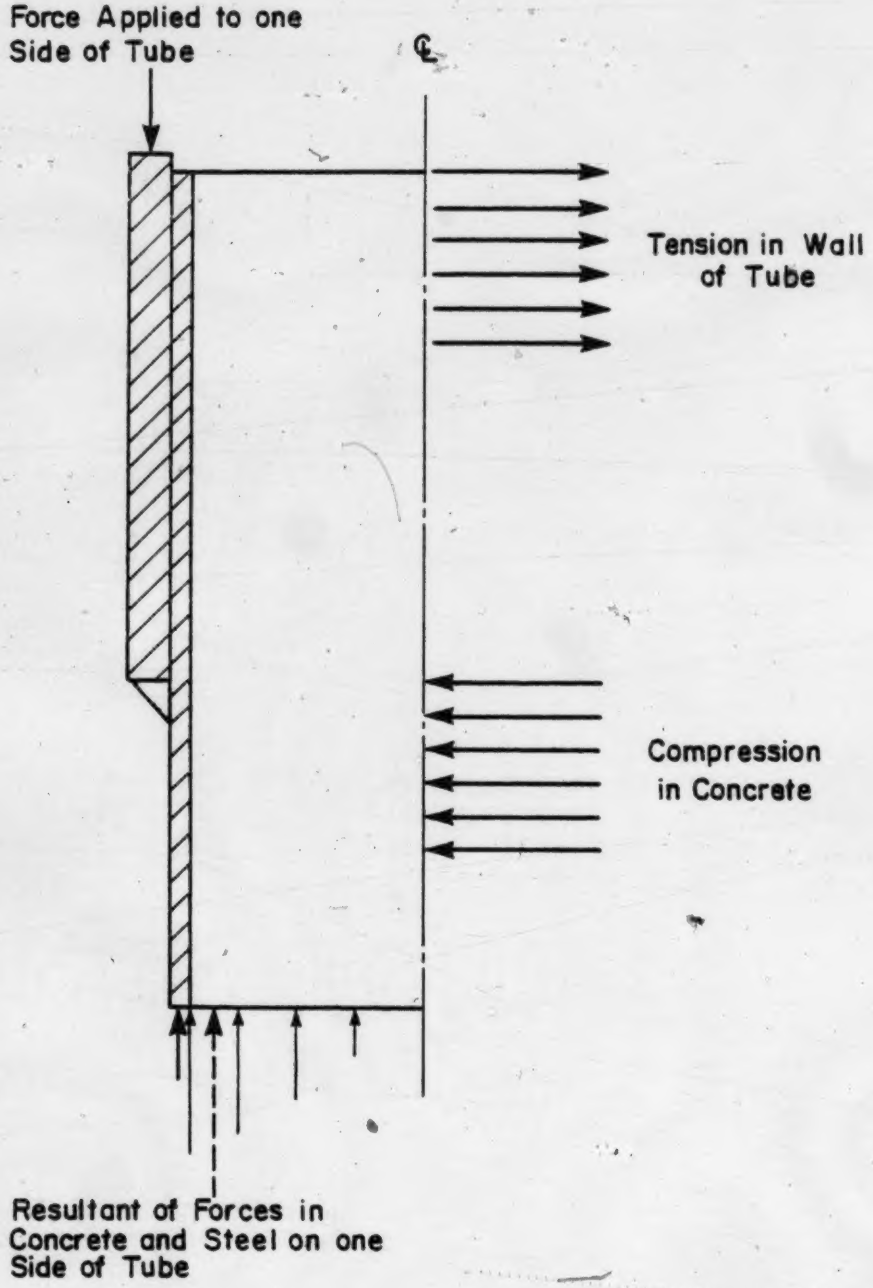
Force Applied to one Side of Tube
℄
Tension in Wall of Tube
Compression in Concrete
Resultant of Forces in Concrete and Steel on one Side of Tube

Figure 6.4 Macro-Interlocking - Friction Load Transfer at Top of Column

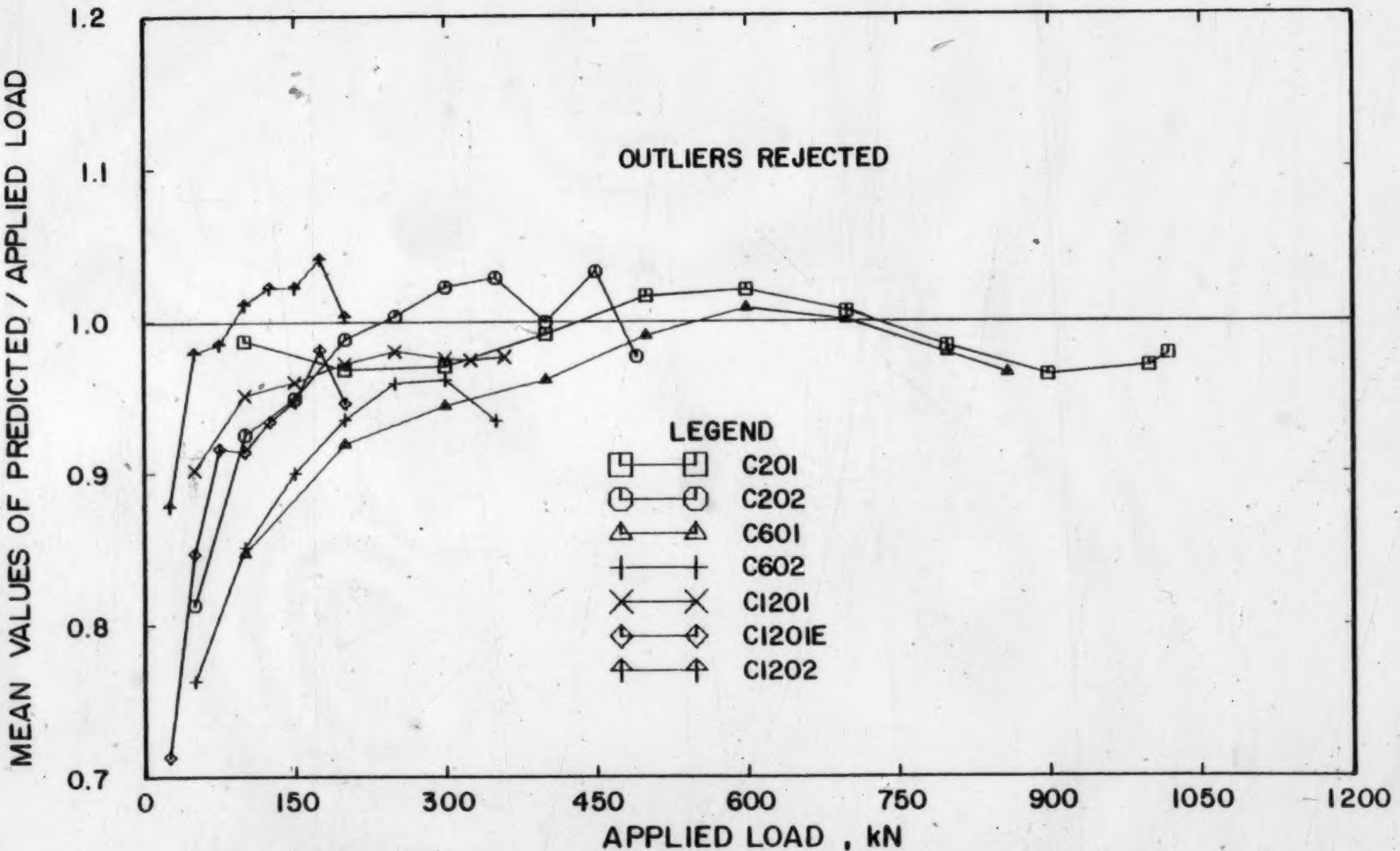

Figure 6.5 Ratios of Predicted to Applied Loads of the Mean Loads for Steel Columns, Based on Stub Column Data

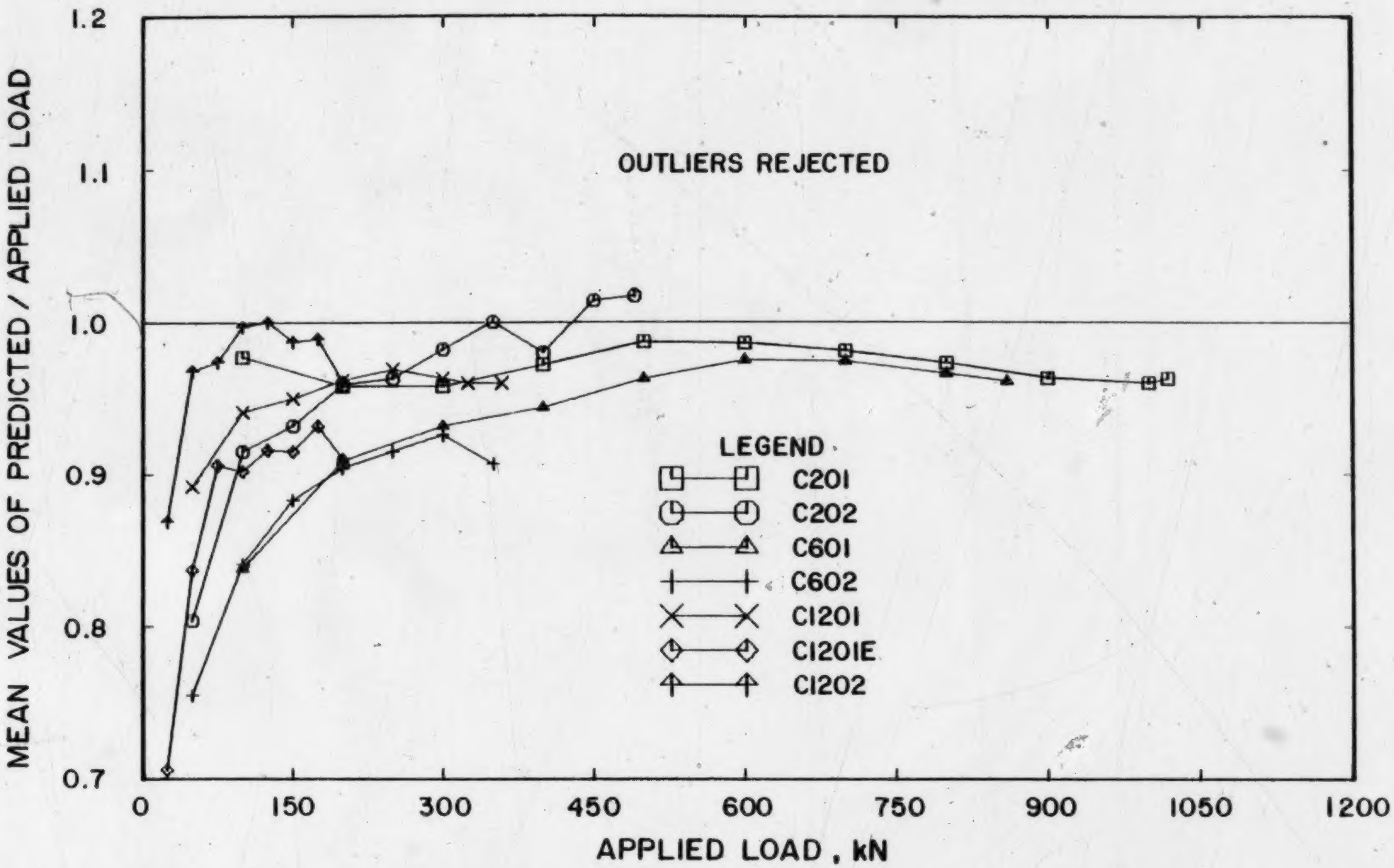

Figure 6.6 Ratio of Predicted to Applied Loads of the Mean Loads for Steel Columns, Based on Tension Coupons and Longitudinal Residual Stress Data

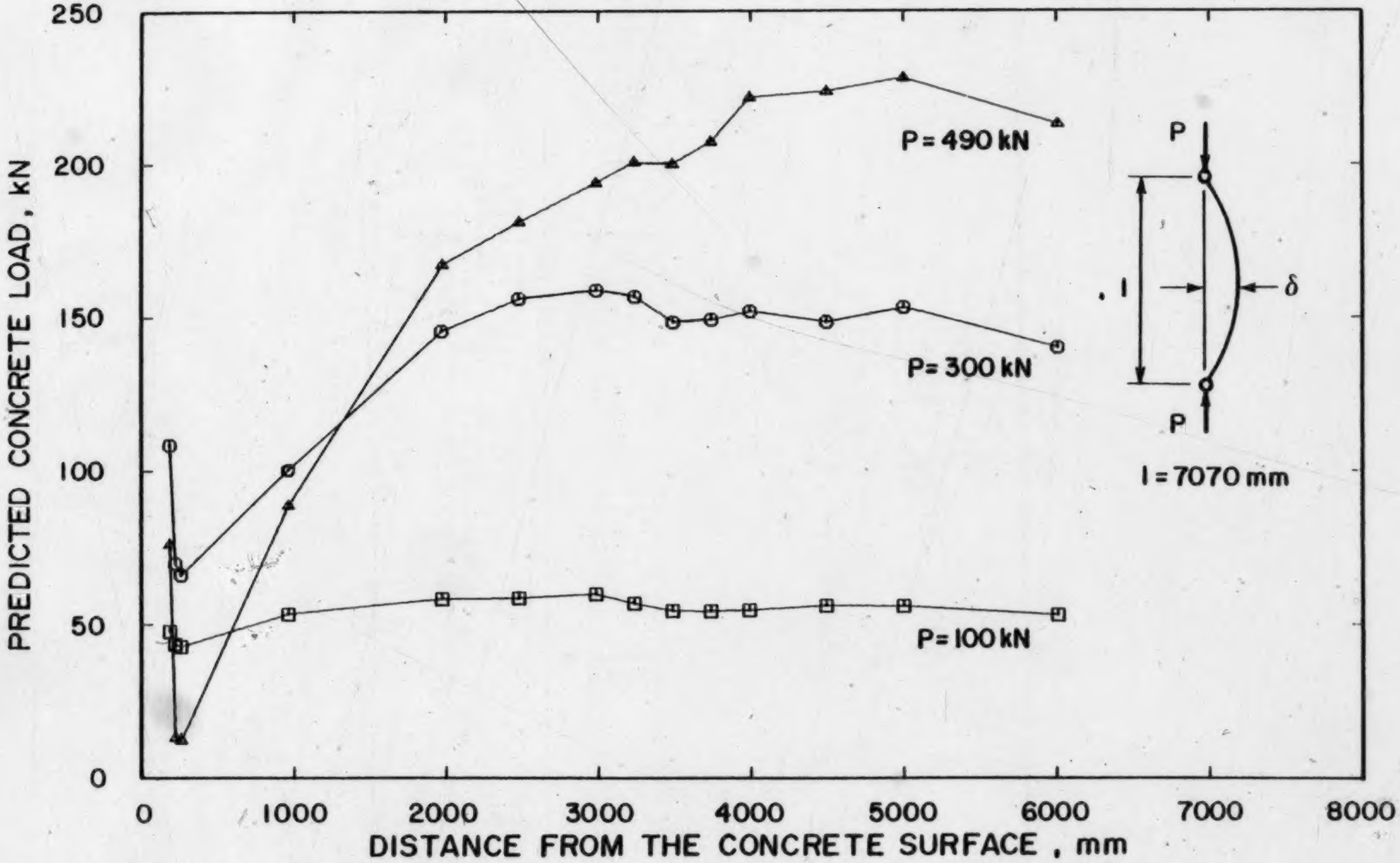

Figure 6.7 Concrete Load Distributions for Column C1205

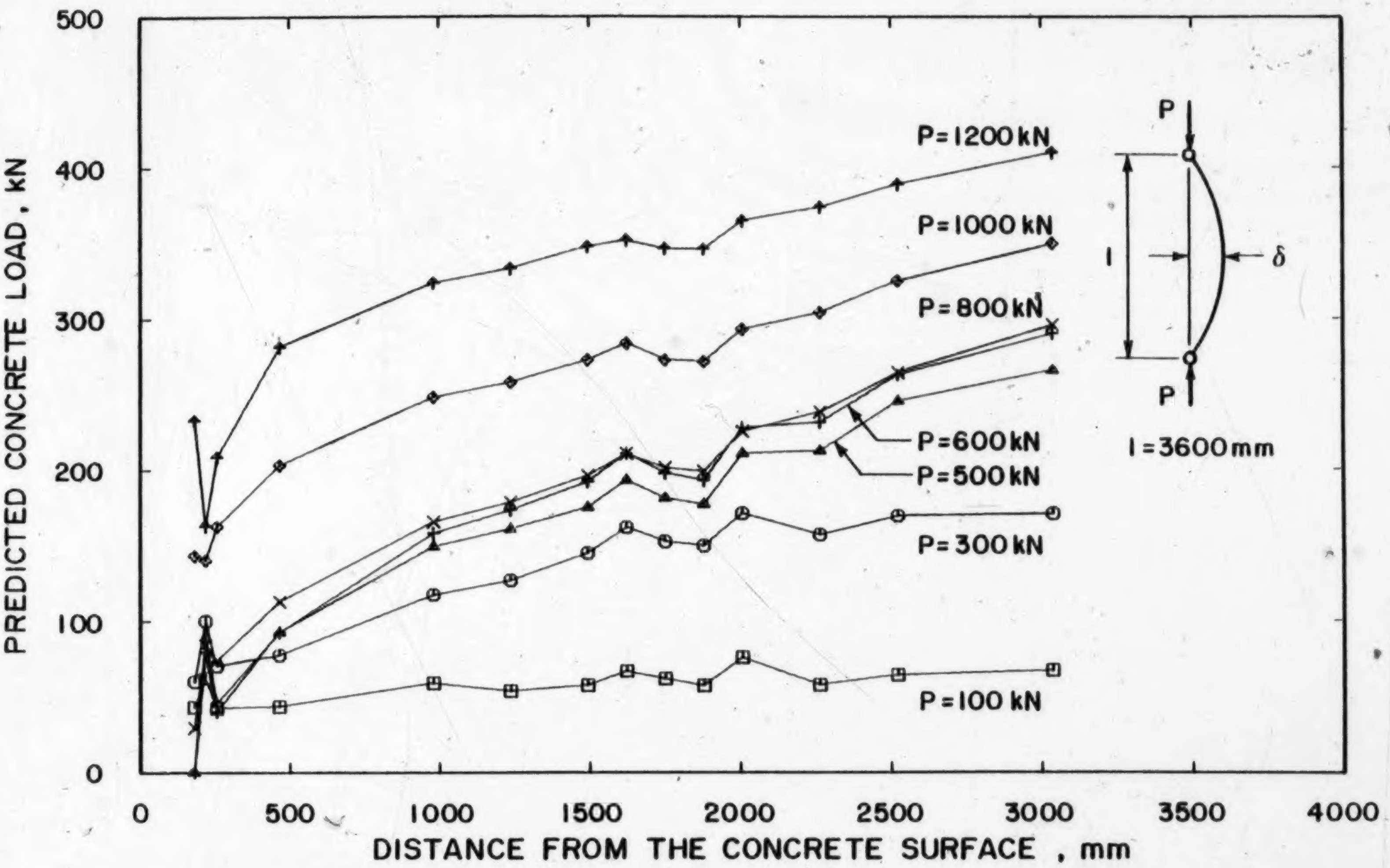

Figure 6.8 Concrete Load Distributions for Column C605

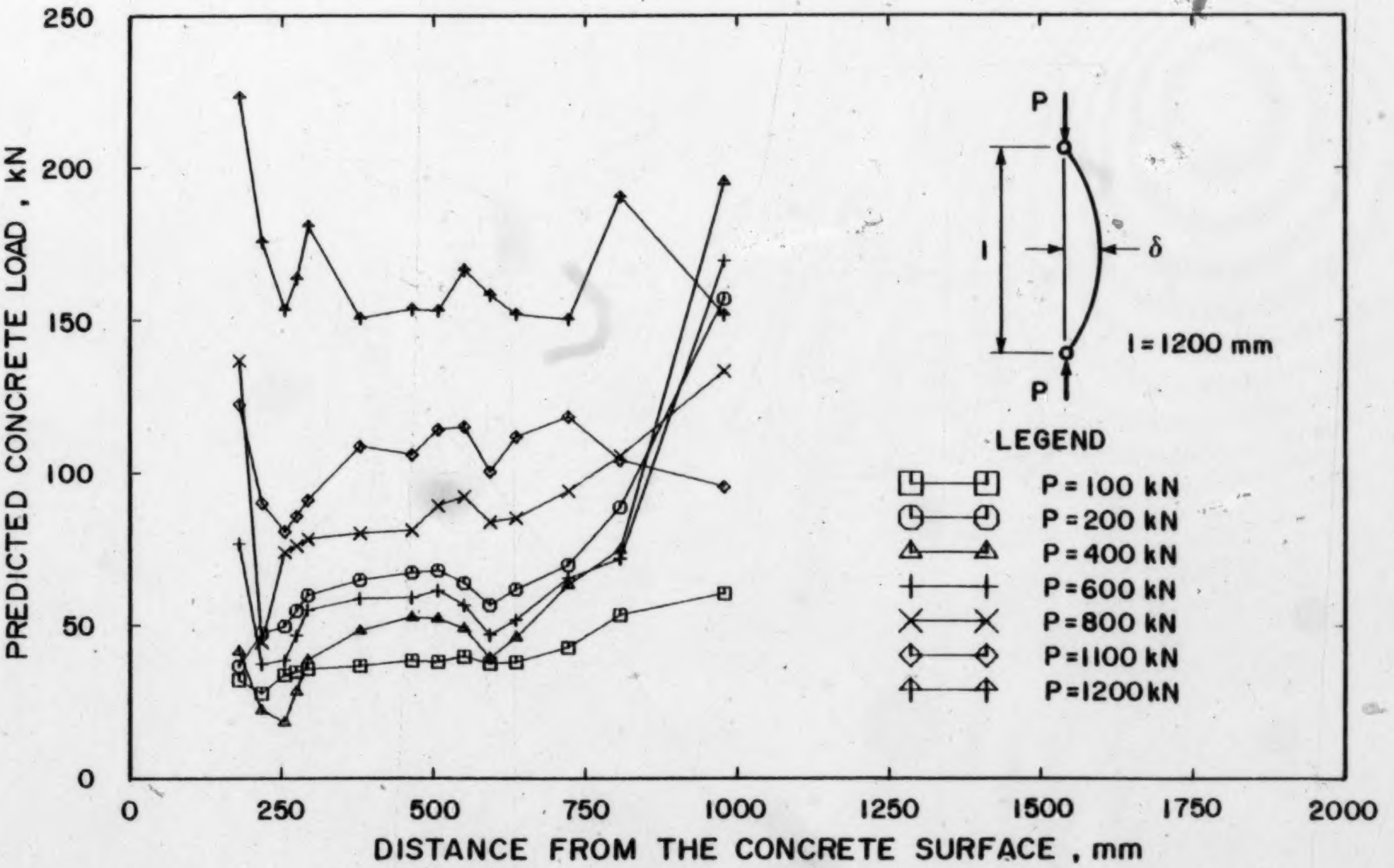

Figure 6.9 Concrete Load Distributions for Column C205

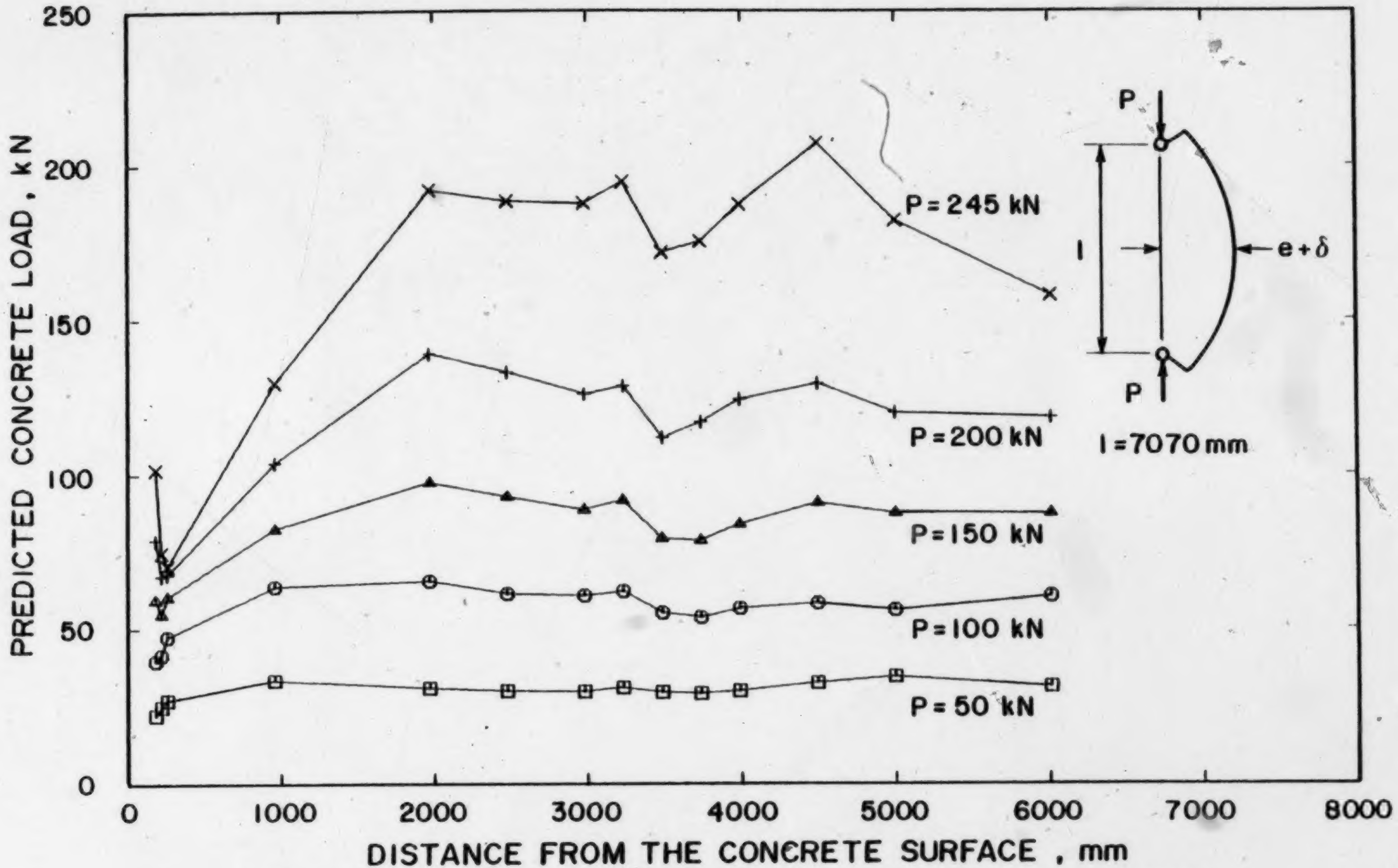

Figure 6.10 Concrete Load Distributions for Beam Column C1206

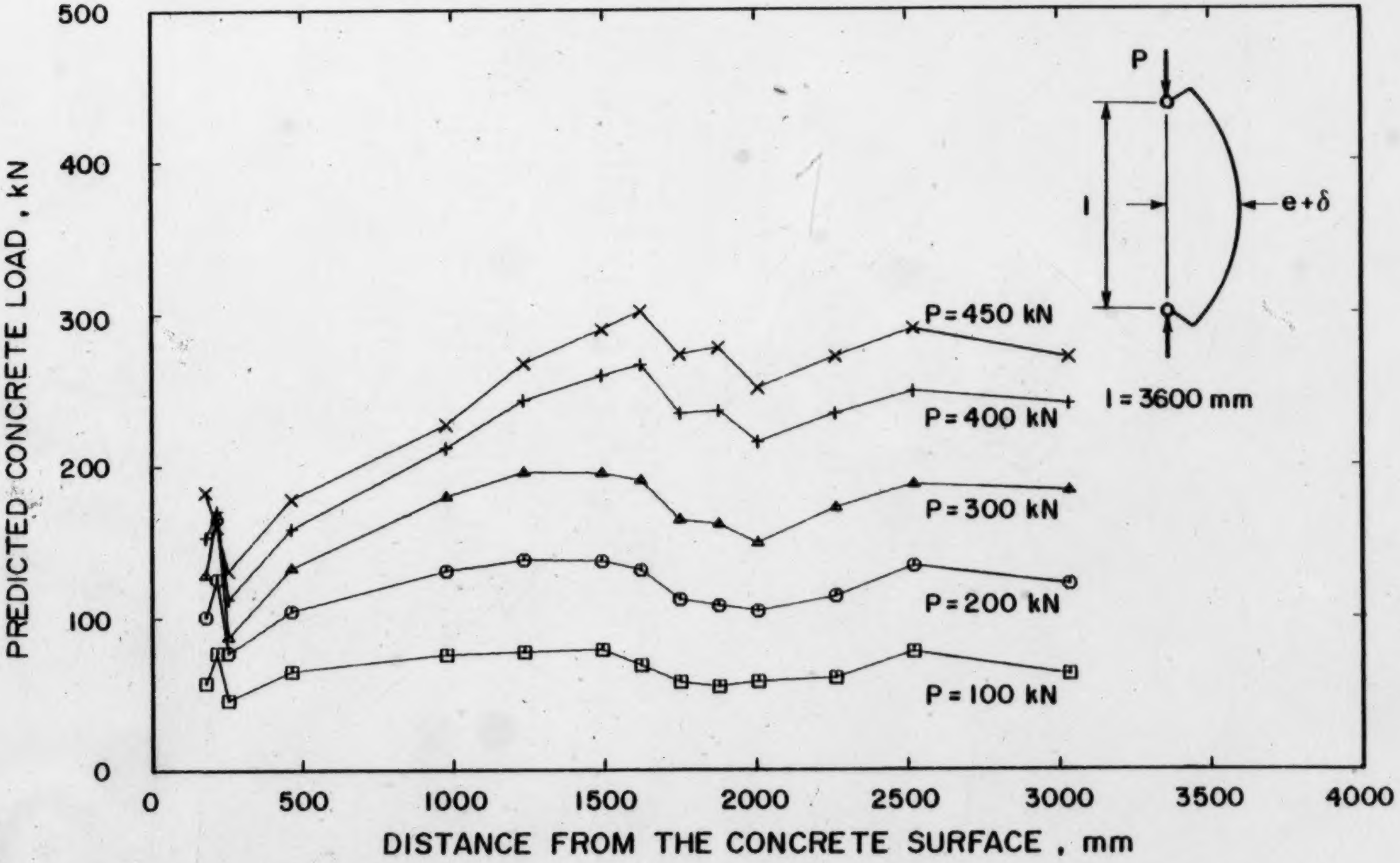

Figure 6.11 Concrete Load Distributions for Beam Column C606

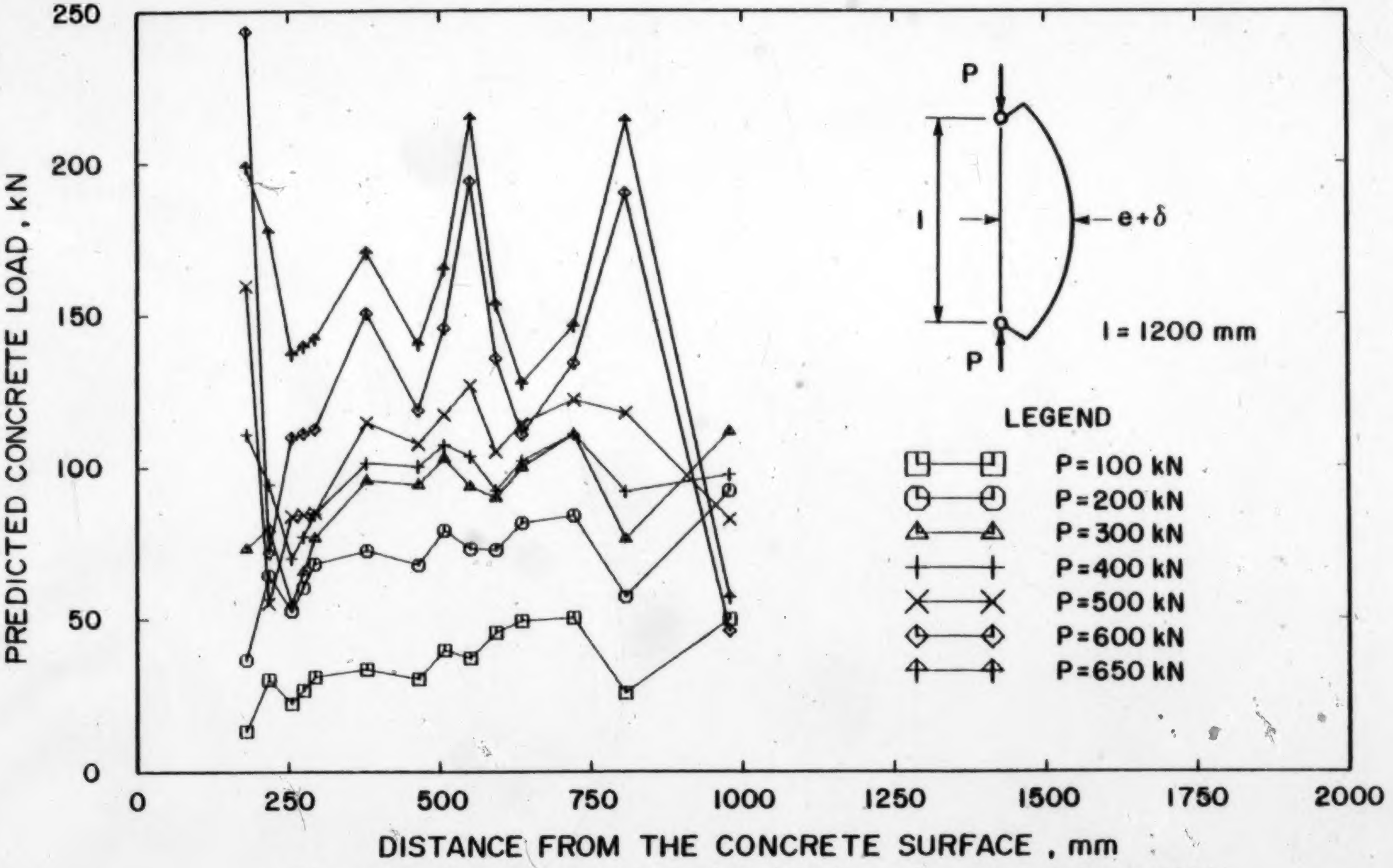

Figure 6.12 Concrete Load Distributions for Beam Column C206

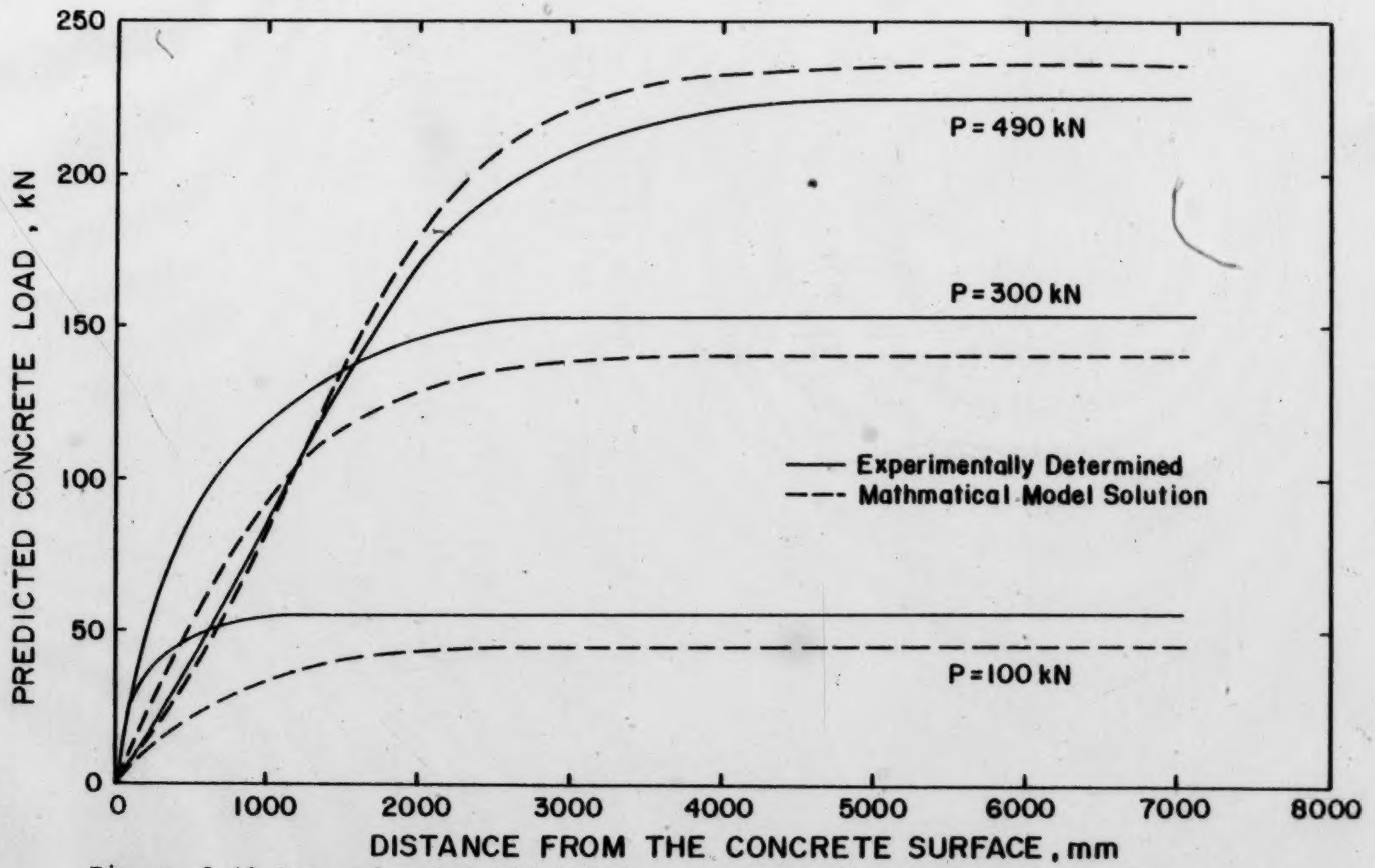

Figure 6.13 Assumed and Predicted Concrete Load Distributions for Column C1205

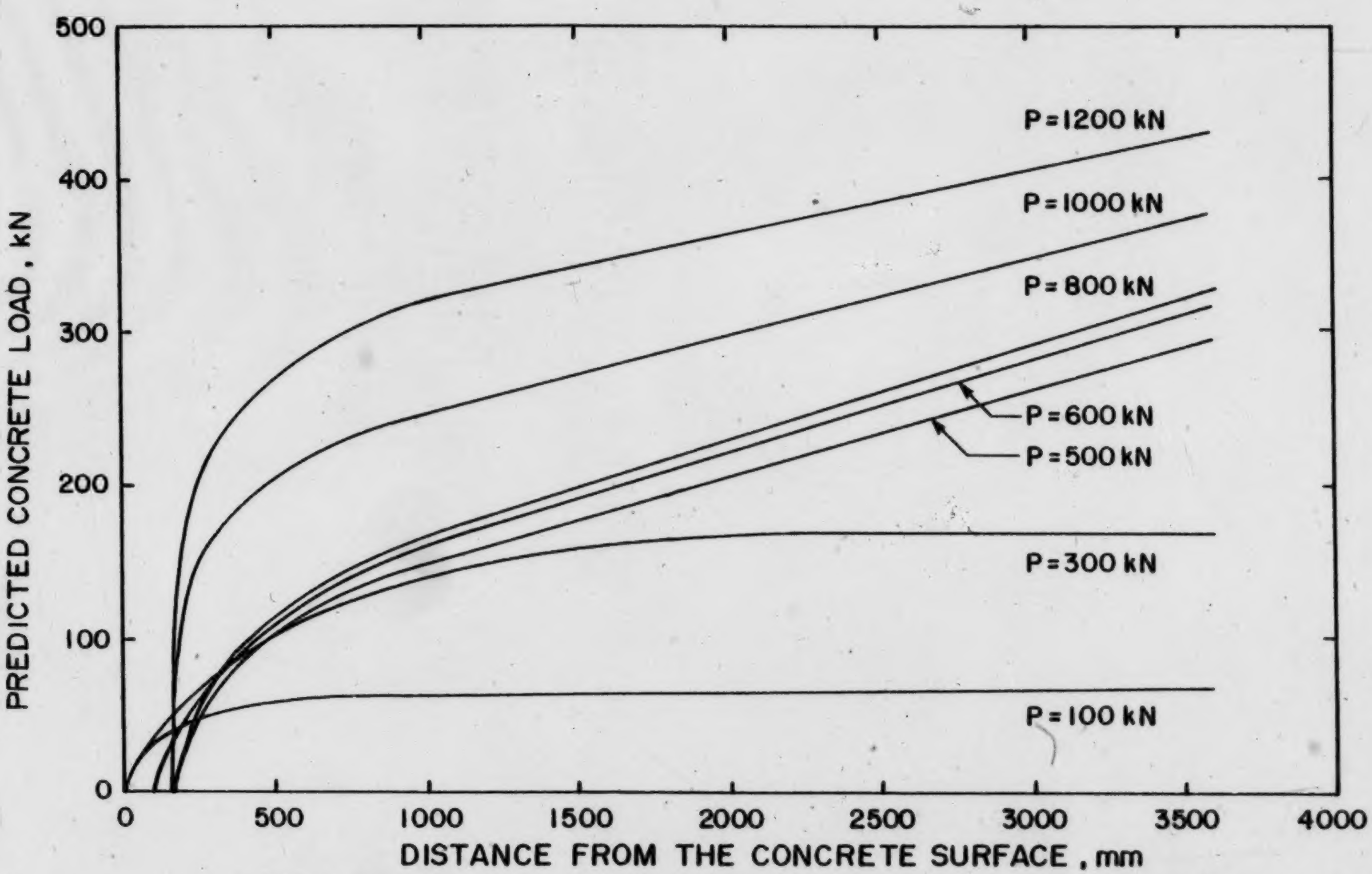

Figure 6.14 Assumed Concrete Load Distributions for Column C605

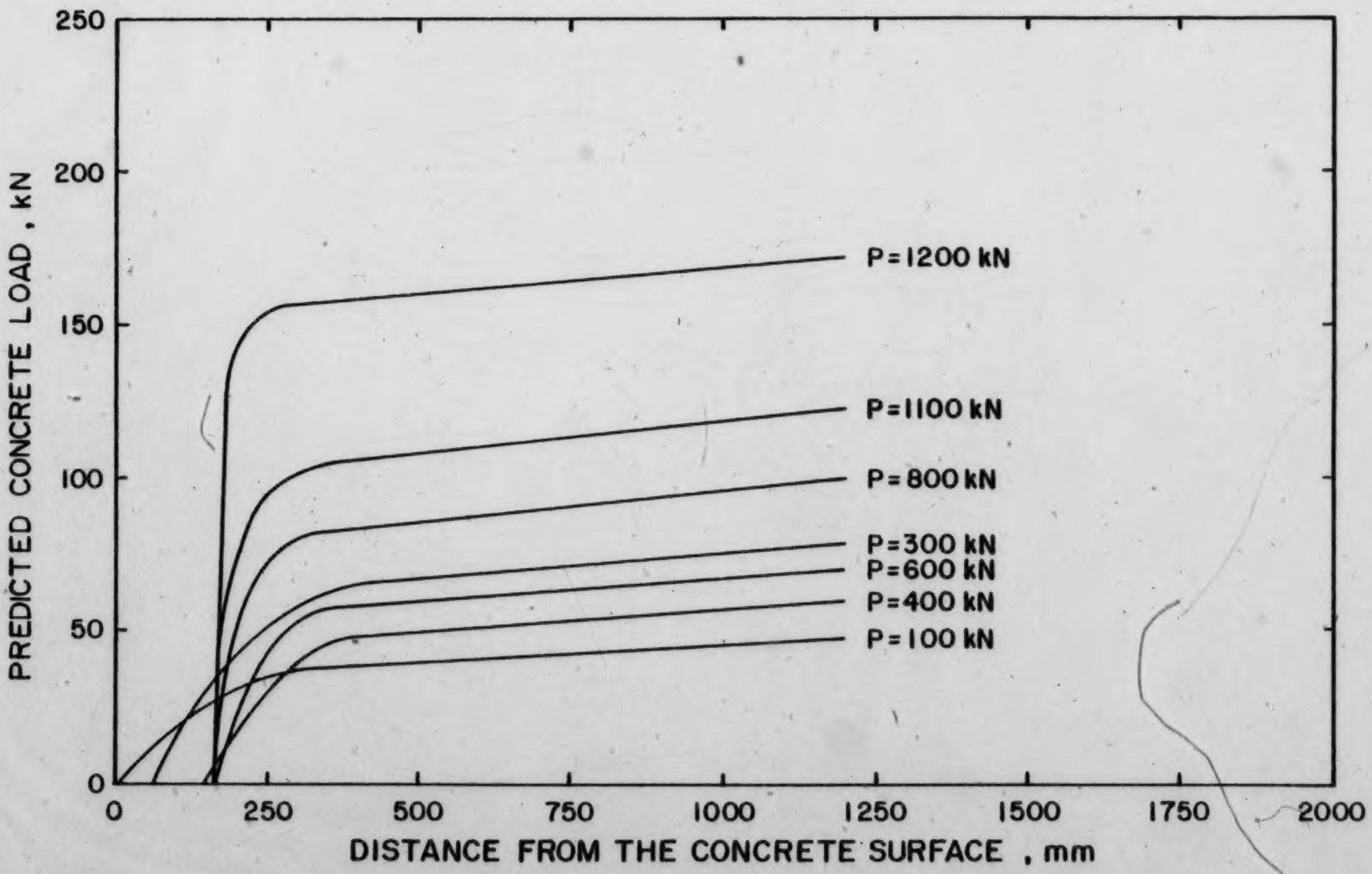

Figure 6.15 Assumed Concrete Load Distributions for Column C205

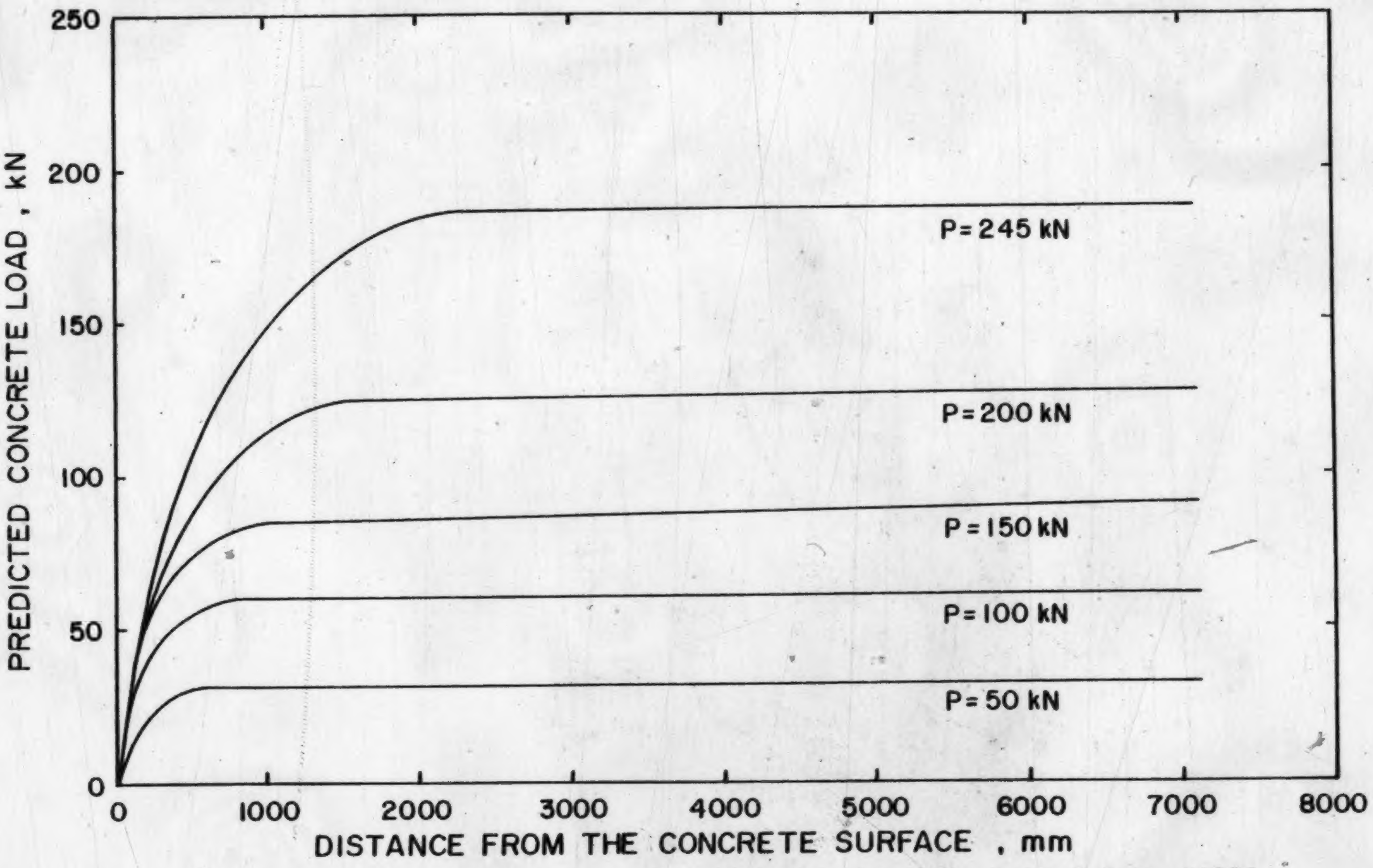

Figure 6.16 Assumed Concrete Load Distributions for Beam Column C1206

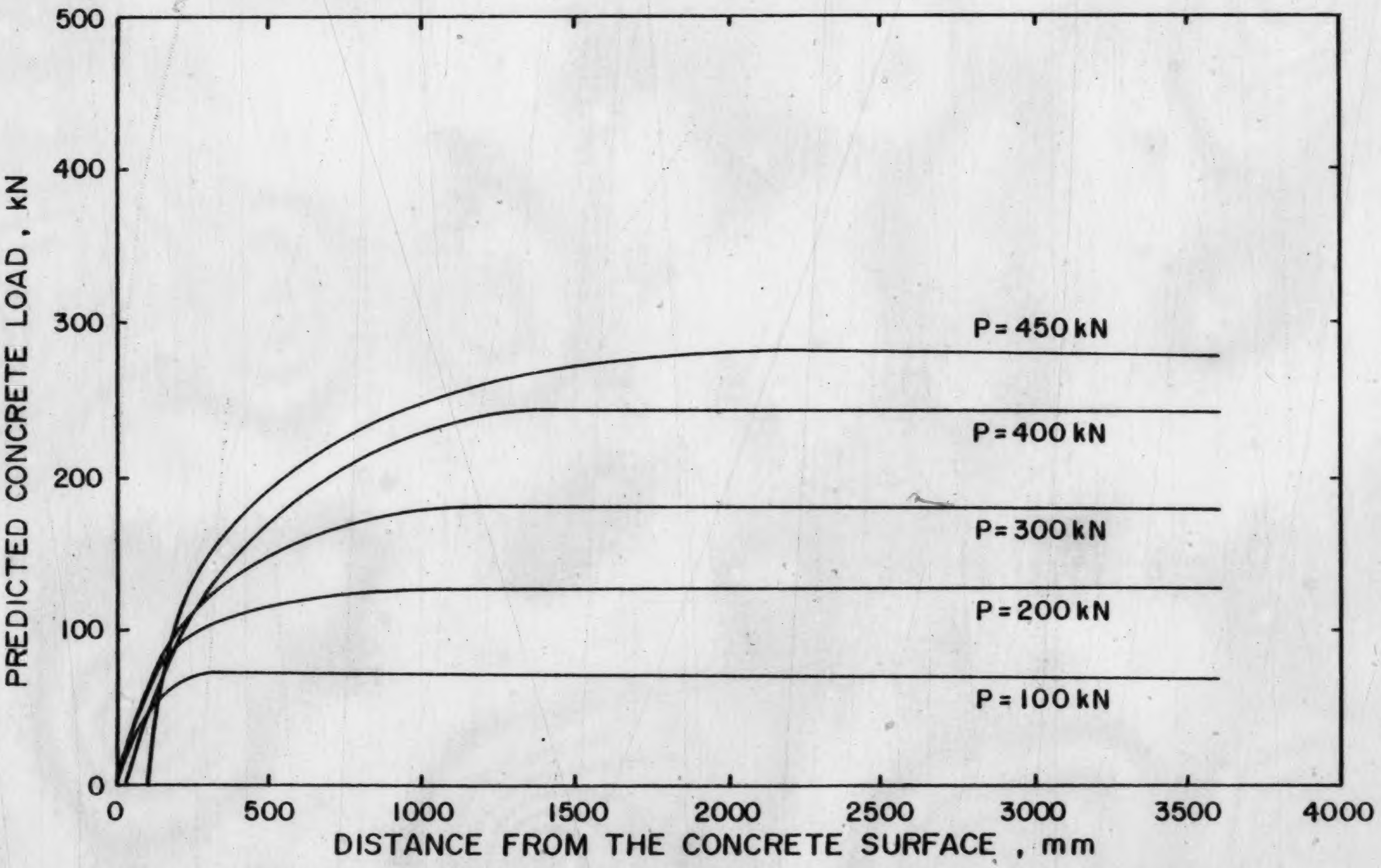

Figure 6.17 Assumed Concrete Load Distributions for Beam Column C606

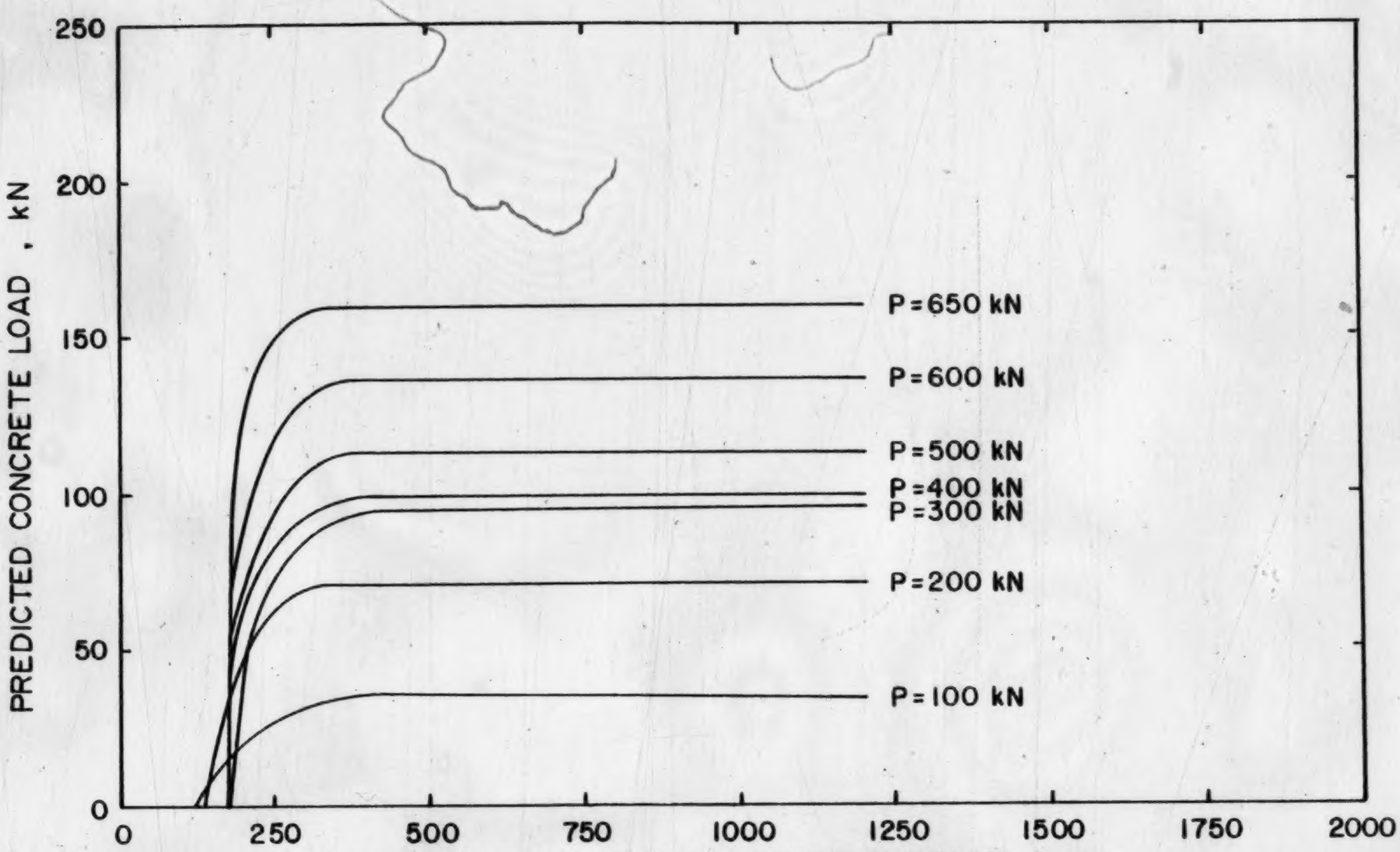

Figure 6.18 Assumed Concrete Load Distributions for Beam Column C206

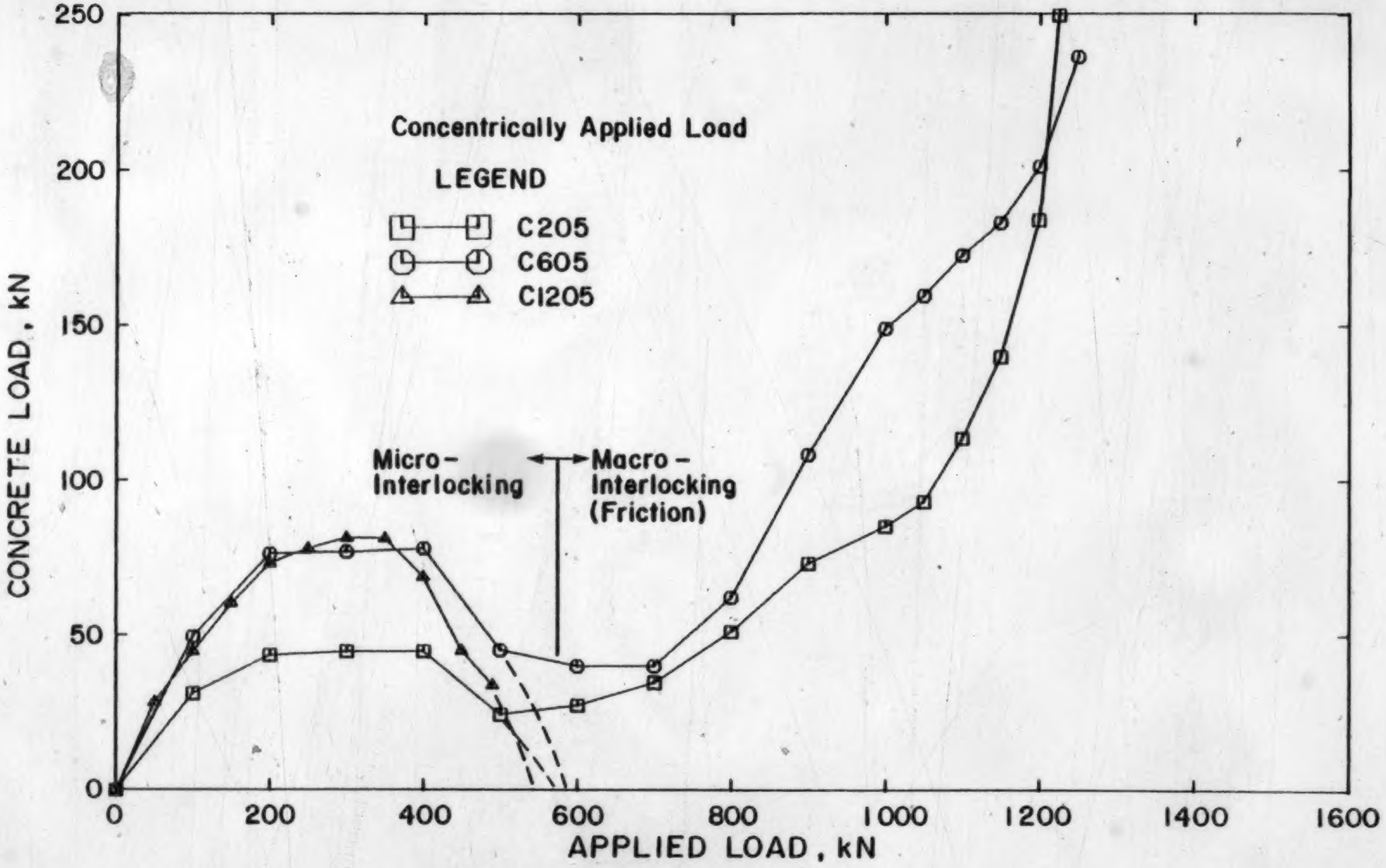

Figure 6.19 Load Transfer Mechanisms in the Region just Below the Connection Plates for Concentrically Loaded Columns

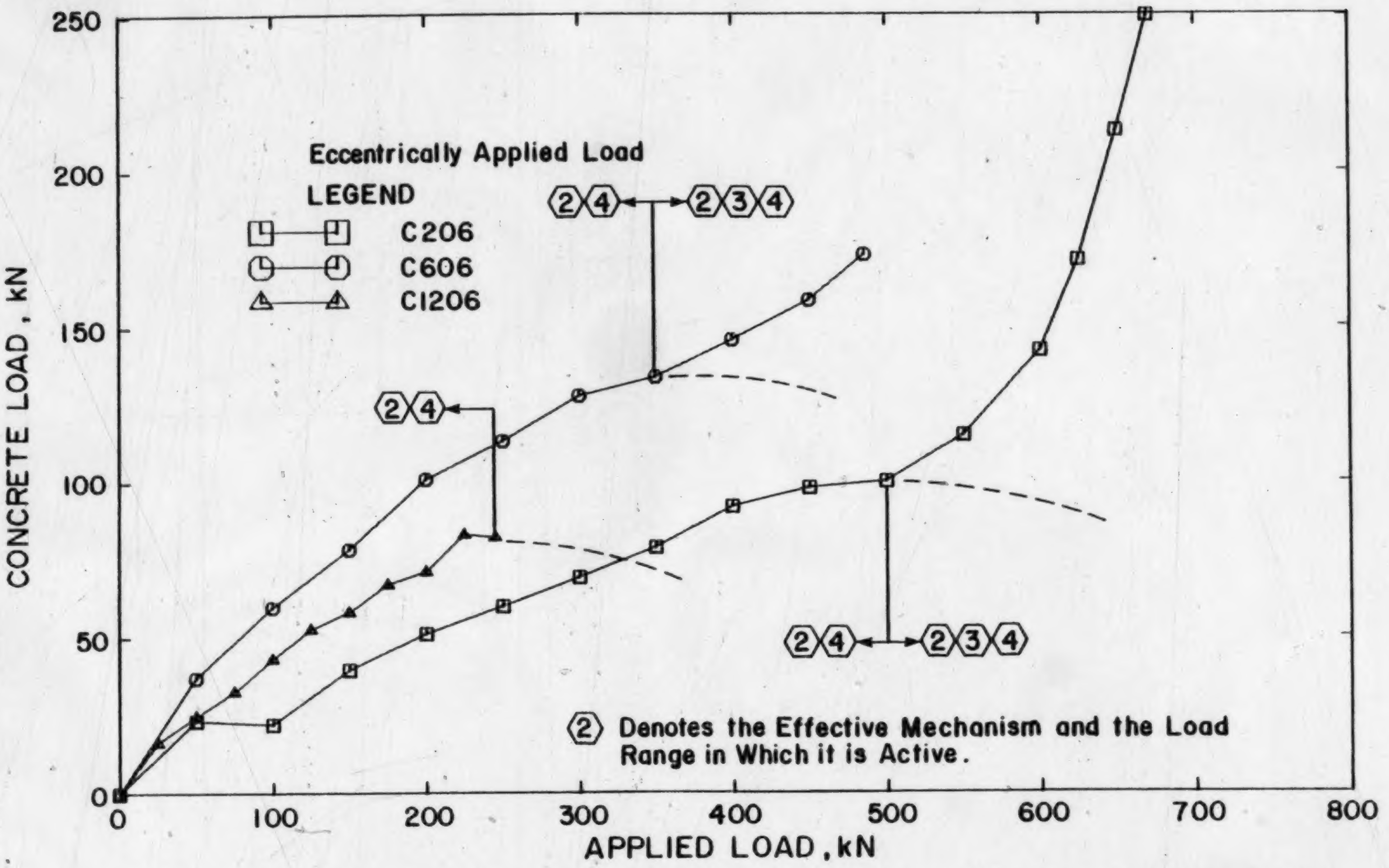

Figure 6.20 Load Transfer Mechanisms in the Region just Below the Connection Plates for Eccentrically Loaded Columns

7. ULTIMATE LOADS

7.1 General

Ultimate loads obtained from tests on steel and composite beam columns are compared with ultimate loads predicted by various codes and standards. The relative merits and deficiencies are discussed in light of the comparison. In all cases the data are presented in the form of interaction diagrams relating axial load and moment, and curves giving the maximum strength as a function of steel slenderness ratio when loaded concentrically or eccentrically. The predicted curves are based on the measured geometric and strength properties of the given section.

In Section 7.2 the results of tests on steel columns, without concrete, are compared to the ultimate loads calculated in accordance with CSA Standard CAN3-S16.1-M78. Section 7.3 presents a comparison of the results from tests on the strain compatible columns with the values as given by the design method proposed for the CSA Standard CAN3-S16.1-M84, an alternate design method for the same standard but not adopted, the design method proposed by the Structural Stability Research Council (SSRC)-Task Group 20, and European Convention for Constructional Steelwork (ECCS) recommendations. These methods have been developed on the basis of strain compatible conditions. The moment resistance of the composite section is briefly discussed in Section

7.3.5. A comparison between the results obtained in the strain compatible cases with the non-strain compatible cases is given in Section 7.4. A summary of the salient points is given in Section 7.5.

7.2 Strength of Hollow Structural Steel Sections

The maximum axial loads and corresponding moments for all the steel beam columns tested are plotted in Figure 7.1 in the form of an interaction diagram. Also drawn in this figure are the CSA CAN3-S16.1-M78 interaction lines obtained from strength and stability Equations 13.8.1(a), 13.8.1(b) of that code for Class 2 sections, and Equations 13.8.3(a), 13.8.3(b) for Class 3 sections, for slenderness ratios of 20, 60, and 118. For Class 2 and Class 3 sections the solutions to the strength and stability equations were based on a plastic and an elastic moment resistance of the section, respectively. These interaction lines are shown as dashed lines for Class 2 sections and solid lines for Class 3 sections in Figure 7.1. For uniaxial bending and without the resistance factor ϕ, these equations become:

for strength,

$$\frac{C_f}{C_r} + \frac{M_f}{M_r} \leqslant 1.0 \qquad (7.1)$$

where, $$C_r = AF_y \qquad (7.2)$$

for stability,

$$\frac{C_f}{C_r} + \frac{\omega M_f}{M_r\left(1 - \frac{C_f}{C_e}\right)} \leq 1.0 \qquad (7.3)$$

where, C_e = Euler buckling strength of the steel section
C_f = Compressive force in a member under axial load
C_r = Compressive resistance of a member as defined by Clause 13.3.1 (cold formed section)
M_f = End moment of the beam column
M_r = Moment resistance of a member as defined by Clause 13.5(a) for Class 1 and Class 2 sections and Clause 13.5(b) for Class 3 sections
ω = Coefficient used to determine equivalent uniform bending effect in beam columns, for this particular case $\omega = 1.0$

The test section, a 152.4 x 152.4 x 4.78 HSS, is normally a Class 2 section based on nominal dimensions and yield strength, with a b/t ratio of 27.88 which is slightly less than 28.06, the Class 2 limit of $525/\sqrt{F_y}$. Based on the measured width, thickness and yield strength, however, the test section would be classified as a Class 3 section with a b/t ratio of 30.40 which exceeds the Class 2 limit of 26.62. Although the section may be classed as 2 or 3 depending on the nominal or measured values of b/t and yield strength, the transition in behaviour from one classification to another is not a stepwise function and some intermediate behaviour may be obtained.

In general the test results lie above the interaction lines for the respective slenderness ratios. The results for the two tests on beams (B21 and B25) give mean test to predicted ratio of 1.375 and 1.176, based on the section developing an elastic and plastic moment resistance, respectively. These values are attributed to the facts that:

1. The stress strain characteristics for the section (see the steel stub column stress strain curve in Figure 4.4) shows that the section was able to obtain stress levels higher than the nominal yield stress determined by the 0.2% offset before local buckling occurred.
2. The walls of the section bulge slightly outward increasing both the values of the elastic and plastic section moduli and hence the moment resistance of the section.

The same test data is presented in another form in Figure 7.2, along with curves relating the compressive strength to slenderness ratio for concentrically and eccentrically loaded columns. The curves are obtained from the expressions given in CSA CAN3-S16.1-M78 for strength and stability, Equations 13.8.1(a), 13.8.1(b) for Class 2 sections, which are based on a plastic moment resistance, and Equations 13.8.3(a), 13.8.3(b) for Class 3 sections, which are based on an elastic moment resistance. The curve for an eccentricity of 65.0 mm represents the radial line in Figure 7.1 for which the moment is equal to 0.065 times the axial load.

As the curves based on CSA CAN3-S16.1-M78 have been drawn based on the measured cross sectional and strength properties, the comparisons here relate only to the accuracy of the code equations as given by the test load to predicted load ratios, and show that the predicted curves are about 9 to 15 per cent conservative. It is understood that the column curves given in S16.1 were in fact derived, not for HSS, but for W shapes with particular out-of-straightness and residual stress patterns. It appears that the HSS columns tested gave strengths greater than the predicted values because the mean out-of-straightness value of 1/12600 was considerably less than the 1/1000 assumed by Bjørhovde (1972) in the development of these curves. This is borne out by:

1. The differences are not significant for the columns loaded at an eccentricity of 65.0 mm.
2. For concentrically loaded columns where the influence of initial out-of-straightness on the ultimate strength of a column is the greatest, the difference in test load to predicted load values is a maximum, as shown clearly on Figure 7.2, for a slenderness ratio of 60 and less when the slenderness ratio is smaller and greater than this value.

A summary of test to predicted ratios for this test series is given in Table 7.1, with the means, standard deviations and coefficients of variation given in Table 7.6. The test to predicted ratios vary from 0.996 to 1.436 with a mean value of 1.152 and a coefficient of variation of 0.112 when the comparison is made on the basis of a Class 3 section. Based on the nominal classification of the section as a Class 2, the test to predicted ratios vary from 0.996 to 1.228 with a mean value of 1.090 and a coefficient of variation of 0.0685.

7.3 Strength of Strain Compatible Concrete Filled Hollow Structural Sections

7.3.1 CAN3-S16.1-M84

The maximum axial loads and corresponding moments for all the composite beam columns tested are plotted in Figure 7.3 in the form of an interaction diagram. Square and octagonal symbols represent the ultimate loads obtained from the strain compatible and non-strain compatible tests, respectively. Also drawn in the figure are interaction bands as obtained from the proposed Clause 17.8 CSA CAN3-S16.1-M84, for columns with slenderness ratios based on the steel section alone of 20, 60, and 118. These bands represent the range of concrete strengths, as determined by Equation 4.4, for concrete ages of 27 to 55 days, for the test period of the composite beam columns. Two sets of bands have been drawn. The lightly shaded and cross hatched bands represent an analysis based on an elastic, and a plastic moment resistance of the steel section, respectively.

For concrete filled hollow structural rectangular sections subject to uniaxial bending and without the resistance factors ϕ and ϕ_c, the equations become:

for strength,

$$\frac{C_f - C_r'}{C_r} + \frac{M_f}{M_r} \leqslant 1.0 \tag{7.4}$$

where, C_r = Steel squash load as defined by Equation 7.2

for stability,

when $C_f > C_r'$

$$\frac{C_f - C_r'}{C_r} + \frac{\omega\, M_f}{M_r\left(1 - \frac{C_f - C_r'}{C_e}\right)} \leqslant 1.0 \tag{7.5}$$

when $C_f \leqslant C_r'$

$$M_f < M_r \tag{7.6}$$

where, C_r = Compressive resistance of a member as defined by Clause 13.3.1 (cold formed HSS section)
where, C_r' = Compressive resistance of the concrete as defined in Clause 17.8.2 by Equation 7.7

$$C_r' = 0.85 A_c f_c' \lambda_c^{-2}\left[\sqrt{1 + 0.25\,\lambda_c^{-4}} - 0.5\,\lambda_c^{-2}\right] \tag{7.7}$$

in which,
A_c = Concrete area, mm²

f_c' = Compressive strength of concrete at 28 days

λ_c = Non-dimensional slenderness ratio for the concrete core as defined by equation 7.8

$$\lambda_c = \frac{Kl}{r_c}\sqrt{\frac{f_c'}{\pi^2 E_c}} \tag{7.8}$$

where,
E_c = Elastic modulus of concrete considering the effects of long term loading. For normal weight concrete, with expressed in MPa, this may be taken as:

$$E_c = (1 + S/T)\ 2500\sqrt{f'_c} \qquad (7.9)$$

in which,
S = Short term load on the column
T = Long term load on the column
K = Effective length factor, a value of 1.0 for all pinned ended columns
l = Column length
r_c = Radius of gyration of the concrete area, A_c

For this analysis and for the comparison of test to predicted ultimate loads, the compressive strength, f'_c and the elastic modulus, E_c of the concrete were calculated from mathematical expressions, Equations 4.4 and 4.5, which were fitted to those values obtained experimentally.

The same data is presented in another form in Figure 7.4, along with the curves relating the compressive strength to steel slenderness ratio for concentrically and eccentrically loaded columns. The predicted curves are plotted as bands to reflect the change in strength of the concrete and the type of analysis as discussed previously. Also drawn is the Euler buckling strength of the composite column as given by:

$$C_{ec} = \left(A_s F_y + 0.85 A_c f'_c\right) / \lambda^2_{comp} \qquad (7.10)$$

where, λ_{comp} = Slenderness ratio for the composite column and is defined as follows

$$\lambda_{comp} = \frac{Kl}{\pi}\sqrt{\frac{\tau\ A_s F_y + 0.85\ \tau'\ A_c f'_c}{E_s I_s + \eta\ E_c I_c}} \qquad (7.11)$$

in which,

τ, τ' = Coefficients reflecting an increase in strength of the section due to the development of a triaxial state of stress in the concrete. For rectangular HSS both coefficients have a value of 1.0.

η = Coefficient reflecting the effects of long term loading, normally taken as 0.4.

A summary of test to predicted values for this analysis and the strain compatible test series is given in Table 7.2, with means, standard deviations, and coefficients of variation given in Table 7.6.

In Figure 7.3 it is found that the data for strain compatible tests (square symbols) fits the predicted curves closely, with the exception of beam test B22. This is clearly illustrated by the means and the coefficients of variation of the test to predicted ratios for column and beam column data for both analyses. Excluding test B22, the test to predicted ratios vary from 0.932 to 1.192 with mean values of 1.066 and 0.979, and coefficients of variation of 0.0813 and 0.0765 for columns and beam columns, respectively, when the comparison is made on the basis of a Class 3 section. Considering a Class 2 classification, again excluding test B22, the test to predicted ratios vary from 0.872 to 1.192 with mean values of 1.066 and 0.918, and coefficients of variation of 0.0813 and 0.0606 for column and beam columns, respectively.

Considering that the composite beam column strength is the sum of the individual strengths of the steel tube and the concrete core, it becomes apparent that the same variations would occur in predicting the steel load contribution as described in Section 7.2. It should be noted that the contribution of the concrete to the column strength is based on the tangent modulus theory and that no account has been made to reduce the strength for initial out-of-straightness. The analysis does, however, make a good prediction for strain compatible composite beam columns.

For analyses based on an elastic and plastic moment resistance of the steel section, the test to predicted ratios for test B22 are 1.759 and 1.505 respectively. These values indicate that the estimate of moment resistance for the composite section based on the steel section alone is very conservative. It also suggests that:

1. The concrete stabilizes the steel walls and prevents local buckling. This is consistent with the fact that a significant plastification of the steel had occurred prior to an outward buckling of the upper flange. Compressive steel strains in excess of 8000×10^{-6} to 10000×10^{-6} were measured prior to local buckling. For this section, the test results should be compared with the analysis based on the plastic section modulus of the steel i.e. - the section should be classified as a Class 1 or a Class 2 section.
2. The concrete makes a considerable contribution to the moment resistance of the section.

7.3.2 CAN3-S16.1-M84 (Alternate Proposal, Not Adopted)

The test data for composite beam columns has been plotted in Figure 7.5 in the form of a load-moment interaction diagrams and in Figure 7.6 in the form of column curves relating the axial load to slenderness ratio based on the steel section alone, for concentrically and eccentrically loaded columns. As previously discussed, the square and octagonal symbols represent the ultimate loads obtained from strain compatible and non-strain compatible tests, respectively. The bands show the range of beam column strength corresponding to concrete age between 27 and 55 days, and the lightly shaded and cross hatched bands denote whether the analysis was based on the moment resistance of the section being elastic or plastic. The interaction diagrams, column curves and Euler curve for the test section composite column have been drawn on the appropriate figure.

These curves have been formulated using the alternate S16.1-1984 proposal which was not adopted. For uniaxial bending and without the resistance factors ϕ and ϕ_c the equations for rectangular HSS become:

for strength,

$$\left(\frac{C_f}{C_{ro}}\right)^2 + \frac{M_f}{M_r} \leq 1.0 \qquad (7.12)$$

where, C_{ro} = Squash load for a composite column

$$C_{ro} = A_s F_y + 0.85 A_c f'_c \qquad (7.13)$$

for stability,

$$\left(\frac{C_f}{C_{rc}}\right)^2 + \frac{\omega\ M_f}{M_{rc}\left(1 - \frac{C_f}{C_{ec}}\right)} - \frac{0.85A_c f'_c}{A_s F_y}\frac{C_f}{C_{ro}}\left(1 - \frac{C_f}{C_{rc}}\right) \leq 1.0 \qquad (7.14)$$

where, C_{ec} = Euler buckling strength of a composite column, as defined by Equation 7.10

C_{rc} = Compressive resistance of the composite section and is to be taken as a value equal to C_r given in Clause 13.3.1 or Clause 13.3.2 according to the type and Class of HSS with AF_y replaced by $\tau A_s F_y + 0.85\tau' A_c f'_c$ and λ replaced by λ_{comp} as described by Equation 7.11.

M_{rc} = Pure bending moment resistance of the composite section, neglecting any area of concrete in tension and is given by the following equation.

$$M_{rc} = M_r + \left[\frac{0.5(b - 2t)^2 A_c t F_y}{A_c + 4t(b - 2t)\,\zeta}\right] \qquad (7.15)$$

in which, $\zeta = F_y / 0.85f'_c$ (7.16)

A summary of test to predicted ratios for this analysis and the strain compatible test series is given in Table 7.3, with means, standard deviations, and coefficients of variation given in Table 7.6.

As shown in Figures 7.5 and 7.6 the test values for concentrically loaded columns generally lie above the range of predicted values. Test to predicted ratios vary from 0.971 to 1.158, with a mean value of 1.052 and a coefficient of variation of 0.064. As discussed in section 7.2 the difference between the test and predicted values for this column curve may be attributed to the facts that:

1. The column curves are derived for W shapes, not concrete filled HSS, and
2. The initial out-of-straightness of these columns is considerably less than that used in the derivation of this curve.

For eccentrically loaded columns the test to predicted ratios vary from 0.883 to 1.053, with a mean of 0.940 and a coefficient of variation of 0.104 when the comparison is made on the basis of a Class 3 section. Based on a Class 2 classification, the test to predicted values vary from 0.824 to 0.960 with a mean of 0.877 and a coefficient of variation of 0.0883.

Although the parabolic interaction equation is 6 to 12 per cent unconservative in predicting the beam column loads, it approximates the moment resistance of the composite section more closely. Test to predicted ratios for test B22 are 1.531 and 1.334 based on an elastic and plastic moment resistance, respectively. The contribution of the concrete to the moment resistance of the composite section clearly is not understood. Although this method accounts for some concrete contribution, as shown in Figure 7.5 and Equation 7.15, it grossly under estimates the magnitude of that contribution. With the exception of the beam test, CAN3-S16.1-1984 gives a slightly more conservative answer with less variation.

7.3.3 Structural Stability Research Council, SSRC - Task Group 20

The test data for composite beam columns is presented in Figure 7.7 in the form of a load-moment interaction diagram and in Figure 7.8 as column curves relating the axial load to the slenderness ratio based on the steel alone, for concentrically and eccentrically loaded columns. The square and octagonal symbols represent the ultimate loads obtained from strain compatible and non-strain compatible tests, respectively. The bands show the range of beam column strengths corresponding to concrete ages between 27 and 55 days, and the lightly shaded and cross hatched bands denote whether the analysis was done based on the moment resistance of the section being the elastic or plastic section modulus of the HSS. The interaction diagrams, column curves and Euler curve for the test section composite column have been drawn on the appropriate figure.

These curves have been formulated using the proposal for composite columns as reported by SSRC - Task Group 20 (1979). As discussed previously in section 2.4, the SSRC - Task Group 20 proposal is based on the AISC equations for strength and stability with modified values of yield stength, modulus of elasticity, radius of gyration and section modulus to account for the composite section. Expressing these equations in terms of load, instead of allowable stresses and without safety factors, and using the notation of CSA Standard S16.1 for resistances, these equations take on the form:

for strength,

$$\left(\frac{C_f}{C_r}\right)^2 + \frac{M_f}{M_r} \leqslant 1.0 \qquad (7.17)$$

where, C_r = Squash load of the column by given by Equation 7.18

$$C_r = A_s F_{my} \qquad (7.18)$$

where, F_{my} = Modified value of yield stress for a composite column

$$F_{my} = F_y + 0.85 f'_c \frac{A_c}{A_s} \qquad (7.19)$$

for stability,

$$\left(\frac{C_f}{C_r}\right)^2 + \frac{M_f}{M_r\left(1 - \frac{C_f}{C_{ec}}\right)} \leqslant 1.0 \qquad (7.20)$$

where, C_{ec} = Elastic buckling strength for a composite column

$$C_{ec} = \frac{\pi^2 E_m A_s}{\left(\frac{Kl}{r_m}\right)^2} \qquad (7.21)$$

C_r = Compressive resistance of the member and is given by the Johnson parabola (1976)

when $\frac{Kl}{r_m} \leqslant C_c$

$$C_r = \left[1 - \frac{1}{2}\left(\frac{\left(\frac{Kl}{r_m}\right)^2}{C_c^{\,2}}\right)\right] F_{my} A_s \qquad (7.22)$$

$$\text{when} \quad \frac{Kl}{r_m} > C_c \qquad C_r = C_{ec} \tag{7.23}$$

where, C_c = Slenderness ratio corresponding to an Euler stress $F_{my}/2.0$

$$C_c = \sqrt{\frac{2\pi^2 E_m}{F_{my}}} \tag{7.24}$$

E_m = Modified modulus of elasticity for a composite column

$$E_m = E_s + 0.4E_c \frac{A_c}{A_s} \tag{7.25}$$

r_m = Modified radius of gyration for a composite column

S_m = Modified section modulus for a composite column

It should be noted that for rectangular HSS the values of S_m and r_m are those of the steel section.

A summary of test to predicted ratios for this analysis and the strain compatible test series is given in Table 7.4, with the means, standard deviations and coefficients of variation listed in Table 7.6.

Although the results fit the prediction within satisfactory limits, this method tends to deviate from a physical interpretation by using modified geometric and material properties and hence this leads the designer further from a true understanding of the problem. Application of the Johnson parabola with an assumed maximum residual compressive stress of 0.5 F_{my}, Equation 7.22, is an over simplified approach and in the case of composite columns is incorrect. This assumption leads to unconservative predictions for columns with inelastic behaviour and with slenderness ratios greater than C_c as shown in both Figures 7.7 and 7.8.

In general the strain compatible test results, with the exception of B22, are modelled fairly closely using the elastic solution and parabolic interaction curve. The test to predicted ratios vary from 0.920 to 1.197, with a mean of 0.984 for axially loaded columns and 1.038 for eccentrically loaded columns. The corresponding coefficients of variation are 0.0569 and 0.138, respectively. For the plastic analysis, the test to predicted ratios vary from 0.8713 to 1.072 with a mean of 0.983 for axially loaded columns and 0.951 for eccentrically loaded columns, with corresponding coefficients of variation of 0.0569 and 0.112, respectively. As in the CAN3-S16.1-M84 analysis, the pure moment resistance of the composite section is based on the steel alone and yields the same test to predicted ratios for test B22.

7.3.4 ECCS Recommendations

The test data for composite beam columns is presented in Figure 7.9 in the form of load-moment interaction diagrams and in Figure 7.10 as column curves relating the axial load to slenderness ratio based on the steel alone, for concentrically and eccentrically loaded columns. The square and octagonal symbols represent the strain compatible and non-strain compatible tests respectively. The bands in this case show the range of beam column strength corresponding to concrete age between 27 and 55 days for an analysis based on a composite plastic moment resistance.

These curves have been formulated using ECCS Recommendations as given by the Technical General Secretariat of the ECCS (1981) in their publication Composite Structures. The interaction equation for rectangular HSS used in Figure 7.9 is of the form:

$$N = N_u K_1 \;/\; \left(1.0 + (K_1 - K_2)\,\frac{N_u e}{M_u}\right) \qquad (7.26)$$

where, e = Given eccentricity
K_1 = Non-dimensional coefficient which describes the shape of Column Curve 'a' as a function of column slenderness. The values are interpolated from the given table
K_2 = Non-dimensional Coefficient determined by Basu and Sommerville (1969) which defines the maximum axial load corresponding to an applied moment equal to the plastic moment capacity of the composite section, as a function of column slenderness. The expression for K_2 is given by Equation 7.27.
N = Compressive force in the member
N_u = Squash load as defined by Equation 7.31
M_u = Ultimate resistance of the section

Basu and Sommerville's non-dimensional coefficient, K_2 is a function of steel section type, column slenderness, the applied end moments and the material and geometric properties of the composite section. The coefficient is given by an equation of the form:

$$K_2 = K_{2(1=0)}\{[90 - 25(2\beta - 1)(1.8 - a) - \bar{\eta}\,\bar{\lambda}]/30(2.5 - \beta)\} \tag{7.27}$$

with limits given as $0 \leq K_2 \leq K_{2(1=0)}$

where,

$$K_{2(1=0)} = 0.9a^2 + 0.2 \leq 0.75 \tag{7.28}$$

a = Concrete contribution parameter

$$a = 0.83\, f_{cu} A_c / N_u \tag{7.29}$$

β = The ratio of the smaller to the larger of end moments, 1.0.

$\bar{\eta}$ = 100 for columns designed to curve 'a'. For this composite section, however, a comparison between Basu and Sommerville and the ECCS Recommendations yields a value of η=83.

After simplification Equation 7.27 becomes:

$$K_2 = K_{2(1=0)}[(45 - 25a - 83\,\bar{\lambda}) / 45] \tag{7.30}$$

The squash load of the composite section is given by an equation of the form:

$$N_u = A_s f_{sy} + 0.83\, A_c f_{cu} \tag{7.31}$$

where, f_{sy} = Yield strength of the steel section
f_{cu} = Compressive strength of concrete

The maximum moment on the section for any given axial load is given as the ultimate moment resistance of the section which is defined as follows:

$$M_u = N_{us} e_u \tag{7.32}$$

where, e_u = Ultimate eccentricity of the composite section which corresponds to the distance from the elastic to the plastic neutral axis

$$e_u = \frac{1}{2A_s}\left\{A_s h + 2b_f t^2 - \frac{(A_s - 2b_f t)^2}{pb + 4t}\right\} \qquad (7.33)$$

N_{us} = Squash load for the steel given as,

$$N_{us} = A_s f_{sy} \qquad (7.34)$$

in which,
- b = Inside dimension of the tube parallel with the axis of bending
- b_f = Outside dimension of the tube parallel with the axis of bending
- h = Inside dimension perpendicular to the axis of bending
- p = $0.48 \times 0.83 \frac{f_{cu}}{f_{sy}}$
- t = Wall thickness

The equivalent slenderness ratio $\bar{\lambda}$ is given as:

$$\bar{\lambda} = \sqrt{\frac{N_u}{N_{cr}}} \qquad (7.35)$$

where, N_u = Squash load given by Equation 7.31

N_{cr} = Euler critical load given by the following equation

$$N_{cr} = \frac{\pi^2}{l_k^2}\left(E_{ce} I_c + E_s I_s\right) \qquad (7.36)$$

in which,
E_{ce} = Effective Concrete Elastic Modulus given as:

$$E_{ce} = 0.82 \times 600\ f_{cu} \qquad (7.37)$$

l_k = Effective column length

Except in the case of very slender columns with large values of the concrete distribution parameter, a, a reduction in the concrete modulus to account for the effects of the time dependent strains of concrete is not required for concrete filled hollow structural sections. For this analysis and for the comparison of the test to predicted ultimate loads, the compressive strength f_c' and the elastic modulus E_c of the concrete were calculated from mathematical expressions, Equations 4.4 and 4.5 which were fitted to those values obtained experimentally. A summary of test to predicted ratios for this analysis and the strain compatible test series is given in Table 7.5, with means, standard deviations and coefficients of variation listed in Table 7.6.

As shown in Figures 7.9 and 7.10, the test values for concentrically loaded columns lie close or within the predicted range. The test to predicted ratios vary from 0.957 to 1.060, with a mean value of 1.015 and a coefficient of variation of 0.0393. The closeness of fit is attributed to the fact that the ECCS uses multiple column curves and the selection of the appropriate curve depends on the steel section type. The column curve used here represents a family of sections which exhibit the same behaviour as the HSS. In the development of the ECCS multiple column curves the initial out-of-straightness was taken as 1/1000, after Beer and Schultz (1970). For columns with smaller initial out-of-straightnesses, this assumption leads to a maximum deviation of test to predicted values for columns of an intermediate slenderness ratio, as discussed in section 7.2 and as shown in Figure 7.10.

The ECCS Recommendations recognizes that the concrete stabilizes slender steel elements such that the steel section is capable of achieving its full plastic capacity. The relative contribution attributed to the concrete to the moment resistance of the composite section is still quite small. This leads to a conservative prediction of the ultimate moment capacity. The test to predicted ratio of test B22 is 1.377.

The ECCS Recommendations have adopted Basu and Sommerville's (1969) work for the design of rectangular composite columns subject to uniaxial bending. Their solution excludes the moment amplification factor which reflects a decrease in strength due to secondary moments, i.e. P-Δ effects. This effect is accentuated as the slenderness ratio of a column increases, as shown in Figure 7.9, and leads to unconservative results for the columns tested at an eccentricity of 65.0 mm. The test to predicted values for these columns vary from 0.771 to 1.058, with a mean of 0.913 and a coefficient of variation of 0.157.

7.3.5 Ultimate Moment Resistance of the Composite Section

Of the four methods presented here, two base the analysis for the ultimate moment resistance of the composite section on the elastic moment capacity of the steel alone, and the other two base the analysis on the plastic moment capacity of the steel with a minor contribution for the concrete acting in compression and lying above the plastic neutral axis. All of these methods conservatively predict the moment resistance of the composite section and give test to predicted ratios for test B22 varying from 1.334 to 1.759. Based on an ACI solution and a maximum compressive stress in the concrete of $0.9 f'$ the test to predicted ratio for test B22 was 1.383. Because of this conservative prediction of the ultimate moment capacity of this section some researchers have suggested that parabolic interaction equations fit the data more closely. However, if the correct ultimate moment capacity of the composite section is predicted, then a straight line interaction curve with an amplification factor which reflects the decrease in strength due to $P-\Delta$ effects and the reduced flexural stiffness due to cracking of the concrete core, would be a more appropriate formulation. Based on the behaviour of the beam under load and measurements made the increased moment capacity of the composite section should be accounted for.

Recognizing that plane sections remain plane and knowing that strain compatibility was enforced at both ends of the beam, suggests that the concrete would have the same strain gradient as the steel section. Strains of the magnitude of 8000×10^{-6} to 10000×10^{-6} were measured on the compression face of the tube prior to failure. Richart, et al. (1929) have determined that concrete subject to compressive stresses greater than 2000 microstrains undergoes a rapid volumetric expansion. The rectangular hollow structural section restrains this expansion, enhancing the composite action between the two materials and developing a state of triaxial stress. Development of this stress state in the concrete would in fact account for the ultimate moment values for both the strain and non-strain compatible beam tests being close to the same value. Part of the increase in moment capacity of the composite section tested over that given by various design methods is due to the increased compressive resistance of the concrete under a state of triaxial stress.

The remaining increase in moment capacity is attributed to the fact that, the steel was able to obtain a plastic stress distribution without local buckling occurring, with the maximum stress corresponding to the ultimate strength as opposed to the yield strength of the section.

Based on the cross section, measured values of ultimate strength from coupon tests, an increased compressive resistance of the concrete of 1.7 f_c', and a plastic stress distribution, the moment capacity of the section was calculated to be 78.0 kNm. The test to predicted ratio of the ultimate moment capacity for test B22 is 1.064.

7.4 Non-Strain Compatible Versus Strain Compatible Beam Columns

7.4.1 Comparison of General Behaviour

The load-deflection curves for all composite column tests with concentrically and eccentrically applied loads are shown in Figures 5.6 and 5.7 respectively. Apart from the ultimate loads obtained, the general load-deflection behaviour of the non-strain compatible columns is comparable to the corresponding strain compatible columns. There is no relative difference in the flexural stiffness between the two types.

Concentrically loaded columns with slenderness ratios of 60 and 118, and all eccentrically loaded columns failed identically, by overall buckling. As discussed in Section 5.2.2, test specimen C205, a non-strain commpatible, concentrically loaded 1200 mm long column, failed by an outward local buckling of all four tube walls accompanied by slip of the steel tube relative to the concrete core, where the strain compatible counterpart, test specimen C203 failed by both outward local buckling of the tube and crushing of the concrete. For test specimen C205, the reduced load carrying capacity, the failure mode and the relatively small loads in the concrete at failure can in part be attributed to the fact that shrinkage had occurred in the concrete core. Shrinkage cracks were noticed along the concrete steel interface at the top and prior to testing at a concrete age of 55 days. Such cracks were not observed in any other specimen.

7.4.2 Comparison of Ultimate Loads

In general the ultimate loads obtained by a non-strain compatible column is a direct function of the effectiveness of load transfer from the steel to the concrete core by one or more of the load transfer mechanisms as described in Chapter 6. Naturally, for strain compatible columns, load transfer is not a question. Figure 7.11 shows the ratio of ultimate load capacity of the non-strain compatible to the strain compatible composite beam columns.

From the limited data a relationship exists among the ratio of the ultimate loads of these two types, the slenderness ratio of the column and the eccentricity of the applied load. The difference between the ultimate loads of the two types decreases with an increase in the slenderness of the column and/or an increase in the eccentricity of the applied load. This family of curves can be simplified with an approximate empirical relationship formulated as follows, shown by dashed lines in Figure 7.11.

$$R = \left(0.7 + 0.004\,\frac{Kl}{r}\right)\left(1 + 0.17\,\frac{e}{b}\right) \qquad (7.38)$$

for values of $e/b < 2.5$ and $Kl/r < 75$

where, b = outside dimension of a rectangular HSS in the plane of the eccentric load
e = Eccentricity of the applied load in mm
Kl/r = Slenderness ratio of the column based on the steel section
R = Ratio of the ultimate load carrying capacity of non-strain compatible to strain compatible composite beam columns

This equation suggests that ultimate load carrying capacity of non-strain compatible beam columns with applied loads at an eccentricity greater than 2.5b and/or a slenderness ratio greater than 75 can be predicted by various standards, without any reduction in strength. For columns within the range specified, the strength obtained from these standards should be multiplied by the value R, as obtained from Equation 7.37. The ratio of the ultimate moment capacities for the corresponding beam tests B24 and B22 is 0.964.

7.5 Summary

In tests conducted to establish the strength of concrete filled HSS beam columns of varying slenderness ratios, strain compatibility of the steel and the concrete at the ends of the column has been ensured by applying load to both materials as discussed in the survey of experimental work by Budijanto (1983). Current and proposed codes also require that this is the case by recommending that the designer provide some shear transfer mechanism in order to load both materials simultaneously.

An examination of the ultimate load carrying capacities predicted by the current or proposed design methods presented in this chapter, with respect to the ultimate loads obtained from the strain compatible test series shows that:

1. With reasonable accuracy all these methods are able to predict the ultimate load capacity of composite beam columns, with the exception of the ultimate moment

capacity.

2. All methods under-estimate the concrete contribution to the ultimate moment capacity of the composite section.
3. Few tests have been done on composite beam columns in the region approaching and including pure flexural behaviour.

The ultimate moment capacity of these composite sections can be predicted closely when the ultimate strength of the steel section, an increased compressive resistance of the concrete to account for the development of triaxial stresses, and a plastic stress distribution are used in the solution.

A direct comparison of the ultimate loads between the strain compatible and non-strain compatible composite beam columns indicates that for the practical range of slenderness ratios from 30 to 90, the reduction in load carrying capacity varies from 0 percent to a maximum of 18 per cent for concentrically loaded columns and less for eccentrically loaded columns.

Table 7.1 Test to Predicted Ratios for Steel Beam Columns and Beams by CAN3-S16.1-M78

TEST NO.	TEST LOAD	$M = SF_y$	$\frac{TEST}{PRED.}$	$M = ZF_y$	$\frac{TEST}{PRED.}$
		BEAM COLUMNS			
STUB1	1035.2	999.7	1.036	-	-
STUB2	995.6	999.7	0.996	-	-
C201	1007	963.1	1.046	963.1	1.046
C601	868	720.5	1.205	720.5	1.205
C1201	357	318.0	1.123	318.0	1.123
C202	485	407.3	1.191	443.7	1.093
C602	347	318.9	1.088	343.1	1.011
C1201E	197	176.3	1.117	185.1	1.064
C1202	197	176.3	1.117	185.1	1.064
		BEAMS			
B21	67.9	47.3	1.436	55.3	1.228
B25	62.2	47.3	1.315	55.3	1.125

Table 7.2 Test to Predicted Ratios for Composite Beam Columns and Beams by CAN3-S16.1-M84

TEST NO.	TEST LOAD	$M = SF_y$	$\frac{\text{TEST}}{\text{PRED.}}$	$M = ZF_y$	$\frac{\text{TEST}}{\text{PRED.}}$
		BEAM COLUMNS			
STUB3	1697.6	1643.9	1.033	-	-
STUB4	1727.8	1645.7	1.050	-	-
C203	1517	1584.6	0.957	1584.6	0.957
C603	1271	1066.2	1.192	1066.2	1.192
C1203	476	434.2	1.096	434.2	1.096
C204	721	676.5	1.066	735.8	0.980
C604	479	513.9	0.932	549.0	0.872
C1204	243	258.4	0.940	269.7	0.901
		BEAMS			
B22	83.2	47.3	1.759	55.3	1.504

Table 7.3 Test to Predicted Ratios for Composite Beam Columns and Beams, CAN3-S16.1-M84 Alternate Method (Not Adopted)

TEST NO.	TEST LOAD	$M = SF_y$	$\frac{\text{TEST}}{\text{PRED.}}$	$M = ZF_y$	$\frac{\text{TEST}}{\text{PRED.}}$
		BEAM COLUMNS			
STUB3	1697.6	1643.9	1.033	-	-
STUB4	1727.8	1645.7	1.050	-	-
C203	1517	1561.9	0.971	1561.9	0.971
C603	1271	1097.2	1.158	1097.2	1.158
C1203	476	453.8	1.049	453.8	1.049
C204	721	684.6	1.053	751.2	0.960
C604	479	541.5	0.885	581.4	0.824
C1204	243	275.2	0.883	287.2	0.846
		BEAMS			
B22	83.2	54.4	1.531	62.4	1.334

Table 7.4 Test to Predicted Ratios for Composite Beam Columns and Beams by SSRC-Task Group 20

TEST NO.	TEST LOAD	$M = SF_y$	$\frac{\text{TEST}}{\text{PRED.}}$	$M = ZF_y$	$\frac{\text{TEST}}{\text{PRED.}}$
BEAM COLUMNS					
STUB3	1697.6	1643.9	1.033	-	-
STUB4	1727.8	1645.7	1.050	-	-
C203	1517	1594.5	0.951	1594.5	0.951
C603	1217	1267.7	0.960	1267.7	0.960
C1203	476	517.7	0.920	517.7	0.920
C204	721	602.4	1.197	672.6	1.072
C604	479	480.2	0.998	527.0	0.909
C1204	243	264.1	0.920	278.9	0.871
BEAMS					
B22	83.2	47.3	1.759	55.3	1.504

Table 7.5 Test to Predicted Ratios for Composite Beam Columns and Beams by ECCS

TEST NO.	TEST LOAD	$M = ZF_y$	$\frac{\text{TEST}}{\text{PRED.}}$
	BEAM COLUMNS		
STUB3	1697.6	1628.8	1.042
STUB4	1727.8	1630.5	1.060
C203	1517	1585.0	0.957
C603	1217	1194.2	1.019
C1203	476	476.5	0.999
C204	721	681.3	1.058
C604	479	525.8	0.911
C1204	243	315.2	0.771
	BEAMS		
B22	83.2	60.4	1.377

Table 7.6 Test to Predicted Ratio Statistics

COLUMNS

TYPE	n	$\bar{x}$	σ	V
STEEL[2]	5	1.081	0.0831	0.0768
COMPOSITE[1] (CAN3-S16.1-M84)	5	1.066	0.0866	0.0813
COMPOSITE[2] (CAN3-S16.1-M84)	5	1.066	0.0866	0.0813
COMPOSITE[1] (CAN3-S16.1-M84[3])	5	1.052	0.0675	0.0641
COMPOSITE[2] (CAN3-S16.1-M84[3])	5	1.052	0.0675	0.0641
ECCS[1]	5	1.015	0.0399	0.0393
SSRC-TASK GROUP 20[1]	5	0.983	0.0559	0.0569
SSRC-TASK GROUP 20[2]	5	0.983	0.0559	0.0569

BEAM COLUMNS

TYPE	n	$\bar{x}$	σ	V
STEEL[1]	4	1.132	0.0529	0.0467
STEEL[2]	4	1.058	0.0341	0.0322
COMPOSITE[1] (CAN3-S16.1-M84)	3	0.979	0.0749	0.0765
COMPOSITE[2] (CAN3-S16.1-M84)	3	0.918	0.0556	0.0606
COMPOSITE[1] (CAN3-S16.1-M84[3])	3	0.940	0.0978	0.104
COMPOSITE[2] (CAN3-S16.1-M84[3])	3	0.877	0.0729	0.0832
ECCS[1]	3	0.913	0.144	0.157
SSRC-TASK GROUP 20[1]	3	1.038	0.143	0.138
SSRC-TASK GROUP 20[2]	3	0.983	0.0559	0.0569

Table 7.6 con't...

Table 7.6 continued

BEAMS

TYPE	n	$\bar{x}$	σ	V
STEEL[1]	2	1.375	0.0852	0.0620
STEEL[2]	2	1.176	0.0728	0.0619
COMPOSITE[1] (CAN3-S16.1-M84)	1	1.759	-	-
COMPOSITE[2] (CAN3-S16.1-M84)	1	1.504	-	-
COMPOSITE[1] (CAN3-S16.1-M84[3])	1	1.531	-	-
COMPOSITE[2] (CAN3-S16.1-M84[3])	1	1.334	-	-
ECCS[1]	1	1.377	-	-
SSRC-TASK GROUP 20[1]	1	1.759	-	-
SSRC-TASK GROUP 20[2]	1	1.504	-	-

BEAMS AND BEAM COLUMNS

TYPE	n	$\bar{x}$	σ	V
STEEL[1]	11	1.152	0.130	0.112
STEEL[2]	11	1.090	0.0746	0.0685
COMPOSITE[1] (CAN3-S16.1-M84)	9	1.114	0.256	0.230
COMPOSITE[2] (CAN3-S16.1-M84)	9	1.065	0.192	0.180
COMPOSITE[1] (CAN3-S16.1-M84[3])	9	1.068	0.194	0.182
COMPOSITE[2] (CAN3-S16.1-M84[3])	9	1.025	0.156	0.152
ECCS[1]	9	1.022	0.162	0.158
SSRC-TASK GROUP 20[1]	9	1.089	0.266	0.225
SSRC-TASK GROUP 20[2]	9	1.030	0.190	0.185

NOTES:
1. The solution is based on the elastic moment resistance of the steel or composite section.
2. The solution is based on the plastic moment resistance of the steel or composite section.
3. Alternate method not adopted.

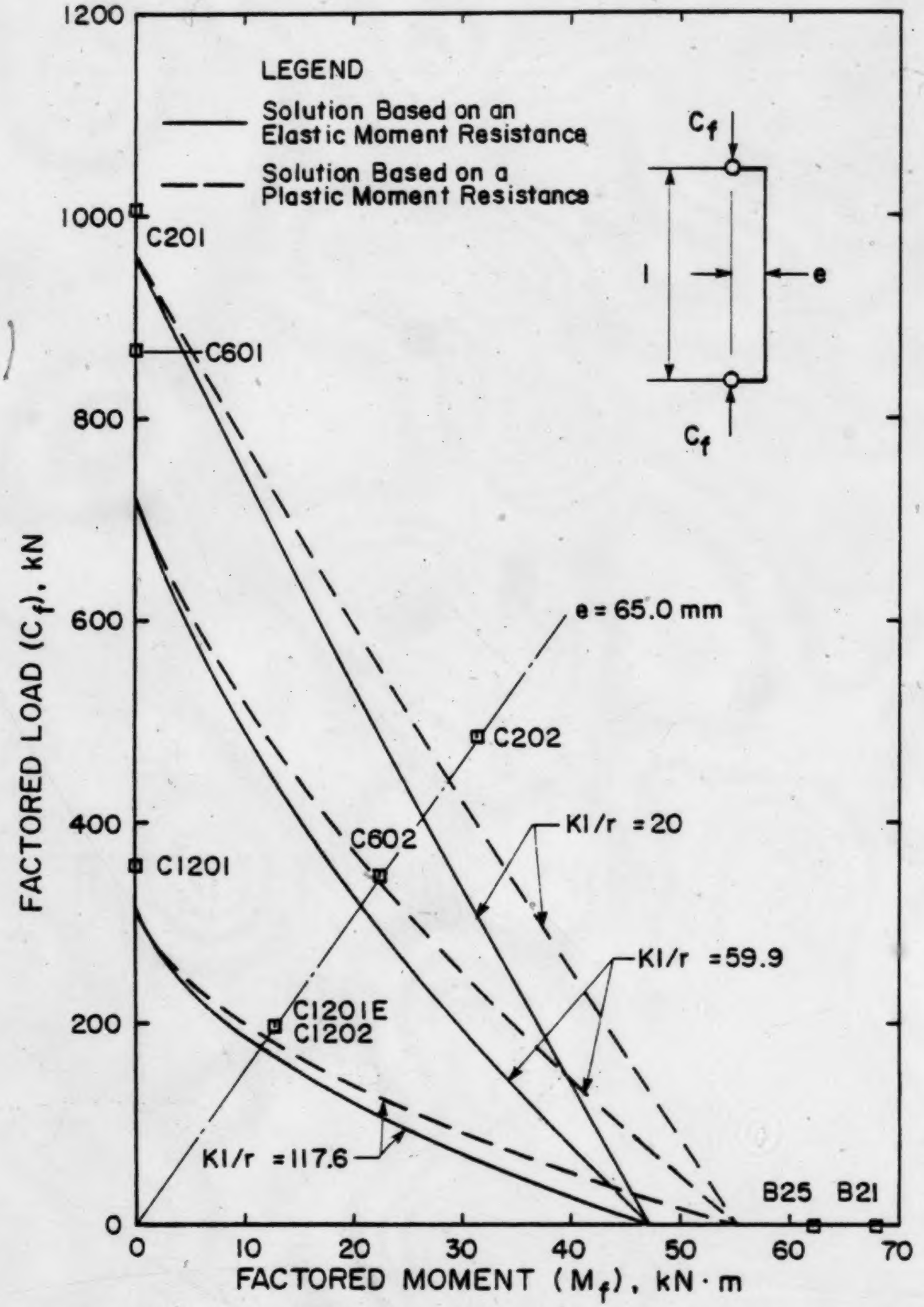

Figure 7.1 Axial Load-Moment Interaction Diagram for Steel Columns, CAN3-S16.1-M78

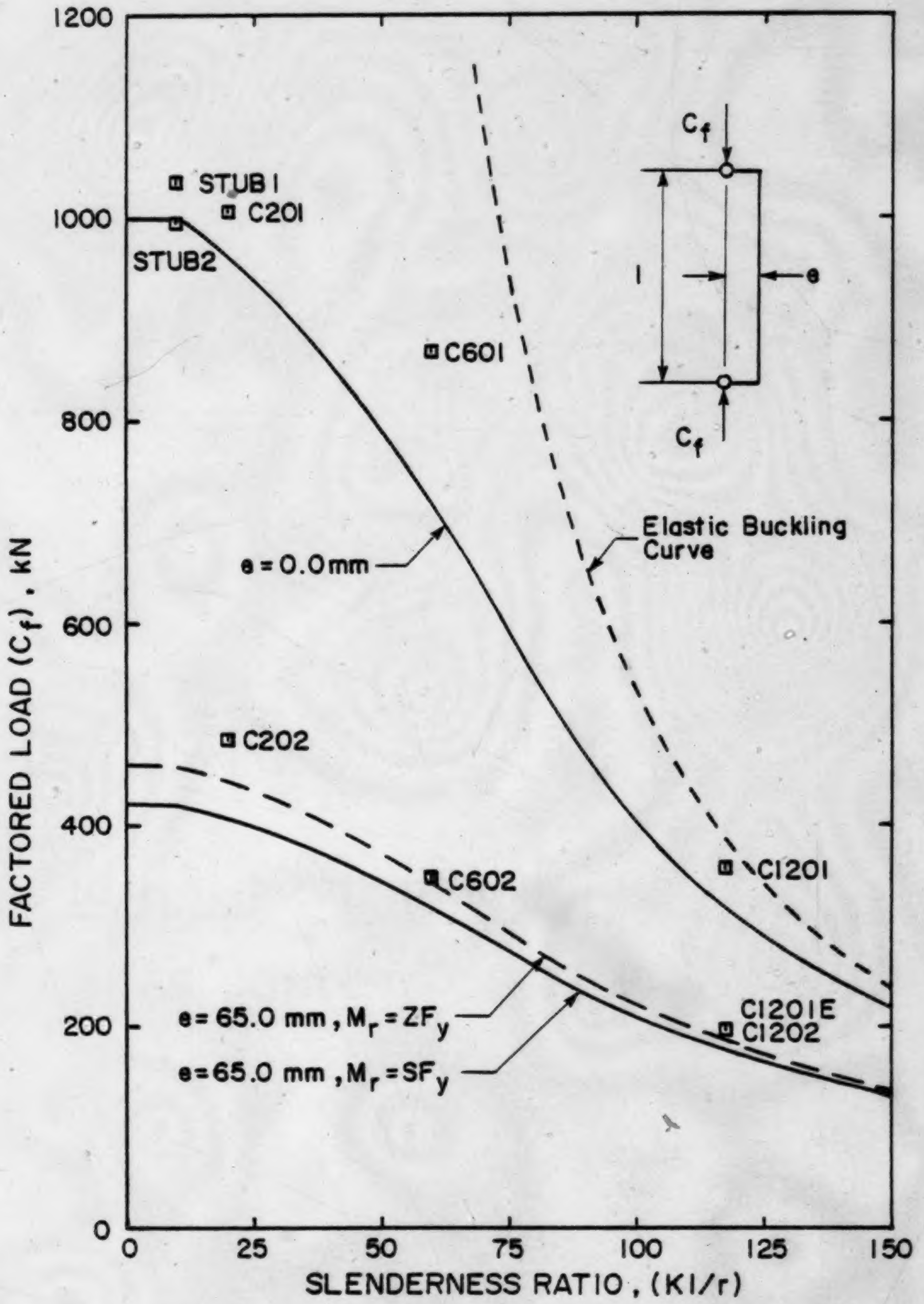

Figure 7.2 Column Curves for Steel Columns, CAN3-S16.1-M78

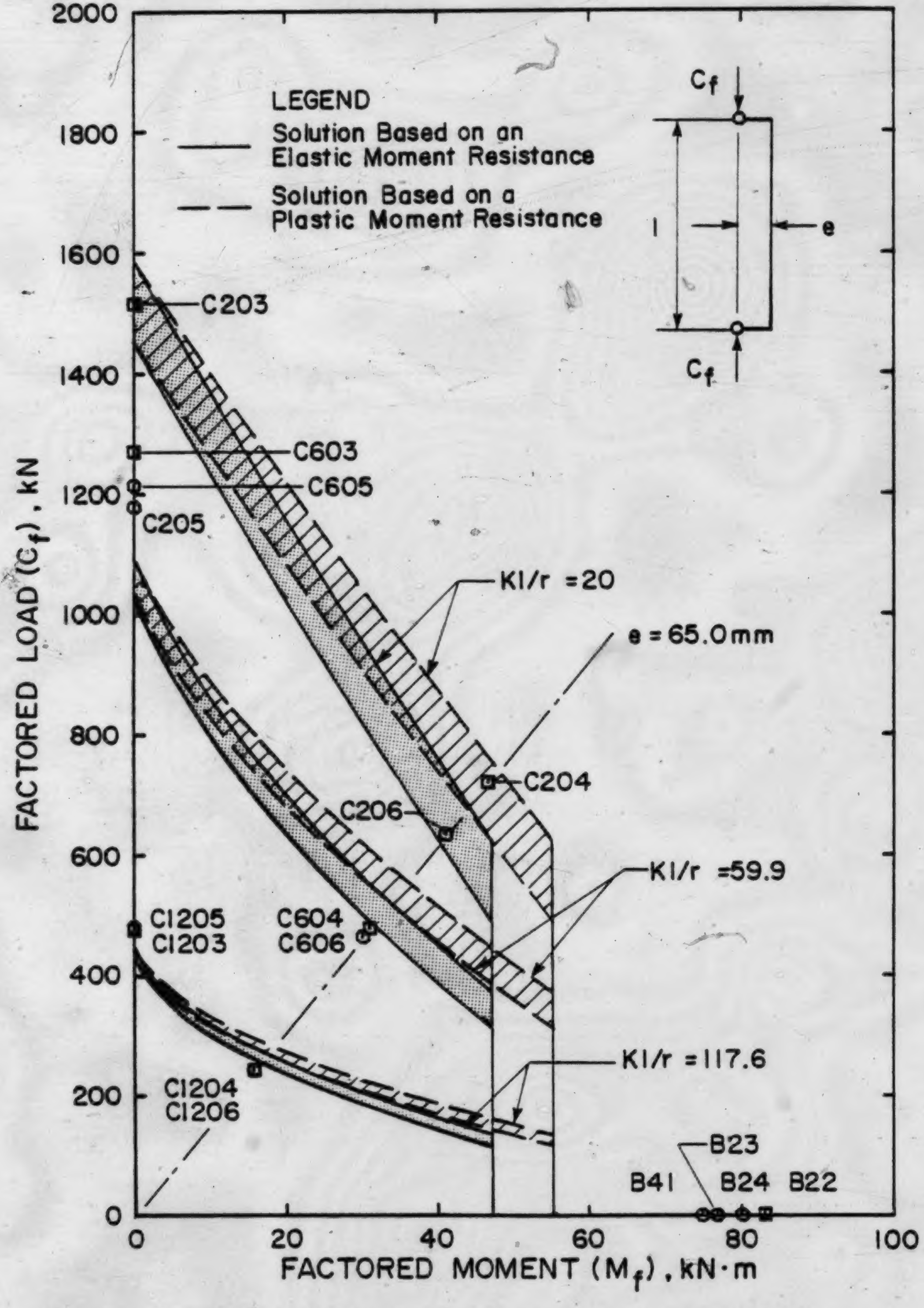

Figure 7.3 Axial Load-Moment Interaction Diagram for Composite Columns, CAN3-S16.1-M84

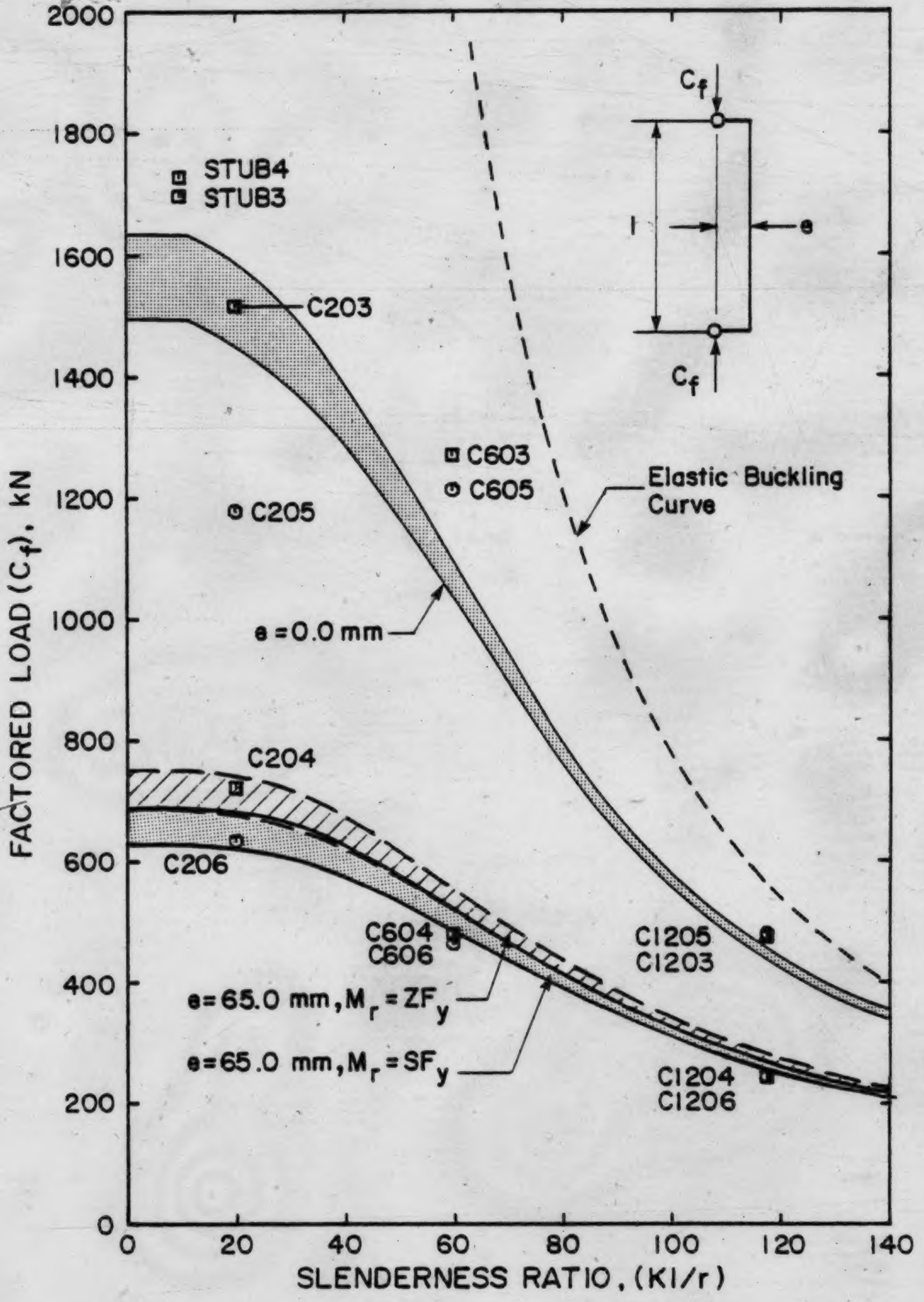

Figure 7.4 Column Curves for Composite Columns, CAN3-S16.1-M84

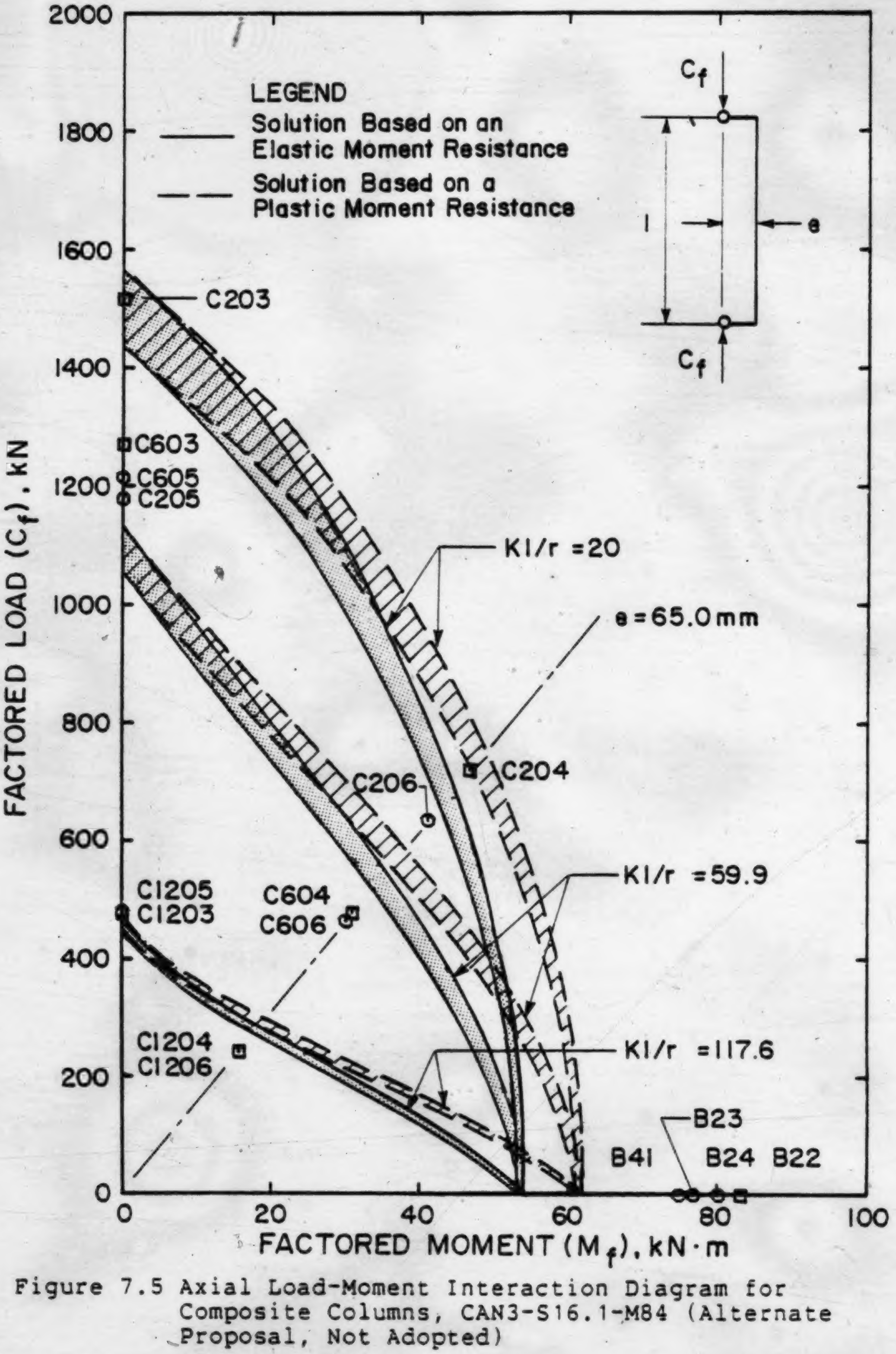

Figure 7.5 Axial Load-Moment Interaction Diagram for Composite Columns, CAN3-S16.1-M84 (Alternate Proposal, Not Adopted)

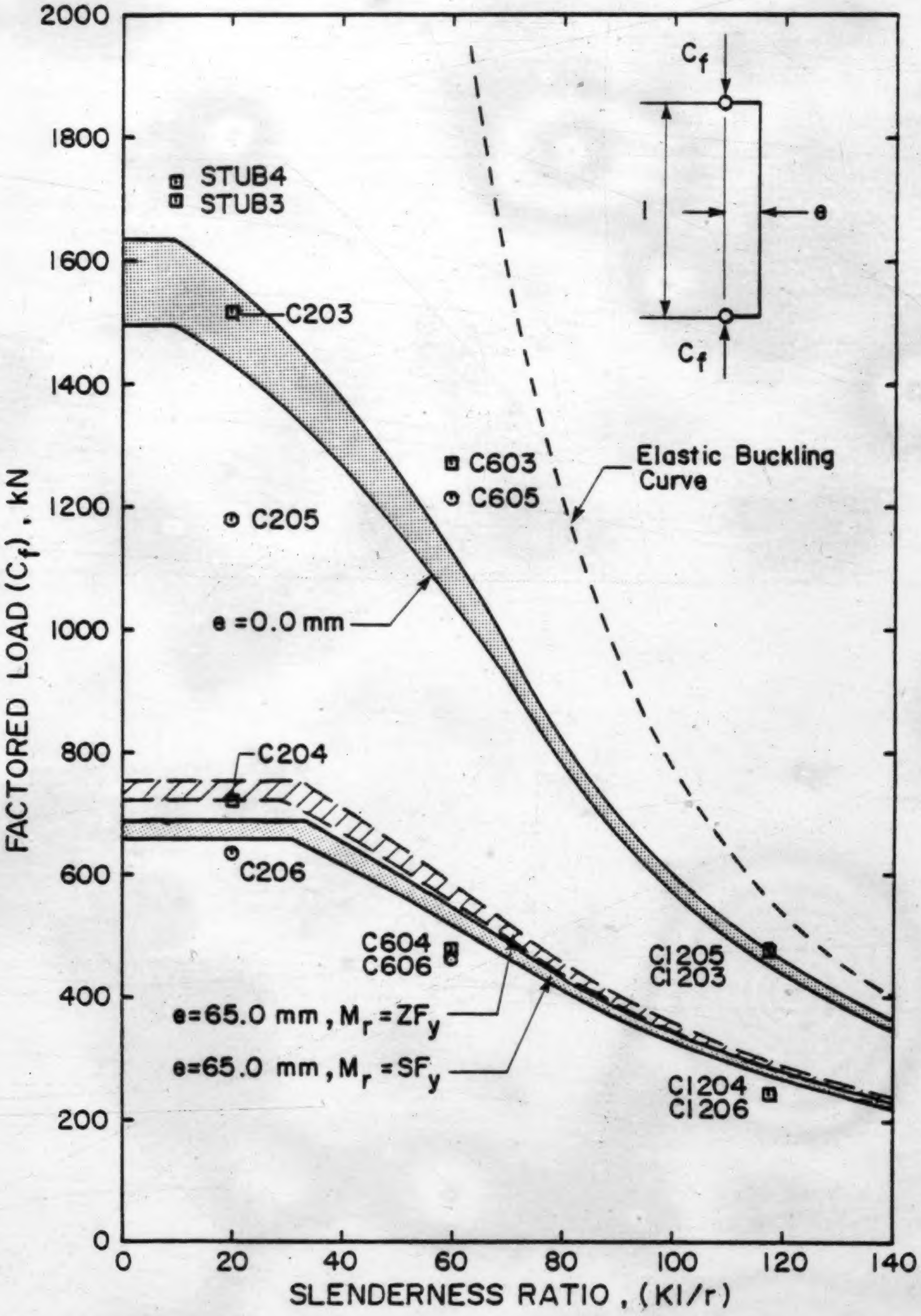

Figure 7.6 Column Curves for Composite Columns, CAN3-S16.1-M84 (Alternate Proposal, Not Adopted)

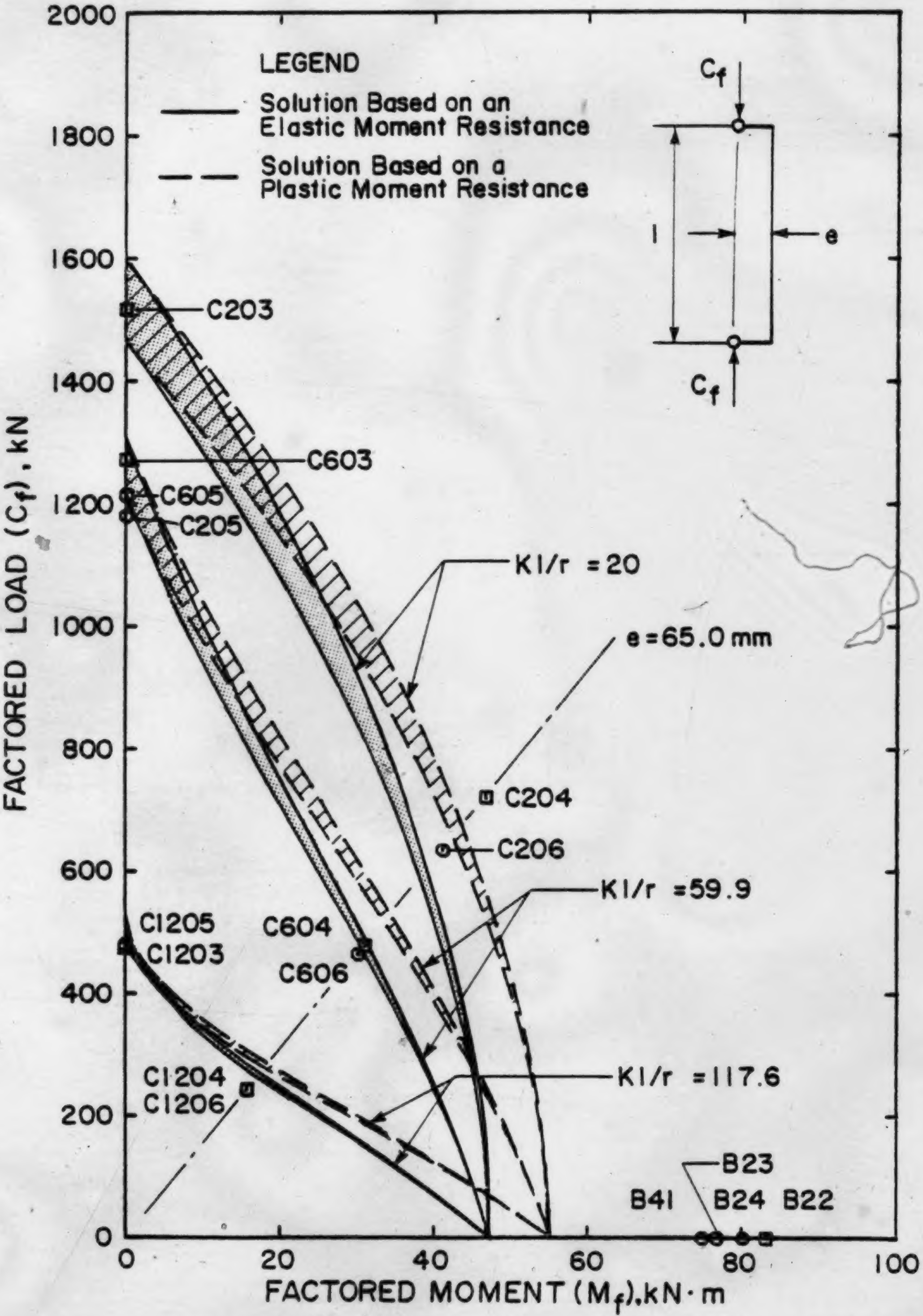

Figure 7.7 Axial Load-Moment Interaction Diagram for Composite Columns, SSRC Method

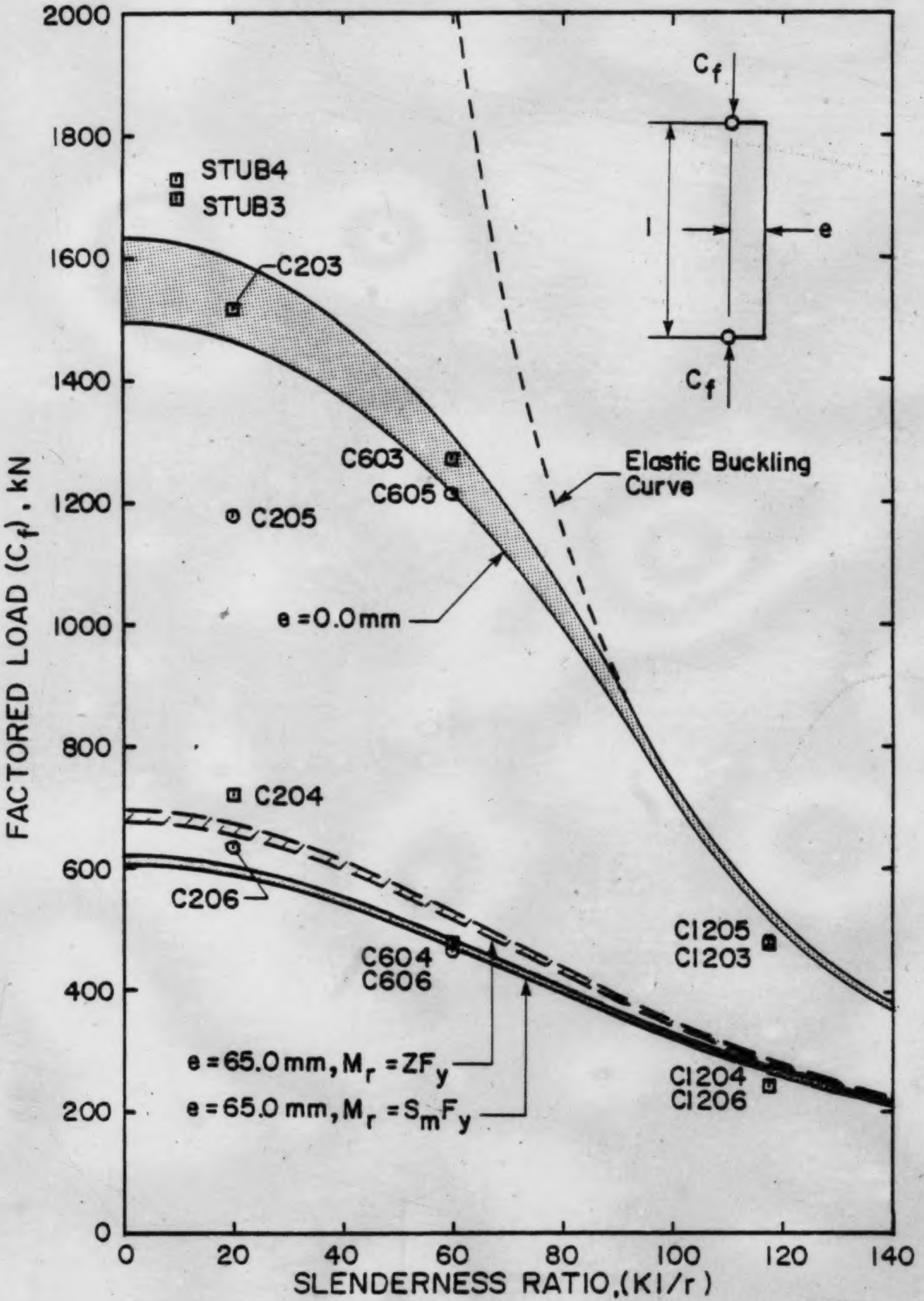

Figure 7.8 Column Curves for Composite Columns, SSRC Method

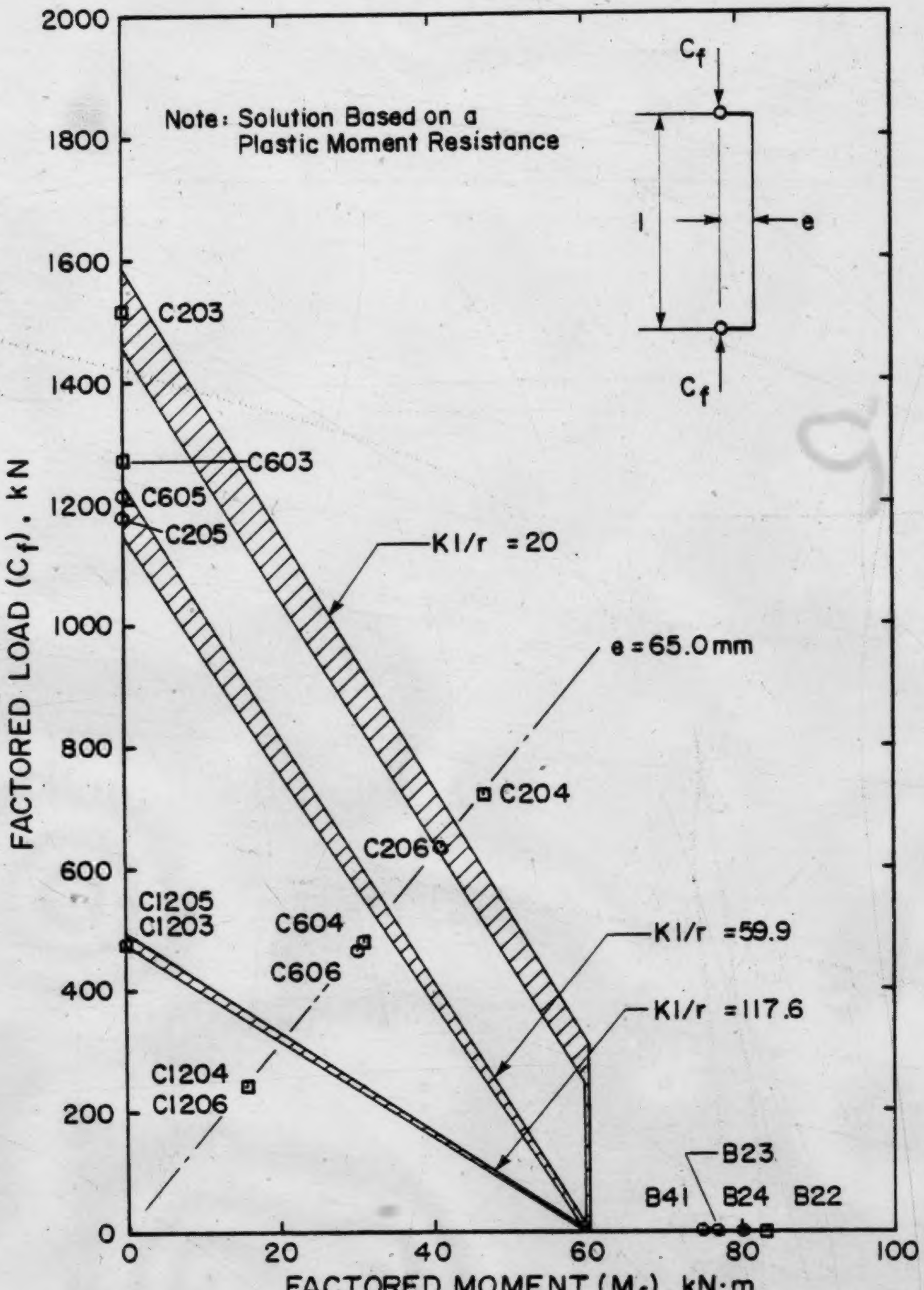

Figure 7.9 Axial Load-Moment Interaction Diagram for Composite Columns, ECCS Recommendations

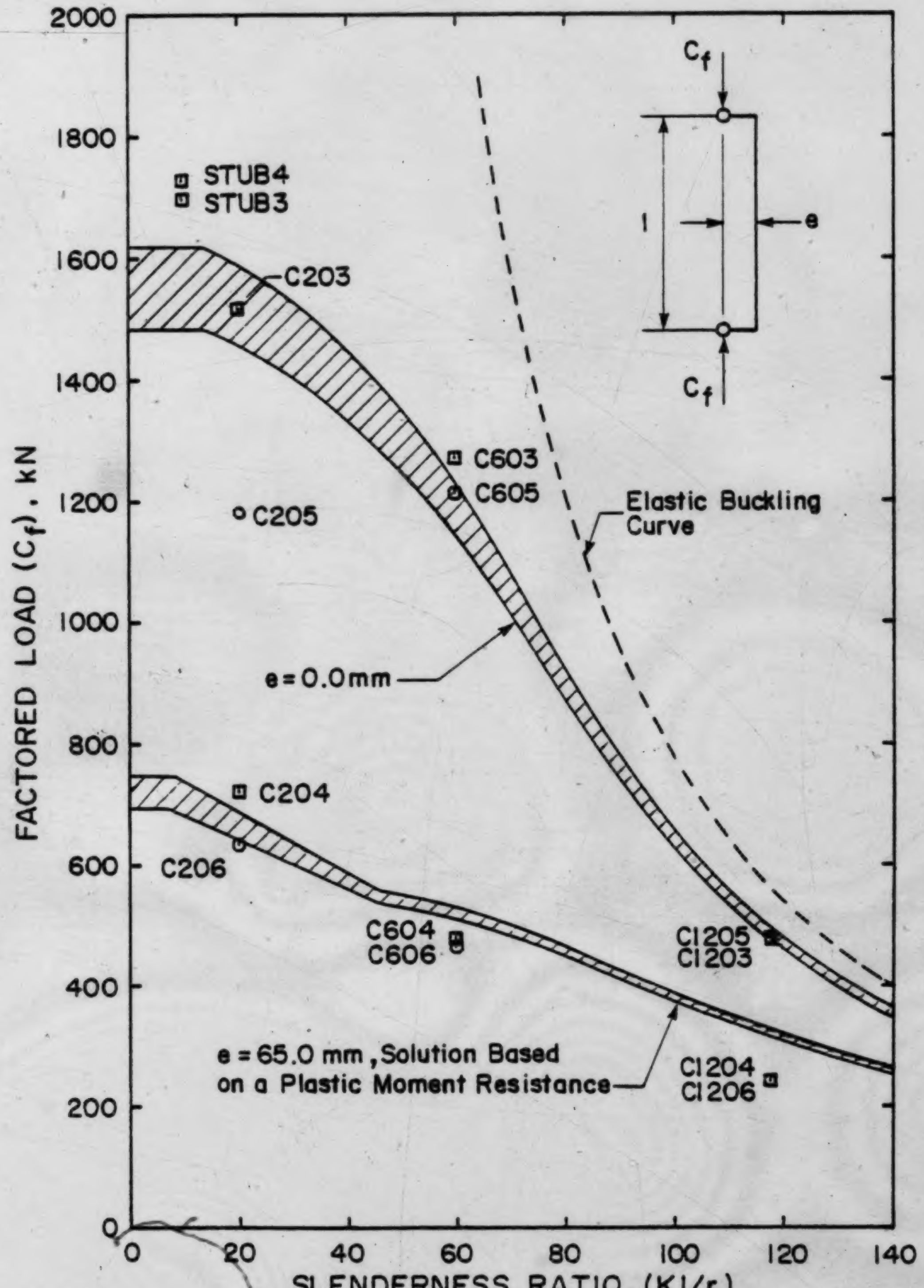

Figure 7.10 Column Curves for Composite Columns, ECCS Recommendations

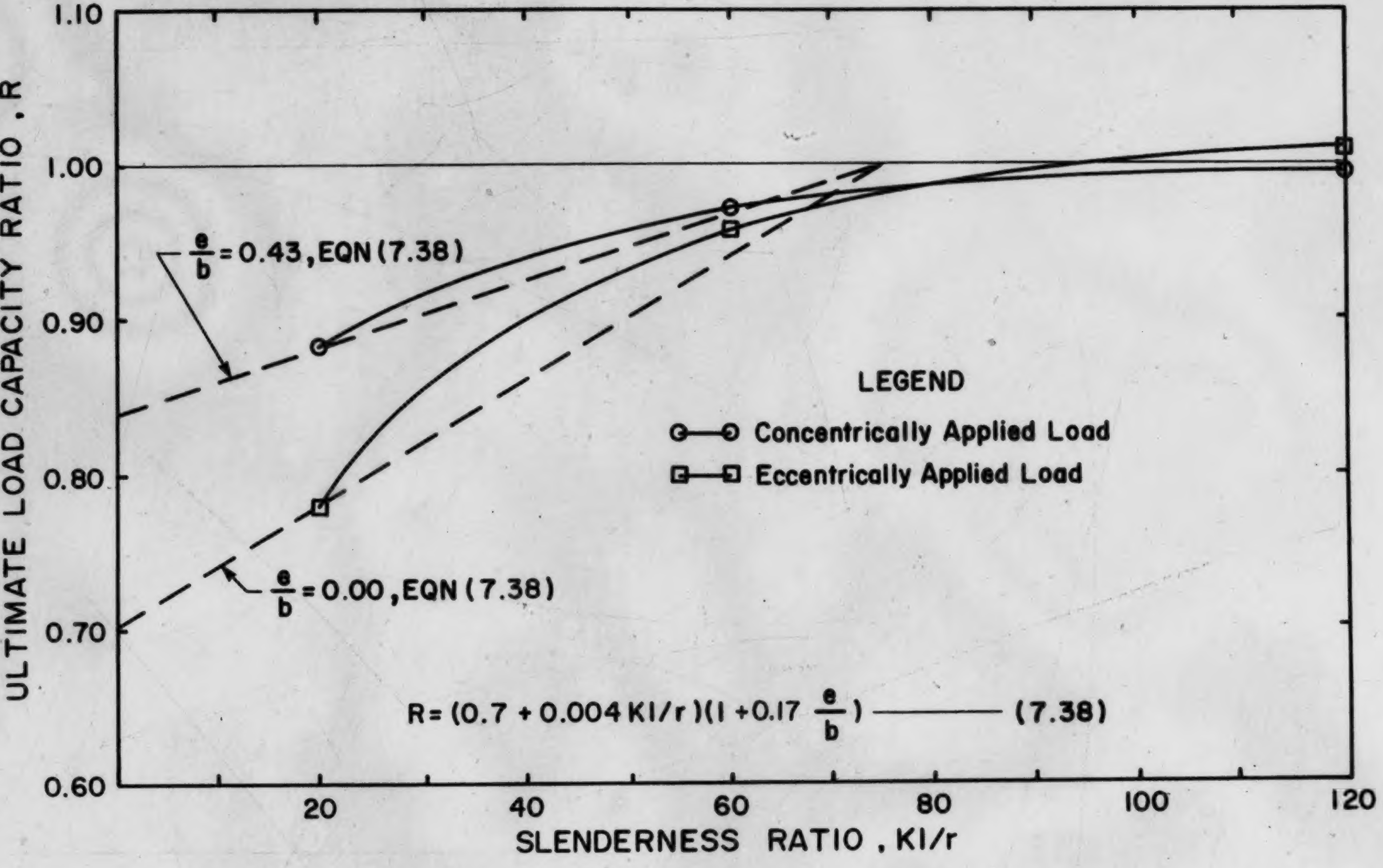

Figure 7.11 Ultimate Load Capacity Ratio of Non-Strain Compatible to Strain Compatible Composite Beam Columns

8. SUMMARY, CONCLUSIONS AND RECOMMENDATIONS

8.1 Summary

An experimental and analytical program was undertaken to determine:

1. The change in behaviour and ultimate load carrying capacity of concrete filled HSS beam columns when strain compatibility was not ensured at the point on the beam column where the load was introduced.
2. The load transfer mechanisms between the steel shell and the concrete core for the non-strain compatible cases.

The ultimate load carrying capacity and the behaviour of the beam columns was established by nineteen tests of pinned-ended columns on HSS 152 x 152 x 4.78, with slenderness ratios of 20, 60, and 118 as determined by the radius of gyration of the steel section alone. The tests were conducted on bare steel tubes and concrete filled tubes, with and without strain compatibility at the upper end. The load was either applied concentrically or with a constant eccentricity of 65 mm (0.43b). The ultimate moment capacity of the section was determined by six beam tests on HSS members, which were empty or concrete filled, with and without strain compatibility. Material properties and behaviour were established from a series of ancillary tests which included stub column tests on steel and concrete filled strain compatible tubes, residual stress measurements, tension coupons, concrete cylinders and concrete prisms.

Analysis of the load sharing characteristics involved the establishment of the load carried by the steel along the length of the column at any particular applied load level from strain measurements and material properties. The concrete load was then calculated by subtracting the steel load from the applied load and the load distributions for both materials were drawn. The analysis was calibrated against the test results obtained from the steel beam column tests. From the concrete load distributions for the non-strain compatible beam column test series, four load transfer mechanisms have been identified. In brief these are as follows:

1. Adhesion due to chemical reactions and/or suction forces resulting from capillary action during the hydration process.
2. Micro-interlocking of surface irregularities of the steel shell and the cement paste in contact with it.
3. Friction due to the pinching of the concrete core by the steel shell due to localized deformations resulting from the eccentricity of the applied loads on the connection and/or the buckling restraint provided by the concrete.
4. Binding or curvature effect which results from imposing deformations on two materials of different flexural stiffnesses and/or from a volumetric increase of the concrete core caused by micro-cracking which is due to excessive compressive strains.

A mathematical model, governing equation and solution are presented for the load transfer mechanism referred to as micro-interlocking.

The ultimate loads obtained from the steel and the strain compatible composite beam column tests are compared with those predicted by various codes and standards. For steel beam columns the comparison was made with CAN3-S16.1-M78 and for composite beam columns with:

1. CAN3-S16.1-M84
2. CAN3-S16.1-M84 (Alternate proposal, not adopted)
3. SSRC-Task Group 20
4. ECCS Recommendations

It should be noted that the comparison of the beam column strengths, is strictly speaking, only valid for the strain compatible test series since all the design recommendations have been developed assuming that strain compatible conditions are imposed at the load points. The relative merits and deficiencies of these methods are discussed in light of the comparison. Based on experimental observation, a plausible formulation is presented for the determination of the ultimate moment capacity of concrete filled HSS.

The behaviour and ultimate loads for the non-strain compatible test series are compared with corresponding tests from the strain compatible test series. Based on the limited data from this test series an expression has been derived to express the reduced ultimate load capacity of an non-strain compatible column compared to a strain compatible column as a function of the steel slenderness ratio and the eccentricity of applied load.

8.2 Conclusions and Recommendations

1. To determine an accurate value for the modulus of elasticity of a steel from a stress-strain curve where the yield point is not well defined, it is recommended that a moving average technique be used in conjunction with a least squares fit.
2. The cold forming process reorientates the metal crystals in the corners of a rectangular HSS shape. This preferred orientation increases the value of the modulus of elasticity and makes the material in this part of the section considerably less ductile than the surrounding material in the flats. The yield strength gain is attributed to another effect of cold working and that is the strain hardening phenomena.
3. Compressive longitudinal residual stresses of up to thirty percent of the yield strength were found in the corners of the HSS. In general the residual stresses for the remaining sections were small and/or tensile with a maximum tensile residual stress of 16 percent of the yield strength occurring adjacent to the weld. The yield points are not well defined on the stress-strain curves for the flat, corner and weld sections. This is attributed to the large variation of longitudinal residual stresses through the thickness of the section

which ranged from 30 to 90 percent of the yield stress found in these sections.

4. Analysis of the composite stub columns tested indicates that:
    a. the squash load of the composite section is equal to the sum of the squash loads for the steel and concrete sections,
    b. there is no confinement action on the concrete core by the steel tube,
    c. the concrete restrains the steel tube from local buckling.
5. Although the classification of steel sections is discrete in design standards, the transition in behaviour between two classes is not. From the tests performed, it is recommended that concrete filled Class 3 HSS be classified as a Class 1 or 2 section because of the stabilizing effect the concrete has in preventing local buckling of the steel tube.
6. An analysis of column end fixity, based on the steel column data and an assumed deflected shape of a half sine wave, shows that the knife edge fixtures behaved as pinned ends.
7. The mean value for the out-of-straightness of these members was found to be 1/12600, which is much less than the specified tolerance limit of 1/500.
8. The load deflection curves for all beam column tests exhibited normal characteristics. Apart from the

ultimate loads obtained, the general load deflection behaviour of the non-strain compatible beam columns is comparable to the corresponding strain compatible beam columns. There was no difference in the flexural stiffness between these two types.

9. The mean and coefficient of variation of the ratio of predicted to applied load for the load carried by the steel based on steel column tests, measured strains, and material properties was 0.974 and 0.035 respectively, for calculations based on the stub column data and 0.953 and 0.036 respectively, for calculations based on the tension coupon data coupled with residual stress patterns.
10. The ultimate loads reached in tests of non-strain compatible columns were a direct function of the effectiveness of the load transfer from the steel to the concrete core by one or more of the load transfer mechanisms.
11. Adhesion is an elastic brittle load transfer mechanism. This is an effective mechanism only when the relative slip between the two materials is negligible and/or shrinkage has not occurred and generally cannot be taken into consideration.
12. The load transfer mechanism referred to as micro-interlocking allowed a significant amount of load to be transferred along the length of the column but was only effective in regions of low slip. The concrete load

distribution as determined from the solution of the governing differential equation derived herein and an assumed shear transfer function showed excellent agreement with that of column C1205, which was subject to conditions where this was the only effective load transfer mechanism.

13. The friction type, macro-interlocking load transfer mechanism was independent of the relative slip between the two materials, is governed by localized effects and is the most prominent and dominant of all load transfer mechanisms.
14. The binding type macro-interlocking load transfer mechanism occurred in beam columns subject to an eccentrically applied load and with curvature greater than ten microradians. Characteristically, relatively little slip occurred when this mechanism came into play.
15. All design methods investigated here were able to predict the ultimate load capacity of strain compatible beam columns with reasonable accuracy, but not the ultimate capacity of beams or of those beam columns approaching pure flexural behaviour. No conclusive statements can be made as to which method is best due to the limited data used in the comparison.
16. From the design methods examined the range of test to predicted ratios of ultimate moment capacity of the composite section was 1.33 to 1.76. It is suggested that the augmented strength was due to the development of a

triaxial stress state in the concrete core, and the ability of the steel section to fully plasticize with the maximum stress being the ultimate strength of the steel section. Given an ultimate moment capacity of the composite section as determined with these increased strength values and a plastic stress distribution, it is recommended that a straight line interaction curve with an amplification factor which reflects the decrease in strength due to P-Δ effects and the reduced flexural stiffness due to cracking of the concrete core would be the most appropriate formulation.

17. Current design methods are based on imposing strain compatible conditions at loading points or at points on the columns where the load is introduced. It is recommended that a simple formulation be considered to reduce the ultimate load capacity for columns where strain compatibility is not ensured. Such a formulation has been developed based on the limited data from this test series. It is a function of the column slenderness ratio (as determined by the radius of gyration of the steel section alone) and the eccentricity of the applied load. For the practical range of slenderness ratios from 30 to 90, the reduction in load carrying capacity when strain compatibility is not ensured varies from 0 per cent to 18 per cent for concentrically loaded columns and less for eccentrically loaded columns.
18. Shrinkage of the concrete for this structural element

may be neglected since the exposed area of concrete is relatively small and exposure time during construction is short.

8.3 Future Work

From this investigation it is concluded that further research is required in the following areas:

1. Analytical work is required to develop mathematical models for the macro-interlocking type load transfer mechanisms. These models should be verified experimentally.
2. A larger sample of data is required on the behaviour and the ultimate load capacity of non-strain compatible pinned-ended beam columns for both circular and rectangular sections. Tests should be conducted on columns with a practical range of slenderness ratios and eccentricities of applied load. Load transfer mechanisms should be monitored.
3. The ultimate moment capacity for both circular and rectangular composite sections should be thoroughly investigated.
4. Another major area of study is beam column assemblage and connection behaviour. It is envisaged that a series of tests would be conducted on interior and exterior assemblages of two and three storey column lifts subject to uniaxial and biaxial bending under realistic loads. Beams framing into the columns between splice levels

would be connected to the steel shell with connections typical of HSS construction. The application of load and the load distribution in both the concrete and steel should be monitored.

REFERENCES

AMERICAN SOCIETY FOR TESTING AND MATERIAL. 1961. Standard Test Method for Young's Modulus at Room Temperature. ASTM E111-61 Part(10), Philadelphia, Penn.

AMERICAN SOCIETY FOR TESTING AND MATERIAL. 1961. Standard Test Method for Poisson's Ratio at Room Temperature. ASTM E132-61 Part(10), Philadelphia, Penn.

AMERICAN SOCIETY FOR TESTING AND MATERIAL. 1977. Standard Methods and Definitions for Mechanical Testing of Steel Products. ASTM A370-77 Part(1), Philadelphia, Penn.

AMERICAN SOCIETY FOR TESTING AND MATERIAL. 1971. Splitting Tensile Strength of Cylindrical Concrete Specimens. ASTM C496-71, Philadelphia, Penn.

AMERICAN SOCIETY FOR TESTING AND MATERIAL. 1966. Test Methods for Compression Members. Symposium Presented at the Sixty-ninth Annual Meeting, American Society for Testing and Materials, 26 June - 1 July, Atlantic City, N. J.

ANSOURIAN, P. 1976. Connections to Concrete-Filled Tube Columns. International Association for Bridge and Structural Engineering Publications, 36-I-1976.

BASU, A. K. 1967. Computation of Failure Loads of Composite Columns. Proceedings Institution of Civil Engineers, London, Vol. 36, Paper 6980.

BASU, A. K., and HILL, W. F. 1968. A More Exact Computation of Failure Loads of Composite Columns. Proceedings Institution of Civil Engineers, London, Volume 40.

BASU, A. K., and SOMMERVILLE, W. 1969. Derivation of Formulae for the Design of Rectangular Composite Columns. Institution of Civil Engineering, London, Supp. Paper 72065.

BEER, H., and SCHULTZ, G. 1970. The Theoretical Basis of the New Column Curves of the European Convention of Construction Steelwork (In French). Construction Metallique, No. 3, September.

BERTERO, V. V., and MOUSTAFA, S. E. 1970. Steel-Encased Expansive Cement Concrete Column. Proceedings American Society of Civil Engineers. Journal of the Structural Division, Vol. 96, No. ST11, Paper 7660, November.

BLEICH, F. 1952. The Buckling of Metal Structures. Mc-Graw-Hill Book Co., New York, N. Y.

BJØRHVODE, R. 1972. Deterministic and Probabilistic Approaches to the Strength of Steel Columns. Ph.D. Thesis, Lehigh University.

BODE, H., and BERGMAN, R. 1981. Concrete Filled Structural Hollow Sections. Merkblatt 167, Beratungsstelle fur Stahlverwending, English Translation No. TD 1402 BISI 20258 by H. E. Worner, Steel Users Advisory Council.

BRANDZAEG, A., RICHART, F. E., and BROWN, R. L. 1929. The Failure of Plain and Spirally Reinforced Concrete in Compression. Bulletin No. 190, Engineering Eperimental Station, University of Illinois, Urbana.

BURDIJANTO, P. 1983. Design Methods for Composite Columns. Project Report G83-6, McGill University, May.

CANADIAN STANDARDS ASSOCIATION. 1977. Methods of Test for Concrete. National Standard of Canada CSA CAN3-A23.2-M77, Rexdale, Ont.

CANADIAN STANDARDS ASSOCIATION. 1977. Flexural Strength of Concrete (using simple beam with third point loading). National Standard of Canada CSA CAN3-A23.2-8C, Rexdale, Ont.

CANADIAN STANDARDS ASSOCIATION. 1977. Compressive Strength of Cylindrical Concrete Specimens. National Standard of Canada CSA CAN3-A23.2-9C, Rexdale, Ontario.

CANADIAN STANDARDS ASSOCIATION. 1977. Splitting Strength of Cylindrical Concrete Specimens. National Standard of Canada CSA CAN3-A23.2-13C, Rexdale, Ontario.

COMITE EUROPEEN DU BETON. 1972. Complements aux Recommandations Internationales CEB-FIP-1970. Bulletin d'Information No. 74, January 1971 (Revision March 1972).

COTTRELL, A. H. 1967. An Introduction to Metallurgy. William Clowes and Sons Ltd., London, Great Britain.

DOWLING, P. J., JANSS, J., and VIRDI, K.S. 1976. The Design of Composite Steel-Concrete Columns. Appendix to Introductory Report, Second International Colloquium on Stability, European Convention for Constructional Steelwork.

ESTUAR, F. R., AND TALL, L. 1967. Testing of Pinned-End Steel Columns. Test Methods for Compression Members. ASTM STP419, American Society for Testing and Materials,

FURLONG, R. W. 1967. Strength of Steel-Encased Concrete Beam Columns. Proceedings, American Association of Civil Engineers, Journal of the Structural Division, ST5, Vol. 93, Paper No. 5492, October.

FURLONG, R. W. 1969. Strength of Steel-Encased Concrete Beam Columns (Closure). Proceedings, American Association of Civil Engineers, Journal of the Structural Division, ST1, Vol. 95, January.

FURLONG, R. W. 1976. AISC Column Design Makes Sense for Composite Columns, Too. American Institute of Steel Construction Engineering Journal, Vol. 13, No. 1, 1st Quarter.

GALAMBOS, T. V., and KETTER, R. L. 1957. Further studies of Columns Under Combined Bending and Thrust. Fritz Engineering Laboratory Report No. 205 A.19, Lehigh University.

GALAMBOS, T. V. 1968. Structural Members and Frames. Prentice-Hall Inc., Englewood Cliffs, N. J.

GARDNER, N. J. 1968. Use of Spiral Welded Steel Tubes in Pipe Columns. Proceedings, American Concrete Institute, Vol. 65, No. 11, November.

GARDNER, N. J., and JACOBSON, E. R. 1967. Structural Behaviour of Concrete Filled Steel Tubes. Proceedings, American Concrete Institute, Vol.64, No. 7, July.

GIDDINGS, T. W. 1972. Fire Resistant Construction Using HSS. The International Symposium on Hollow Structural Sections, Comite International pour le Developpement et l'etude de la Construction Tubulaire (Cidect), May.

Hollow Structural Sections - Design Manual for Concrete Filled HSS Columns. 1981. Cidect Monograph #5, Stelco (Canadian Addition), January.

JAMES, M. L., SMITH, G. M., AND WOLFORD, J. C. 1977. Applied Numerical Methods for Digital Computation with Fortran and CSMP. Harper and Row Publishers, Inc.

JANSS, J. Composite Steel-Concrete Construction. Part 3. Tests on Concrete Filled Tubular Columns. Report Published by the Centre of Scientific Research and Industrial Techniques of Metal Fabrication (CRIF), Brussels, Belgium.

JANSS, J. 1974. Ultimate Load of Axially Loaded Concrete Filled Tubes (In French). CRIF Report MT101, Liege, Belgium. November.

JOHNSON, R. P. 1975. Composite Structures of Steel and Concrete Granada Publishing Limited, London.

KATO, B., and KANATINI, H. 1966. Experimental Studies on Concrete Filled Steel Tubular Columns. Steel Structures Laboratory Report, Department of Architecture, Faculty of Engineering, Tokyo University, October.

KLINGSCH, W. 1979. Investigation of the Fire Resistance of Tubular Steel Columns Strengthened with Concrete. Lecture, GIPEC Conference, Zurich, November.

KLÖPPEL, V. K., and GODER, W. 1957. Investigations of the Load Carrying Capacity of Concrete Filled Steel Tubes and Development of a Design Formula. Der Stahlbau, Berlin (In German), Vol. 26, No. 1, January.

KNOWLES, R. B., and PARK, R. 1969. Strength of Concrete Filled Steel Tubular Columns. Proceedings American Society of Civil Engineers. Journal of the Structural Division, Vol. 95, No. ST12, Paper 6936.

KNOWLES, R. B., and PARK, R. 1970. Axial Load Design for Concrete Filled Steel Tubes. Proceedings American Society of Civil Engineers. Journal of the Structural Division, Vol. 96, No. ST10, Paper 7597.

KNOWLES, R. B. 1973. Composite Steel and Concrete Construction. Butterworth and Co. (Publishers) Ltd., London.

MAY, I. M. 1978. Crossed Knife-Edge Joints for Testing Columns. Proceedings Institution of Civil Engineers, London, Vol. 65.

MOUSTAFA, S. E. 1968. Steel Tubes and Expansive Cement Concrete Composite Columns. Ph.D. Thesis Presented to the University of California, at Berkley, Berkley, California, SEMS Report No. 68-8.

NAGARAJA RAO, N. R., LOHRMANN, M., and TALL, L. 1966. Effect of Strain Rate on the Yield Stress of Structural Steels. Journal of Materials, Vol. 1, No. 1.

NARAYANAN, R. 1982. Axially Compressed Structures, Stability and Strength. Applied Science Publishers Ltd., New York, N.Y.

NEOGI, P. K. 1967. Concrete Filled Tubular Columns. Ph.D. Thesis, Imperial College, University of London.

NEOGI, P. K., SEN, H. K., and CHAPMAN, J. C. 1969. Concrete-Filled Tubular Steel Columns Under Eccentric Loading. The Structural Engineer, Vol.47, No. 5.

PERRY, AND LISSNER. 1962. The Strain Gauge Primer. 2nd ed. McGraw-Hill Book Company, New York, N. Y.

REDWOOD, R. G. 1981. The Treatment of Composite Columns in CSA S16.1. Canadian Standards Association - S16 - Task Group on Composite Construction Report, September.

REDWOOD, R. G. 1982. CSA S16 Subcommittee on Composite Construction Report to S16 Committee. Canadian Standards Association - S16 - Task Group on Composite Construction Report, May.

REDWOOD, R. G. 1983. Design of Concrete Filled HSS. Canadian Standards Association - S16 - Task Group on Composite Construction Report, February.

REHM, G. 1961. Über die Grundtagen des Vorbundes zwischen Stahl und Beton. In German. Deutscher Ausschuss für Stahlbeton Publication No. 138, Berling Wilhelm Ernst and Sohn. The Basic Principles of the Bond Between Steel and Concrete, English Translation No.134 by C. van Amerongen, Cement and Concrete Association, London, England.

RICHART, F. E., BRANDTZAEG, A., and BROWN, R. L. 1928. A Study of the Failure of Concrete Under Combined Compressive Stresses. Bulletin No. 185, Engineering Experimental Station, University of Illinois, Urbana.

ROIK, K., BODE, H., and BERGMANN, K. 1977. Composite Column Design. Preliminary Report, 2nd International Colloquim on Stability of Structures, Leige, France.

SABNIS, G. M. 1979. Handbook of Composite Construction Engineering. Van Nostrand Reinhold Company, Toronto, Ont.

SABNIS, G. M., HARRIS, H. G., WHITE, R. N., AND MIRZA, M. S. 1983. Structural Modelling and Experimental Techniques. Prentice-Hall Inc., Englewood Cliffs, N. J.

SALANI, H. J., and SIMS, J. R. 1964. Behaviour of Mortar Filled Steel Tubes in Compression. Proceedings, American Concrete Institute, October.

SEN, H. K. 1969. Triaxial Effects in Concrete Filled Tubular Steel Columns. Ph.D. Thesis, Imperial College, University of London.

SOMAYASI, S., AND SHAH, S. P. 1981. Bond Stress Versus Slip Relationship and Cracking Response of Tension Members. American Concrete Institute Journal, May - June.

STRUCTURAL STABILITY RESEARCH COUNCIL. 1976. Guide to Stability Design Criteria for Metal Structures. 3rd ed. Edited by B. G. Johnson, John Wiley and Sons, New York, N. Y.

STRUCTURAL STABILITY RESEARCH COUNCIL, TASK GROUP 20. 1979. A Specification for the Design of Steel-Concrete Composite Columns. American Instite of Steel Construction Engineering Journal, Vol. 16, No. 4, 4th Quarter.

TEBEDGE, N., ALPSTON, G. A., AND TALL, L. 1971. Residual Stresses in Thick Welded Plates. Measurement of Residual Stresses - A Study of Methods, Fritz Laboratory Report No. 337.8, February.

TECHNICAL GENERAL SECRETARIAT OF THE ECCS (EUROPEAN CONVENTION FOR CONSTRUCTIONAL STEELWORK). 1981. Composite Structures. The Construction Press, Ltd., Longman Inc., New York, N. Y.

TODESCHINI, C. E., BIUNCHINI, A. C., AND KESLER, C. E. 1964. Behavior of Concrete Columns Reinforced with High Strength Steels. American Concrete Institute Journal, Vol. 61, June.

TOMII, M., YOSHIMURA, K., AND MORISHITA, Y. 1977. Experimental Studies on Concrete Filled Steel Tubular Stub Columns Under Concentric Loads. International Colloquium on Stability of Structures under Static and Dynamic Loads, May 17 - 19, Washington, D. C.

TOURNAY, M. 1972. Fire Resistance of Concrete Filled HSS. The International Symposium on Hollow Structural Sections, Comite International pour le Developpement et l'etude de la Construction Tubulaire (Cidect), May.

TROKE, R. W. 1976. Improving Strain-Measurement Accuracy with Using Shunt Calibrations. Experimental Mechanics, October.

VAN VLACK, L. H. 1980. Elements of Material Science and Engineering. 4th ed. Addison-Wesley, Don Mills, Ont.

VIRDI, K. S., and DOWLING, P. J. 1972. Composite Columns - Comparison of Test Results with Proposed Interaction Formula for Composite Columns in Biaxial Bending. CESLIC Report, No. CE4, London.

VIRDI, K. S., and DOWLING, P.J. 1973. The Ultimate Strength of Composite Columns in Biaxial Bending. Proceedings Institute of Civil Engineers, Vol. 55, PT. 2, Paper No. 7598. March.

VIRDI, K. S., and DOWLING, P. J. 1976. The Ultimate Strength of Composite Columns in Biaxially Restrained Columns. Proceedings Institute of Civil Engineers, Vol. 61, Paper No. 7860. March.

VIRDI, K. S., and DOWLING, P. J. 1976. A Unified Design Method for Composite Columns. International Association of Bridge and Structural Engineers Memoires 36-II.

WAKABAYASHI, M. 1977. A New Design Method of Long Composite Beam-Columns. Proceedings International Colloquium on Stability of Structures under Static and Dynamic Loads, American Society of Civil Engineers, Washington, D. C. May.

WALKER, A. C. (Editor) 1975. Design and Analysis of Cold-Formed Sections. International Textbook Company Limited.

WINDOW, A. L., AND HOLISTER, G. S. 1982. Strain Gauge Technology. Applied Science Publishers Ltd., Essex, England.

YAM, H. J., and SIMS, J. R. 1981. Design of Composite Steel-Concrete Structures. published by Surrey University Press, London.

YU, C. K., AND TALL, L. 1969. Significance and Application of Stub Column Test Results. Fritz Laboratory Report No. 290.18, Lehigh University, June.